

INSTITUTE OF MINERALOGY AND MINERAL RESOURCES  
TECHNICAL UNIVERSITY OF CLAUSTHAL

**Geology and geochemistry of the Cerro Millo gold prospect,  
southern Peru**



Daniel Hennig

27 January 2005

“Ich zweifle nicht, dass ich vieles ausgelassen habe.  
Ich bin ein Mensch, ich war von meinem Dienst  
voll ausgefüllt und arbeitete an diesem Werk in den  
späten Stunden der Nacht.“

PLINIUS d. Ä. (77 n. Chr.)

Trotzdem sage ich:

“That`s enough, now.“

Mrs Weasley in J. K. ROWLING (1999):  
Harry Potter and the Prisoner of Azkaban.

„Alea jacta est.“

Julius Cäsar (10. Januar 49 v. Chr.)

Hiermit versichere ich, dass die vorliegende Arbeit  
selbstständig und unter Verwendung der  
angegebenen Quellen und Hilfsmittel angefertigt  
wurde.

Daniel Hennig

## Acknowledgements

I would like to thank Professor Bernd Lehmann for supervision, encouragement, confidence and help during the preparation of this diploma thesis.

For second reviewing I thank Professor Kurt Mengel and Dr. Karl Strauß.

Particular gratitude is expressed to Dr. Cesar Vidal and the logistic support by Minas Buenaventura SAA.

Dr. Andreas Dietrich is thanked for an introduction to epithermal systems and for suggesting the interesting study area at Pichacani.

I feel obliged to thank Mauro, the sampler, and Clever, the driver and cook for the memorable and funny time, in spite of unfavourable weather and living conditions.

I thank Dr. Rainer Müller for valuable criticism and information concerning volcanic rocks. Ulf Hemmerling prepared the thin and polished sections and Dr. Eike Gierth helped to interpret the latter. Fred Türck and Tobias Riekebrink knew for every computer problem a suitable answer. Amiable Helga Vollbrecht is wished best convalescence. Klaus Herrmann was responsible for EPMA and Dr. M. Siemann for RDA analysis. Sincere thanks are given to all of them.

Dr. Thomas Oberthür is thanked for XRF analysis at BGR; Jens Wittenbrink and Dr. Frank Schultz are thanked for discussion about numerous small and larger problems.

I thank my parents for their belief in me and for financial support to study geology.

Nicole Peter is thanked for her energy and vitality.

## Zusammenfassung

Das Arbeitsgebiet liegt 35 km SW von Puno in der östlichen Westkordillere Süd-Perus.

Die ältesten Gesteine, flach lagernde, andesitische bis latitische Laven, gehören der känozoischen Maure-Gruppe an. Diese werden von Gesteinen der Barroso-Gruppe überlagert, die in ihren stratigrafisch tiefsten Einheiten aus pyroklastischen Gesteinen und aus jüngeren andesitischen bis dazitischen/trachytischen porphyrischen Laven aufgebaut ist.

Die latitischen, leicht verschweißten pyroklastischen Gesteine zeigen ähnlich der sie überlagernden andesitischen bis trachytischen Laven umlaufendes Streichen mit kuppelartiger Orientierung. Die Geländebeobachtung impliziert einen stark erodierten Stratovulkan. Im Hangenden folgen andesitische bis latitische, zum Teil blockig entwickelte Laven unterschiedlicher Herkunft, die aufgrund von tektonischen, petrografischen und geochemischen Untersuchungen vier weiteren vulkanischen Ereignissen zugeordnet werden konnten.

Die Elementverteilungsmuster der am wenigsten alterierten Gesteine zeigen Differentiations- und Kontaminations-Erscheinungen, wie sie für Laven, die an aktiven Kontinentalrändern gefördert werden, typisch sind. Dies schließt die Abreicherung in Nb und Ta, sowie die Zufuhr von Elementen ein, die mobil in Subduktionszonen sind (z. B. Th).

Obwohl das Kartiergebiet im Zuge der andinen Orogenese starken Kompressions-Extensions- und Transtensionskräften ausgesetzt war, sind die Versatzbeträge an den zahlreichen Störungen insgesamt gering.

Ein Epithermalsystem im und unterhalb des Stratovulkans verursachte eine starke und großräumige (2x3 km) hydrothermale Alteration der vulkanischen Gesteine, die „sericitic“/„propylitic“/„argillic“/„advanced argillic“ alteriert und silifiziert sind.

Von besonderer Bedeutung am C° Millo ist die Überlagerung von hypogener „acid-sulfate“ Alteration durch einen oberflächennahen „steam-heated overprint“, der auf „boiling“ und Kondensation von H<sub>2</sub>S in der vadosen Zone zurückgeht. Dabei wird Quarz remobilisiert, der im Bereich des ehemaligen Grundwasserspiegels ausfällt und als silifizierter Horizont (oft als Chalzedon) aufgeschlossen ist. Mehrere dieser Quarzdecken deuten am C° Millo auf eine

lange Aktivität des Hydrothermalsystems verbunden mit synhydrothermalen Erosion des Vulkangebäudes.

Die Ferrikret-Bildung in der südlichsten Qda. und eine Patina von Limonit auf allen stark alterierten pyroklastischen Gesteinen zeigen an, dass am C° Mollo supergene „acid-sulfate“ Alteration durch die Verwitterung von Pyrit ausgelöst wurde.

Die Elementverteilungsmuster der alterierten Gesteine zeigen vom Alterationstypus abhängige Elementbewegungen, die von „propylitic“ bis zu „advanced argillic“ alterierten und silifizierten Gesteinen zunehmen und Verarmung an Hauptelementen und Spurenelementen anzeigen, bei Zufuhr von Arsen, Quecksilber, Antimon, Barium und Wismut. In einer Probe tritt Gold mit 81 mg/t auf.

## Abstract

The C° Millo study area is located 35 km SW of Puno and belongs to the easternmost Western Cordillera of southern Peru.

The oldest rocks in the study area belong to the Cenozoic Maure Group and form dark, mainly flat-lying andesitic to latitic lavas. These rocks are overlain by the Barroso Group, which is built of a lower unit of latitic pyroclastic rocks and of an upper unit of andesitic to trachytic porphyritic lavas. Both units have a cupola-like orientation, and field observation suggests a stratovolcano environment.

Uppermost thick andesitic to latitic, partly blocky lavas group into four volcanic events, as defined by tectonics, petrography and geochemistry.

The element pattern of the least-altered rocks shows the typical differentiation and contamination features of subduction-related volcanic rocks in a thick continental crustal setting. This includes retention of Nb and Ta, as well as addition of subduction-mobile elements (Th).

Although the study area shows plenty of faults and fissures due to compressional/extensional and transtensional regimes during the Andean orogeny, dip separation is low.

An epithermal system in and below the stratovolcano caused pervasive and spacious (3 x 2 km) hydrothermal overprint of the volcanic rocks. The volcanic rocks are sericitic/propylitic/argillic/advanced-argillic and silicic altered.

Of special interest is at C° Millo the overprint of hypogene acid-sulfate alteration by steam-heating, itself based on boiling and condensation of H<sub>2</sub>S in the vadose zone. Thereby quartz is remobilized and fixed in now silicified horizons (mainly chalcedony) at the paleo-water table. Multiple blanket levels imply at C° Millo a long activity of the hydrothermal system accompanied by synhydrothermal erosion.

Ferricrete in the southernmost Qda. and a patina of iron oxyhydroxides on all strongly altered pyroclastic rocks indicate at C° Millo also supergene acid-sulfate alteration by weathering of pyrite.

The element pattern of the altered rocks reflects mobilization trends, which increase from propylitic to advanced argillic and silicified rocks and include depletion/dilution in most major elements, minor elements and trace elements.

Arsenic, zircon, antimony, barium, mercury, bismuth and gold (in only one sample with 81 g/t) are hydrothermally enriched.

# Table of Contents

<u>Acknowledgements .....</u>	<u>III</u>
<u>Zusammenfassung .....</u>	<u>IV</u>
<u>Abstract .....</u>	<u>VI</u>
<u>Enclosures .....</u>	<u>X</u>
<u>Geological Mapping .....</u>	<u>1</u>
1. Introduction .....	1
1.1 Location and infrastructure of the study area.....	1
1.2 Field work and map base.....	2
1.3 Climate .....	3
1.4 Vegetation .....	3
1.5 Topography .....	3
1.6 Hydrogeography.....	4
1.7 Regional geology.....	5
1.7.1 Geotectonic framework and plate tectonic setting.....	5
1.7.2 Morphostructural units and crustal structure of the Central Andes .....	6
1.8 Mining and exploration .....	10
2. Petrography and lithostratigraphy .....	13
2.1 Maure Group .....	13
2.1.1 Huancarane event .....	13
2.1.1.1 Porphyro-aphanitic lava: Latite.....	13
2.1.1.2 Porphyritic lava: Andesite.....	14
2.2 Barroso Group .....	14
2.2.1 Millo event .....	14
2.2.1.1 Pyroclastic rock: Latite.....	14
2.2.1.2 Ignimbrite (unwelded pumice flow deposit): Latite.....	15
2.2.1.3 Ignimbrite (partly welded pumice flow deposit): Latite .....	15
2.2.1.4 Fine- to medium-grained crystal-bearing ashtuff: Latite .....	16
2.2.1.5 Subvolcanic pyroclastic rock: Latite .....	17
2.2.1.6 Porphyritic lava, undifferentiated: Andesite-trachyte .....	18
2.2.1.7 Coarse-grained block-lava: Andesite .....	19
2.2.1.8 Porphyritic lava .....	20
2.2.2 Qda. Sallaoqueña event .....	21
2.2.2.1 Porphyritic lava: Dacite.....	21
2.2.2.2 Medium- to very-coarse-grained block-lava: Dacite .....	21
2.2.3 Colpacachi event I and II .....	22
2.2.3.1 Coarse- to very-coarse-grained block-lava: Dacite.....	22
2.2.3.2 Porphyritic lava .....	22
2.2.3.3 Aphanitic lava: Andesite-dacite .....	22
2.2.3.4 Porphyritic lava .....	23
2.2.3.5 Very coarse-grained block-lava .....	23
2.2.3.6 Porphyritic lava: Andesite-latite.....	23
2.2.3.7 Medium-to very-coarse-grained block-lava: Latite.....	24
2.2.3.8 Porphyritic lava: Latite.....	25
2.2.4 Chichupunt event.....	26
2.2.4.1 Porphyritic lava: Latite.....	26
2.2.5 Dikes and domes .....	26

2.2.5.1	Amphibole-biotite-bearing porphyritic dike: Latite .....	26
2.2.5.2	Dikes and chimneys undiff.: Andesite-latite .....	27
2.2.5.3	Lava domes: Andesite-latite .....	27
2.3	Quaternary .....	28
2.3.1	Debris flow/lahar: Latite .....	28
2.3.2	Colluvium.....	29
2.3.3	Colluvial fan.....	29
3.	Tectonics .....	30
3.1	General stratification .....	30
3.2	Fault tectonics .....	33
3.2.1	General overview from remote sensing .....	33
3.2.2	Mapping area.....	34
3.3	Interpretation of tectonic features related to the Andean stress field.....	35
4.	Geological evolution .....	37
<u>Diploma Thesis .....</u>		<u>41</u>
5.	Hydrothermal Alteration .....	41
5.1.	Alteration halos/facies of the “high-sulfidation”-type .....	41
5.1.1	Propylitic alteration .....	41
5.1.2	Sericitic alteration .....	41
5.1.3	Argillic alteration .....	42
5.1.4	Advanced argillic alteration .....	43
5.1.5	Silicification .....	45
5.1.6	Veins and horizons of chalcedony .....	45
5.1.7	Vuggy silica.....	46
5.1.8	Solfatara alteration .....	46
5.2	Spatial overview of the alteration halos/facies.....	47
6.	Mineralization .....	48
6.1	Supergene mineralization/superficial duricrust formation.....	48
6.1.1	Ferricrete .....	48
6.2	Hypogene Mineralization.....	49
7.	Geochemistry .....	51
7.1	Sampling.....	51
7.2	Sample preparation and analysis .....	51
7.3	Data screening .....	52
7.4	Data evaluation.....	54
7.5	Petrology .....	54
7.5.1	Classification of least-altered rocks .....	54
7.5.2	Major element distribution of least-altered rocks .....	61
7.5.3	Trace elements and rare earth element pattern of least-altered rocks .....	64
7.5.5	Rock classification of the altered rocks.....	73
7.5.6	Geochemistry of the hydrothermal alteration.....	75
7.6	Frequency distribution of As, Sb, Ba and Hg .....	91
7.7	Spatial distribution of As, Sb, Ba, Hg and Au .....	93
7.8	Physical-chemical background of the hydrothermal system.....	96
8.	The hydrothermal system .....	102
9.	Conclusion.....	107
<u>References: .....</u>		<u>108</u>

<u>Appendix .....</u>	<u>113</u>
<u>Abbreviations .....</u>	<u>113</u>
<u>Glossary of terms .....</u>	<u>113</u>
<u>Photographs .....</u>	<u>116</u>
<u>Tables .....</u>	<u>128</u>

## **Enclosures**

Enclosure 1:	Geological map of C° Millo, SE Peru (1:10.000)
Enclosure 2:	Geological sections of C° Millo, SE Peru (1:10.000)
Enclosure 3:	Hydrothermal alteration and mineralization, C° Millo, SE Peru (1:10.000)
Enclosure 4:	Sections through the hydrothermal system of C° Millo, SE Peru (1:10.000)
Enclosure 5:	Lithological and structural interpretation from remote sensing, C° Millo, SE Peru
Enclosure 6:	Sample and outcrop location map, C° Millo, SE Peru (1:10.000)
Enclosure 7:	CD: C° Millo data (ASTER & LANDSAT satellite images, ASTER digital elevation model, 3d images of C° Millo area, structural arc map interpretation, real-color picture, geochemical maps, corel maps & sections etc.)

# Geological Mapping

## 1. Introduction

### 1.1 Location and infrastructure of the study area

The rectangular mapping area (UTM Coordinates  $367-370$ ,  $8225-8228$ ) covers 12 km<sup>2</sup> and belongs geomorphologically to the easternmost part of the Cordillera Occidental.

The location is in the Department Puno, 35 km southwestward from the western lobe of Lake Titicaca (Fig. 1). The two nearest villages of greater importance are San Antonio de Esquilache, about 10 km SSW, and Pichacani, about 15 km SE.

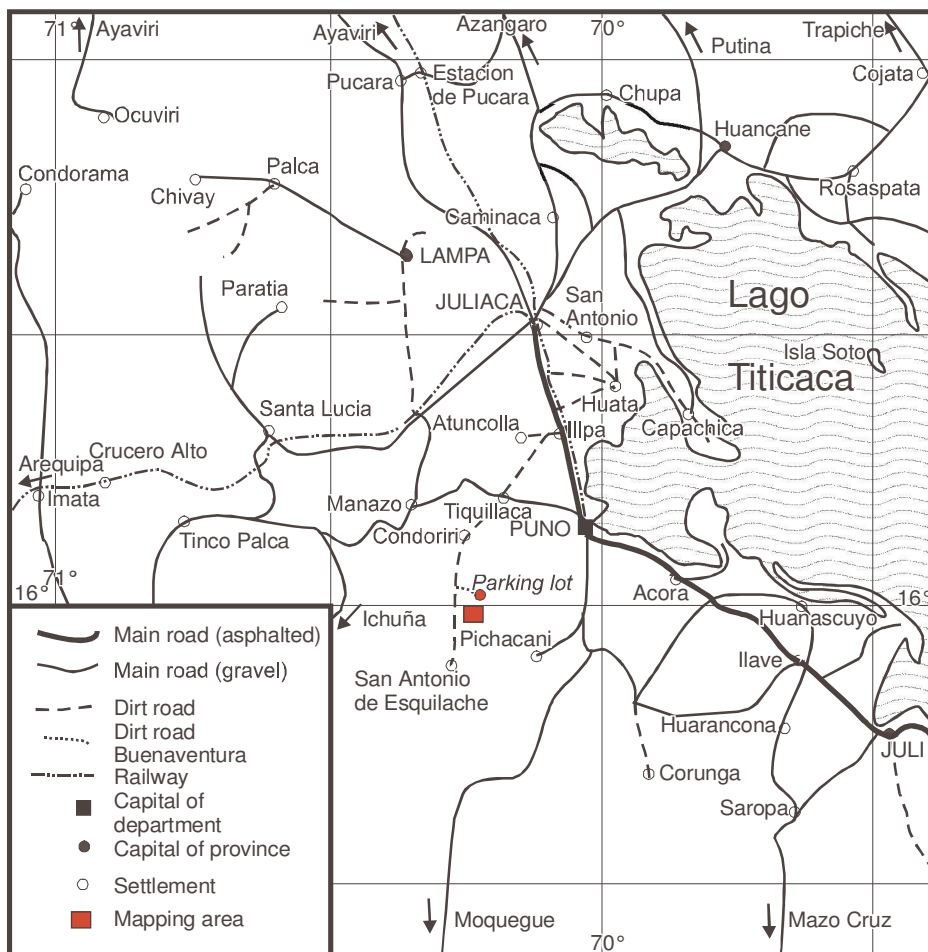


Fig. 1: Location of the mapping area and infrastructure in the Departamento Puno/South Peru.

The mapping area is uninhabited but in the periphery are some indio settlements which assure their base of life by breeding llamas, alpacas and sheeps. These houses are only reachable on

foot. Two main indio trails traverse the mapping area, one leads up the Qda. Millo and the other one follows Qda. Sallaoqueña (Enclosure 6).

The mapping area can be reached by jeep from Juliaca, driving on the main road S to Puno, and, turning SW on a dirt road after 20 km at Illpa. The villages Sillastadi (28 km), Tiquillaca (56 km) and Condoriri (68 km) are passed. Leaving the dirt road at km 86 on a Buenaventura prepared dirt track to SE leads after 95 km distance from Juliaca to a “parking lot” from which the camp is reached after a walk of half an hour (Fig. 1).

## **1.2 Field work and map base**

The field work took place from mid-August to mid-September with weekend shopping breaks at Juliaca (Fig. 1). Minas Buenaventura SAA provided a jeep with driver/cook and sampler. The camp consisted of three tents, two for sleeping and one for cooking and working.

The outcrop conditions in the field are moderate. Some outcrops alternate - especially in morphologically flatter parts - with vast areas of recent to subrecent sandy sediment cover and rock debris. The situation is complicated by a patina of iron oxides and iron oxyhydroxides which coats nearly all altered rocks.

The map base was an “orthophoto”, a georeferenced air photograph, at a scale of 1:10.000. Location in the field was by topographic features and GPS.

An ASTER (Advanced Spaceborne Thermal Emission and Reflection Radiometer) satellite image of the Terra satellite, launched in December 1999 as part of NASA’s Earth Observing System (EOS) provides a regional overview. The scene has been bought on the ASTER homepage of the USGS and includes a DEM (Digital Elevation Model) (<http://edcimswww.cr.usgs.gov/pub/imswelcome/>).

The image (hdf file) and the DEM were georeferenced by the ERDAS imagine 8.6 software. On this base a real-color picture was generated. The DEM and the ASTER scene have been combined with the ENVI 4.0 software to generate a spatial model of the mapping area (Enclosure 7: CD, 3d images). A satellite image at a scale of 1:25.000 was developed with the ERDAS Map Composer, which itself has been edited with the ESRI software ArcView GIS 3.2 and ArcMap (Enclosure 5: Structural interpretation from remote sensing).

### 1.3 Climate

The Peruvian climate is very variable and reaches from tropical in the lowland to arctic in the High Andes.

The Western Cordillera ranges in altitude range from 3300 to 5000 m asl. Median annual temperatures range from 8°C at 3300 m to 0°C at the snow-line (TROLL et al. 1980). The cold and dry season is from May till August.

From September begins the rainy season, which lasts till March. In that period thunderstorms with flurrys of snow, hailstorms and rainflurrys are frequent. The measured temperatures in the field were from 5 to 12°C during the day and descending down to -16°C at night.

According to TROLL et al. (1980) the mapping area is part of the dry Puna (to the south of 15°S) with annual precipitations of less than 400 mm. Most rain (70-80%) falls between September and March (PALACIOS et al. 1993).

The Andes show a typical high-mountain climate, subdivided into Tierra caliente, Tierra templada, Tierra fria, Tierra helada and Tierra nevada. Accordingly, the mapping area with an altitude range from about 4650 asl. to 4980 m asl. belongs to the Tierra helada (froststage, 4500-5000 m asl.) which is defined by sporadic vegetation and perennial frost (TROLL et al. 1980).

### 1.4 Vegetation

Caused by the cold, dry and windy conditions in the dry puna the “puna vegetation” is scanty. Plants are in general small xerophytes living near the ground. To defy the dryness they have special adaptations to avoid desiccation.

The ground is locally covered - especially in the flat valleys – with stable, prickly bunch-grasses (“paja brava”) of *Festuca orthophylla* and *Stipa obtusa* forming tussocks. Thola shrubs (*Parastrephia lepidophylla*) are found at some sheltered areas.

In wetlands the typical bog flora of *Isoetes* spp. and *sphagnum* is present.

At higher levels the grass loses its dominance and cushion and rosette herbs of *Azorella* are the predominant life forms (WEBERBAUER 1945).

### 1.5 Topography

In the center of the study area is the NNE-SSW striking C° Millo (highest point in the mapping area with 4980 m asl) which leads in the south to C° Zorrichata by modifying the direction to ENE-WSW and slowly sloping downwards. This topographic high is rimmed by

the Qda. Millo in the NW, the smaller Qda. Quelluire in the S and the Qda. Sallaoqueña in the E and SE (see enclosures).

In the northwestern corner of the area lies C° Supa. The eastern boundary is formed in the northern part of C° Sallaoqueña and in the south of C° Chunco. Two small lakes, Lag. Calacruz in Qda. Millo and Lag. Quelluire at the beginning of Qda. Quelluire and two bogs in the northern Qda. Sallaoqueña and at the westside of C° Chunco provide a certain diversity. C° Zorrichata, the southern part of C° Sallaoqueña and the upper part of the western C° Chunco fall nearly vertical. The other slopes show more or less moderate gradients.

Some outcrops on the C° Millo are of turtle-back form and indicate glaciation. Glacial valleys of wide extent and rounded U-form are overprinted by V-shaped valleys along the recent drainage pattern.

### 1.6 Hydrogeography

The study area is part of a continental divide (Fig. 2). The brooks at the westside of C° Millo generally drain to the Pacific, whereas the drainage pattern on the eastside is oriented towards the Lago Titicaca (Altiplano).

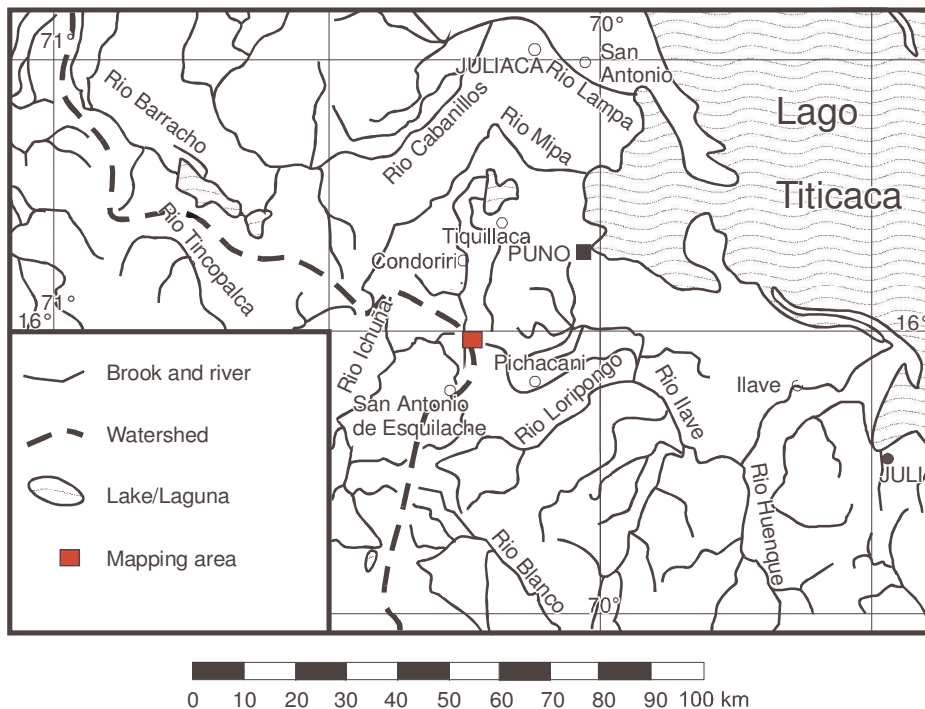


Fig. 2: Main drainage elements in the Departamento Puno/South Peru.

## 1.7 Regional geology

### 1.7.1 Geotectonic framework and plate tectonic setting

The Andes are the classical example of a volcanoplutonic orogen, at a destructive plate boundary, where oceanic lithosphere (Nazca Plate) is subducted under the South-American Plate (Fig. 3). Subduction is active since at least 200 Ma, however, the uplift of the Andes took place during the last 30 Ma only.

South America migrates roughly westwards at a present day rate of 3 cm/a. Between 2°S and 23°S, the Nazca Oceanic Plate migrates to E/ESE at a velocity of ~6 cm/a. The resulting convergence rate between the two plates is about 9 cm/a (SIMKIN et al. 1994).

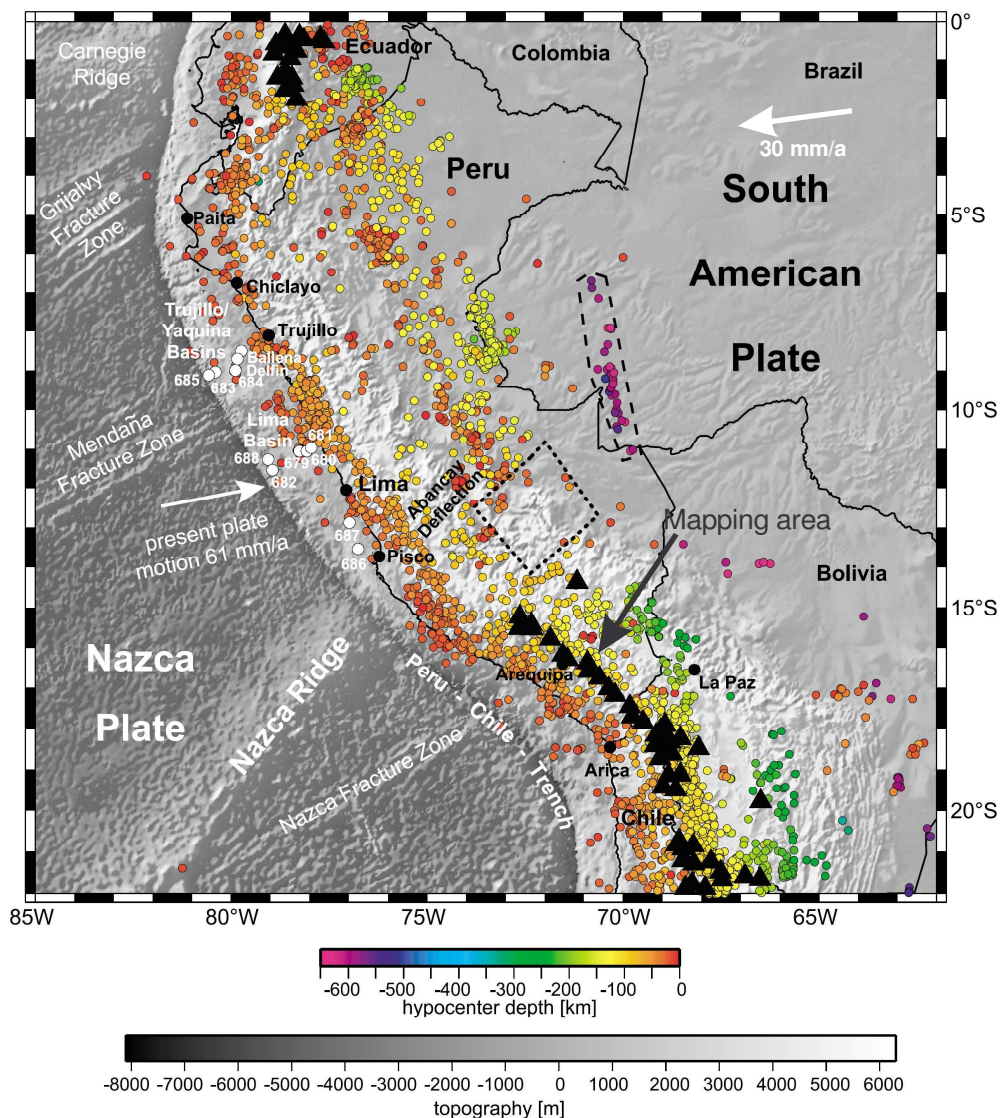


Fig. 3: Map of South America showing the geotectonic framework of the Andes, earthquakes with hypocenters, the volcanic zones (NVZ, CVZ) and the mapping area situated near the recent Central Volcanic Zone of the Central Andes. Note the gap in the intermediate depth seismicity (70-300 km) (dotted line) and the presence of deep seismic events (500-650 km) beneath Brazil (dashed line) (adapted from HAMPEL 2004).

The mapping area is located close to the recent Central Volcanic zone. The northward continuation of this zone has no volcanism which only reappears 1500 km N in the Northern Volcanic zone of Ecuador and Colombia. The volcanic inactivity is probably due to flat slab subduction (Fig. 3).

Flat slab subduction is given when the subducted oceanic plate changes direction from an angle of 30° towards a flat trajectory (at 100 km depth) and follows the base of the continental lithosphere (JAMES & SACKS 1999). Flat subduction is thought to result from anomalously thick oceanic lithosphere (ridges, plateaus, seamounts) which leads to elevated buoyancy of the subducting plate.

### **1.7.2 Morphostructural units and crustal structure of the Central Andes**

Southern Peru is divided into six morphostructural units; the Coastal Ranges, the Western Cordillera/Cordillera Occidental, the Altiplano, the Eastern Cordillera/Cordillera Oriental, the Subandean Zone and the Foreland. In the Coastal Ranges relief is low (<300 m), and sediments are accumulated in wide alluvial plains.

The Western Cordillera is built of deformed Paleozoic metamorphic rocks and Mesozoic sedimentary rocks, such as limestones, conglomerates, arenites, greywackes, pelites and volcanic rocks. They are intruded to the W by Mesozoic plutons (Mesozoic arc) and unconformably covered to the E by abundant volcanic rocks (Tertiary arc), which are mainly made of Cenozoic volcanic rocks of intermediate to acid composition forming stratovolcanoes, lava flows, domes and ignimbrite plateaus (Fig. 4).

The Eastern Cordillera is chiefly made of Paleozoic to Tertiary intrusions and volcanic rocks (inner arc of Southern Peru; KONTAK et al. 1984). The basement consists of Proterozoic phyllites and micaschists overlain by up to 15.000 m thick Paleozoic psammites and pelites. The Cordillera is bordered to the W and SW by a nearly continuous E-verging thrust and fold belt involving mainly Mesozoic sedimentary rocks (Fig. 5).

Longitudinal valleys separate S of 13°S the Eastern and Western Cordillera evolving southwards into an endorheic basin (Altiplano) which is a tectonic graben, refilled in its center with up to 14.000 m of Cretaceous and Tertiary sediments (Fig. 5).

The deformed Subandean Zone is mainly built up of faulted and folded Mesozoic to Tertiary sedimentary rocks and of Paleozoic sedimentary and metamorphic basement, which are thrust to the NE or E onto the eastern Forelands.

The eastern Forelands are made of either wide alluvial plains receiving Quaternary sediments (northern Peru), or slightly uplifted, fault-controlled zones underlain by the crystalline basement of the Brazilian Shield (southern Peru, Bolivia).

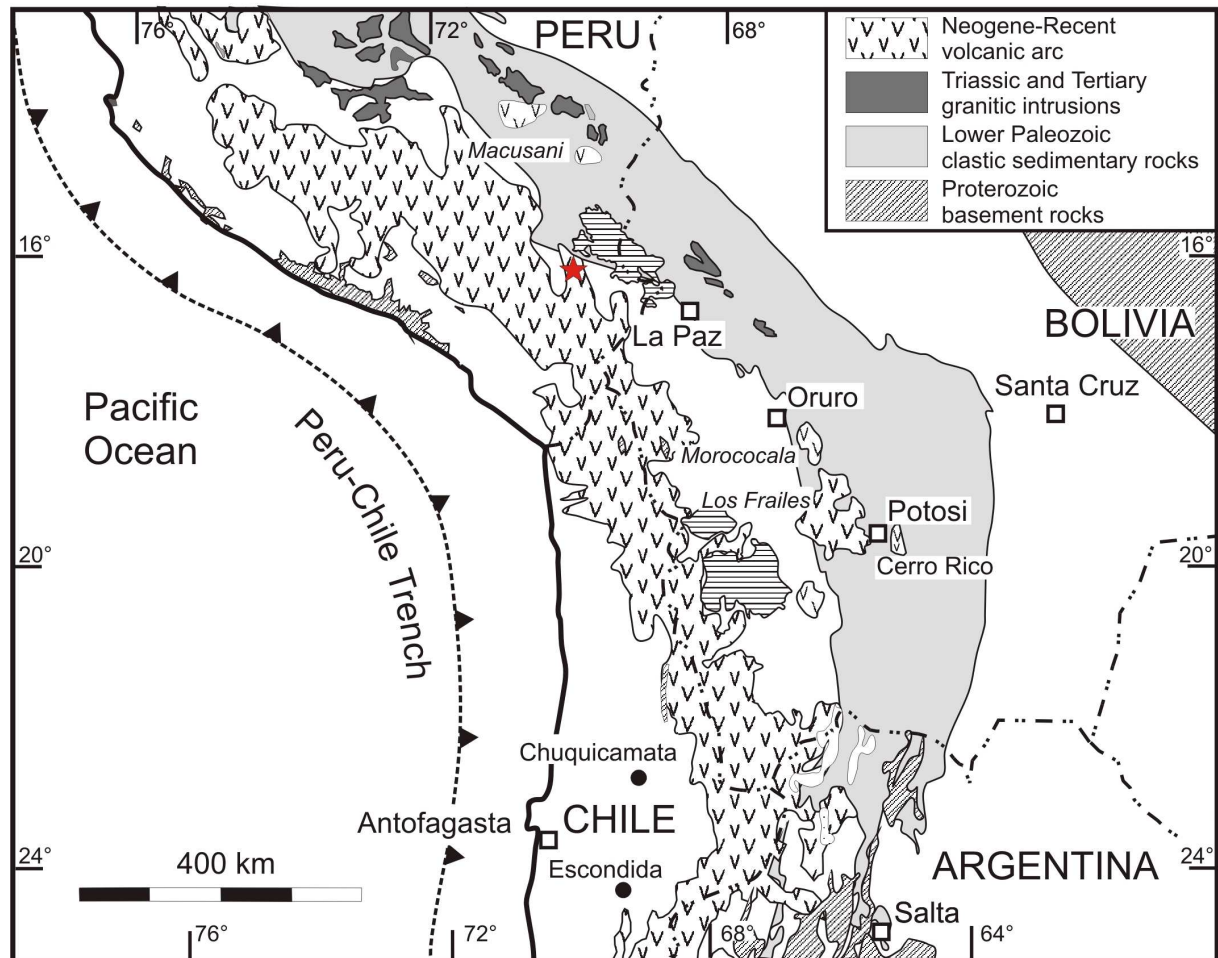


Fig. 4: Map showing geological and morphostructural units of the Central Andes. The location of the mapping area is marked by a star (adapted from DIETRICH 1999).

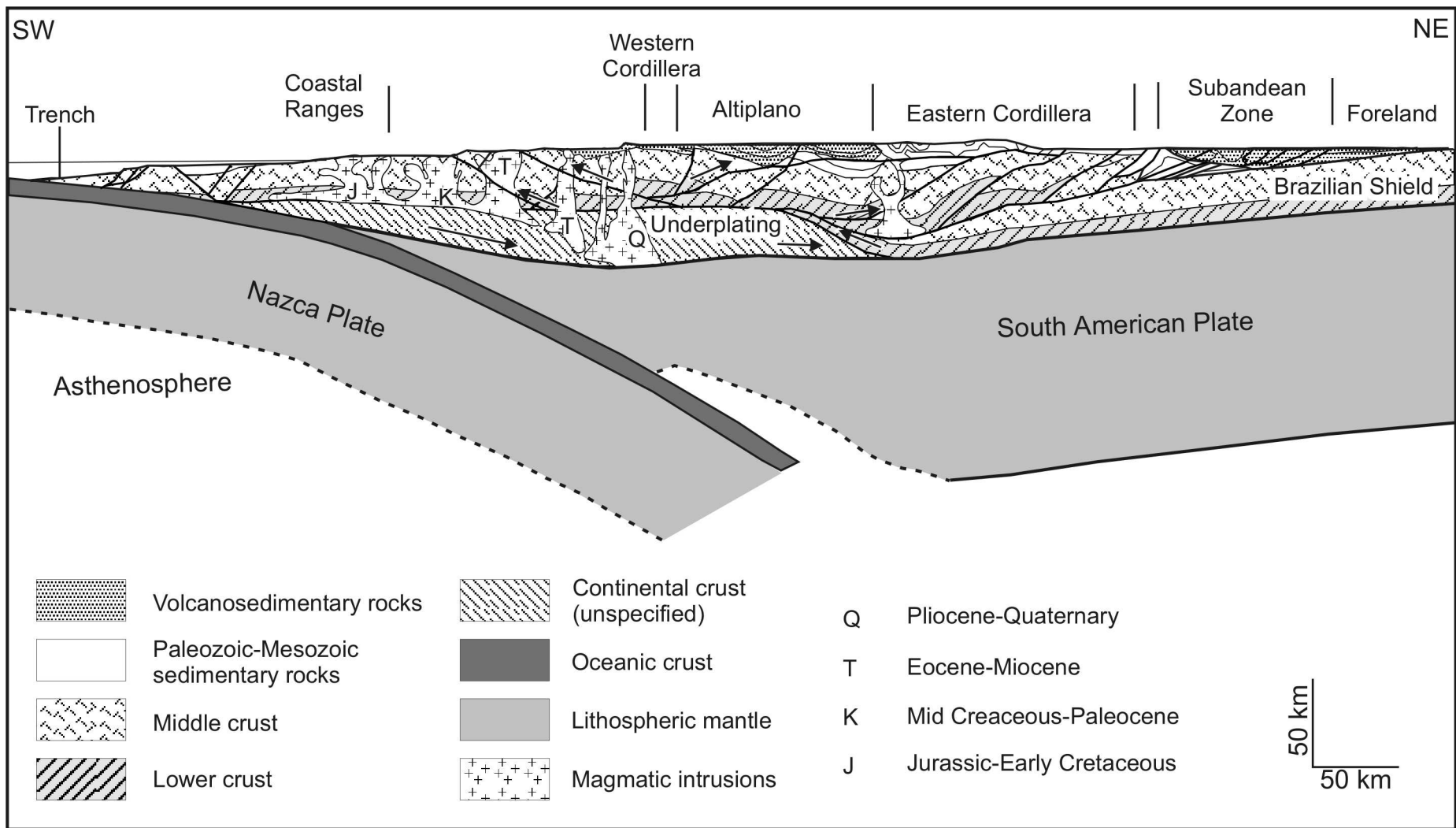


Fig. 5: Simplified geological section through the Central Andes south of Lake Titicaca (adapted from JAILLARD et al. 2000).

### 1.7.3 Rocks of the mapping area: The Maure and Barroso Group

The rocks of the study area are part of the Sillapaca Volcanic Sequence (JENKS 1946) which is divided by the Quechua II unconformity (8 Ma) into the Miocene Sillapaca Group and the Upper Miocene to Present Barroso Group (BENAVIDES-CÁCERES 1999).

Age data on the Sillapaca Group lie in between 16.9 to 8.0 Ma (MCKEE and NOBLE 1989). The Sillapaca Group largely consists of dacite, trachyte, andesite and trachyandesite. The rocks fall within the high K series of PECCERILLO and TAYLOR (1976) and within the alkaline series of KUNO (1966). The uppermost Sillapaca Group includes the stratigraphically equivalent Maure Group.

The Maure Group has a maximum thickness of 1.500 m and consists of lavas, ignimbrites, reworked tuffs and soft tuffs which are characteristically light and porous. They include lapilli, crystal and lithic fragments.

The volcanic rocks are interstratified with lacustrine sedimentary rocks, siltstones, and micritic limestones.

The Barroso Group consists largely of andesite lavas and pyroclastic deposits which are arranged in simple or composite stratovolcanoes. In many of the centers, an explosive pyroclastic phase was followed by lava-dominated effusions, often accompanied by volcanic domes (BENAVIDES-CÁCERES 1999). The pyroclastic phases of Strombolian or Pelean type delivered tuffs, ignimbrites and volcanic breccias.

The lavas consist of biotite-augite dacite, trachyandesite, plagioclase-phyric andesite and aphyric basaltic andesite. In the eastern regions, the Barroso volcanic rocks are of shoshonitic (ARAMAKI et al. 1984) or of K-rich trachyandesitic chemism. Age data exist from two sites near Puno and from one site near Juli, ranging from 5.6 to 6.7 Ma (Fig. 6).

Both groups are underlain by the Oligocene to Miocene Tacaza Group and the Eocene to Miocene Puno Group. The Tacaza Group is mainly built of volcanics, the Puno Group of conglomerates and arenites.

## 1.8 Mining and exploration

The mapping area is situated in a traditional Ag-polymetallic vein district. The deposits consist mainly of small veins related to a regional NW-SE striking fault system (Fig. 6). For characteristics see Table 1.

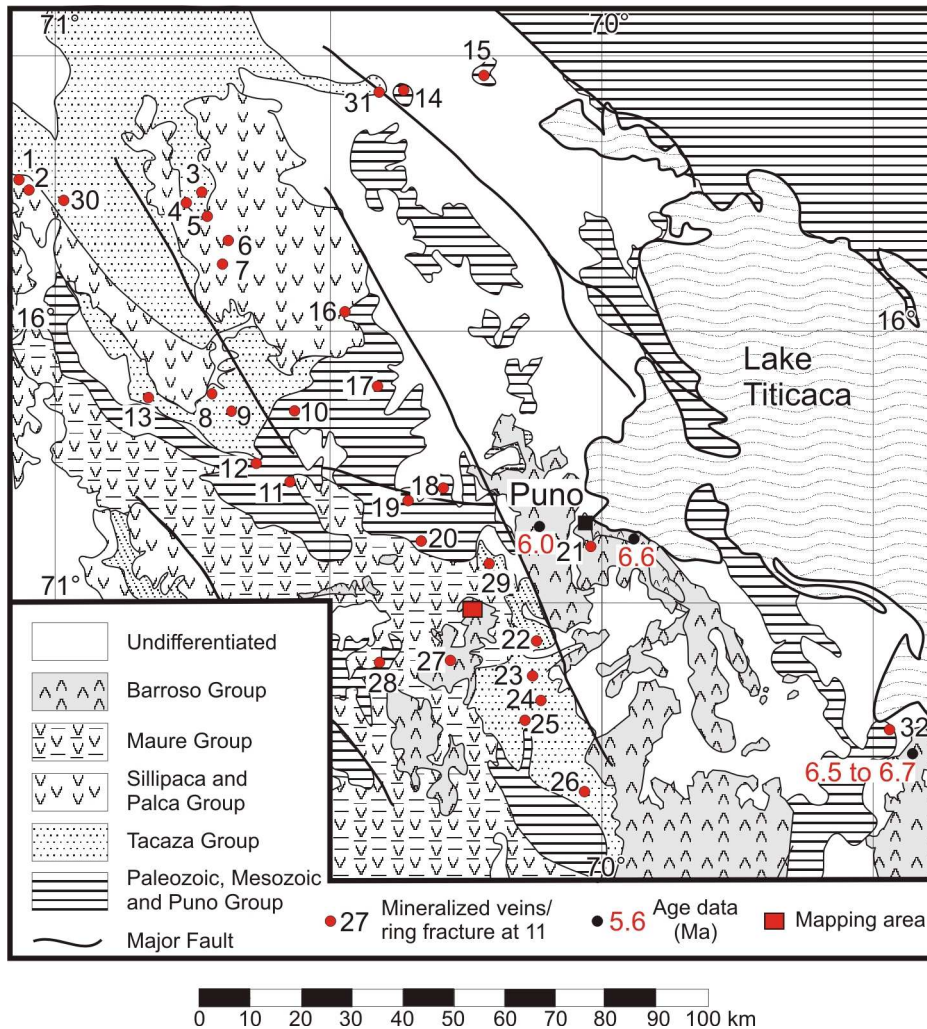


Fig. 6: Map showing simplified geology, the main fault system, the location of working and abandoned mines, and the mapping area in the Departamento Puno/South Peru (adapted from PALACIOS et al. 1993).

Table 1: Metal content, structure and mineralogy of mines marked in Fig. 6 (adapted from PALACIOS et al. 1993).

Mine	State	Metals	Host	Mineralogy
1 Condorama	Closed	12.8 oz/t Ag, 2 % Pb 2 % Zn	Vein	Silver minerals, galena, sphalerite, chalcopyrite
2 Antonido Raimondii	Active	10 oz/t Ag	Vein	Chalcopyrite, galena
3 Palca	Active	7 % Pb, 2 % Zn 1 % Cu, 3 oz/t Ag	Vein	Chrysocolla malachite, azurite, silver minerals, chalcopyrite
4 Raquel	Closed	Ag?	Vein	Galena, sphalerite, chalcopyrite, pyrite, covellite, malachite, marcasite, anglesite, manganese oxides
5 Quilca	Closed	Ag?	Vein	Pyrite, galena, sphalerite, chalcopyrite
6 Pomasi	Active	3 oz/t Ag, 5 % Pb Au?	Vein	Chalcopyrite, native silver, chalcocite, tetrahedrite, argentite, galena, sphalerite
7 Cofre	Active	2 oz/t Ag, 4 g/t Au 2 % Zn, 5 % Pb	Vein	Galena, chalcopyrite, sphalerite
8 Tacaza	Closed	Cu?	Vein	Chalcocite, chrysocolla, bornite, malachite, native copper, galena, azurite, digenite
9 Santa Barbara	Active	12 oz/t Ag, 1 % Pb 0.5 % Cu	Vein	Tetrahedrite, galena, sphalerite, chalcopyrite, chalcocite
10 Berenguela	Closed	1.26 % Cu, 4.28 oz/t Ag, Mn?	Vein	Psilomelane, pyrolusite, iron oxyhydroxides, silver in Mn covellite, malachite, azurite, pyrite, chalcopyrite, native silver, chrysocolla
11 Ccellocello	Active	8-12 oz/t Ag, 5 % Pb 2 % Zn	Vein	Galena, pyrite, sphalerite
12 Copacabana	Active	8-20 oz/t Ag, 2 % Pb 1 % Zn	Vein	Tetrahedrite, galena, sphalerite, chalcopyrite
13 Ichocollo	Closed	Ag?, Cu?	Vein	Chalcopyrite, galena
14 El Carmen	Closed	Ag?, Sb?	Vein	Galena, stibnite, pyromorphite
15 Ccera	Closed	Ag?, Sb?	Vein	Stibnite, marcasite
16 Choychani	Closed	4 oz/t Ag, 25 % Pb	Vein	Galena, silver minerals, chalcocite, pyrite
17 Porvenir	Closed	2 % WO <sub>3</sub> , 1 % MoS <sub>2</sub>	Vein	Wolframite, molybdenite, pyrite
18 Las Rosales	Active	1.5 oz/t Ag, 12 g/t Au 1% Cu	Vein	Chalcopyrite, pyrite with gold, bornite, native gold
19 Aladino	Closed	Cu?, Pb?, Zn?	Vein	Pyrite, chalcopyrite, galena bornite, sphalerite
20 Paltapata	Active	5 oz/t Ag, 8 g/t Au, 1.6 % Cu	Vein	Chalcocite, native copper, malachite, pyrite
21 Laykakota	Closed	Ag?, Au?, Pb?, Cu?	Vein	Galena, argentite, sphalerite, chalcopyrite, native gold, tetrahedrite, arsenopyrite, pyrite
22 Anchanchune	Closed	Ag?, Pb?	Vein	Galena, pyrite, cerussite,
23 Pichacani	Closed	Ag?, Pb?	Vein	Galena, chalcopyrite, malachite,
24 Guadalupe	Closed	Ag?, Pb?, Cu?	Vein	Galena, malachite, oropiment?
25 Jayojayune	Active	1,5 oz/t Ag, 6% Pb, 8% Zn	Vein	Galena, sphalerite, chalcopyrite, chrysocolla, pyrite
26 Rosario	Closed	Ag?, Pb?	Vein	Galena, chalcopyrite, malachite
27 San Antonio de Esquilache	Closed	3 oz/t Ag, 3 % Pb, 4 % Zn	Vein	Galena, sphalerite, chalcopyrite, pyrite, malachite, stibnite, tetrahedrite, proustite, argentite
28 Jesus Maria	Closed	Ag?, Cu?	Vein	Chrysocolla, malachite, galena, tetrahedrite, chalcopyrite, native silver

Fig. 7 shows latest data of high-sulfidation gold deposits and gold claims in South Peru. The C° Millo prospect is located within the Southern Peru Trend of high sulfidation epithermal gold deposits such as Mazo Cruz, Aruntani, Santa Rosa (belonging to Aruntani) and Rescatada. The prospect is located 50 km NW of Aruntani and 120 km SE of Rescatada. Several claims surround the study area.



Fig. 7: High-sulfidation epithermal gold deposits/prospects in southern Peru ([www.geologix.da/s/puno.asp](http://www.geologix.da/s/puno.asp)).

The study area has been explored by Minas Buanaventura SAA for epithermal gold. Samples were taken and C° Millo was traversed by two sample channels (trenches/trincheras) of 30 cm width (Enclosure 6: sample and outcrop location map). One crosses C° Millo Norte (230 m) the other crosses C° Millo Sur (570 m). Samples were taken from every running meter. In areas covered with gravel and sand, trenches of up to two meters depths were dug to reach the bed rock.

The surficial survey was complemented by drilling at the top of C° Millo Sur and C° Millo Norte ( 200 m depth) (Enclosure 6).

## **2. Petrography and lithostratigraphy**

Field work defined at least six volcanic events, which are separated by unconformities.

The first event (Huancarane event) correlates with the Maure Group and is named after the village of Huancarane, southwestward of the mapping area. The second event is already part of the Barroso Group, called here the Millo event, with its postulated volcanic center at C° Millo. The third phase, the Qda. Sallaoqueña event, has its center in the northern Qda. Sallaoqueña. The Colpacachi events are named after the settlement Colpacachi, northeastward of the study area. The lavas of the two phases have the same flow direction but are separated by an unconformity at C° Chunco (Enclosure 2: Geological sections). The sixth volcanic event (Chichupunt) delivered lava from SE by probably nowadays still preserved volcanic edifices (Enclosure 5: Lithological and structural interpretation from remote sensing).

The dikes and domes cannot be arranged in detail to the volcanic events, due to the low number of samples and their strong petrographic and geochemical affinity (chapt. 3).

They are attached below the Barroso lavas. For possible stratigraphic correlation see geologic evolution (chapt. 4).

The following descriptions of individual stratigraphic units give in the chapter headings: first the rock pheno-type according to texture (field term), followed by rock type according to chemical data.

### **2.1 Maure Group**

#### **2.1.1 Huancarane event**

The first volcanic event is characterized by effusive volcanism which delivered two differently textured lavas from SW to W.

##### **2.1.1.1 Porphyro-aphanitic lava: Latite**

This unit is about 150 m thick, and is represented by sample 77962.

Outcrop situation: The rock unit occupies 400 m<sup>2</sup> in the southwestern corner of the study area. It is morphologically inconspicuous.

Hand specimen: The layering planes of the rock (1-5 cm), partly plane and partly convolute, are enhanced by brownish weathering. Medium-grained, euhedral, trachytoid-textured phenocrysts of plagioclase are set in a bluish-grey groundmass with fine-grained disseminated ore minerals.

Microscopic observation: Phenocrysts form about 15 vol% of the rock and consist of two plagioclase generations. A bigger, tabular type with sizes up to 1.2 mm is zoned and partly aggregated to glomerocrysts. Some minerals are completely altered with only the crystal outline preserved (ghost-texture). The smaller lath-like type varies between 0.1 and 0.5 mm. The very fine-grained, grey groundmass consists of a trachytic mineral assemblage with plagioclase, quartz and subhedral opaques. Lath-like apatite crystals up to 1 mm occur in nests.

### **2.1.1.2 Porphyritic lava: Andesite**

This unit is about 320 m thick, and is represented by samples 77280, 77964, 77965 and 77970.

Outcrop situation: The lava flow lies roughly flat in the southern Qda. Millo and occupies 1.5 km<sup>2</sup>.

Hand specimen: The trachytoid porphyritic rock consists of a dark-grey to black groundmass which encloses white to reddish, tabular plagioclase crystals (1 to 6 mm) and some smaller biotite and amphibole crystals.

Microscopic observation: The phenocrysts form 10-15 vol% of the rock. Albitic twinned plagioclase (70 vol%) shows sieve-texture in its center. Biotite (13 vol%) is up to 2 mm large, and amphibole (12 vol%) is up to 1.5 mm in diameter. Both minerals are partly brownish oxydized and rimmed by black edging up to total opacitization. Some bay-like quartz crystals (5 vol%) have corroded shape. The pilotaxitic groundmass consists of plagioclase microlites, hematite and magnetite (0.02-0.13 mm). Limonite gel occurs in the groundmass and on plagioclase. Finely allotted apatite laths up to 0.5 mm occur in and attached to plagioclase.

## **2.2 Barroso Group**

### **2.2.1 Millo event**

The Millo event starts with thick pyroclastic rocks, overlain by a suite of porphyritic lava.

#### **2.2.1.1 Pyroclastic rock: Latite**

This unit is about 270 m thick, and is represented by samples 77269-77271, 77295, 77963 and 77964.

Outcrop situation: The strongly altered (argillic, advanced-argillic) strata in the middle of the mapping area dip with low angles away from C° Millo Norte and C° Millo Sur. The unit is morphologically inconspicuous, except for silicified ridges located at faults and fissures.

Hand specimen: Most of the rock is altered beyond recognition. The color varies (white, grey, red, brown) due to the differing alteration minerals and varying content of iron oxides and iron oxyhydroxides. At 77271, 77295 and 77964 the rock shows vuggy silica texture.

Microscopic observation: The phenocryst assemblage is given by plagioclase (70 vol%), biotite (15-20 vol%), amphibole (5-10 vol%) and quartz (5 vol%).

Plagioclase ghosts are sometimes broken and reach sizes of 3 mm. Dark biotite and amphibole ghosts indicate pre-alteration opacitization. Quartz is partly euhedral and partly of bay-like habit. Some roundish lava fragments, mainly composed of plagioclase laths occur at 77270. The groundmass is totally altered to a fine-grained mineral assemblage of quartz and clay minerals. Accessory: zircon.

### **2.2.1.2 Ignimbrite (unwelded pumice flow deposit): Latite**

Each flow/cooling unit is about 5-10 m thick. The rock type is represented by samples 77281 and 77282.

Outcrop situation: The strata are located at the eastern slope of C° Millo and at C° Millo Norte. Weathering leads to coatings of iron oxides and iron oxyhydroxides.

Hand specimen: The rock is pervasively altered (silicification and argillic to advanced-argillic alteration), and consists of light-colored lithic fragments up to 4 cm in size set in a grey groundmass. Primary mineral constituents cannot be determined.

Microscopic observation: The rock fragments are set in a groundmass with about 10 vol% of phenocrysts. Most of the phenocryst phase is strongly altered and broken plagioclase (70 vol%). Euhedral biotite (0.2-2 mm, 20 vol%) and amphibole (0.2-0.8 mm, 8 vol%) are characterized by dark opacitization rims. Quartz (2 vol%) shows corrosion features. The lithic rock fragments are strongly silicified and seem to be altered pumice. The groundmass is altered to a mineral assemblage of quartz, alunite, clay minerals and iron oxyhydroxides. Rock texture is chaotic. Accessory: zircon.

### **2.2.1.3 Ignimbrite (partly welded pumice flow deposit): Latite**

Each flow/cooling unit is about 8-15 m thick. The rock type is represented by samples 77955, 77963 and 77971.

Outcrop situation: The rock dips with low angles away from C° Millo and forms distinctive crests with a notch of 0.1-2 m height at the base of each flow/cooling unit (Fig. 8; Appendix, Photo 7).

The widespread areas underlain by pyroclastic rocks are covered by sandy sediments, the rocks are intensively altered and coated by a patina of iron oxides and iron oxyhydroxides.

Hand specimen: One rock variant consists of a grey-colored groundmass with grey lava fragments and some white pumice (lower part of 77971 and 77955). The other rock type is grey-colored with white pumice fragments from 0.2 to 15 mm which, at 77971, are fiamme-like developed (Fig. 8). The pumice itself is sometimes reddish oxydized.

Microscopic observation: Due to intensive alteration, primary magmatic minerals are absent, except for corroded quartz. The estimated modal composition (according to ghost textures) is about 65 vol% plagioclase, 15 vol% biotite, 15 vol% hornblende and 5 vol% quartz.



Fig. 8: Partly welded, argillic-altered ignimbrite at Trinchera IV (channel sampling by Buenaventura SAA) (Own sample number: 77971). Right from the hammer is fiamme-like developed pumice. Below on the right is a notch, where the rock unit is unwelded, and erodes easier.

#### **2.2.1.4 Fine- to medium-grained crystal-bearing ashtuff: Latite**

This unit is about 10 m thick, and is represented by sample 77972.

Outcrop situation: The ashtuff builds a small, slightly W dipping remnant of 70x100 m located on C° Millo Sur. Characteristics of the unit are its porous and rough surface, the light grey colour, the high weatherability and its break down in fine-sandy particles.

Hand specimen: The strongly altered rock has 5 vol% phenocrysts set in a grey matrix (Fig. 9).

Microscopic observation: The rock is heavily altered to clay minerals, and displays contours of broken plagioclase and dark rimmed amphibole.



Fig. 9: Crystal bearing ashtuff at 77972. The fine-grained rock has a porous and rough surface.

#### **2.2.1.5 Subvolcanic pyroclastic rock: Latite**

This unit is about 20 m thick, and is represented by samples 77273, 77283 and 77956.

Outcrop situation: At C° Millo Norte the rock unit forms an oval depression of 200x400 m covered by sandy detritals (Appendix, Photo 5). At the central and southern part of the mountain the rock occurs as a dike (30-100 m wide) without morphological expression. It is characterized by vertical bedding and its brecciated texture.

Hand specimen: The rock is intensively altered, its color varies from white over reddish to grey, and it is composed of light angular rock fragments from 1-6 cm in diameter with flow texture and smaller (0.5-2 cm) light green, roundish, porous pumice fragments. The rock carries additionally some bluish-grey fragments. The only preserved primary magmatic mineral is quartz (0.5-3 mm in size).

Microscopic observation: The rock has about 15 vol% phenocrysts, of which about 60 vol% is plagioclase, which is only determinable by its crystal shape. Biotite and hornblende are opacitized or totally altered to an undistinguishable fine-grained groundmass.

### **2.2.1.6 Porphyritic lava, undifferentiated: Andesite-trachyte**

This unit is about 350 m thick, and is represented by samples 77268, 77272, 77284, 77285, 77287-77289, 77292, 77958-77961, 77966, 77967 and 77969.

Outcrop situation: The porphyritic lava rims the pyroclastic rocks at C° Millo and is propylitically altered. At faults and fissures alteration is more intensive (silicification, argillic alteration and advanced argillic alteration).

Hand specimen: The porphyritic rock consists of white to greenish plagioclase, occasionally with red oxidation rims, clear sanidine and some quartz set in a grey to black groundmass. The three felsic minerals show seriate grain-size distribution, from 0.5 to 5 mm in diameter. Mafic minerals are biotite and hornblende from 0.5 to 2 mm in diameter. The two minerals show different degree of opacitization. Flow texture is perfectly preserved and is enhanced by weathering along partings from 1 to 5 cm in thickness (Fig. 10).

Microscopic observation: The phenocrysts form 15-20 vol% of the rock, of which plagioclase is 65-80 vol%, biotite 10-20 vol%, hornblende 4-10 vol%, quartz 0-3 vol%, clinopyroxene 0-2 vol% and sanidine 0-2 vol%.

Plagioclase phenocrysts from 0.5-7 mm in diameter are partly euhedral, partly broken and corroded. The mineral is complexly twinned (Carlsbad, pericline and albite twins) with normal and oscillatory zoning. In some sections a first generation of small and corroded phenocrysts is enclosed by a second larger one. Due to slight alteration, the anorthite-rich core of some crystals shows sieve-texture.

Biotite has a size from 0.1 to 1 mm. The opacitization ranges from incipient black edging to total transformation into an assemblage of fine-grained spinel, clinopyroxene, magnetite and hematite. Hornblende (0.3-3 mm) undergoes the same process. Clinopyroxene is anhedral to subhedral with sizes between 0.1 to 0.5 mm. The main part of the groundmass is built of trachytic orientated plagioclase microlites, enclosing some intersertal glass, limonite gel, subhedral hematite and magnetite. Accessory minerals: zircon and apatite.

The unit is in the northern part of the mapping area (77284) and at 77958 more evolved (trachytic chemism) and has higher amounts of oxybiotite and glass.



Fig. 10: Propylitically altered porphyritic lava at 77289. Plagioclase phenocrysts are transformed to a mineral assemblage of chlorite, carbonate, muscovite and epidote, the groundmass is altered to chlorite.

#### 2.2.1.7 Coarse-grained block-lava: Andesite

This unit is about 30 m thick, and is represented by samples 77286 and 77968.

Outcrop situation: The strata are dipping flatly NW from C° Supa. Due to high weatherability, caused by the composition of lava fragments and lava matrix, the rock body is preserved in patches only. Outcrop sections at C° Supa show lava fragments up to 1.5 m in diameter. The matrix to fragment ratio is about 1:3. On weathering more resistant lava fragments morphologically stand out (Fig. 11).

Hand specimen: The rock is composed of a light greenish-grey “lava groundmass” built up of bleached plagioclase, euhedral, booklet-like biotite and euhedral amphibole in fine-grained matrix. The bluish-grey lava fragments (0.5-5 cm) are of angular to subangular shape and contain plagioclase with glassy lustre and euhedral biotite.

Microscopic observation: The phenocryst assemblage of the andesite consists of 70 vol% plagioclase, 15 vol% biotite, 10 vol% amphibole, 3 vol% sanidine and 2 vol% quartz.

Plagioclase in the fragments is euhedral and shows complex twinning features (albite and Carlsbad twins). Grain size distribution is seriate (0.5 to 2 mm). Plagioclase in the “matrix” is bigger (0.5 to 3 mm), often broken and slightly corroded. Complex twinning is rare.

Biotite in the lava fragments is mainly fresh and tabular-euhedral with sizes from 0.3 to 3 mm. Biotite in the “lava matrix” shows kinkbands, curved crystal planes and fan-like ends and displays all states of opacitization.

Euhedral amphibole occurs in the fragments and in the lava with sizes between 0.3 and 3 mm. In the lava it is often completely opacitized. Sanidine, mainly attached to the outermost part of plagioclase and indicating its zonation, is lath-like, shows Carlsbad twins and transversal fractures. Opaque minerals are magnetite and hematite. Bay-like corroded quartz is restricted to the enclosing lava and has the same grain size as plagioclase. The matrix of the lava fragments is built of trachytic plagioclase laths and biotite.



Fig. 11: Cross-section through propylitically altered, coarse-grained block-lava (andesite) at 77968. Lava fragments (partly rounded and partly angular) are set in a “groundmass” of porphyritic lava, which is more altered due to higher permeability.

#### **2.2.1.8 Porphyritic lava**

This unit is about 5 m thick and has not been sampled due to its minor stratigraphic importance.

A patch of 20x100 m outcrops on C° Supa. The dark colored rock has plagioclase, biotite and amphibole.

## 2.2.2 Qda. Sallaoqueña event

The Qda. Sallaoqueña event delivered lavas dipping with steep angles to SE.

### 2.2.2.1 Porphyritic lava: Dacite

This rock unit is about 40 m thick, and is represented by samples 77299 and 77951.

Outcrop situation: The grey-colored rock is characterized by a rough surface caused by resistant plagioclase phenocrysts, which stand out from the weathered rock surface.

Hand specimen: The seriate porphyritic, trachytoid rock consists of 25 vol% phenocrysts. Euhedral plagioclase up to 25 mm in diameter, biotite and amphibole (0.3-1 mm) are set in a grey groundmass. The rock is partly altered (plagioclase to clay minerals).

Microscopic observation: The phenocryst assemblage consists of zoned plagioclase (80 vol%), Fe-rich, partly corroded biotite (15 vol%), green to brown euhedral amphibole (5 vol%) and some corroded quartz (<1 vol%).

Plagioclase shows penetration twins and knee-shaped contact twins. Poikilitic intergrowth aggregates are common (biotite in plagioclase, and plagioclase in biotite). The texture is dominated by trachytic, and pilotaxitic orientated plagioclase laths. Reddish, opaque minerals (hematite?) occur disseminated in the matrix. Microcrystalline titanite “eggs” are arranged in nests especially in/on plagioclase and euhedral, rod-shaped apatite occurs widespread. The main accessory is zircon which forms dark pleochroitic halos in biotite.

### 2.2.2.2 Medium- to very-coarse-grained block-lava: Dacite

This unit is about 5 m thick, and is represented by sample 77950.

Outcrop situation: The block-lava is restricted, due to erosion, to three small deposits at northern C° Sallaoqueña and is characterized by up to 70-cm-large, rounded lava fragments, set in a “lava matrix”. The rock is weathered.

Hand specimen: It shows porphyritic lava fragments (3-4 cm) in a “lava matrix”.

Microscopic observation: The rock has about 15 vol% phenocrysts. Plagioclase 80 vol%, iron-biotite 8 vol%, amphibole 10 vol% and corroded quartz 2 vol%. The groundmass consists of plagioclase laths. Apatite, zircon and titanite “eggs” are accessories.

### **2.2.3 Colpacachi event I and II**

The volcanic rocks of the Colpacachi events are well stratified lavas, delivered from E to NE.

#### **2.2.3.1 Coarse- to very-coarse-grained block-lava: Dacite**

This unit is about 100 m thick, and is represented by sample 77952.

Outcrop situation: The rock body at southern C° Sallaoqueña is preserved in patches and undergoes weathering due to its structure of roundish lava-boulders up to 1 m in diameter set in a “lava matrix” (ratio of components to lava 1:5). In the course of weathering the “lava boulders” are selectively exposed and stand statue-like on the bedrock.

Hand specimen: The “lava boulders” and “lava matrix” are of porphyritic texture. Phenocrysts (15-20 vol%), mainly white, trachytoid plagioclase, are set in a bluish-grey groundmass.

Microscopic observation: Zoned plagioclase dominates the phenocryst assemblage (80 vol%), followed by 10 vol% Fe-rich biotite, amphibole and quartz (both 5 vol%). Quartz (5 vol%) is corroded and has bay-like habit. The groundmass, mainly built of trachytic plagioclase laths is partly propylitically altered. Accessories: titanite “eggs” in nests and apatite on plagioclase, some euhedral zircon.

#### **2.2.3.2 Porphyritic lava**

This unit is about 80 m thick.

Outcrop situation: The rock unit lies between the southern C° Sallaoqueña and the Qda. Sallaoqueña. The rock unit is fresh, except of slight propylitic alteration.

Hand specimen: The porphyritic rock consists of white plagioclase phenocrysts, occasionally with red oxidation rims, clear sanidine and some quartz set in a grey to black groundmass. The felsic minerals show seriate grain-size distribution from 0.5 to 4 mm in diameter. Biotite and hornblende (0.5-2 mm) are opacitized. Flow texture is preserved and is enhanced by weathering along partings from 1 to 5 cm in thickness.

#### **2.2.3.3 Aphanitic lava: Andesite-dacite**

This unit is about 140 m thick, and is represented by samples 77290 and 77291.

Outcrop situation: The lava forms a prominent cuesta in the southern Qda. Sallaoqueña, is partly altered (propylitic) and parts in parallel up to 1 cm thick layers.

Hand specimen: The color of the rock ranges from brownish/reddish-grey to black. Fine-grained sanidine phenocrysts show trachytoid texture.

Microscopic observation: The phenocrysts of the microcrystalline rock constitute about 5 vol%. Subhedral sanidine, with transversal fractures, sometimes in glomerocrysts, is the major phenocryst phase (65 vol%, 0.2-2 mm). Euhedral, often twinned green amphibole (20 vol%, 0.4-0.8 mm) shows dark rims and channels of oxyamphibole on cleavage planes. Microlites of magnetite, hematite and clinopyroxene indicate its opacitization. Biotite (5 vol%, <0.5 mm) occurs nearly fresh and partly with dark rims of oxybiotite. Opacitization leads to a fine-grained intergrowth of clinopyroxene-magnetite-spinel. The euhedral plagioclase (5 vol%, up to 1 mm) is zoned. Subhedral clinopyroxene (up to 0.3 mm) is rare. The matrix is built of trachytic-textured (pilotaxitic type) plagioclase (80 vol%). Opaque minerals (20 vol%) reach 0.025 mm. Some oval and elongated vesicles occur.

#### **2.2.3.4 Porphyritic lava**

This unit is about 230 m thick.

Outcrop situation: The first lavaflow at C° Chunco forms a surface of truncation on top of distinct crest of aphanitic lava. The rock is fresh.

Hand specimen: The volcanic rock consists of a grey groundmass and white to greenish plagioclase of medium to very-coarse grain size. Biotite and amphibole are relatively rare.

#### **2.2.3.5 Very coarse-grained block-lava**

This unit is about 25 m thick.

Outcrop situation: The block-lava at the east slope of C° Chunco is built of up to 2 m large lava fragments set in a porphyritic lava groundmass.

#### **2.2.3.6 Porphyritic lava: Andesite-latite**

This unit is about 40 m thick, and is represented by samples 77274 and 77276.

Outcrop situation: The lava at C° Chunco is erosionally resistant and forms the upper vertical slope.

Hand specimen: The seriate porphyritic rock is convolutedly layered and bears 1 to 5 mm large plagioclase and smaller opacitized biotite and amphibole. The groundmass is partly reddish-oxidized and shows trachytoid texture. At 77274 the rock is silicified.

Microscopic observation: About 15-20 vol% of the rock is built up of phenocrysts. Plagioclase (70 vol%, 0.5-7 mm) is complexly twinned (Carlsbad and albite twins) and the close arrangement of the albite lamellae indicates high anorthite content. The majority of plagioclase is normal-zoned. Biotite (20 vol%, 0.5-3 mm) and amphibole (10 vol%, 0.1-0.3 mm) are strongly opacitized. The groundmass is mainly formed by lath-like plagioclase

microlites (70 vol%), amphibole and biotite microlites (together 25 vol%) and opaque minerals (5 vol%). Plagioclase is mainly oriented in flow direction and shows occasionally glomerocrystic growth. The rock has autoliths with phenocrysts smaller than 0.1 mm.

Accessories: euhedral zircon, apatite-laths, titanite, partly in “eggs” and partly euhedral.

#### **2.2.3.7 Medium-to very-coarse-grained block-lava: Latite**

This unit is about 35 m thick, and is represented by sample 77278.

Outcrop situation: The block-lava at the northern C° Chunco is flat lying, propylitically altered and has lava fragments from 2 mm to 1 m. The larger particles (>1 cm) are rounded, the smaller ones angular to subangular. On weathering these components stand out.

Hand specimen: The rock is oxydized, due to elevated permeability. The fragment to matrix ratio is about 1:3 and the fragment colors vary (white, grey and red). Matrix and rock fragments carry biotite (about 1 mm in diameter) and plagioclase (Fig. 12).

Microscopic observation: The phenocrysts in the lava components constitute about 10 vol%. Plagioclase (about 70 vol%, <5 mm) is euhedral and zoned. Biotite (20 vol%, iron rich) between 0.6 and 1.2 mm in diameter, is occasionally broken and shows incipient opacitization (black edging). Euhedral amphibole (10 vol%) is between 0.12 and 0.5 mm in size.

The phanocrysts of the “matrix” are 20 vol%. Plagioclase (80 vol%) is altered to carbonate/epidote and encloses biotite crystals with sagenite structure (Ti-exsolution). Biotite phenocrysts (10 vol%) and amphibole (8 vol%) are totally opacitized. Some corroded quartz.

The matrix is built up of trachytic plagioclase microlites, limonite gel and opaque minerals.



Fig. 12: Propylitically altered block-lava (Latite) (77278).

#### 2.2.3.8 Porphyritic lava: Latite

This unit is about 35 m thick, and is represented by samples 77277 and 77279.

Outcrop situation: The lava builds the flattened top of C° Chunco. Due to vertical jointing and horizontal layering the rock forms columns (30-300 cm high) (Appendix, Photo 9). In areas where joints are not dominant, weathering follows flow unit boundaries and dissects roundish “layerheads”.

Hand specimen: Irregular fractures pervade the rock, which has a grey groundmass and reddish-oxidized areas parallel to flow layering. Phenocrysts are 20 vol% of the rock. Polysynthetically twinned plagioclase has seriate grain size distribution from 0.5 to 10 mm in diameter. Biotite and amphibole form together 20 vol%. Amphibole is aligned with flow direction.

Microscopic observation: Plagioclase (75 vol%) is mainly zoned, twinned and shows corrosion bays. Euhedral biotite (15 vol%, 0.35-2 mm) and euhedral amphibole (7 vol%, 0.25-2 mm) are of brownish color (iron-rich) and display intensive pleochroism. Some of the crystals are opacitized. Vesicles are rimmed with limonite. Subhedral to allotriomorphic quartz phenocrysts (2 vol%) are bay- or tube-like corroded, broken and holey. Subhedral clinopyroxene (augite, 1 vol%) reaches sizes up to 1.5 mm.

The matrix of the holocrystalline rock is built of pilotaxitic, microcrystalline plagioclase laths and crystallites (maybe plagioclase). Hematite and magnetite occur in microlites. Euhedral zircon up to phenocryst size and apatite prisms/columns occur.

## **2.2.4 Chichupunt event**

The lava of the Chichupunt event was delivered from S to SE.

### **2.2.4.1 Porphyritic lava: Latite**

This unit is about 20 m thick and is represented by sample 77275.

Outcrop situation: The dark colored lava outcrops at the southern border of the mapping area and is characterized by a rugged surface with sharp edges and many fractures.

Hand specimen: The porphyritic lava has a bimodal plagioclase phenocryst distribution. One plagioclase population has seriate diameters from 0.5 to 3 mm; the other population has coarse-grained phenocrysts from 1 to 3 cm in diameter. The white plagioclase phenocrysts are flow-aligned within a bluish-grey groundmass.

Microscopic observation: The phenocrysts are about 25 vol% of the rock, of which plagioclase is about 80 vol%, biotite 10 vol%, amphibole 5 vol% and clinopyroxene 5 vol%. Zoned plagioclase is often broken along twin-lamellae. Iron-rich biotite and amphibole are altered (chloritization). Amphibole shows opacitization to dark rimmed phantoms. Euhedral to subhedral clinopyroxene is altered to serpentine minerals.

The matrix is built up of small plagioclase laths and other slightly yellow colored crystallites. Plagioclase is orientated along flow direction. Opaque minerals, hematite and magnetite, are regularly distributed. Euhedral zircon columns form phenocrysts (around 1 mm large). Euhedral, rod-shaped apatite is associated with plagioclase.

## **2.2.5 Dikes and domes**

### **2.2.5.1 Amphibole-biotite-bearing porphyritic dike: Latite**

This unit is about 30 m thick and is represented by sample 77954.

Outcrop situation: The dike at the eastern flank of C° Millo Norte could be mapped and determined by the distinct vertical layering and the vertical alignment of phenocrysts.

Hand specimen: The rock is of seriate porphyritic texture. White, trachytoid plagioclase ranging from 1 to 6 mm in diameter, and mafic minerals (about 40 vol% of the phenocrysts), mainly biotite and secondarily amphibole (0.3-2 mm) are set in a greenish-grey groundmass. Some autoliths and xenoliths with diameters up to 2 cm occur in the rock.

Microscopic observation: The phenocrysts are about 25 vol%, of which tabular, euhedral and zoned plagioclase (65 vol%), biotite (20 vol%, partly oxydized), euhedral amphibole (8 vol%) and anhedral sanidine (7 vol%) with fractures are the major components.

The altered matrix is mainly built of trachytic-textured plagioclase microlites. Biotite is sometimes enclosed by large plagioclase phenocrysts and biotite is also poikilitically enclosing plagioclase laths of sizes from 0.03-0.3 mm. Opaque minerals are rare. Vesicles (<1 mm, 1-2 vol% of the matrix) partly subrounded and partly elongated, occur. Accessory minerals are columnar zircon (in biotite) and lath-like apatite with transversal fractures. The latter occurs on plagioclase, biotite and in the groundmass.

#### **2.2.5.2 Dikes and chimneys undiff.: Andesite-latite**

The dikes vary in thickness (20-400 m), and are represented by samples 77296 and 77297.

Outcrop situation: The dikes are located on the mountain ridge of C° Millo, on the westslope of C° Millo Norte, and in Qda. Sallaoqueña.

The dikes and chimneys have inconspicuous topographic expression and are distinguished by relatively fresh lava material within altered host rocks, and by vertical to subvertical layering.

Hand specimen: The rock has a grey groundmass, is seriate-porphyrific with flow aligned plagioclase (0.5-10 mm) and some highly altered pyroclastic rock fragments. At the surface the groundmass is bleached and the phenocrysts are opacitized. The rock is cut by fractures.

Microscopic observation: The hypocrySTALLINE rock consists of 25 vol% porphyrocrysts; mainly plagioclase (80 vol%, two generations), biotite (10 vol%), amphibole (7 vol%) and sanidine (3 vol%). Subhedral plagioclase is zoned and sometimes twinned. Anhedral biotite and amphibole have diameters between 0.2 and 1.5 mm. Euhedral sanidine shows fractures.

The groundmass of plagioclase laths and glass is trachytically textured and in some cases cut by quartz veinlets. Ore minerals (hematite and magnetite) are finely dispersed.

Small lath-shaped, euhedral apatite and zircon microlites are finely distributed in the rock.

#### **2.2.5.3 Lava domes: Andesite-latite**

The lava domes are 50 and 80 m thick, and are represented by sample 77953.

Outcrop situation: Two domes occur in the study area. One (150 m x 80 m x 20 m) is in the northern Qda. Sallaoqueña and the other (120 m x 50 m x 25 m) is situated in the northwestern part of the study area. They are characterized by vertical to subvertical layering (Fig. 13).

Hand specimen: The phanocrystalline, seriate-porphyrific rock is characterized by a blue-grey groundmass with reddish, oxidized flow-layer boundaries, caused by alteration. The

white and trachytoid-orientated plagioclase phenocrysts range in size from 0.2 to 30 mm. Mafic minerals are biotite and amphibole, up to 3 mm large.

Microscopic observation: The rock is built of 40 vol% phenocrysts. Plagioclase is 85 vol%, biotite 7 vol%, sanidine 3 vol%, amphibole 3 vol%, clinopyroxene 1 vol% and quartz 1 vol%. Plagioclase occurs in two variants: (1) Euhedral phenocrysts with 1-3 mm in diameter (2/3 of all plg), (2) glomerocrysts or anorthositic rock fragments with diameters up to 7.5 mm, (1/3 of all plg). A minor part of plagioclase shows resorption and intergrowth features. The groundmass is composed of plagioclase laths and crystallites (plagioclase?). The texture is mainly trachytic. Microcrystalline opaque minerals (hematite and magnetite) are widespread in the rock. Anhedral, microcrystalline apatite and some euhedral zircon are disseminated.

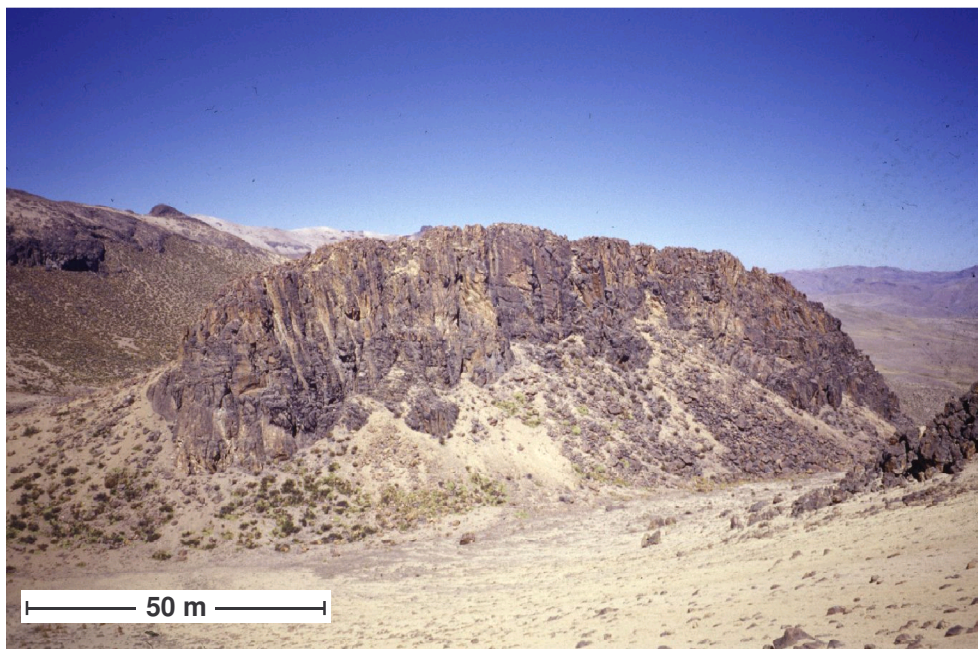


Fig. 13: Dome in the northwestern part of the mapping area, characterized by vertical to subvertical layering. Strongly altered C° Millo in the background.

## 2.3 Quaternary

### 2.3.1 Debris flow/lahar: Latite

This rock unit is about 2 m thick, and is represented by sample 77293.

Outcrop situation: The rock body is flat lying and contains abundant angular fragments (<1.5 m) set in a yellow to brown groundmass, indicating strong oxidation.

Hand specimen: At hand specimen scale (Fig. 14) rock fragments from 0.1 to 1.5 cm in diameter dominate. The clasts are mainly angular to subangular. Some are roundish. The colors vary (white, reddish, grey), indicating different lithologies or alteration processes.

Microscopic observation: The rock is supported by a dark fine-grained groundmass. The fragments, mainly altered (propylitized, argillic and advanced-argillic alteration) lava fragments and some pyroclastic rock material show plagioclase, biotite and amphibole phenocrysts. Biotite is occasionally broken and opacitized like amphibole. Secondary pore space, apparently generated in the groundmass, is filled by cryptocrystalline, brownish-red limonite forming concentric to shelled aggregates, and by kaolinite.



Fig. 14: Lahar deposit at 77293. The rock has abundant variably altered, angular rock fragments, set in a groundmass of iron oxyhydroxides (ferricrete formation).

### 2.3.2 Colluvium

Colluvium occurs in the southwestern part of the area, with up to 7 m thickness. The rock debris consists of angular to subangular lava fragments and some pyroclastic rock fragments coated by iron oxides and iron oxyhydroxides. Grain size varies between 1 cm and 50 cm.

### 2.3.3 Colluvial fan

A colluvial fan covers the southern slope of C° Millo Sur. It has a maximum extent of 300x150 m with up to 5 m thickness and is built of angular to subangular blocks of pyroclastic rocks coated with a patina of oxides. Grain size varies between 10 cm and 1 m.

### **3. Tectonics**

#### **3.1 General stratification**

Lavas of the Huancarane event (Maure Group) are delivered from W to SW (Enclosure 2 and Fig. 18a). The porphyro-aphanitic lava dips with a mean angle of about 40°NE. It is overlain by porphyritic lava dipping 10 to 25°NE, which indicates levelling of the given paleorelief.

Pyroclastic rocks and lavas of the Millo event (Barroso Group) are unconformably, cupola-like overlying the lavas of the Maure Group (Figs. 15, 16, 17, 18). Especially the flat (10 to 35°) dipping pyroclastic rocks on the western and the eastern slope of C° Millo are distinct in the SCHMIDT stereonet. The vertical layered subvolcanic pyroclastic rocks intrudes the inclined pyroclastites. The porphyritic lava dips with angles between 0 and 70° at both sides of C° Millo, but an average trend of 25° can be assumed from field data on under- and overlying rock units. The high and low incidence angles can be explained by the variable paleorelief. The coarse-grained block-lava at C° Supa strikes out flatly (5-25°) over the porphyritic lava covered itself by the flat-lying porphyritic lava relict on C° Supa.

The Qda. Sallaoqueña event lavas at C° Sallaoqueña dip steeply 30-60°E (Fig. 18b). In the porphyritic lava the plagioclase is orientated both in flow direction (observed rarely) and perpendicular to it (observed often, Enclosure 1). This phenomenon can be explained by varying viscosities within a cooling lava flow. The cooler the lava flow the higher the viscosity and the higher the tendency of the lava to rotate along an axis perpendicular to flow direction.

Block-lavas and porphyritic, unbrecciated lavas of the Colpacachi event I are generally dipping W to SW (Fig. 18c). The coarse to very coarse-grained block-lava at southern C° Sallaoqueña dips with angles between 30 and 45°W, overlain by the porphyritic and the aphanitic lava with angles of incidence between 15 and 60°W. The hangingwall lavafloes show already a gradual decrease in dip (Enclosure 1 and 2).

The brecciated and unbrecciated lavas of the Colpacachi event II are dipping W to SW, but they are separated from the underlying rocks by an unconformity (Fig. 18c). The units show gradual decrease of dip to almost horizontal layering at the mountain summit region, accompanied by vertical parting (Appendix, Photo 9)

The biotite-amphibole bearing porphyritic lava of the Chichupunt event dips 20°NW (Fig. 18d).

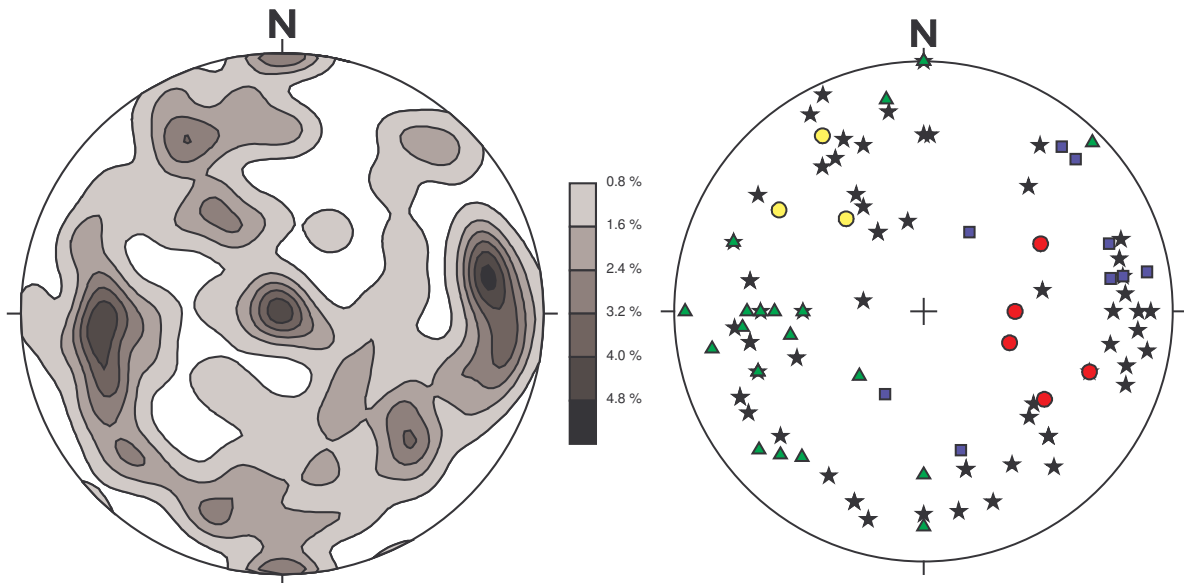


Fig. 15: Plot of all bedding data as points (n=124) in the SCHMIDT stereonet with contour lines. Points are defined by dip-direction and angle of incidence. The darker the area the more data points, lower hemisphere.

Fig. 16: Plot of differentiated bedding data without dikes in the SCHMIDT stereonet as points (n=102). Blue squares represent dip and incidence of the Maure strata, stars are strata belonging to the Millo event, red circles define the Qda. Sallaquena event, green triangles the Colpacachi events and yellow circles the Chichupunt event, lower hemisphere.

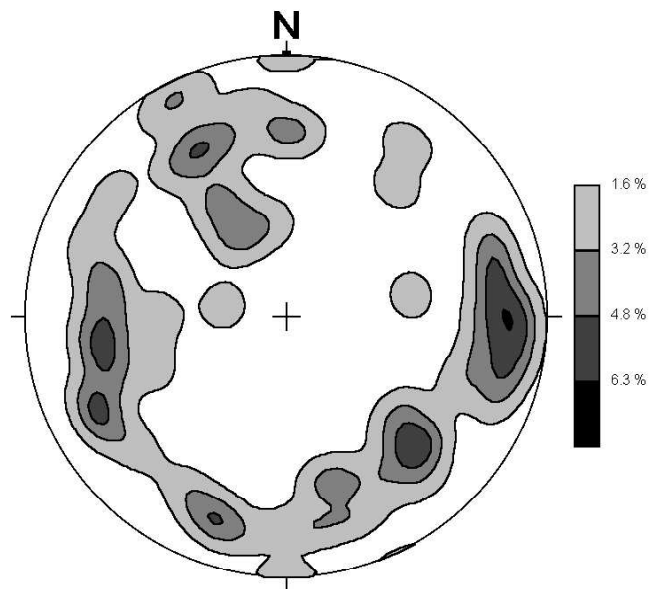
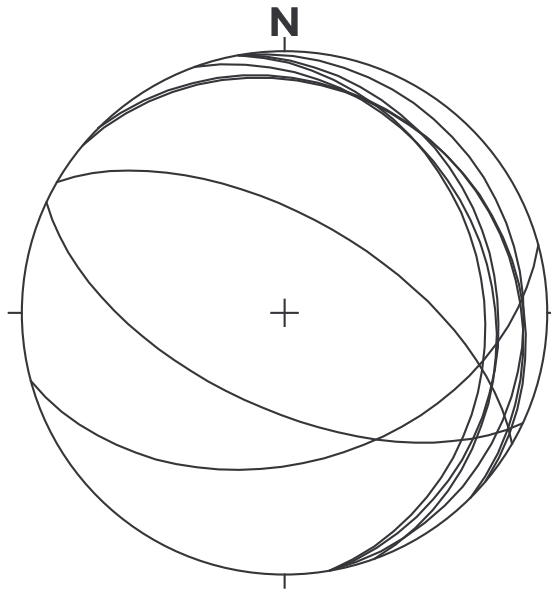
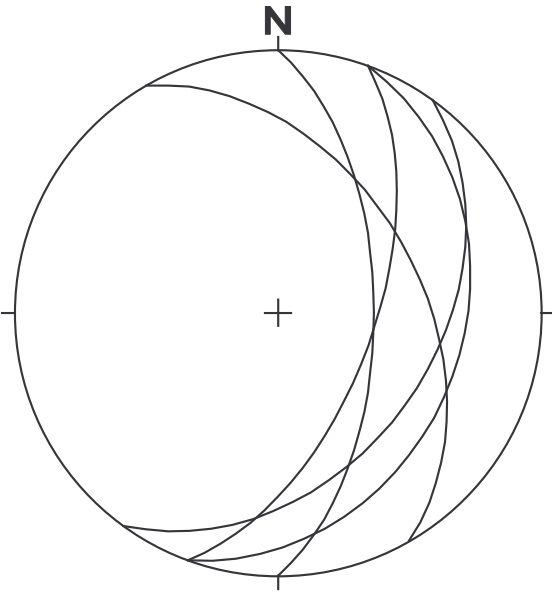


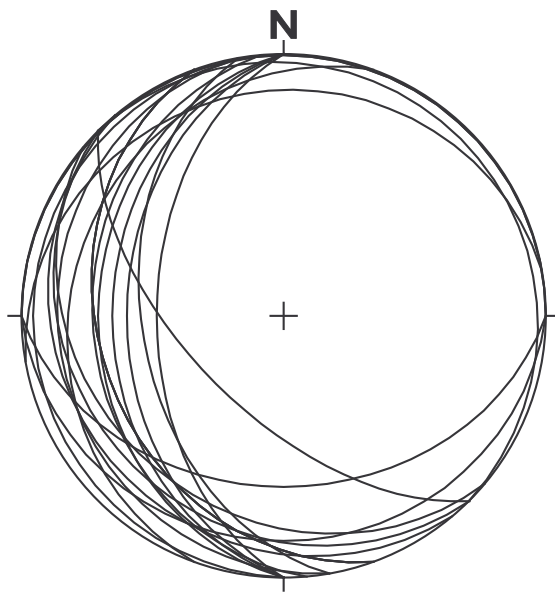
Fig. 17: Plot of the Millo event strata as points with contour lines, (Barroso Group, n=63), lower hemisphere.



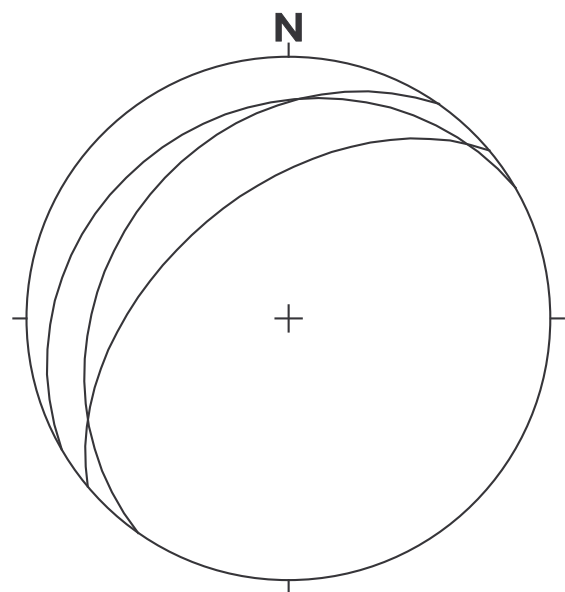
a. Huancarane event strata (Maure Group,  $n=9$ ), lower hemisphere.



b. Qda. Sallaoqueña event strata (Barroso Group,  $n=5$ ), lower hemisphere.



c. Colpacachi event strata (Barroso Group,  $n=22$ ), lower hemisphere.



d. Chichupunt event strata (Barroso Group,  $n=3$ ), lower hemisphere.

Fig. 18: Plot of all field data according to the different volcanic events.

Dikes, chimneys and domes: Dikes and domes are located at main and branch faults (synthetic faults and Riedel shears) at Qda. Millo, at C° Millo and at Qda. Sallaoqueña.

The narrow dikes at the west slope of C° Millo Norte form the prolongation of the outfanning Qda. Millo fault and dip 50° SE. Curved dikes indicate curved faults, changing direction from NNE-SSW in the southern part to W-E in the northern part. The chimney in southern Qda. Millo is located near the Qda. Millo main fault.

The dikes and chimneys at the top of C° Millo are associated with N-S, SW-NE and NW-SE striking faults. The chimneys and the dome at Qda. Sallaoqueña are controlled by the Qda. Sallaoqueña main fault, its horsetails/pinnate fractures and by a NE-SW orientated fault system.

## **3.2 Fault tectonics**

### **3.2.1 General overview from remote sensing**

Structure: The interpretation of the 266 km<sup>2</sup> large area (Enclosure 5: Lithological and structural interpretation from remote sensing) defined four main fault directions: NE-SW, NW-SE, N-S and E-W. The NE-SW striking faults are very prominent and extend for up to 10 km, similar to the second fault direction. N-S striking faults reach up to more than 15 km length and cut all other systems. They show dextral wrenching, proved by synthetic flexing features. The fourth W-E striking system is relatively rare and characterized by lateral extent of about 1-7 km. It is intersected by the NE-SW system and is therefore referred to be the oldest. The mapping area shows the NE-SW, the N-S and the tributary W-E system (Enclosure 5).

Volcanic edifices: The ASTER scene shows a high amount of pearl necklet-like oriented volcanic edifices W, S and SE of the study area. Several explanations are possible.

(1) The mapping area is close to the ancient volcanic arc of the Cordillera Occidental (satellite image: 2-5 km). (2) Another factor may be erosional level, i. e. deeper erosion in the N of the mapping area, so that volcanic edifices are not preserved any more. (3) The roundish alignment of the volcanic edifices can be interpreted as a ring-structure or a caldera-complex with a diameter of over 20 km. There appears to be a NNE orientated corridor, marked by dome structures and fault lines, on which northeastern end lies the study area.

### 3.2.2 Mapping area

Structure: The mapping area comprises a plenitude of faults and fissures (Enclosure 1), which are mainly determined by the “orthophoto”. The lineations were recognized in the field by crests of silicified rocks, by outcropping fault surfaces and flexing of country rock. Due to strong alteration most of the faults could not be further determined. However, the lack of displaced strata and major offsets indicates that fault movement was of minor importance.

Two fault directions are predominant. One system strikes NE-SW to NNE-SSW, the other one NW-SE. The NE-SW system offered more measurable planes than the second, perpendicularly oriented system (Enclosure 1, Fig. 19).

The following normal faults were identified: a normal fault at C° Sallaqueña dips 35°SW, a normal fault at the westslope of C° Millo Sur dips 75°NW and a normal fault which crosses C° Zorrichata in NW-SE direction with a lateral extent of about 230 m and a dip of 90°. The C° Millo side is relatively upthrown, fault striation plunges with 90°. 200 m further SE tectonic striation bears NW-SE and indicates a second tectonic phase of dextral movement.

The following dextral faults were identified: a nearly N-S striking (90° dip) fault in the SW corner of the mapping area, a 85°NW dipping fault at C° Zorrichata, a fault striking W-E with a vertical fault plain at the eastern slope of C° Millo Norte and three faults striking N-S to NW-SE at the northern slope of C° Millo Norte. Their net slip direction is expressed morphologically by dislocation of silicified ridges. The fault surface could not be determined but seems to be vertical as expressed as straight line in the map.

A combined normal and sinistral fault is located at the SE slope of C° Millo Sur. The fault plain dips 70°SE. The fault striation plunges NE with 10 and 75°NE.

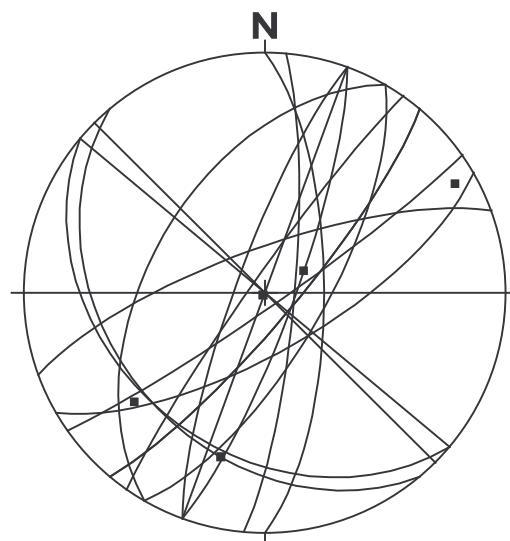


Fig. 19: Stereonet of faults (n=18) and fault striations (n=6) in the mapping area, lower hemisphere.

Attrition breccias and polished fault surfaces with tectonic striae occur at outcrops 249 and 250. Synthetic Riedel shears with angles of 10-20° to the main fault plane are often developed as crescentic grooves indicating the sense of fault movement. Further weakening of the fault area partly led to plucking of phacoids.

### **3.3 Interpretation of tectonic features related to the Andean stress field**

From Late Oligocene onwards the Andean margin was controlled by the W to WSW motion of South America and the E to ENE motion of the Nazca Plate (Figs. 3 and 20).

Even though recent subduction is of high-stress character the Western Cordillera and the western part of the Altiplano are situated in a N-S orientated extensional regime. Compressive stresses are located in the Subandean Belt (Figs. 5 and 20).

The generally steep to vertical dipping normal and strike-slip faults indicate upper crustal deformation with relatively small shear-stress rates. It can be assumed that the majority of faults were generated or reactivated earlier when compressional deformation affected the Western Cordillera (Tertiary Quechua phases).

The system of NW-SE and NE-SW trending faults can be explained by the Mohr circle, which generally shows that highest shear stresses affect planes orientated 45° to  $\sigma_1$  (W-E). The N trending faults can be well explained by the perpendicular orientated compression, which has been reactivated in recent times by the N-S extensional regime (Fig. 20). The W-E trending faults have been probably generated in the Tethyan phase or Atlantic phase when a predominantly W-E orientated wrenching regime was active (JAILLARD et al. 2000). These faults were reactivated to buffer internal stresses due to not exactly opposite orientated convergence of the two plates and they were counterdrawn to the Cenozoic volcanic rocks.

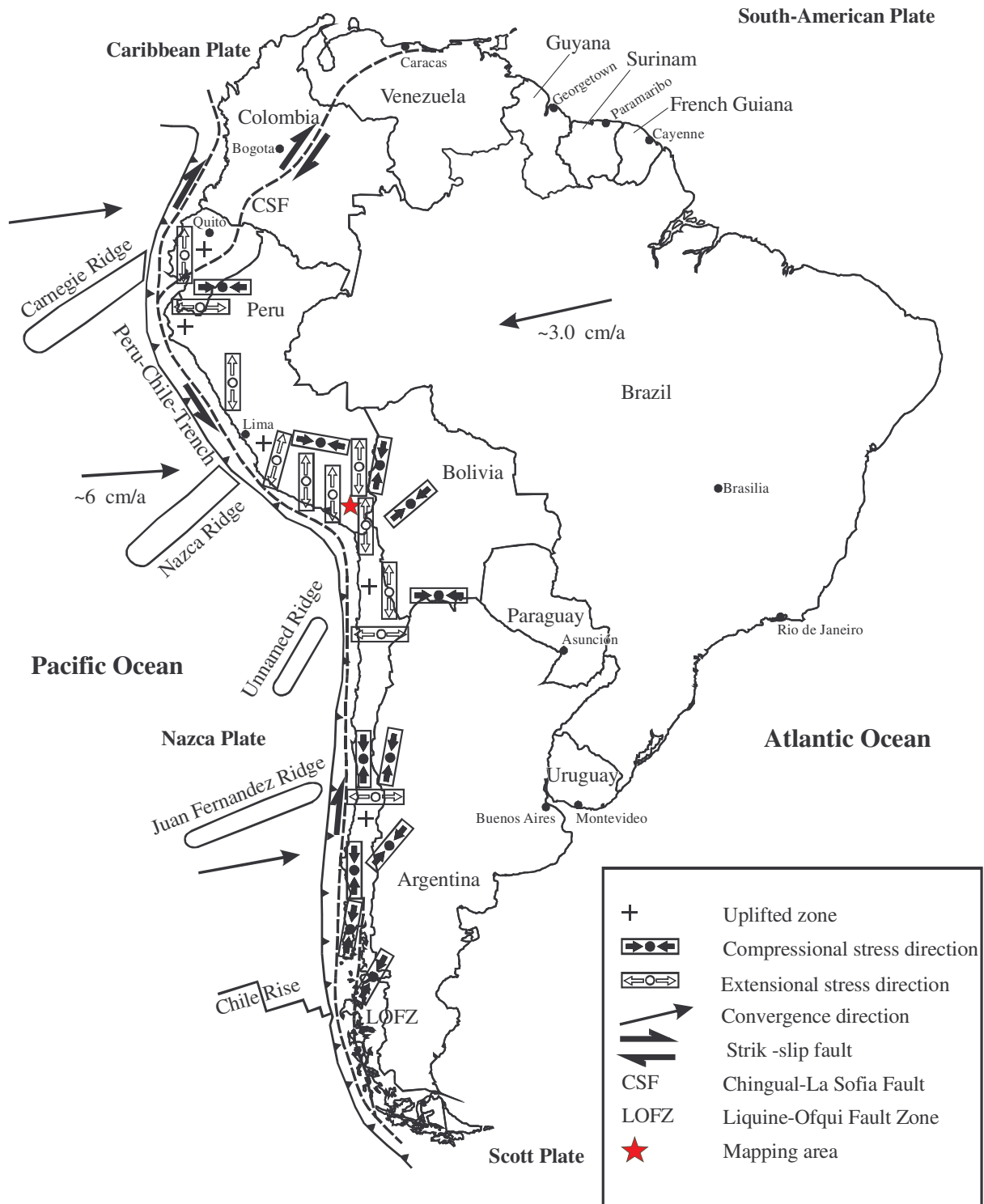


Fig. 20: Principal directions of stress deduced from structural analysis of Quaternary and active faults. The location of the mapping area is marked by a star (adapted from JAILLARD et al. 2000).

#### **4. Geological evolution**

Huancarane event: The uppermost Miocene Sillapaca Group equivalent to Maure Group (~10-9 Ma) consists in the study area of generally flat lying, andesitic lava flows similar in facies all over the Western Cordillera and the adjacent plateau (BENAVIDES-CÁCERES 1999). The flow layering indicates transport from SW to NE.

The Quechua II tectonic phase (9-7 Ma) results from the eastward thrusting of the Paleo-Andes onto the Brazilian shield, by which the arc zones were rapidly uplifted and the fault system at C° Millo was probably generated or reactivated.

Tectonic folding is not seen in the C° Millo region probably due to the high crustal level.

The Quechua III event (7-5 Ma) shows further E-W shortening, characterized by strike slip and reverse faulting in southern Peru (MÉGARD 1984). Uplift for the southern Peruvian Andes is estimated at 1300 m since the Late Miocene, of which 200-300 m would be of Quaternary age (BENAVIDES-CÁCERES 1999).

An extensional regime (6.7-5 Ma) triggers the emplacement of lavas (CARLIER et al. 1996) and is documented in the study area by the deposition of the Barroso volcanic rocks, which unconformably (erosional surface) overlie the Maure porphyritic lava.

Millo event: The Barroso volcanic rocks were delivered from an eroded volcanic center, with a complexly formed vent/feed-region at the mountain ridge of C° Millo and C° Zorrichata. The emplacement of the vent is controlled by faults and fissures (Enclosure 1).

The volcanic center appears to be an eroded stratovolcano due to its enormous size, the bimodality of volcanic strata, the complex internal tectonics and the intensive hydrothermal alteration.

The deposited tephra indicate a first explosive period and show similar to all other C° Millo strata circulating dip around the vent area of the topographic high. Incidence angles of about 25° indicate the ancient slope of the polygenetic volcano.

Facies-models for the Barroso ignimbrites could be reconstructed at the younger pyroclastic rocks at two trenchera outcrops (77971 and 77955). The relatively large diameter (<15 cm) of the juvenile pyroclasts as well as the comagmatic volcanic rock material accumulates at the lower to central part of the flow and indicates a short transport distance.

The dense lava material is predominantly located at the base of the flow unit and the less dense pumice dominates the central and upper part of the flow. A fine-grained ash layer on top of the main ignimbrite body, generated when small ash particles are blown out from hot gases, occurs at sample locality 77971 (Fig. 8).

A characteristic notch at the base of the flow unit is typical of many ignimbrites at the C° Millo. The notches result from higher weatherability, which is according to SMITH (1960) explainable by lower welding due to faster cooling at the base of a “simple cooling unit”. The porous pumice from the central to upper, hot and slowly cooling part of the unit in contrast shows welding (Fig. 8).

The undifferentiated pyroclastic rocks and ignimbrites are overlain by the crystal-bearing ashtuff, which probably represents the uppermost part of a coated ignimbrite flow unit, or a distal tephra fallout deposit.

The youngest recorded pyroclastic rock material from the vent region of the C° Millo stratovolcano is the subvolcanic pyroclastic rock, which suggests a former pyroclastic rock cover on the present surface of C° Millo.

If a constant dip of the uppermost preserved pyroclastic rock material is assumed, the hanging wall of the strata would be located at about 5100 m asl on C° Millo Sur (Enclosure 2: Geological section ABCD).

The thick porphyritic lava represents the “Barrosonian” change in eruption style i. e. from the early explosive period to more lava-dominated eruptions. The eruption fissure on the mountain ridge of C° Millo becomes inactive and new dikes were generated on the already weakened top of C° Millo.

The chemism of the lava does not vary significantly from the pyroclastic rocks, but shows stronger geochemical variation (andesite-trachyte). The more trachytic chemism in the northern part of the mapping area might result from an dike eruption at the northern Qda. Millo or Qda. Sallaoqueña.

The “Barrosonian” block-lavas, as documented from C° Supa imply with their angular to subangular fragments elevated viscosity due to polymerization, possibly due to higher SiO<sub>2</sub> content (dacite). Surface cooling due to the long transport distance (>1 km) and break down at constant feed rate is another possible explanation.

The more roundish lava boulders which were also seen in outcrops of weathered and eroded lava flows at C° Millo, indicate that they are erosional remnants of an older flow, which is overrun.

The uppermost Millo event strata is the remnant of porphyritic lava on C° Supa, which probably represents a hotter/faster flow.

The Qda. Sallaoqueña event is characterized by eastward shifting of active volcanism from the C° Millo region to the uppermost Qda. Sallaoqueña and to the west-slope of C° Sallaoqueña documented by one large chimney and three small dikes. The lavas seem to have a more dacitic composition. The block-lava carries only roundish lava fragments and indicates reworking of eroded lava-boulders.

Colpacachi events: The lavas of the Colpacachi events I and II record further eastward shift of the volcanic activity; outside of the study area. All strata dip SE. Youngest strata lie horizontally (Enclosure 2).

The beginning of the sequence is again of relative acid character (dacitic). The coarse- to very-coarse-grained block-lava implies reworking of a weathered footwall lava, of identical mineralogy.

The porphyritic and aphanitic lava on top remain acidic (andesite-dacite). The former is penetrated by the southernmost chimney in Qda. Sallaoqueña, which indicates a reactivation of volcanic activity with minor importance in the study area.

The porphyritic lava on top must be weathered and eroded in a longer lasting non-depositional phase, because the very-coarse-grained block-lava, which belongs already to the Colpacachi event II lies roughly flat and bears rounded-lava fragments of the latter. Transport direction did not apparently change.

The geochemical composition of the porphyritic lava is transitional between andesite and latite followed by the latitic medium- to very-coarse-grained block-lava and the porphyritic lava, which completes the Colpacachi formation.

The medium- to very-coarse-grained block-lava is characterized by both large rounded lava fragments (reworked) and small angular fragments (auto-brecciated). The columnar jointing pattern of the porphyritic lava on C° Chunco is typical of trachyandesitic lavas (SCHMINCKE 2004).

Chichupunt event: The Chichupunt porphyritic lava seems to be delivered from SE probably from the preserved eruption centers outside of the mapping area (Enclosure 5). The flow partly filled valleys, which were essentially similar to the recent ones. The geochemical composition vary from the former rock units.

The youngest rock unit of the mapping area is the lahar of roughly horizontal layering. This unit occurs at the bottom of the southernmost Qda. on top of porphyritic lava. The unit is probably delivered from the C° Millo region, because it bears a lot of strongly altered rock material.

Transport conditions can be imagined as a viscous water-saturated slurry. The solid material is carried in water, which lubricates the flow. The debris flow/lahar has been ferricreted under the influence of emanating groundwater.

Glacial striation on Cerro Millo indicate direction of ice-movement from W to E and from NW to SE.

# Diploma Thesis

## 5. Hydrothermal Alteration

### 5.1. Alteration halos/facies of the “high-sulfidation”-type

#### 5.1.1 Propylitic alteration

In the field propylitically altered lavas can be recognized by slight loss of luster in biotites and a slightly greenish groundmass.

In thin section propylitization is characterized by the assemblage of chlorite, epidote, carbonate, zeolite and quartz. Carbonate is restricted to some plagioclase and amphibole crystals, beginning to form from the rim, from cleavage planes and from the inner Ca-rich core of zoned plagioclase. Carbonate occurs in subhedral crystals up to 0.1 mm, as dark, finer-grained, anhedral crystals and as fine-grained, patchy dark aggregates in the groundmass due to plagioclase breakdown. Subhedral epidote is mainly located on veinlets and holes. It occurs disseminated in the groundmass. Mafic minerals are altered to chlorite, which partly swells up the cleavage planes. Zeolites and quartz form in veins, veinlets and holes.

#### 5.1.2 Sericitic alteration

Sericitic alteration occurs in one sample and could not be determined by field study. The outcrop is morphologically inconspicuous.

The handspecimen is grey colored and has a bleached appearance compared to unaltered rocks. It partly shows vuggy-texture and is relatively hard due to fine-grained intergrowth of quartz and sericite.

The rock in thin section is very homogenous, which indicates pervasive groundmass sericitization. Sericite is extremely fine-grained (<50 µm), pale green to yellow-brown colored and intimately connected to fine-grained quartz. Probable phenocrysts of plagioclase are altered to an even finer-grained mineral assemblage of sericite, kaolinite and quartz, which appears in thin section a little darker.

### 5.1.3 Argillic alteration

Argillic-altered outcrops are typically white or tan in color and may have a brown to orange oxydized surface due to weathering of iron sulfides (mainly pyrite). The outcrops are soft, but intergrowth with quartz (see below) makes the rocks hard and resistant.

In hand specimen, the indicator mineral for argillic alteration, kaolinite ( $\text{Al}_2\text{Si}_2\text{O}_5(\text{OH})_4$ ) could be determined by its softness ( $H=2.5$ ) and sticking to the tongue. It selectively replaces plagioclase phenocrysts; occurs in pervasive groundmass alteration and shows moderate shades of blue (Fig. 21).

In thin section, a kaolinite-type and a smectite-type argillic alteration can be distinguished.

(1) Kaolinite occurs in replacement masses and as vein infill. The colorless to pale yellow crystals show rarely pleochroism. Kaolinite is typically fine-grained and occurs as anhedral crystals, platy flakes, and rarely as crystals with hexagonal, square and triangular outlines. The crystals in the groundmass are in general smaller than the crystals which replace phenocrysts.

(2) Smectite  $(0.5 \text{ Ca,Na})_{0.7}(\text{Al,Mg,Fe})_4[(\text{Si,Al})_8\text{O}_{20}] (\text{OH})_4 n \text{ H}_2\text{O}$  is a general term for a group of clay minerals of which montmorillonite is the most common. Smectite in the study area is very fine grained ( $<0.01 \text{ mm}$ ) and brown due to iron-content. It mainly replaces volcanic glass and appears rarely as open-space fill.



Fig. 21: Argillic-altered porphyritic lava; phenocrysts and groundmass are altered to kaolinite (77294).

#### 5.1.4 Advanced argillic alteration

Advanced argillic alteration is defined by the occurrence of alunite ( $\text{KAl}_3[\text{SO}_4]_2(\text{OH})_6$ ) together with kaolinite.

Outcrops of alunite alteration are commonly white to tan in color, and may be massive to extremely porous. In hand specimen the fine-grained crystals show vitreous luster. In thin section alunite is colorless with low relief and weak birefringence. Interference colors vary from first order grey to second order green. Extinction is parallel and elongation negative. Two different types occur. (1) Euhedral (needle-/"baguette-shaped") to subhedral-tabular alunite, up to sizes of 1.2 mm in diameter, is often zoned, infills vugs, veinlets and selectively alters plagioclase (Fig. 22). The crystals are occasionally rimmed by jarosite. In pores the crystals may form seams or ice-flower like agglomerates.

(2) Anhedral, typically extremely fine-grained alunite (commonly  $<10\ \mu\text{m}$ ) intermixed with kaolinite may give a dark, mottled appearance to the section (Fig. 23). Rare patches of slightly coarser-grained alunite may occur.

X-ray diffraction analysis determined some alunite present in its Ca-bearing Minamiite-type and some in its Na-dominant Natroalunite-type. In enclosure 2 (Hydrothermal alteration and mineralization) alunite-dominated advanced argillic alteration and kaolinite-dominated advanced argillic alteration are distinguished.

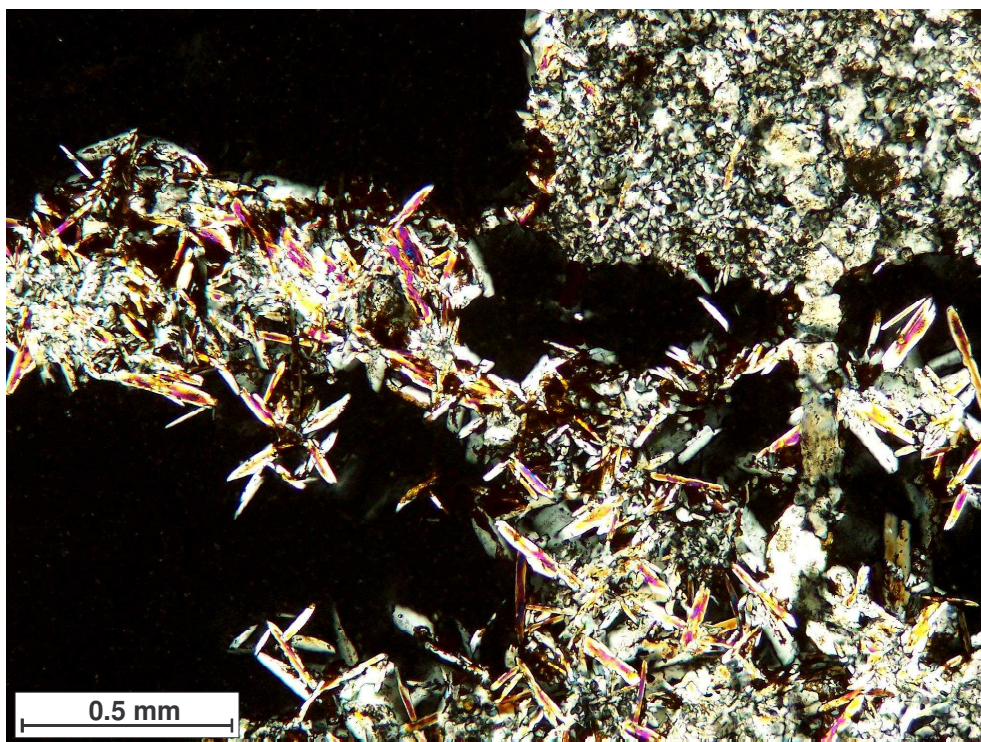


Fig. 22: Photomicrograph (TS 77268; XPL) of euhedral “baguette-like” alunite formed in veins and vugs. This type is characteristic for hypogene acid-sulphate alteration (chapt. 8).

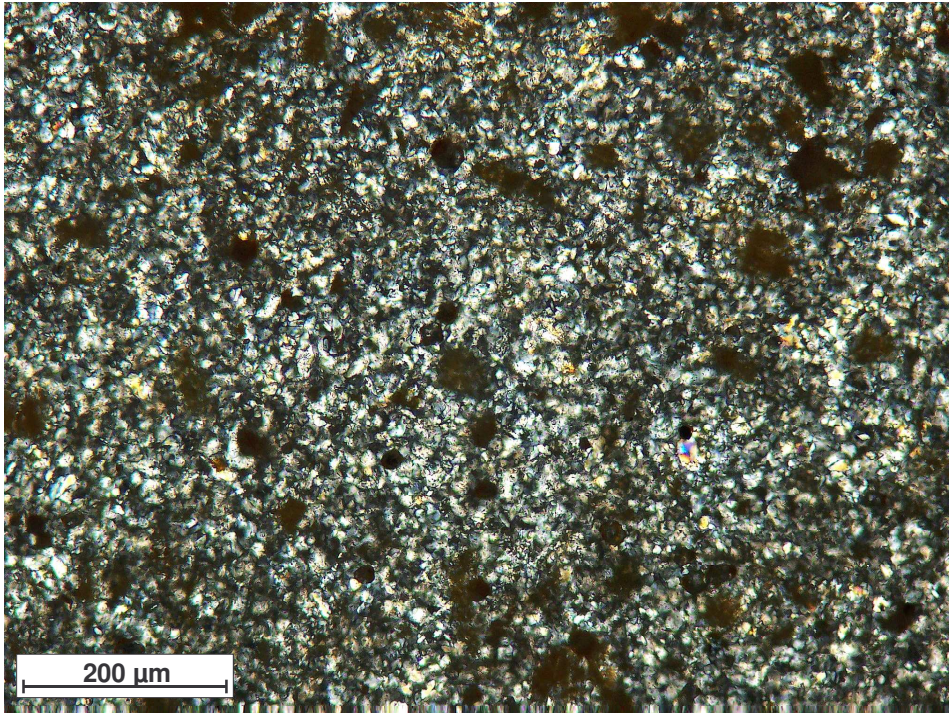


Fig. 23: Photomicrograph (TS 77282; XPL) of anhedral, fine-grained alunite intermixed with kaolinite, quartz, rutile. This type is characteristic for near-surface steam-heated advanced argillic alteration (chapt. 8).

At 77970 and some adjacent outcrops advanced argillic alteration is characterized by late-phase, macroscopic baryte blastesis on veins, in cavities and vugs. Baryte is white-colored and of tabular shape. In thin section the mineral is colorless and tabular (Fig. 24).

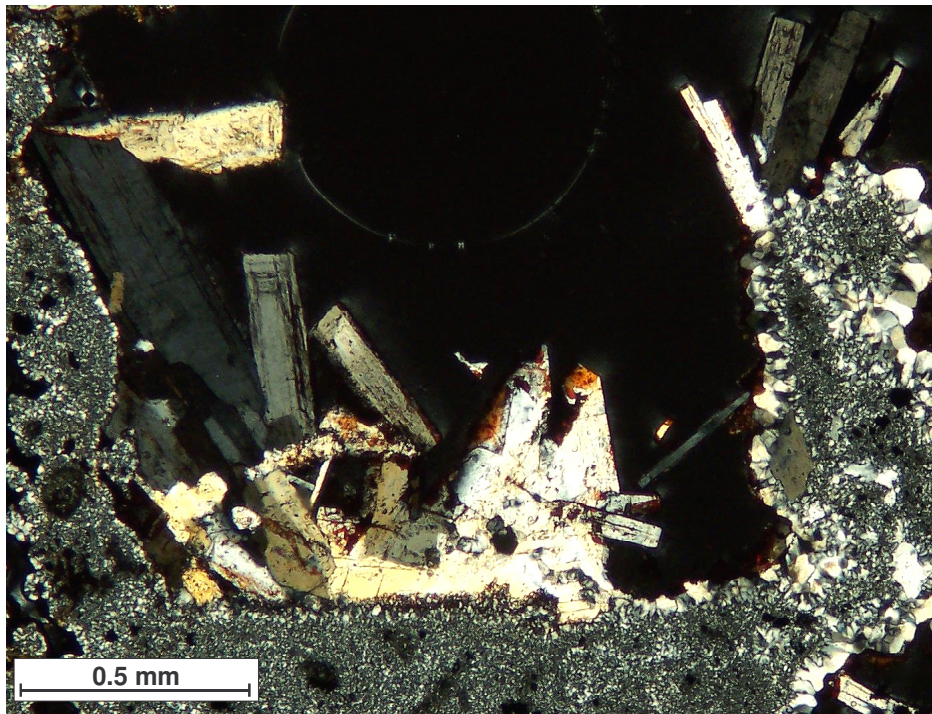


Fig. 24: Large tabular crystals of baryte as infill of a vug overgrown on quartz (TS 77970; XPL).

### 5.1.5 Silicification

Silicification is structurally, paleogeographically and lithologically controlled. Silicified rock occurs as ridges along fault and fissure zones and as more extensive, roughly tabular bodies. In hand specimen the rock is bleached (light-grey to white) and hard.

The thin section is characterized by some microgranular quartz which floods parts of the groundmass up to pervasive silicification and textural destruction. Quartz occurs fine-grained in the groundmass, slightly coarser-grained (or even finer-grained) as replacement of phenocrysts, as fan-like infill and as crystals up to sizes of 1 mm with bay-like intergrown features (buck quartz) infilling vesicles and open fractures (Fig. 25).

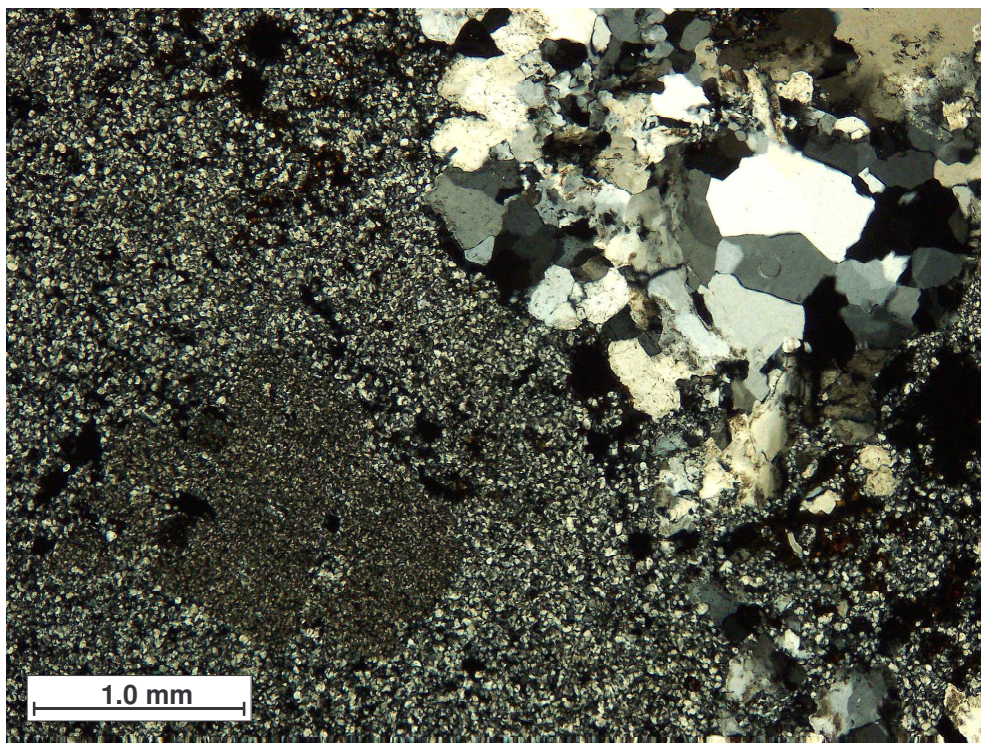


Fig. 25: Three different types of hydrothermal quartz: (1) Very fine-grained intergrown with kaolinite in altered phenocrysts, (2) fine-grained in groundmass and (3) coarse grained (buck quartz) as open-space fill (TS 77961; XPL).

### 5.1.6 Veins and horizons of chalcedony

The veins are variable in thickness and are developed as veinlike to lenslike bodies. Due to the structural control, chalcedony forms ridges with several meters of thickness. The horizons are about 5-75 m thick.

In hand specimen the mainly blue-grey to dark-grey chalcedony shows waxy lustre.

In thin section chalcedony appears as a fine-grained phase, with very fine-grained, disseminated ore minerals. Wavy distribution of ore minerals and slight variation of the optical axes, leads to wavelike habit of the chalcedony (schlieren).

### 5.1.7 Vuggy silica

Some outcrops show vugs with diameters up to 8 cm, which are generated from dissolution of pumice fragments in pyroclastic rocks and xenoliths in lavas (Fig. 26). In hand specimen quartz is usually grey and microcrystalline, with vugs from <1 mm up to 10 mm. The vugs are often lined by quartz, iron oxides and limonite.

In thin section quartz forms a dense mosaic texture. Some vugs are filled by subhedral quartz. Fine-grained rutile occurs as ragged aggregates of subhedral grains and as euhedral, prismatic grains and clusters.



Fig. 26: Acid leached outcrop of vuggy silica altered pyroclastic rock with iron staining (limonite). The very large vugs are leached pumice rock fragments (outcrop 24).

### 5.1.8 Solfatarata alteration

Probably solfatarata altered rocks occur about 150 m E of Lag. Quelluire in a very restricted area. The rock (handspecimen) is strongly argillic-altered and brittle due to swelling. Sulfur appears as a yellow dash. Hand specimen is lost.

## 5.2 Spatial overview of the alteration halos/facies

The study area is characterized by typical zoning of the alteration halos (Enclosure 1). The inner, intensively, advanced-argillic altered zone is mainly hosted by pyroclastic rocks (W of C° Millo Norte), in which small outcrops of structurally controlled vuggy silica alteration are incorporated.

The advanced argillic alteration grades outward (to E and S) into an argillic altered halo likewise in pyroclastic rocks, which follows the mapped outcrop of brecciated subvolcanic pyroclastic rock material. Of special interest is a restricted outcrop of sericitization incorporated by argillic altered rocks on C° Millo Sur related to the subvolcanic rock material. Argillic alteration grading from kaolinite to smectite in the outer parts of the mapping area (77284) occurs in the N of the C° Millo region. The argillic mineral assemblage grades outward into the propylitic altered rocks.

The boundary between advanced argillic and propylitic altered rocks on the west-slope of C° Millo traces nearly perfect the lithological boundary between pyroclastic rocks and porphyritic lava of the Barroso event (Enclosure 1 and 3).

In some more peripheral parts of the study area (C° Supa, C° Sallaoqueña, C° Chunco, S of C° Millo) fresh rock material is preserved, which itself is overlain/underlain by propylitically altered block-lava material.

Among the typical zoning occur advanced-argillic, argillic, propylitic and silicified alteration envelopes along faults and fissures in less-altered rock units.

Of particular interest is the feature that silicification is bound to persistent geographic levels, such as the 4700 m contour line at Qda. Millo/Qda. Quelluire/C° Chunco and the 4800 m contour line at C° Zorrichata/C° Millo. The latter blanket is preserved in patches at the east and north slope of C° Millo Norte. At the top of C° Millo Sur appears to be a further blanket, which roughly follows the 4900 m contour line.

The horizontal shape of silicified horizons, of which the first follows in addition roughly the lithological boundary between the Maure Group and the Barroso Group, implies a control by paleogeography/paleohydrology.

## **6. Mineralization**

### **6.1 Supergene mineralization/superficial duricrust formation**

#### **6.1.1 Ferricrete**

Ferricrete is a sort of duricrust and an indicator of pyrite oxidation and acid rock drainage. Ferricrete forms in the soil profile at the water-table when iron-oxides and iron oxyhydroxides accumulate and fill pore space. Transport and deposition of iron is controlled by fluctuations of the groundwater level. Iron is soluble in reducing acid waters and is precipitated at higher Eh (above 0.4) and/or pH.

Ferricrete in the mapping area can be described as colluvial ferricrete. It is varicolored, brown, reddish-brown to brownish-yellow. The clasts are angular and subangular cobbles-boulders. Pebbles, cobbles and vugs are coated with a fine filamentous iron oxyhydroxide cement (mainly goethite) (Fig. 27).

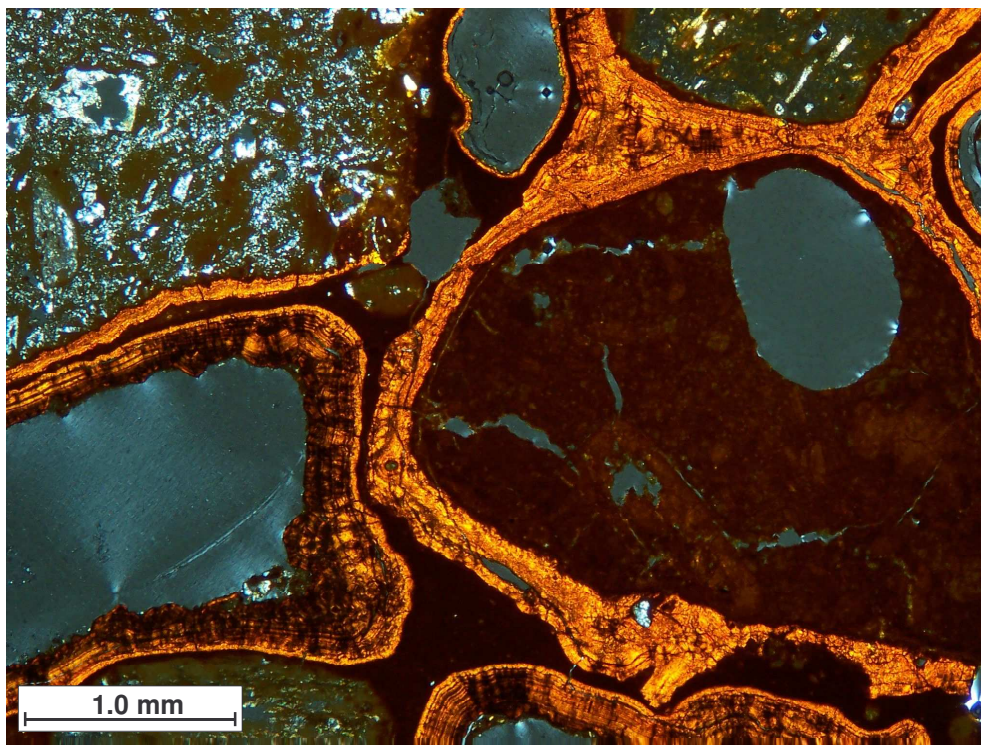


Fig. 27: Photomicrograph: Fine filamentous iron oxyhydroxide cement rimming debris material. Upper left corner shows argillic-altered rock fragment, upper right corner propylitic-altered rock fragment (TS 77293; XPL). See also Fig. 14.

## 6.2 Hypogene Mineralization

The main ore mineral is pyrite, which occurs with grain sizes between 0.005 and 0.5 mm inconsiderable at C° Millo (Fig. 28). The crystals are partly euhedral, but typically exhibit holes, atoll structures and bay-like habit due to silicification and corrosion/oxydation (Fig. 29). Pyrite is intergrown with rutile. There is occasionally a slight zoning, which is according to microprobe analysis due to varying As contents (Fig. 28).

Limonite is very abundant and occurs as veinrims and as open space fill. It shows partly cubic holes which indicates its origin from supergene decay of pyrite.

Only one sample (77970) had an elevated gold content of 81 ppb Au. Ore microscopy and electron microprobe analysis could not locate this gold content. Gold-like,  $\mu\text{m}$ -sized aggregates proved to be Cu-Sn alloy from sample preparation. It is assumed that the gold component of this sample is bound to pyrite.

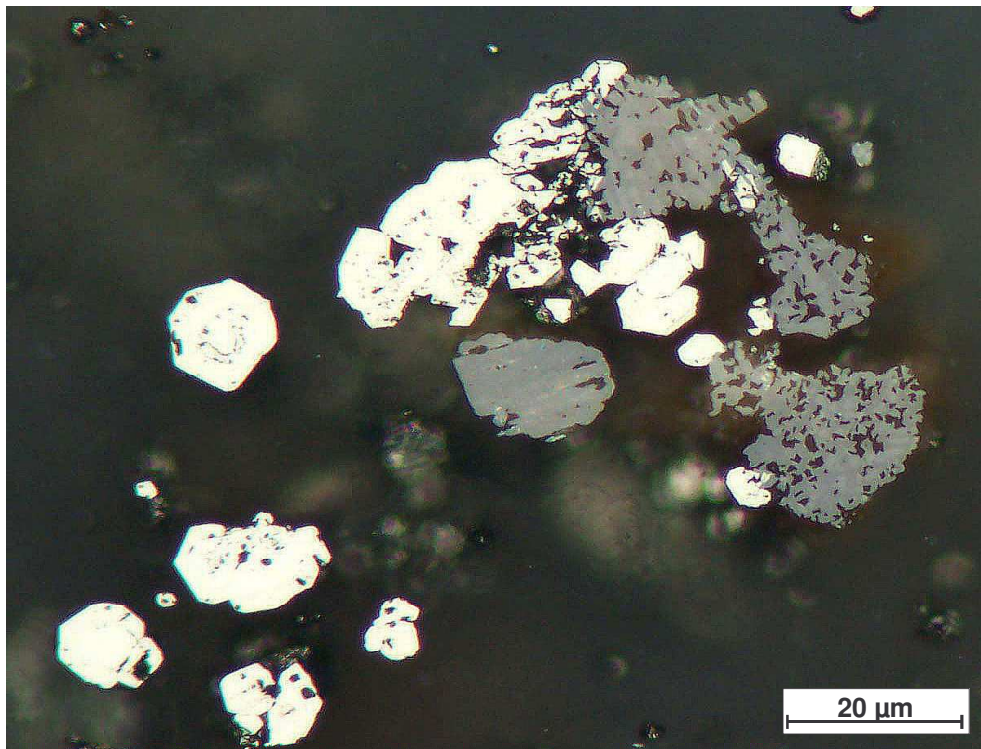


Fig. 28: Photomicrograph of pyrite intergrown with rutile (PS 77970/2; PPL).

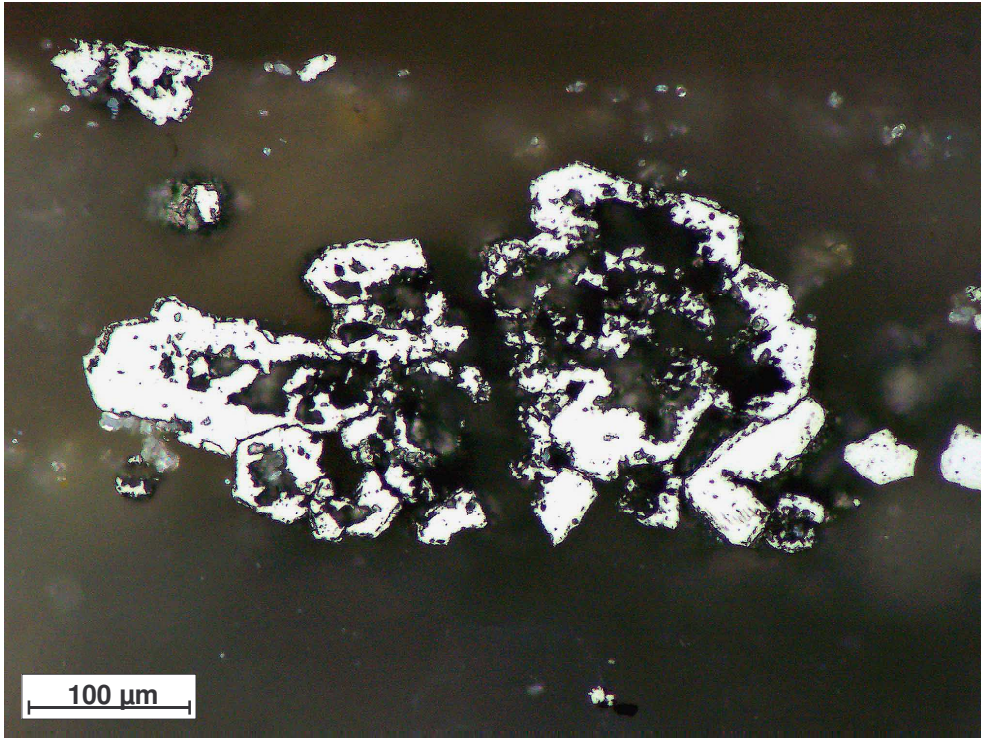


Fig. 29: Photomicrograph of pyrite with atoll structures derived from silicification/oxydation. Some fine-grained hydrothermal zircon (PS 77970/5; PPL).

## **7. Geochemistry**

### **7.1 Sampling**

The sampling aimed for a representative rock spectrum of the different lithologies and alteration facies at the Pichacani gold prospect, and did not follow a systematic spacing.

Sampling was by chips, with about 3-4 kg of chip material and a hand specimen, at 55 sample points.

### **7.2 Sample preparation and analysis**

The hand specimens served for preparation of thin and polished sections; the remainder was kept as reference sample. The rock chips were crushed by a jaw crusher, divided and about 300 g of the split was pulverized in an agate mill.

The rock powder was analyzed by X-ray fluorescence spectrometry (XRF) at Bundesanstalt für Geowissenschaften und Rohstoffe (BGR) in Hannover, and by Actlabs in Canada using the Ultratrace 3 package, which combines instrumental neutron activation analysis (INAA), 4-acid digestion ICP and ICP-MS analysis (Au + 63), plus mercury analysis by cold vapor atom absorption spectrometry.

**XRF** (X-ray fluorescence spectrometry) is a non-destructive technique based on bombarding glass discs (sample + borate flux) by X-rays and measuring the secondary X-ray emission lines generated. Main application is for major and minor element analysis.

**INAA** (instrumental neutron activation analysis) is a non-destructive trace element technique. About 20 g of sample powder are irradiated in a nuclear reactor at constant neutron flux. Each activated element will emit a “fingerprint” of gamma radiation, at a specific energy level, which can be measured and quantified.

**ICP** and **ICP-MS** are based on digestion of 0.25 g of sample powder in 10 ml HClO<sub>4</sub>-HNO<sub>3</sub>-HCl-HF at 200°C (fuming) and dilution to 10 ml with dilute aqua regia (hydrochloric and nitric acids). In **ICP** (inductively coupled plasma emission analysis) a high-frequency generator produces the necessary energy to ionise the atoms in a plasma burner. A highly-resolving spectrometer determines and quantifies the ions.

An **ICP-MS** (inductively coupled plasma emission-mass spectrometer) consists of an ICP unit, a highly resolving Quadrupol-mass spectrometer, which selects the ions and a Channeltron multiplier.

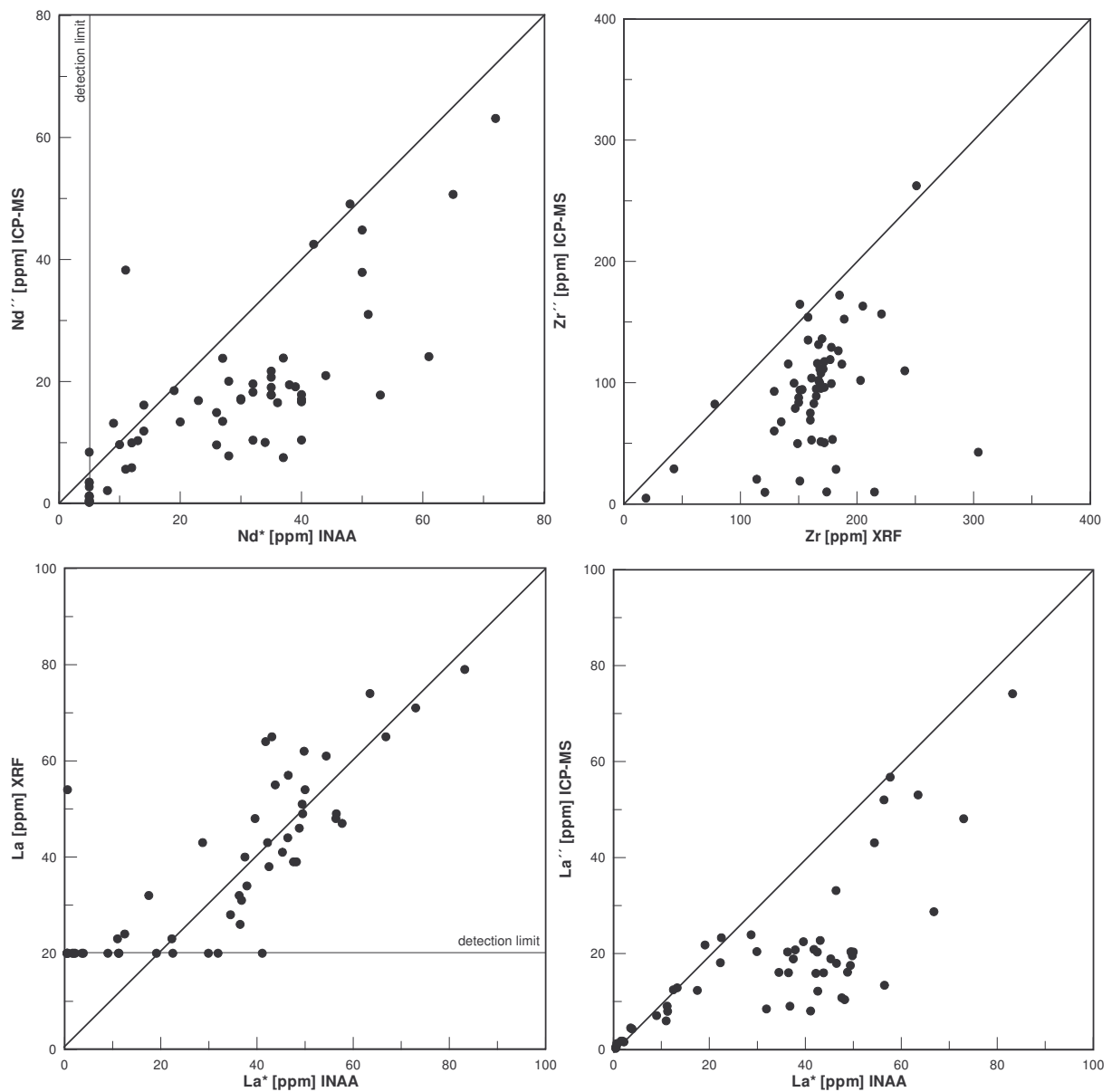
The four-acid digestion does not allow complete dissolution of certain minerals, such as baryte, gahnite, chromite, cassiterite, zircon, sphene and magnetite. Most silicates will be

dissolved, however, some elements will be erratically volatilized, including Si, As, Sb and Au.

AAS-CV (cold-vapor atomic absorption spectrometry) uses the aqua regia digestion, which leaches sulfides, and measures the absorption of Hg hybridized vapors.

### 7.3 Data screening

The problem of incomplete zircon digestion becomes clear, when the determined ICP-MS concentrations of zircon, niobium and some REEs are plotted versus the corresponding INAA and XRF data (Fig. 30).



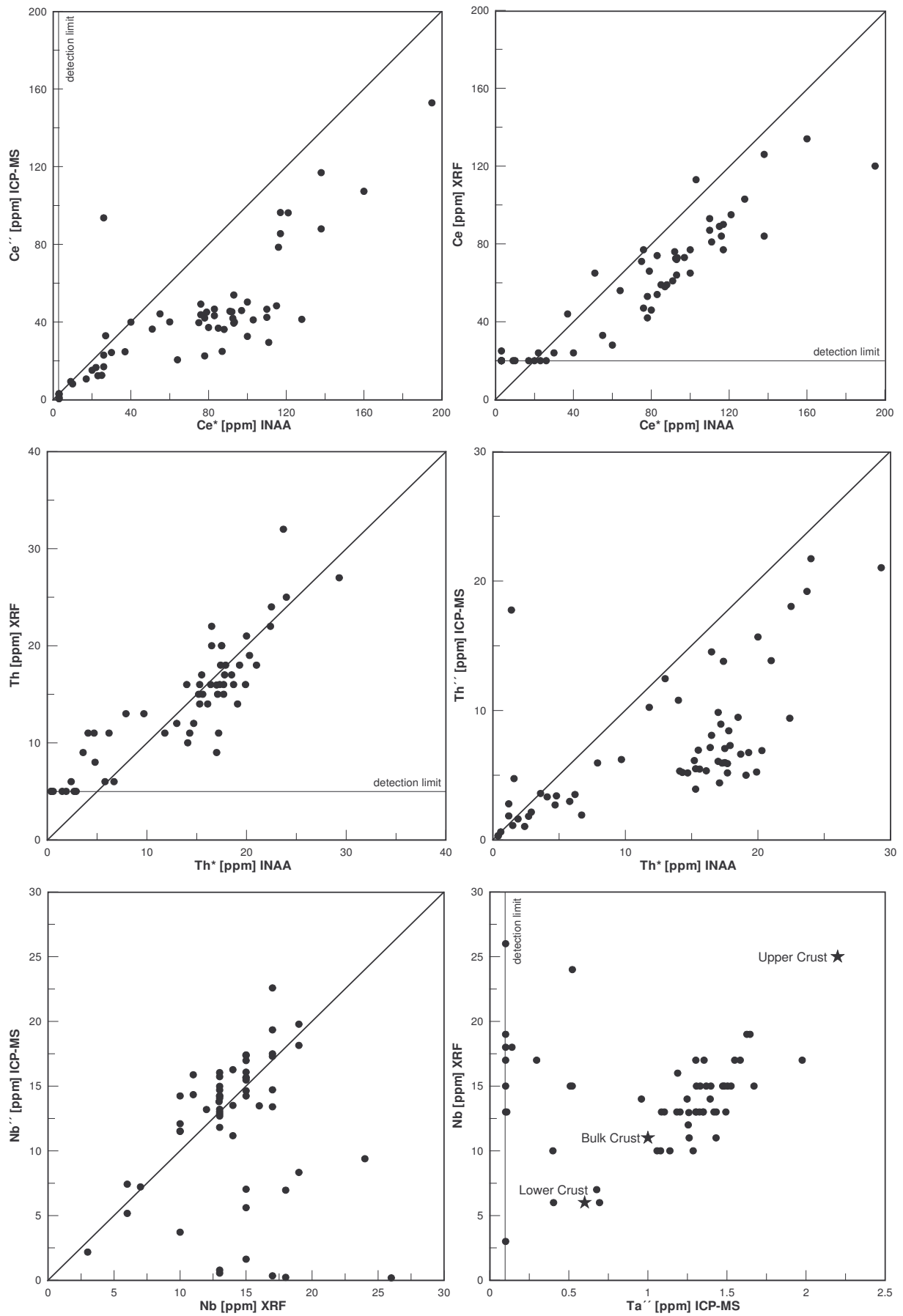


Fig. 30: Colinearity plots of Zr, Nd, La, Ce, Th and bivariate Nb-Ta plot. Diagonal line gives 1:1 colinearity.

Due to the necessity of ICP-MS data for multielement plots and other bivariate plots, the data have been corrected by comparison with the INAA data of La, Ce and Nd.

Correction method: For each sample the proportions La INAA/La ICP-MS, Ce INAA/Ce ICP-MS and Nd INAA/Nd ICP-MS were determined. If either the dividend or the divisor is at or below the detection limit the data set was ignored. The arithmetic mean of the three correction factors for each sample was calculated, which then was used to correct the ICP-MS data on La, Ce, Pr, Nd, Sm, Eu, Gd, Tb, Dy, Ho, Er, Tm, Yb, Lu of each sample. The correction factor is in between 1-3.

Nb is taken from XRF (Fig. 30).

#### **7.4 Data evaluation**

All geochemical data are listed in Table 3, including the multiply analysed elements and the corrected ICP-MS data (marked with co). Data which lie under the detection limit is red colored and give the limit of analytical detection.

In most diagrams the plotted elements are marked by the following symbols: ' =ICP, '' =ICP-MS, ''' =AAS-CV, \* =INAA. XRF data have no symbol.

Upper, Middle, and Lower Crust reference data are generally taken from TAYLOR & MCLENNON (1985).

Data representation was done with Grapher 3.

#### **7.5 Petrology**

##### **7.5.1 Classification of least-altered rocks**

Due to high amounts of groundmass (glass, crystallites and alteration minerals) rock type identification according to modal mineral constituent is inaccurate and the rocks were classified according to geochemical parameters and their normative mineral constituents.

Rock type classification is based on the unaltered and slightly altered rocks of the mapping area. The Na<sub>2</sub>O contents vary between 2.70 and 3.85 wt%, the K<sub>2</sub>O between 3.00 and 3.75 wt%; taking the Huancarane lava flow into account K<sub>2</sub>O goes down to 2.5 wt%.

Table 2: Normative constituents (CIPW) of the least-altered rocks at C° Millo, SE Peru (n. d. =no data).

Sample	Petrography	q wt%	plg wt%	ab wt%	an wt%	or wt%	c wt%	di wt%	hy wt%	il wt%	mt wt%	ap wt%
77296	Dikes and chimneys	17.74	44.35	n. d.	n. d.	20.33	1.83	0.00	11.17	1.60	2.32	0.65
77297	Dikes and chimneys	18.48	45.72	n. d.	n. d.	21.75	1.16	0.00	8.31	1.63	2.28	0.67
77953	Domes	18.99	47.34	n. d.	n. d.	20.39	0.35	0.00	8.66	1.46	2.17	0.63
77954	Amph.-biotite-bearing dike	18.92	47.34	n. d.	n. d.	20.45	0.32	0.00	8.72	1.46	2.16	0.63
77275	Porph. lava, Chichupunt	18.68	48.45	n. d.	n. d.	20.57	1.62	0.00	5.82	1.63	2.57	0.65
77277	Porph. lava Colpacachi II/top of C° Chunco	16.36	50.67	n. d.	n. d.	20.15	0.00	0.01	8.38	1.50	2.35	0.60
77279	Porph. lava Colpacachi II/top of C° Chunco	27.57	40.23	n. d.	n. d.	20.92	3.26	0.00	3.21	2.11	1.88	0.83
77276	Porphyritic lava, Colpacachi II	22.07	43.37	n. d.	n. d.	21.04	3.70	0.00	5.21	1.63	2.60	0.39
77290	Aphanitic lava, Colpacachi I	21.07	47.84	n. d.	n. d.	20.92	0.67	0.00	5.79	1.27	1.93	0.51
77291	Aphanitic lava, Colpacachi I	16.44	47.55	n. d.	n. d.	21.45	0.00	1.42	8.76	1.42	2.35	0.60
77952	Coarse- to v.- coarse-gr. block-lava, Col. I	30.74	34.62	n. d.	n. d.	23.46	4.96	0.00	2.22	1.65	1.39	0.97
77950	Medium- to v.- coarse-gr. block-lava, Salla.	30.42	37.38	n. d.	n. d.	22.52	3.40	0.00	2.53	1.60	1.59	0.56
77299	Porphyritic lava, Sallaqueña	32.70	32.59	n. d.	n. d.	23.28	4.47	0.00	3.09	1.67	1.64	0.56
77951	Porphyritic lava, Sallaqueña	22.24	46.39	n. d.	n. d.	21.22	1.48	0.00	4.64	1.44	2.00	0.58
77968	Coarse-grained block-lava, Millo	27.05	38.82	n. d.	n. d.	22.04	2.85	0.00	4.96	1.63	1.77	0.88
77284	Porphyritic lava, Millo	20.72	44.48	n. d.	n. d.	22.87	2.50	0.00	4.86	1.63	2.07	0.86
77285	Porphyritic lava, Millo	23.08	44.08	n. d.	n. d.	21.33	3.27	0.00	4.11	1.75	1.83	0.56
77288	Porphyritic lava, Millo	15.50	49.18	n. d.	n. d.	19.92	0.00	0.79	10.03	1.56	2.33	0.70
77289	Porphyritic lava, Millo	20.52	45.51	n. d.	n. d.	20.74	0.05	0.00	8.85	1.48	2.25	0.60
77958	Porphyritic lava, Millo	18.77	44.45	n. d.	n. d.	19.44	0.55	0.00	11.63	1.82	2.51	0.83
77966	Porphyritic lava, Millo	14.65	50.96	n. d.	n. d.	18.56	0.00	0.62	9.82	1.88	2.77	0.74
77965	Porphyritic lava, Huancarane	18.68	50.78	n. d.	n. d.	15.42	1.83	0.00	7.95	1.79	2.46	1.09
CLL 93	reference (Palacios et al. 1993)	10.30	51.50	34.20	17.30	18.20	0.00	4.20	12.40	1.60	1.20	0.60
CLL 94	reference (Palacios et al. 1993)	20.90	44.10	31.40	12.70	20.90	3.10	0.00	8.10	1.70	0.90	0.40
CLL 95	reference (Palacios et al. 1993)	13.70	53.40	35.70	17.70	20.70	0.70	0.00	8.40	1.60	0.80	0.70
CLL 96	reference (Palacios et al. 1993)	10.90	49.90	31.90	18.00	17.90	0.00	4.10	14.00	1.40	1.10	0.50
CLL 97	reference (Palacios et al. 1993)	11.70	49.20	33.30	15.90	18.60	0.00	4.50	12.70	1.50	1.10	0.60
CLL 98	reference (Palacios et al. 1993)	11.90	49.90	33.20	16.70	19.10	0.00	4.20	11.80	1.40	1.10	0.60
CLL 99	reference (Palacios et al. 1993)	10.50	51.80	34.80	17.00	17.90	0.00	4.80	11.70	1.60	1.20	0.60
CLL 100	reference (Palacios et al. 1993)	10.10	51.80	36.10	15.70	18.30	0.00	5.00	11.50	1.60	1.10	0.60
CLL 101	reference (Palacios et al. 1993)	9.90	51.30	34.50	16.80	17.70	0.00	5.20	12.50	1.60	1.20	0.60
CHV 22	reference (Palacios et al. 1993)	12.80	50.60	35.20	15.40	18.00	0.00	5.00	10.60	1.40	1.00	0.60
CHV 35	reference (Palacios et al. 1993)	10.50	50.30	37.30	13.00	21.90	0.00	4.50	9.50	1.50	1.00	0.80
CHV 161	reference (Palacios et al. 1993)	14.10	52.60	38.10	14.50	18.20	0.00	4.00	8.40	1.30	0.90	0.50
U. Crust	Upper Crust	15.70	13.60	13.60	n. d.	20.10	n. d.	6.10	9.90	0.95	n. d.	n. d.
B. Crust	Bulk Crust	6.60	53.40	26.20	26.20	6.50	n. d.	8.70	24.10	1.70	n. d.	n. d.
L. Crust	Lower Crust	3.70	54.10	23.70	30.40	2.00	n. d.	9.80	28.60	1.90	n. d.	n. d.

The volcanic rocks at C° Millo are oversaturated with respect to silica and have no normative olivine, nepheline or leucite. Normative quartz, feldspar and plagioclase contents of most samples plot in the modified upper QAPF diagram in the transition zone of the andesite and dacite root field. The block-lavas are tending to rhyodacitic composition (Fig. 31).

Compared with the reference data from PALACIOS et al. (1993), which is derived from the volcanic centers of Huarancante and Calcha normative quartz from the C° Millo rocks is about 5-10 wt% higher, plagioclase is slightly lower and alkali feldspar is slightly higher. These trends seem to be a combination of regional magmatic differences and slight alteration of the C° Millo rocks.

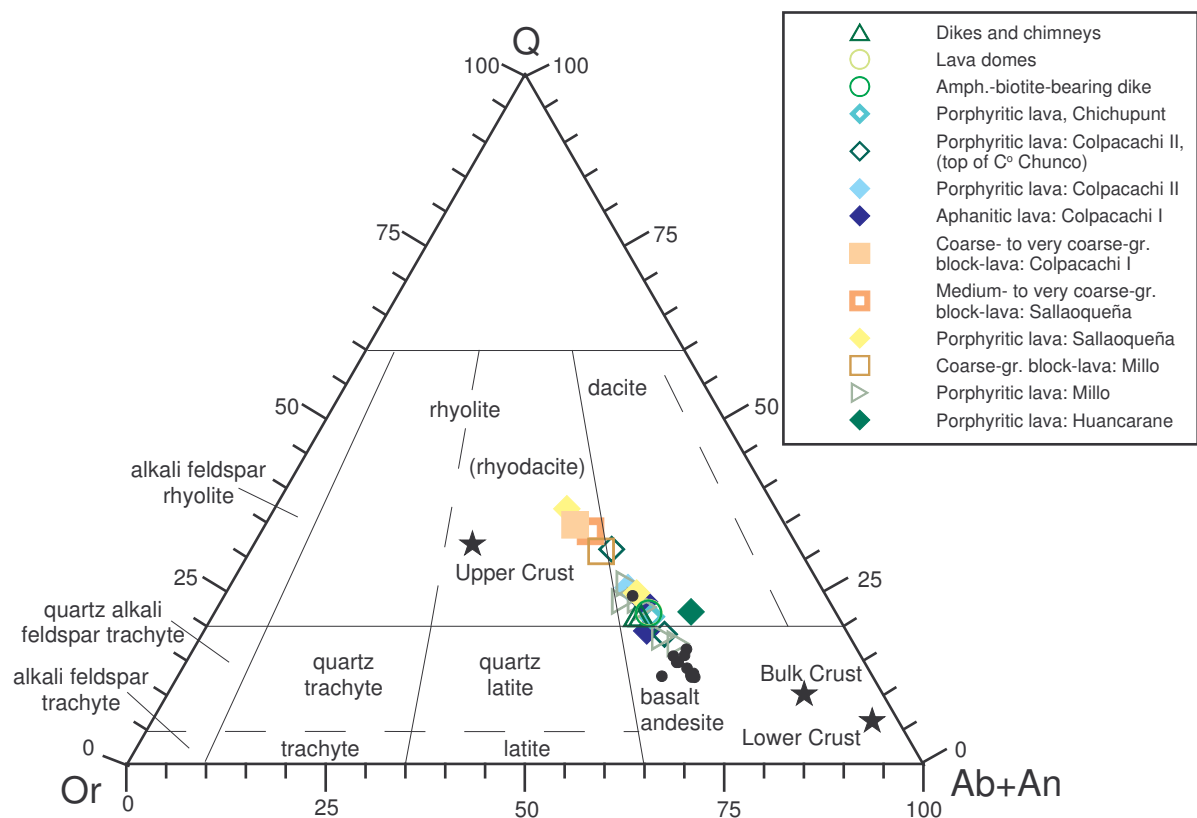


Fig. 31: Classification of the volcanic rocks at C° Millo using the normative constituents (ICPW) and the QAPF diagram (STRECKEISEN 1978). Dark points: reference data from PALACIOS et al. (1993).

More valuable information is derived from the TAS (total alkalis silica) diagram (Fig. 32). All fresh or weakly altered volcanic rocks have subalkaline and intermediate to acid silica composition. Reference data of the Barroso Group from PALACIOS et al. (1993) is nearly congruent to the data of the study area.

The rocks are classified as andesite, trachyandesite, trachyte and dacite. The trachyandesite can be further subdivided as latite ( $\text{Na}_2\text{O}-2<\text{K}_2\text{O}$ , “potassic”). The distinction between trachyte and trachydacite is difficult, because the normative quartz constituents vary in  $q+an+ab+or=100\%$  from 17 to 25 wt% and the influence of slight groundmass silicification is difficult to estimate. Nevertheless it seems that the freshest rocks have normative quartz below 20 wt%. This assumption is justified by the reference ICPW data from PALACIOS et al. (1993) which classify as trachytes.

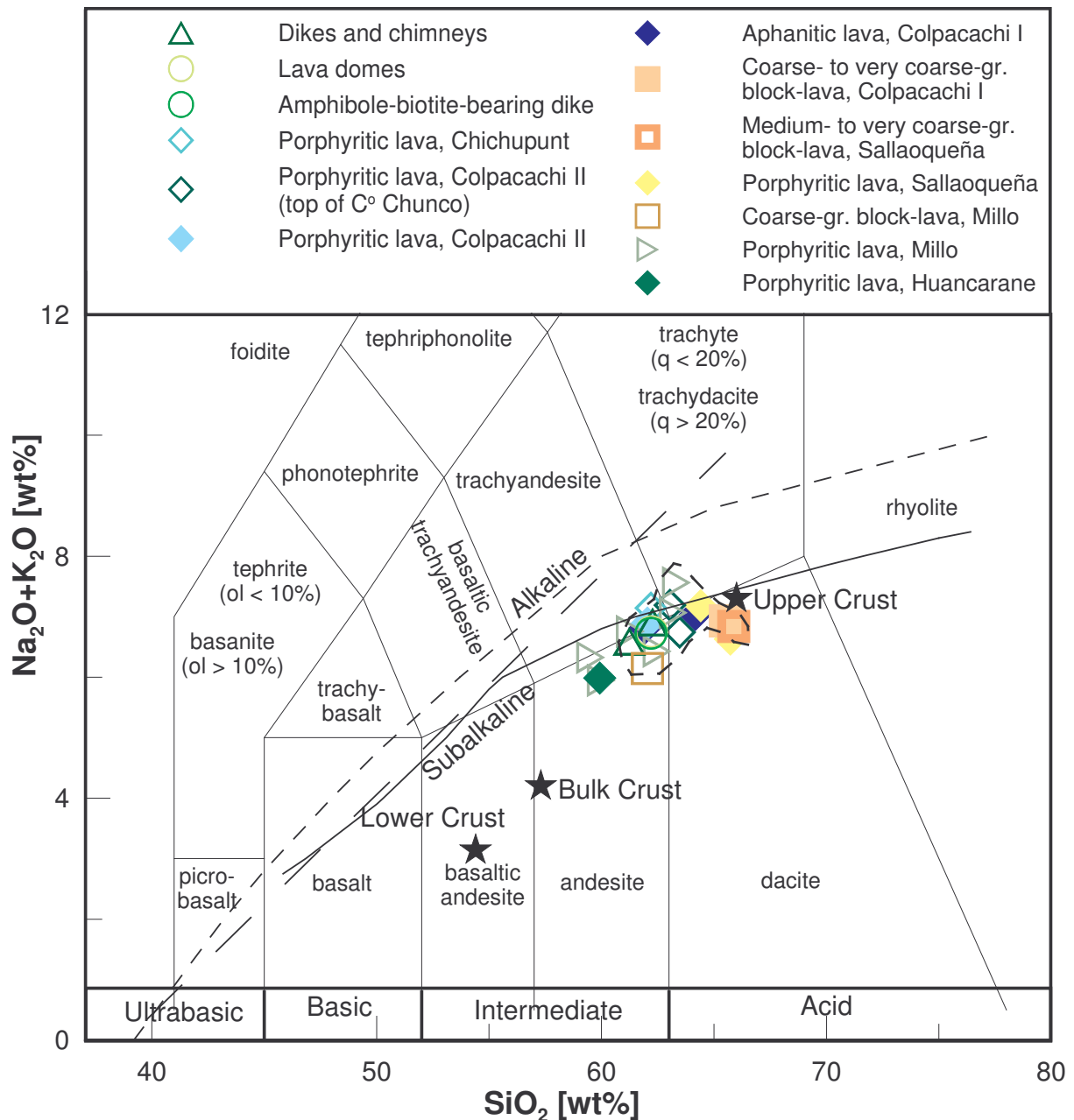


Fig. 32: Chemical classification of the rocks at C° Millo using the TAS diagram (XRF data) (LE BAS et al. 1986). Abbreviations: q=normative quartz, ol=normative olivine. Subdivision into alkaline and subalkaline rocks: continuous line KUNO (1966), widely dashed line MACDONALD (1968), narrowly dashed line IRVINE & BARAGAR (1971). Field with dashed outline: Barroso Group by PALACIOS et al. (1993).

The rock classification according to TAS is confirmed by the  $\text{SiO}_2\text{-Zr/TiO}_2$  diagram (FLOYD & WINCHESTER 1975, Fig. 33).

The data points of the lava domes and the amphibole-biotite-bearing dike as well as the other dikes plot in a very narrow range and suggest an origin from a similar source.

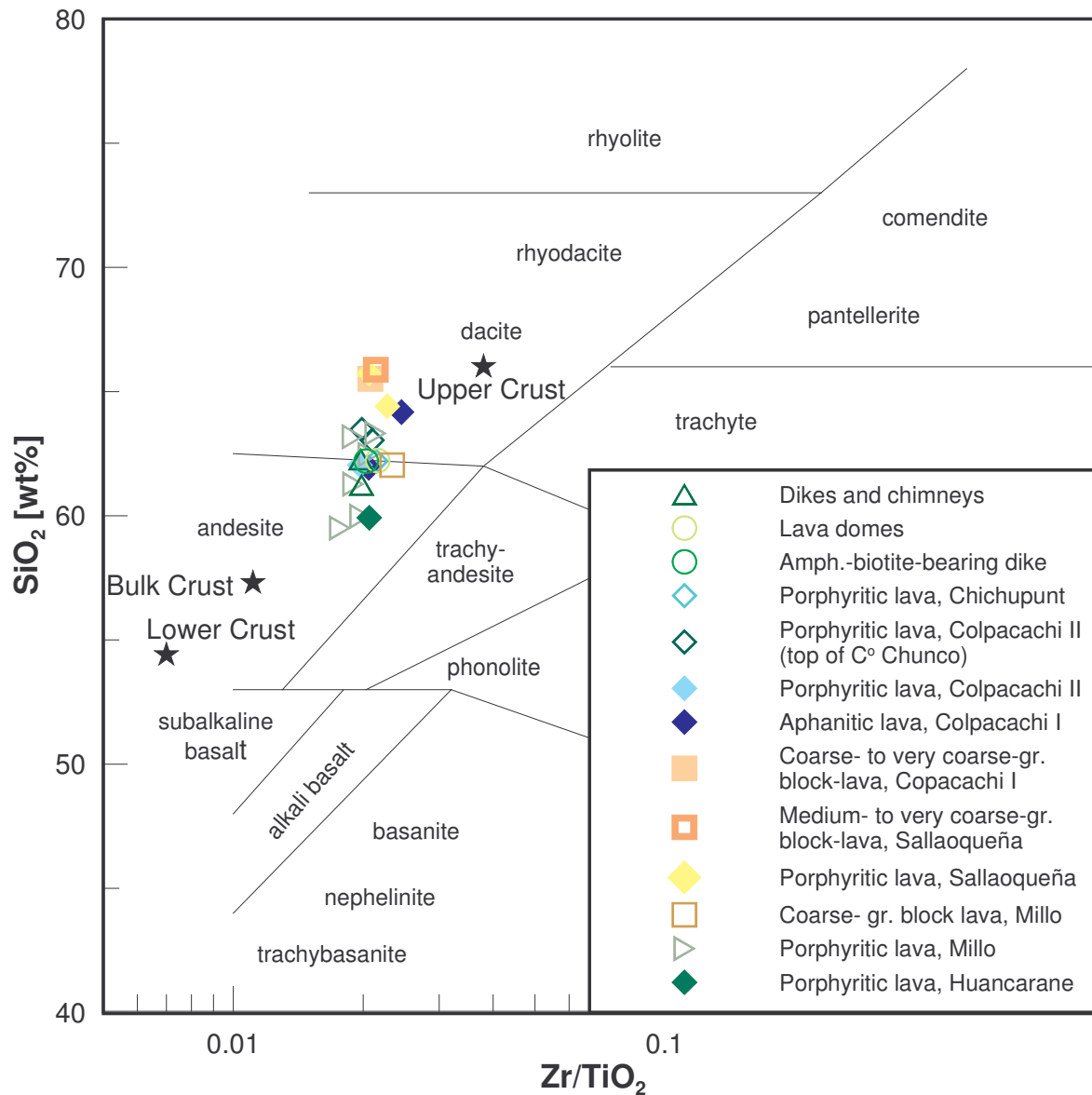


Fig. 33: SiO<sub>2</sub>-Zr/TiO<sub>2</sub> diagram (FLOYD & WINCHESTER 1975) of the least-altered rocks from C° Millo (XRF).

The subalkaline rocks can be further subdivided using the K<sub>2</sub>O vs. silica diagram (Fig. 34). All rocks belong to the calc-alkaline series (RICKWOOD 1989). This also corresponds to the subdivision of IRVINE and BARAGAR (1971) in the AFM diagram (Fig. 35). The andesite and dacite can be qualified as high-K andesite and high-K dacite according to PECCERILLO and TAYLOR (1976).

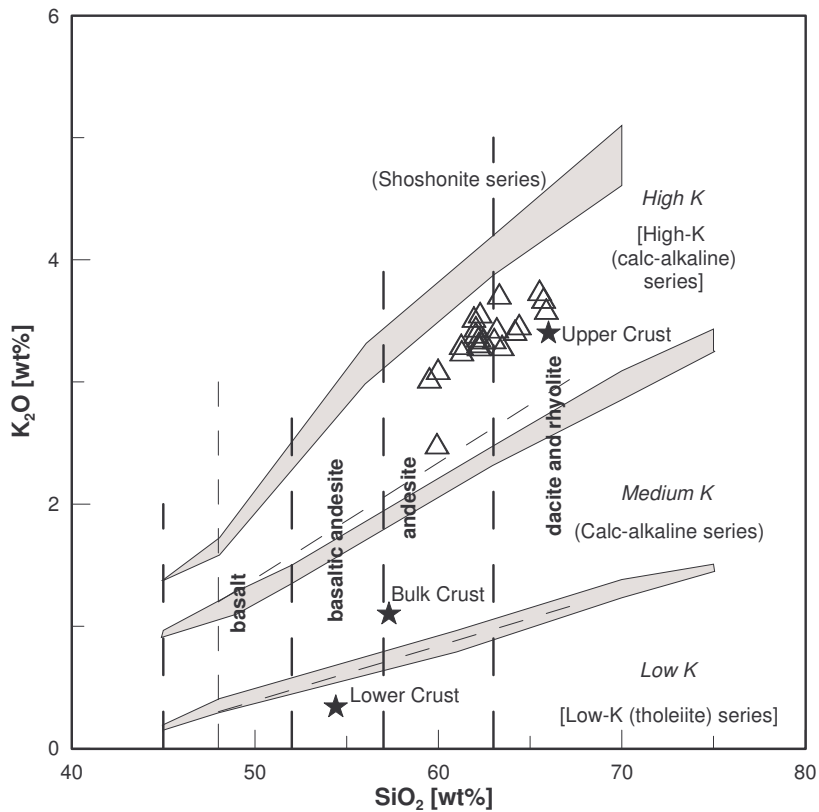


Fig. 34: The subdivision of the subalkalic rocks at C° Millo using the  $K_2O$  vs silica diagram (XRF data). Subdivisions: LE MAITRE et al. (1989) (broken lines with nomenclature in italics), RICKWOOD (1989) (nomenclature in parentheses). Shaded bands: boundary lines of PECCERILLO and TAYLOR (1976), EWART (1982), INNOCENTI et al. (1982), CARR (1985) and MIDDLEMOST (1985).

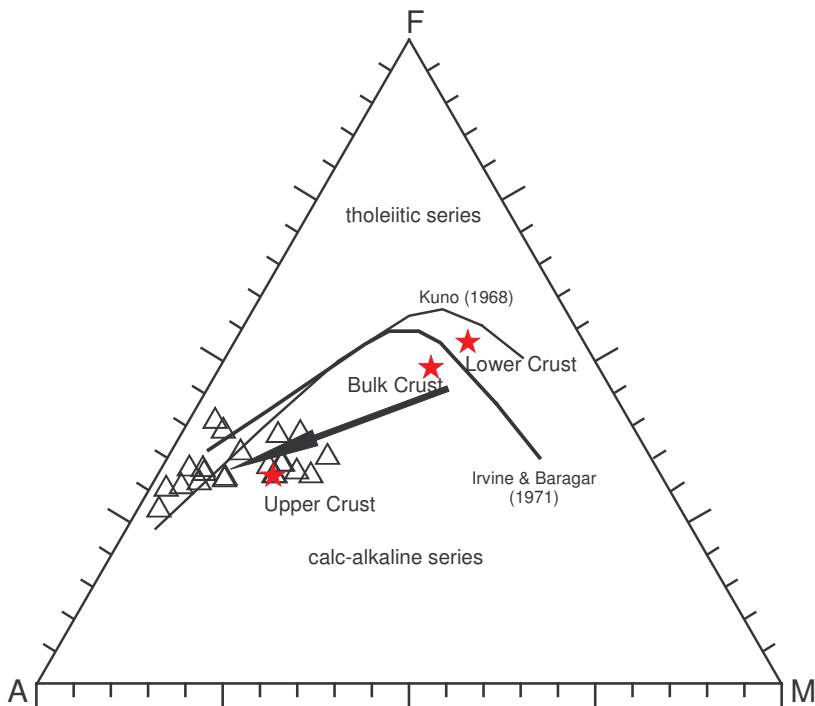


Fig. 35: AFM diagram showing the calc-alkaline field and the tholeiitic field after KUNO (thin line) and IRVINE and BARAGAR (heavy line) (from RICKWOOD 1989). The rocks of the mapping area belong to the calc-alkaline series. Arrow marks the calc-alkaline differentiation trend (CARMICHAEL 1964).

The samples show relatively large scatter in the aluminosity-SiO<sub>2</sub> variation diagram and cover both metaluminous and peraluminous compositions (Fig. 36). The majority of the rocks plot in the I-type field and are therefore derived from melting of igneous rock material. I-type rocks are mainly metaluminous (SHAND 1951).

The elevated Al<sub>2</sub>O<sub>3</sub> concentrations and lowered Na<sub>2</sub>O, K<sub>2</sub>O and CaO concentrations indicate incipient and weak alteration, which mainly affects the more permeable block-lavas but also is evident in the massive lavas.

The occurrence of normative corundum might be an indicator for peraluminosity but can be more likely explained, especially in comparison to the unaltered reference data of PALACIOS et al. (1993), by loss of alkalis in the course of alteration. This corresponds with the occurrence of diopside, amphibole, biotite and titanite in thin section, which are indicators for metaluminosity and the occurrence of hypersthene and diopside in CIPW of the C° Millo rock suite.

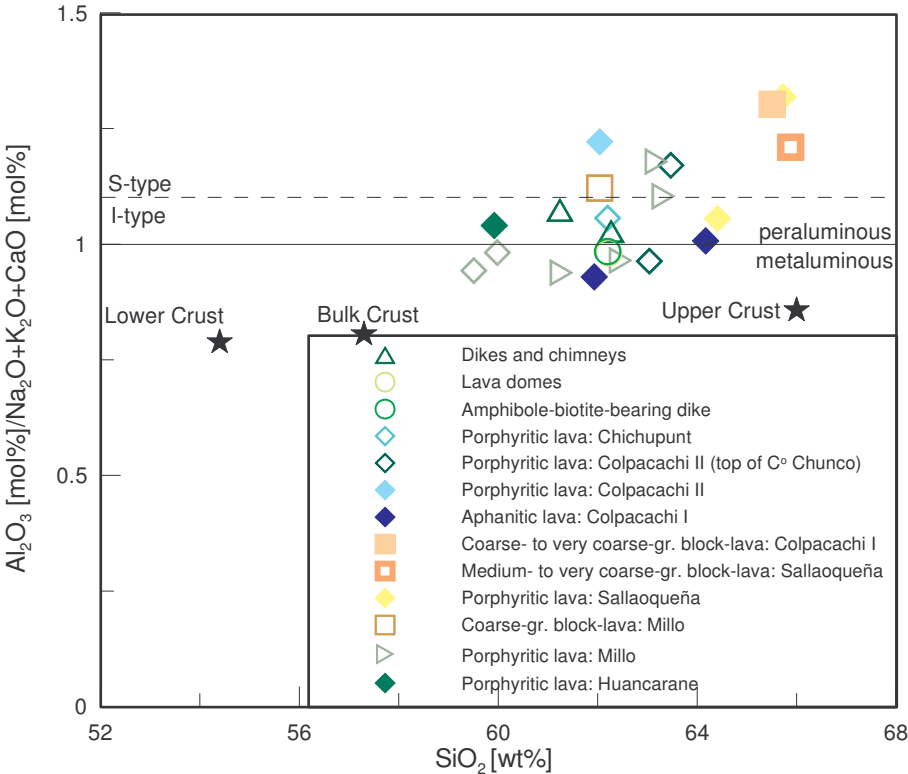


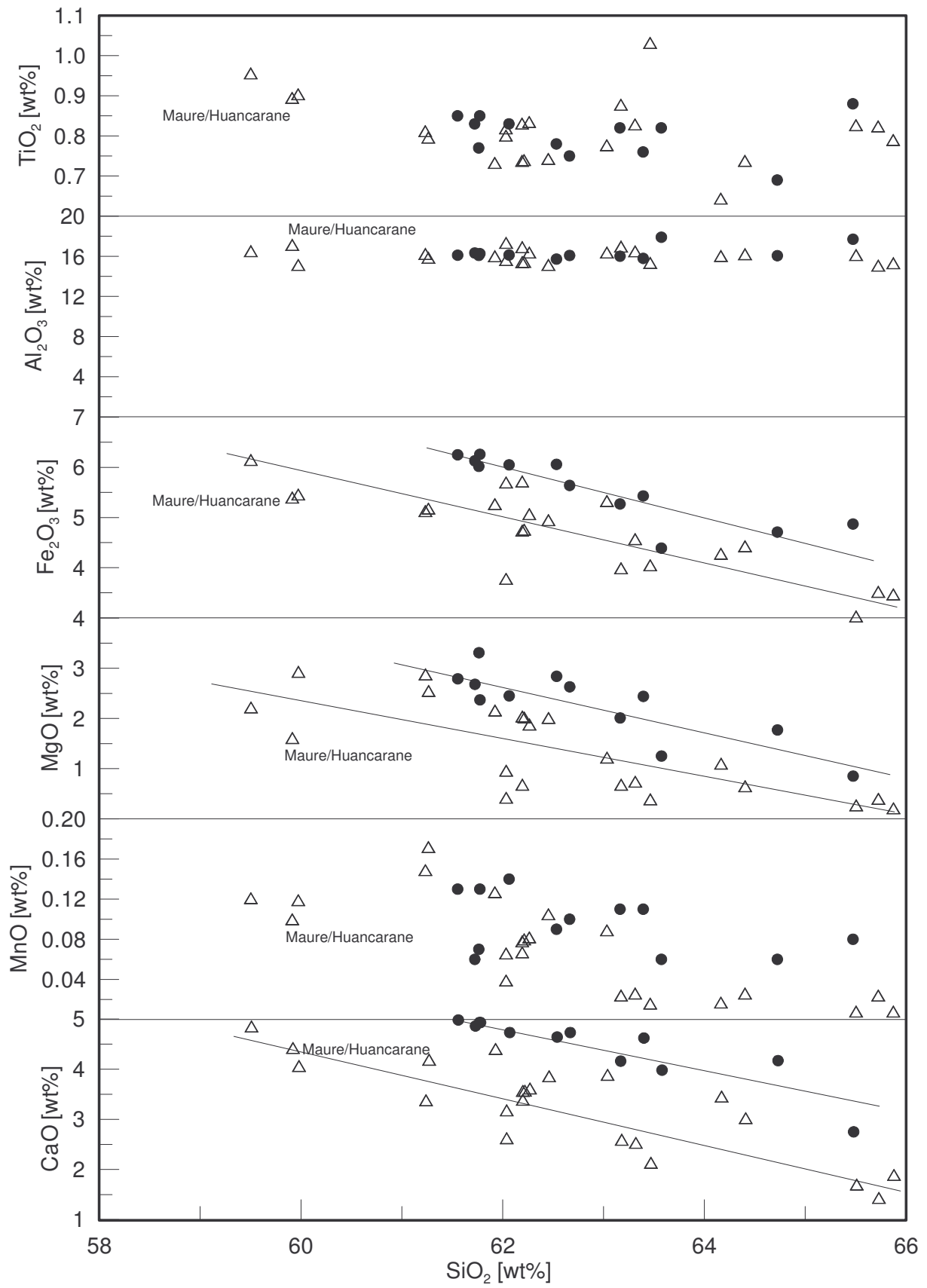
Fig. 36: Aluminosity-SiO<sub>2</sub> variation diagram of the least-altered volcanic rocks of C° Millo (XRF) (Sources: SHAND 1951, CHAPPEL & WHITE 1974).

### 7.5.2 Major element distribution of least-altered rocks

According to HARMON et al. (1984) the Cenozoic volcanic rocks of the Central Andes have  $\text{SiO}_2$  concentrations mainly between 56 and 66 wt% and are andesites-dacites with dacite-rhyolite ignimbrites. The  $\text{SiO}_2$  concentration of the volcanic rocks at C° Millo range between 58 and 66 wt%, in contrast to the Barroso data from PALACIOS et al. (61-66 wt%), and the rocks of the mapping area are andesites-dacites (Fig. 37).

In comparison to the data from PALACIOS et al. (1993) the  $\text{Fe}_2\text{O}_3$ , MgO, MnO, CaO,  $\text{Na}_2\text{O}$  and  $\text{K}_2\text{O}$  data from C° Millo are slightly lower. The  $\text{TiO}_2$ ,  $\text{Al}_2\text{O}_3$  and  $\text{P}_2\text{O}_5$  data are congruent and  $\text{K}_2\text{O}$  is slightly enriched (Fig. 37).

$\text{K}_2\text{O}$  generally behaves incompatibly and thus rocks which are genetically related should define linear trends with  $\text{K}_2\text{O}$  increasing progressively with increasing  $\text{SiO}_2$  as observed in the volcanic rocks of the mapping area and in the reference data (Fig. 37, comp. Fig. 34). Similarly, CaO and  $\text{Fe}_2\text{O}_3$  show negative correlation with silica, confirming the role of plagioclase and magnetite as major fractionating phases in the evolution of the magma.  $\text{TiO}_2$  should behave in the same manner but there is a relatively pronounced scatter.



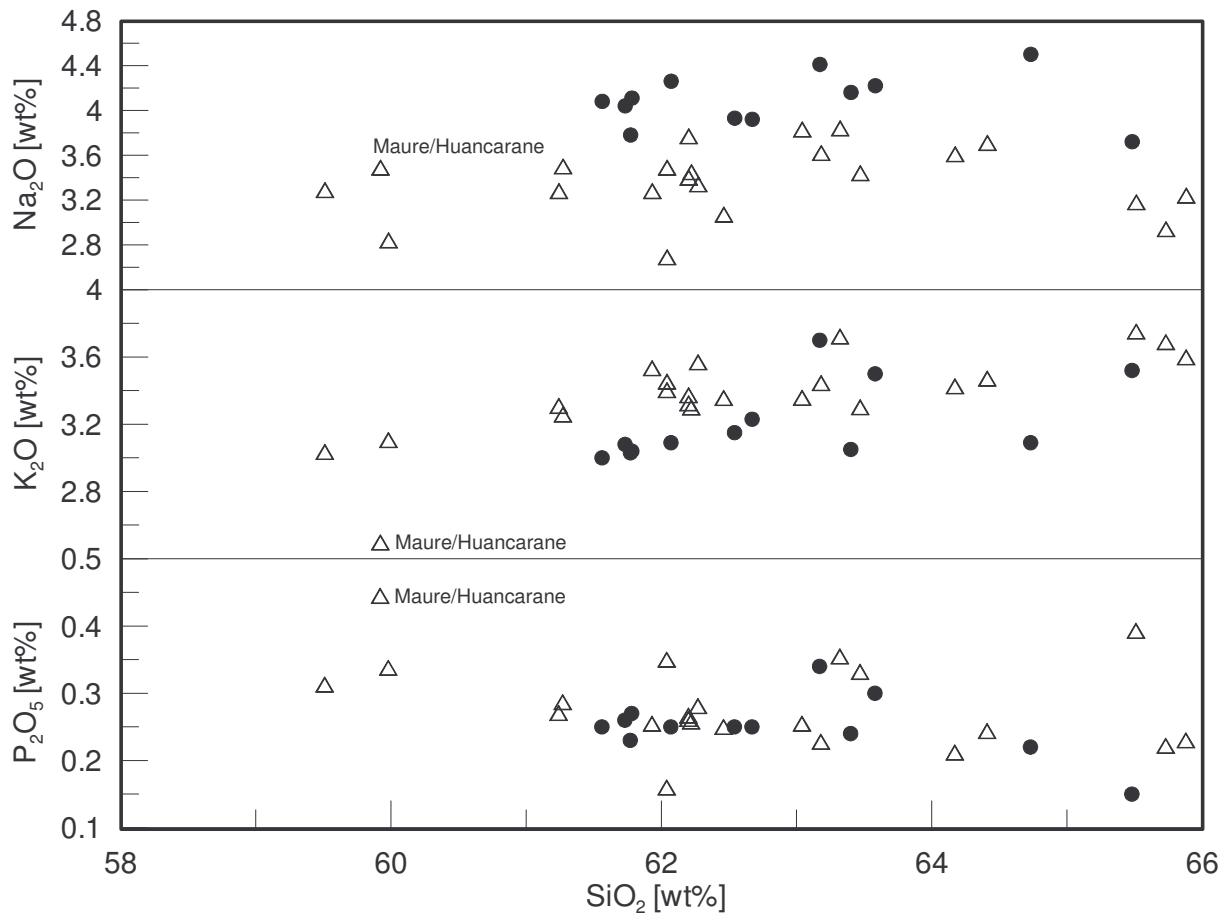


Fig. 37: Harker-diagrams of  $\text{TiO}_2$ ,  $\text{Al}_2\text{O}_3$ ,  $\text{Fe}_2\text{O}_3$ ,  $\text{MgO}$ ,  $\text{MnO}$ ,  $\text{CaO}$ ,  $\text{Na}_2\text{O}$ ,  $\text{K}_2\text{O}$ ,  $\text{P}_2\text{O}_5$  illustrating fractionation of the least-altered rocks at C° Millo (XRF). Solid dot: PALACIOS et al. (1993); open triangle: this study.

$\text{MgO}$  correlates negatively with  $\text{SiO}_2$  indicating ferromagnesian minerals and plagioclase as fractionating phases.  $\text{Al}_2\text{O}_3$ ,  $\text{P}_2\text{O}_5$  and  $\text{Na}_2\text{O}$  show no systematic trend.

The Maure lava has remarkably low  $\text{K}_2\text{O}$  and high  $\text{P}_2\text{O}_5$  which might be explained by lesser amount of crustal contamination. Field evidence indicates that this rock unit is from a different volcanic eruption center.

### 7.5.3 Trace elements and rare earth element pattern of least-altered rocks

The samples studied have the same general trace and rare earth element pattern, which is characterized by enrichment of incompatible elements such as Cs, Rb, Ba, Th, U and REEs in comparison to the primitive mantle (SUN & MC DONOUGH 1995). The compatible elements such as Co, Ni, Cr are depleted (Fig. 38). Ta, Nb, Ti and Y show distinct negative anomalies.

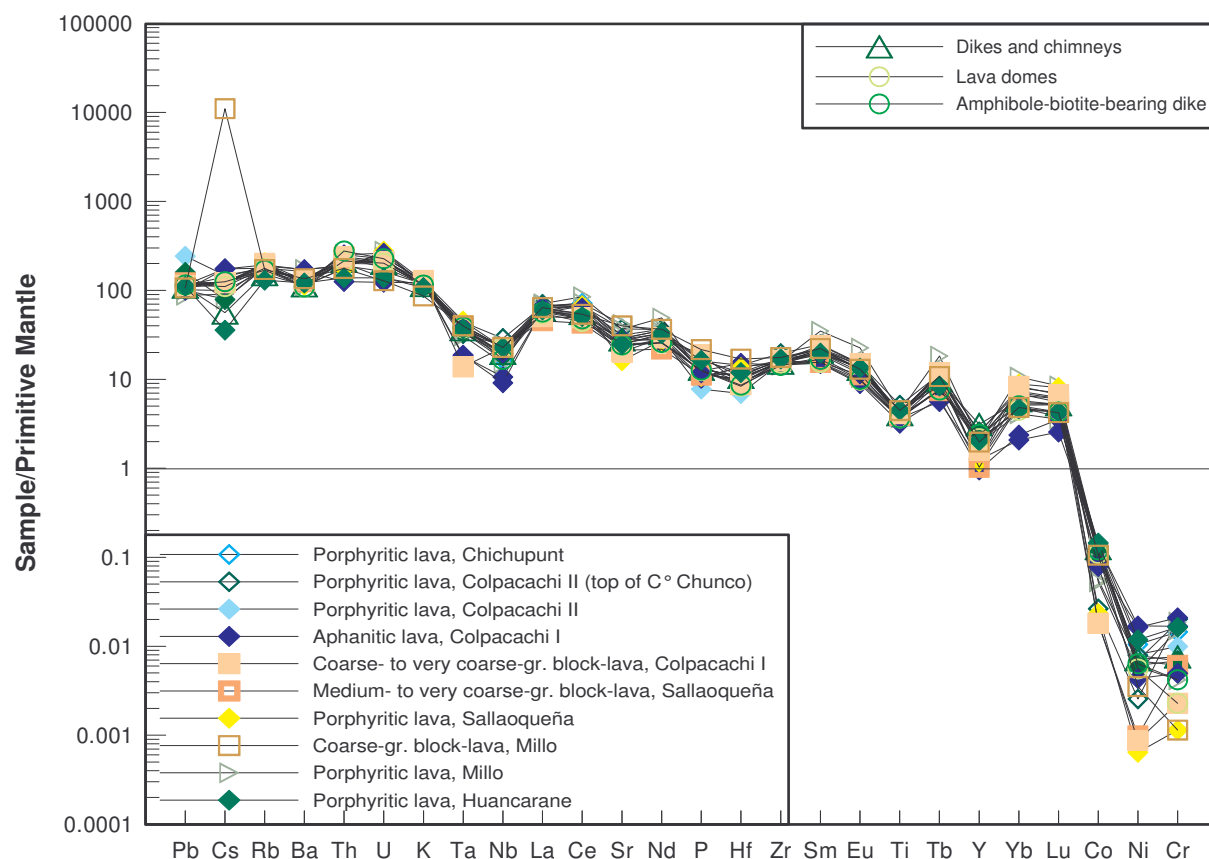


Fig. 38: Trace element distribution of the least-altered rocks at C° Millo normalized to primitive mantle (SUN & MC DONOUGH 1995). Major elements plus Rb, Ba, Nb, Sr, Nd, Zr: XRF; U: INAA; others: ICP-MS, REE data are corrected.

Fig. 39 shows the volcanic rocks of C° Millo according to tectonomagmatic environments as defined by PEARCE et al. (1984), i. e. ocean ridge (ORG), volcanic arc (VAG), within plate (WPG) and collision granites (syn-COLG and post-COLG).

In both diagrams the samples of the mapping area plot in the VAG field and show congruency with the reference data (PALACIOS et al. 1993) and geochemical data of Chilean granites (PEARCE et al. 1984).

The rocks are characterized by relatively high Rb and low Y, Nb, Yb and Ta concentrations. Two samples of aphanitic lava (77290, 77291) are most depleted in Ta, Nb, Y and Yb.

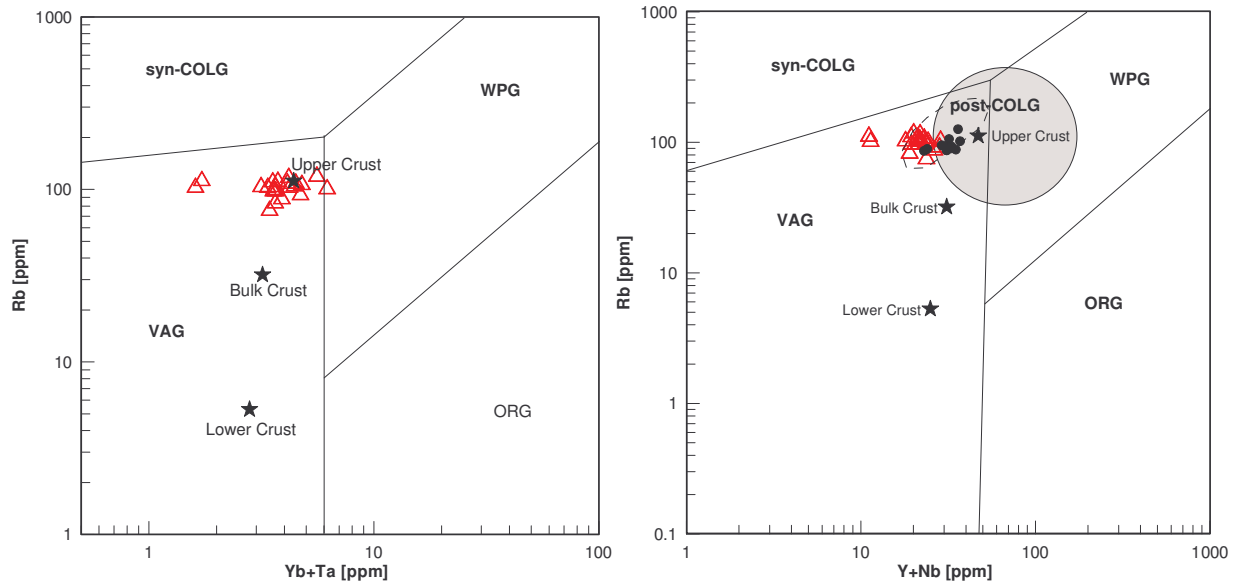


Fig. 39: The Rb-(Y+Nb) and Rb-(Yb+Ta) discrimination diagram for granitic rocks (PEARCE et al. 1984). Black points: reference data Barroso group (PALACIOS et al. 1993), triangles: C° Millo data (Rb, Nb: XRF; Yb, Ta: ICP-MS).

The relatively low Ta, Nb, Y and Ti concentrations in the rocks (Fig. 39) might be explained by storing in garnet and clinopyroxene of the subducted plate (eclogite).

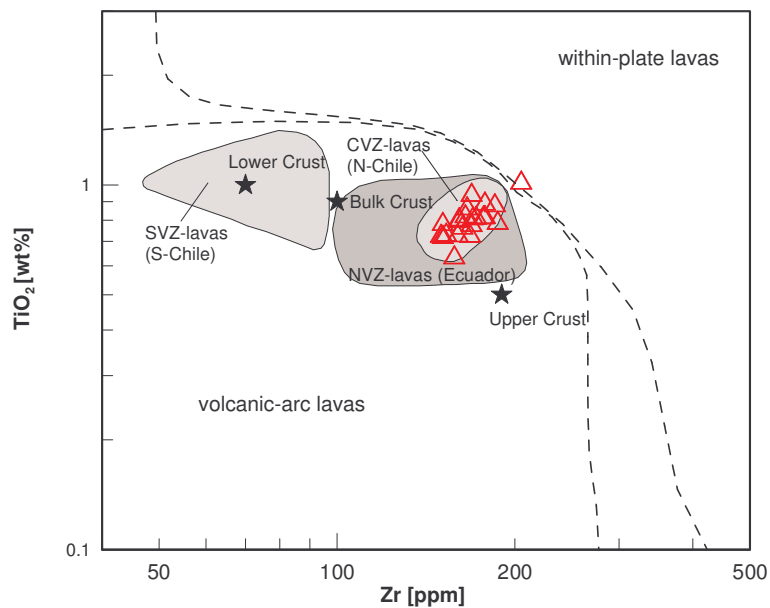


Fig. 40: TiO<sub>2</sub>-Zr variation diagram (XRF data) (THORPE et al. 1984).

THORPE et al. (1984) used the TiO<sub>2</sub>-Zr variation diagram to distinguish between magmatic rocks at active continental margins (volcanic arc lavas) and rocks which were generated in an intraplate setting (Fig. 40). The volcanic rocks of the mapping area plot as volcanic arc lavas.

Fig. 41 shows a modified Th-Ta-Hf diagram for basaltic rocks. The volcanic rocks of the mapping area plot in the VAB field and in the VAB/WPB transition zone (PEARCE 2002). The remarkable depletion of the C° Millo rocks in Ta and Hf in contrast to the relatively high concentration of Th, which is similar in behaviour to Rb, i. e. mobile in subduction zone fluids, indicates enrichment in the mantle wedge. On the other hand, Th is also an indicator for crust-magma interaction, i. e. assimilation of crustal rocks (arrows).

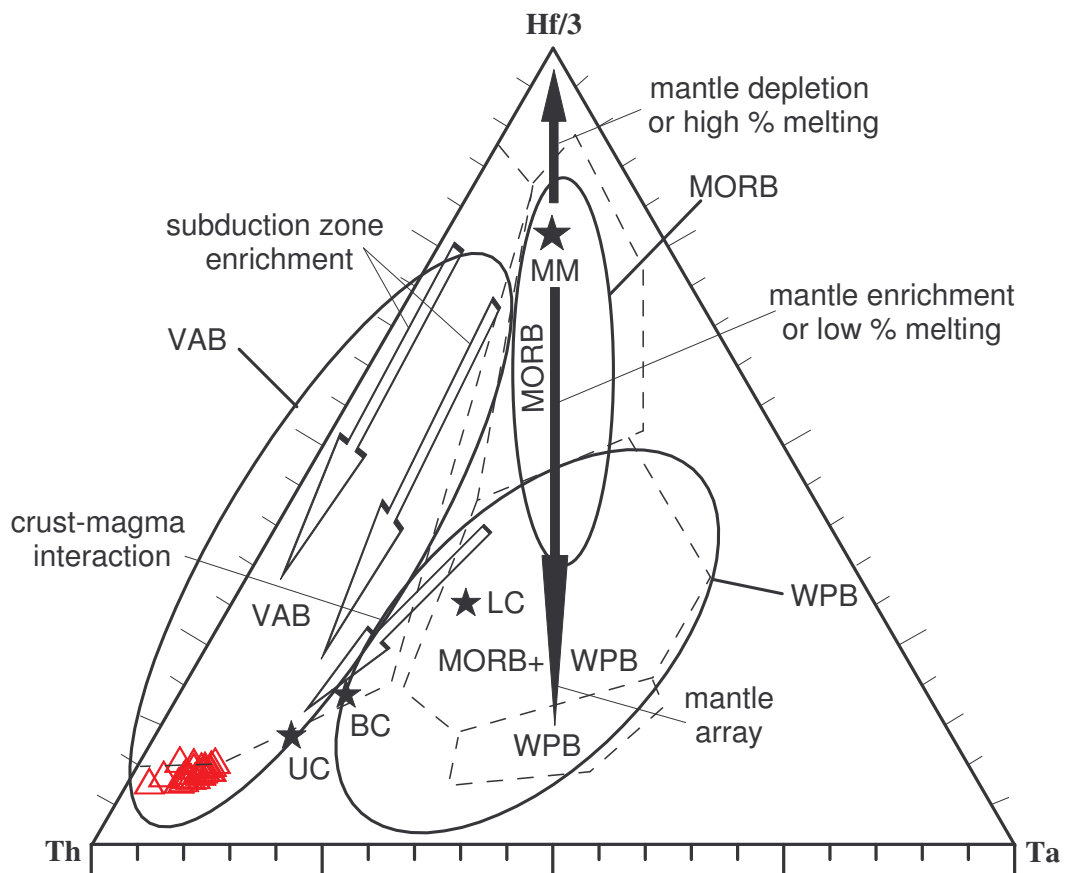


Fig. 41: Th-Ta-Hf triangular diagram distinguishes between WPB (within-plate basalt), MORB (mid-ocean ridge basalt) and VAB (volcanic arc basalt) (WOOD et al. 1979) (dashed lines). MM: Morb-mantle and ellipses indicating basalt fields of PEARCE (2002) (XRF data).

BAILEY (1981) recognized four types of andesite (Fig. 42). The Andean or active continental margin andesite (which could be called Central Andean andesite) is characterized by elevated La/Yb (mainly 12-20), which indicates a high degree of continental crust involved in magma genesis (see below). The low Sc/Ni (below 0.5) is typical for the continental crust and is a further indication of assimilation processes.

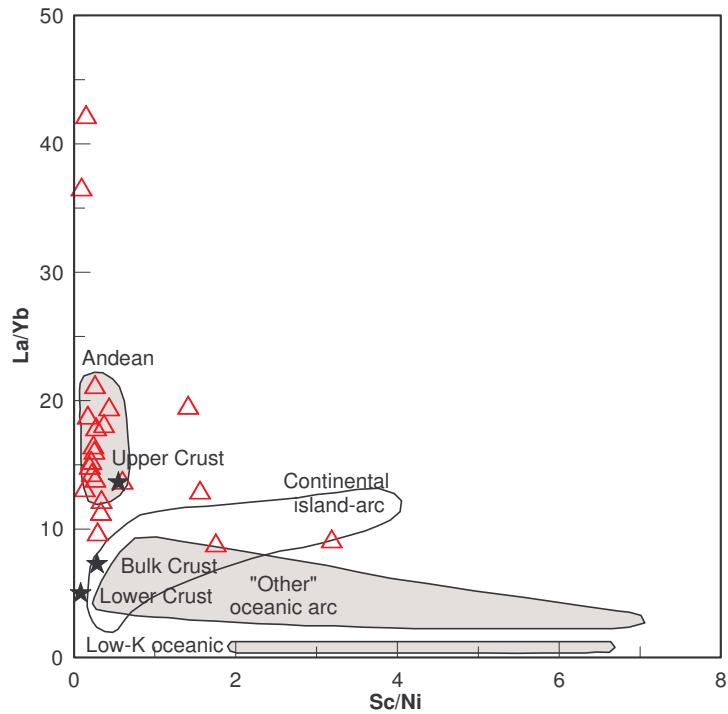


Fig. 42: La/Yb-Sc/Ni discrimination diagram for andesites (Sc: INAA; La, Yb, Ni: ICP-MS) (BAILEY 1981).

PEARCE (2002) plotted Th and Nb both normalized to Yb, of which the element ratio is supposed to be unaffected by partial melting and fractional crystallization (Fig. 43).

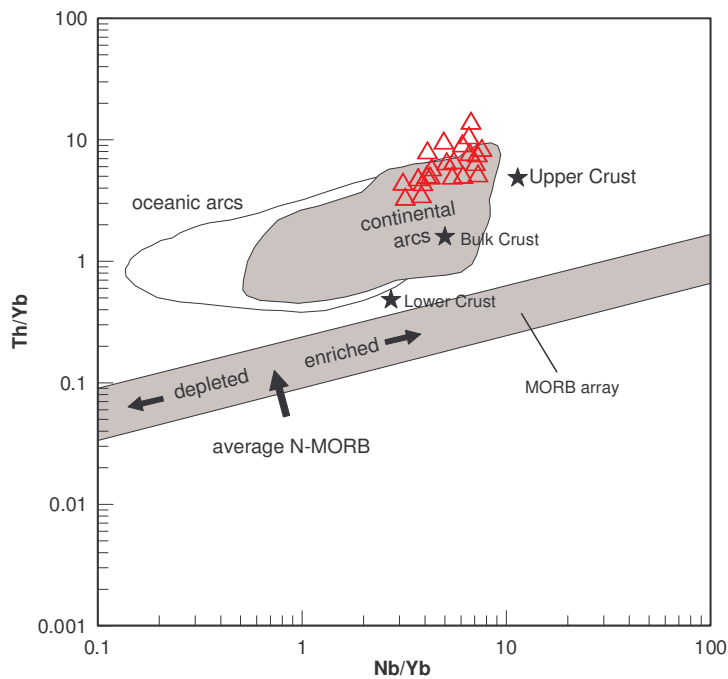


Fig. 43: Th/Yb-Nb/Yb diagram shows subduction-related and oceanic rocks derived from depleted and enriched sources (Nb: XRF; Th, Yb: ICP-MS) (PEARCE 2002).

The samples from C° Millo plot in the upper part of the continental arc field “above” the enriched MORB array. This leads to the conclusion that the Th concentration of the magmas is not explainable by enrichment of the mantle wedge alone and it seems that crustal assimilation plays an important role.

Fig. 44 shows a multielement plot for the REE data, Th, Nb, Ta and Zr normalized to average chondrite (ANDERS & GREVESSE 1989).

Samples of the individual rock units plot close together and display better their identity than in most previous bivariate and triangular rock type classification plots. Especially the aphanitic lava samples show congruency. The porphyritic lava from the Sallaoqueña event has similar Th, Ta, Nb, Zr and LREE abundances. The amphibole-biotite-bearing dike and the lava domes stress once more their petrologic unity.

All rocks, except for aphanitic lava and sample 77285, which was mapped as porphyritic lava of the C° Millo event, have the same slightly enriched upper crust pattern. In comparison to bulk crust and lower crust composition the rocks are strongly enriched in Th and LREE and show slight enrichment of HREE. Taking N-Morb as reference, the enrichment of LREE and a slight depletion of HREE is evident.

The pattern can be interpreted by subduction, magmatic differentiation and crustal contamination. The LILE are mobile during subduction (e.g. Th, La) and are enriched in the mantle wedge. Light REE (e.g. Ce, Pr) are more incompatible than HREE and are therefore enriched during partial melting. Further enrichment of incompatible elements is due to fractional crystallization.

All rocks are characterized by strong negative Ta and Nb anomalies. These anomalies are more pronounced than for continental crust, and therefore indicate the important role of subduction-related processes during which Nb and Ta behave compatible with Al-cpx/garnet and are immobile (KEPPLER, oral communication 2004).

All rocks show a slight, negative Eu anomaly. The ratio of Eu/Eu\* is coherent in all samples and lies between 0.72 and 0.77. Mean value: 0.75. Europium is the only REE which is also present in the divalent state and then replaces Ca<sup>2+</sup> in plagioclase. Therefore the removal of plagioclase from a melt by crystal fractionation will give rise to a negative Eu anomaly in the melt. However, hydrothermal alteration also can lead to preferential Eu mobilization, which is less likely for the least-altered samples.

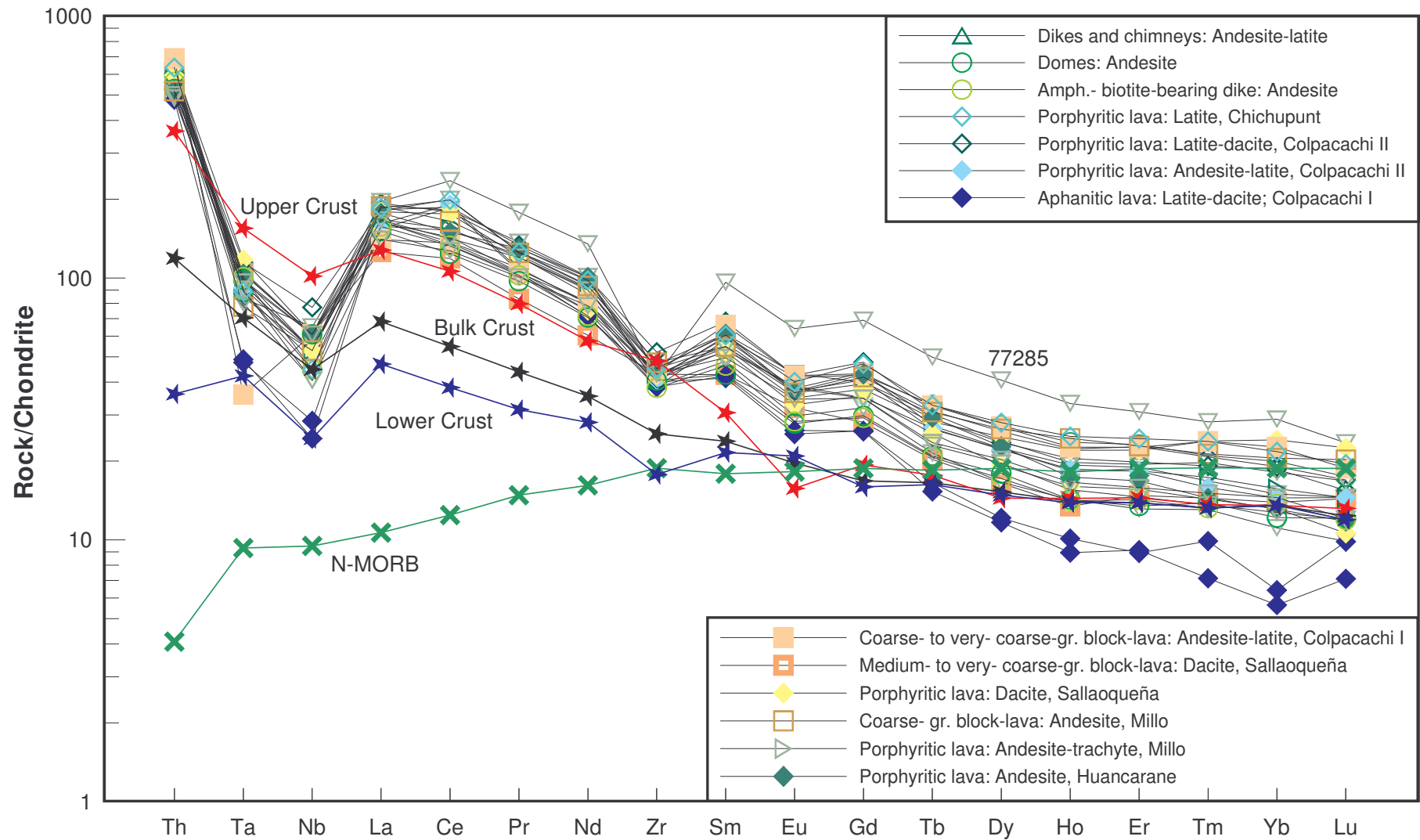


Fig. 44: REE pattern including Th, Ta, Nb and Zr of the least-altered rocks at C° Millo, SE Peru (REE, Th, Ta: ICP-MS; Nb, Zr: XRF). N-morb data from SUN & MC DONOUGH (1995).

### 7.5.4 Short review of published Cenozoic Central Andean isotopic data

JAMES et al. (1976) subdivided the Pliocene to Quaternary volcanic rocks, covering the high Andes of southern Peru, by using trace elements and isotopic geochemistry. They focussed on the Arequipa and Barroso volcanic rocks, which both belong to the Barroso Group (Fig. 45).

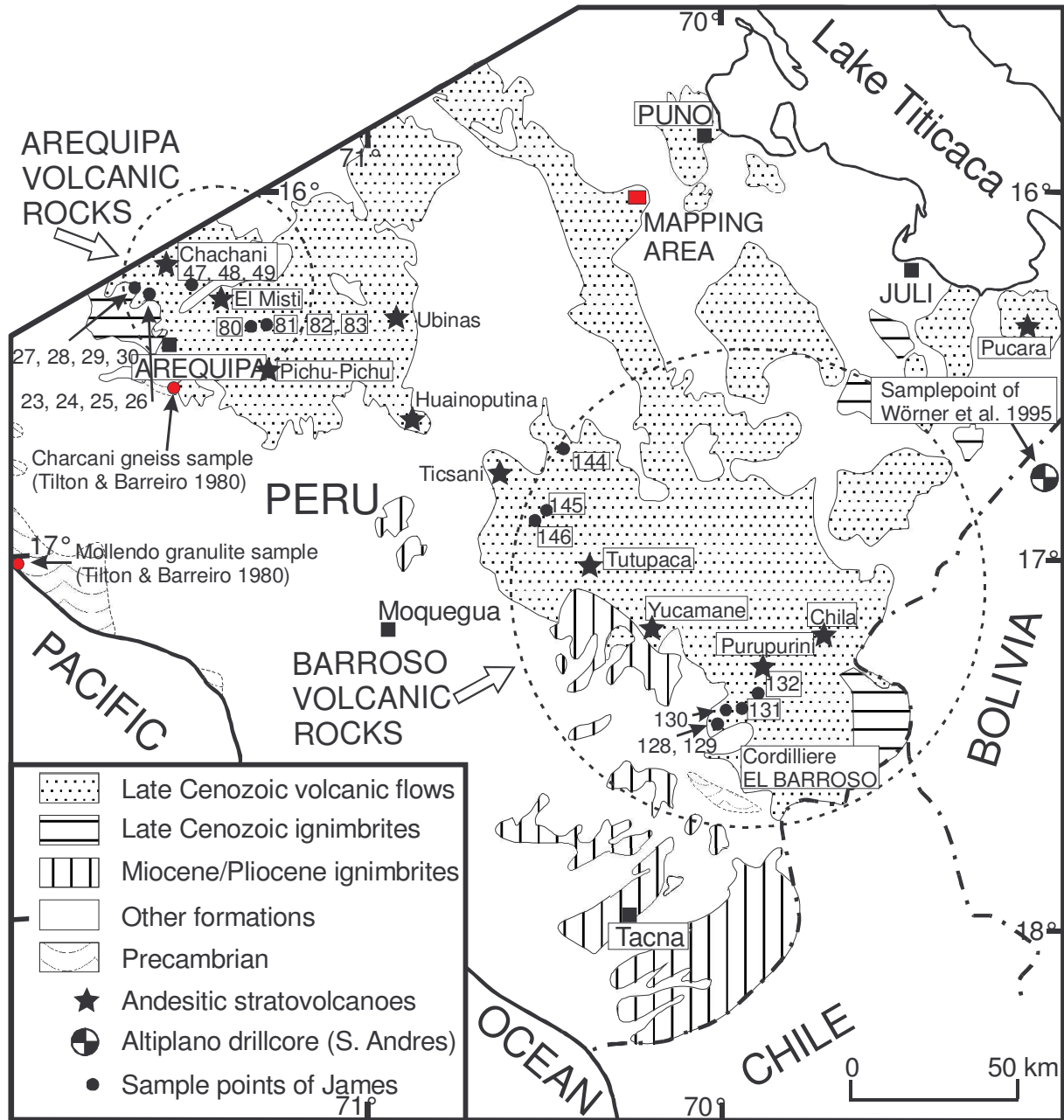


Fig. 45: Strongly simplified geological map of southern Peru with probable extent of the Cenozoic volcanic rocks of the Barroso Group according to JAMES et al. (1976) and JAMES (1982). Location of Altiplano drillcore according to LEHMANN (1978).

The Barroso volcanic rocks of the mapping area are slightly depleted in Sr (~540-680 ppm) and enriched in Rb (~80-115 ppm, Fig. 46) when compared to the reference data of JAMES (1976), and can be interpreted as the most evolved members of a general “Barroso trend”.

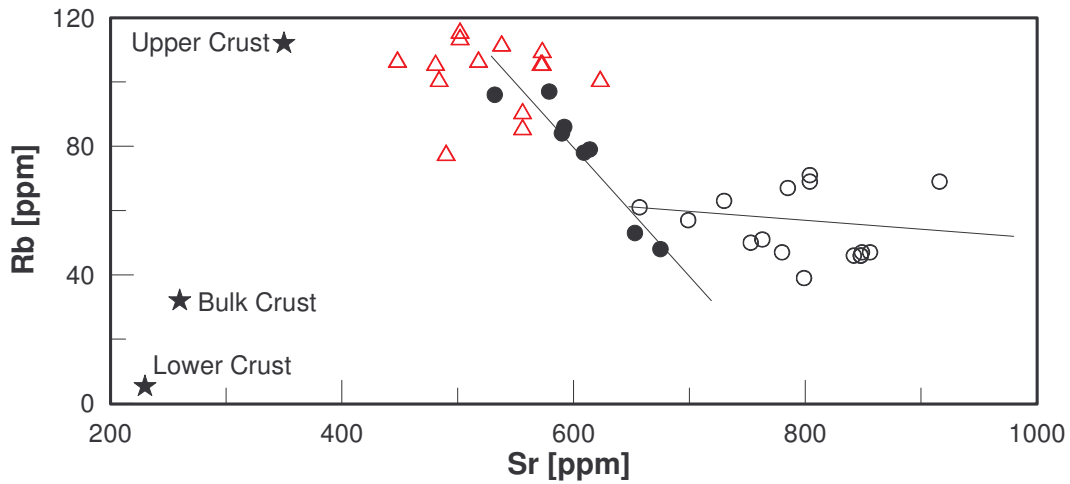


Fig. 46: Variation of Rb and Sr concentration of Cenozoic volcanic rocks in the Central Andes. Open circles: Arequipa volcanic rocks (JAMES 1976), closed circles: Barroso volcanic rocks (JAMES 1976), triangles: C° Millo data excluding Maure Group and altered rocks (own data, XRF). Solid lines define approximate trends (adapted from JAMES 1982).

$^{87}\text{Sr}/^{86}\text{Sr}$  ratios (JAMES 1982) are plotted vs. Rb/Sr (Fig. 47). The correlation of  $^{87}\text{Sr}/^{86}\text{Sr}$  with Rb/Sr probably results from the assimilation of crustal rocks with elevated  $^{87}\text{Sr}/^{86}\text{Sr}$  and relatively high Rb/Sr ratio by a mantle-derived magma (JAMES 1982).

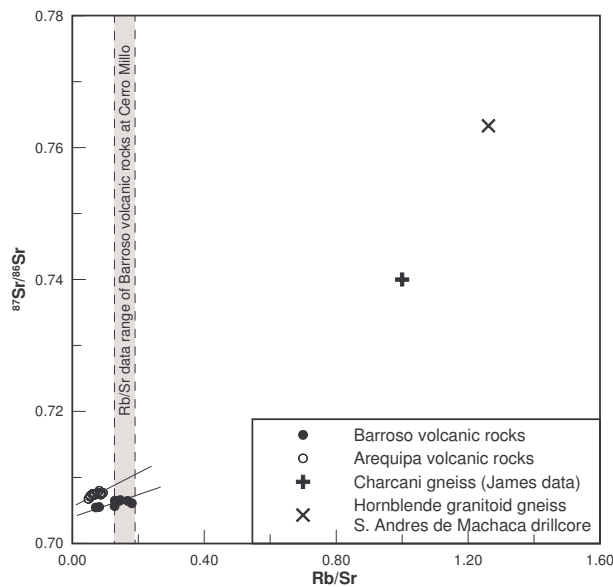


Fig. 47:  $^{87}\text{Sr}/^{86}\text{Sr}$  vs. Rb/Sr. Own data: XRF (Sources: JAMES et al. 1976, JAMES 1982, WÖRNER 1995).

The isotope ratios of Sr and Nd reveal the full range of petrogenesis from magma formation in the mantle wedge without crustal assimilation in Ecuador to significant assimilation of

crystalline basement rocks for the Barroso/Arequipa volcanic rocks, plotting in the continental crust quadrant (Fig. 48). The data are located far from the DMM component and close to EM 1 (Enriched Mantle, HART 1988). Therefore it is not attributable to metasomatic alteration of the mantle wedge alone. The data suggest crustal contamination of around 3 % (calculated Sr ratio of JAMES (1982) in primary Barroso lava: 0.705).

The contamination model is consistent with the REE pattern, which has mainly continental signature (Fig. 44).

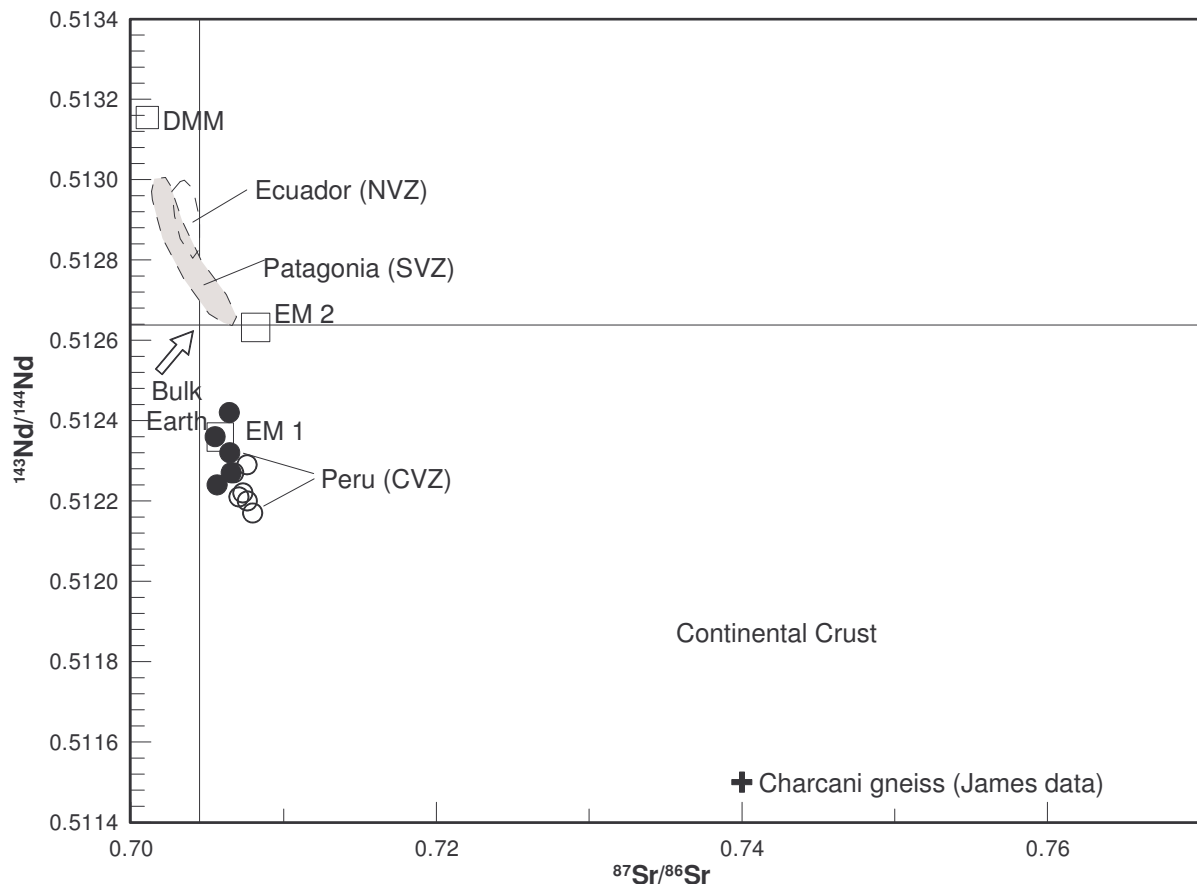


Fig. 48: Sr-Nd mixing diagram of Late Tertiary andesites and basalts of the Andes. Symbols as in Fig. 47 (Sources: HAWKESWORTH et al. 1979b, HART 1988, JAMES 1982, WÖRNER et al. 1995).

The radiogenic isotope ratios of the volcanic rock suites suggest that the two volcanic series could have evolved from a similar source, interacting predominantly with a single crustal contaminant, here represented by the Proterozoic Charcani gneiss of southern Peru (Fig. 49).

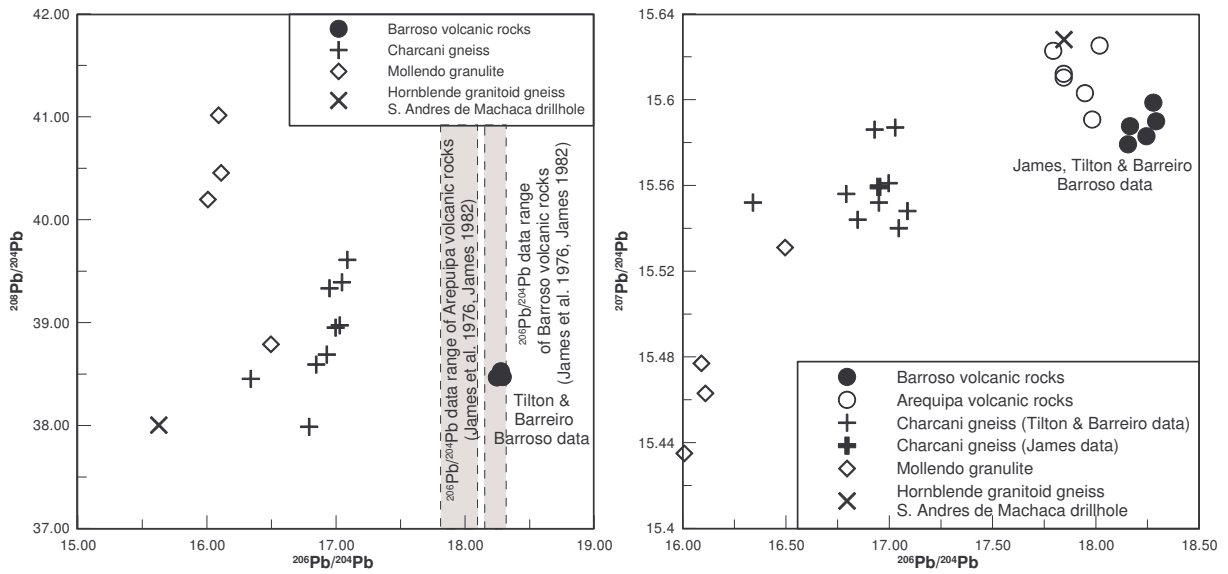


Fig. 49: Radiogenic isotopic variations in Barroso and Arequipa volcanic rocks and their isotopic relationship to the crystalline basement rocks of the Arequipa Massif (Sources: JAMES et al. 1976, JAMES 1982, LEEMAN unpublished data, TILTON & BARREIRO 1980).

### 7.5.5 Rock classification of the altered rocks

Alteration has largely obliterated the primary mineralogy, and the mobility of major elements such as Na, K, and Si does not allow to use the TAS diagram. Therefore, immobile elements are used, with Zr/Ti as a proxy for Si, and Nb/Y as a proxy for total alkalis (Fig. 50).

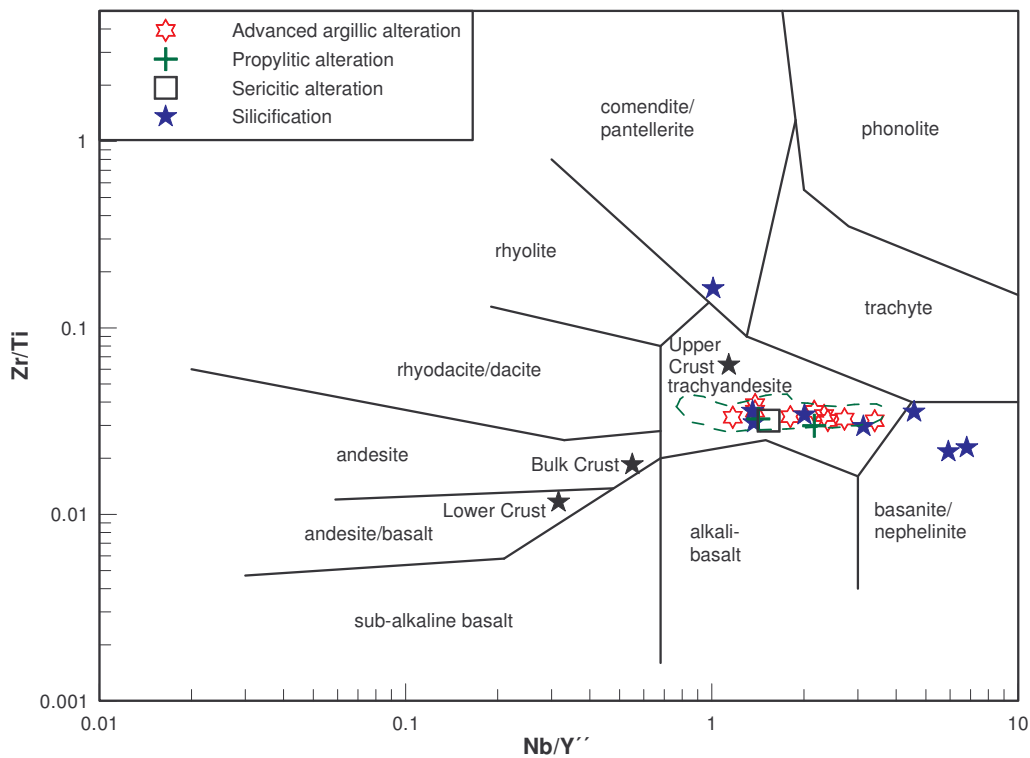


Fig. 50: Classification of altered rocks according to WINCHESTER & FLOYD (1977). Green dashed area marks data range of least-altered rock equivalent. Some highly silicified rocks with Nb/Y > 10 plot outside of the diagram (Ti, Zr, Nb: XRF; Y: ICP-MS).

In analogy to the least altered rocks, which are plotted for reference in Fig. 50, the altered rocks can be classified as trachyandesite or latite, respectively. The tendency towards basanite/nephelinite and trachyte (shift to higher Nb/Y) is probably due to mobility of Y.

The  $\text{SiO}_2\text{-Zr/TiO}_2$  diagram shows the advanced argillic altered rocks plotting congruent to the least-altered rock data in the andesite to dacite root field (Fig. 51). Silicification leads to rhyolitic chemism.

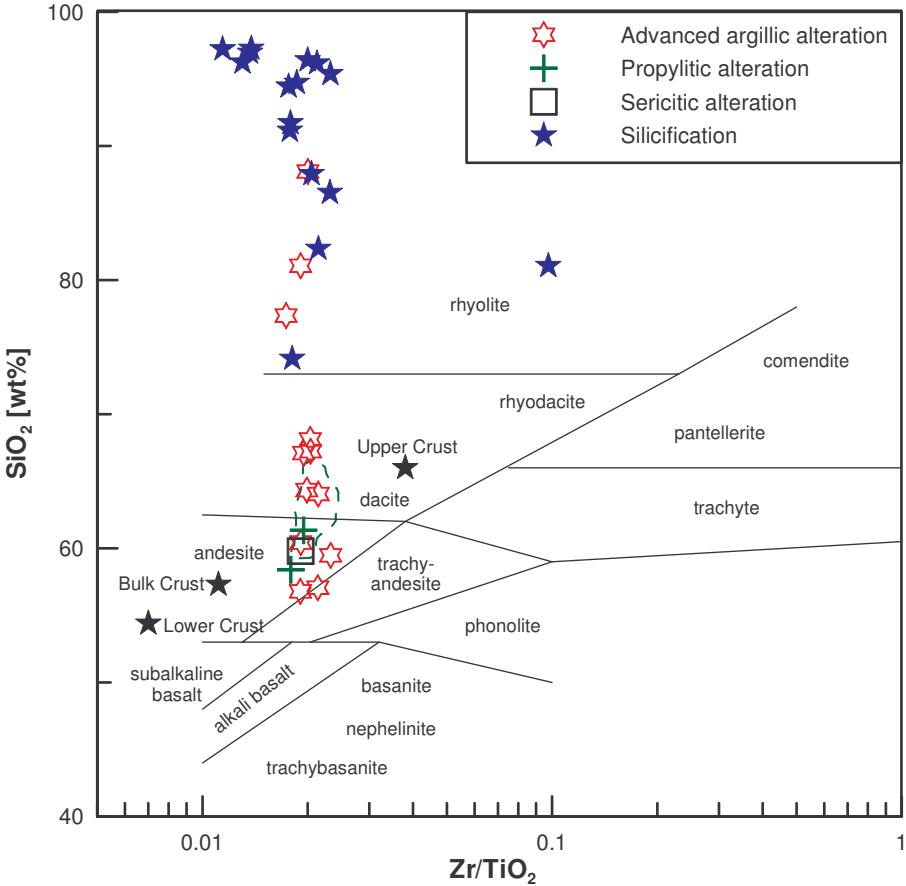


Fig. 51:  $\text{SiO}_2\text{-Zr/TiO}_2$  diagram according to WINCHESTER & FLOYD (1977). Data range of the least-altered rocks is marked by a dashed line (XRF data).

### 7.5.6 Geochemistry of the hydrothermal alteration

Hydrothermal alteration results from water-rock interaction during which the primary magmatic mineralogy/composition of the rock is modified due to mobilization of certain elements (addition and removal).

The altered rocks at C° Mollo display both alkali enrichment ( $\text{Na}_2\text{O} + \text{K}_2\text{O} > 4 \text{ wt}\%$ ) and depletion ( $\text{Na}_2\text{O} < 2.5 \text{ wt}\%$ ,  $\text{K}_2\text{O} < 3 \text{ wt}\%$ ).

The advanced argillic altered rocks have characteristically high sulfur concentrations (7.3-1.9 wt% S, mean=4.3 wt% S, n=12). Silicification is characterized by silica abundances between 97 and 74 wt%  $\text{SiO}_2$  (mean: 91.2 wt%  $\text{SiO}_2$ , n=16). The remainder, two propylitic altered rocks are separated from the sericitic altered rock sample by lower  $\text{Na}_2\text{O}$  and  $\text{K}_2\text{O}$ .

An overview of element mobilization give Figs. 52 and 53 in which mean element concentrations of the several alteration styles are normalized to the least-altered rock equivalent.

The mobility of the elements generally increases from propylitic and sericitic to advanced argillic alteration and silicification.

Major elements: Advanced argillic altered rocks are enriched and sericitic/propylitic altered rocks are slightly depleted in silica.

Distinct depletion show  $\text{Fe}_2\text{O}_3$ , MnO, MgO, CaO and  $\text{Na}_2\text{O}$  in advanced argillic altered rocks, which is caused by break-down of plagioclase and biotite. Silicified rocks show in addition a drastic depletion of  $\text{Al}_2\text{O}_3$  which is due to dilution of clay minerals such as kaolinite, illite and smectite (Fig. 52).

Propylitic alteration leads to slight depletion in MnO, MgO, CaO,  $\text{Na}_2\text{O}$  and  $\text{K}_2\text{O}$ , whereas the same elements appear to be slightly enriched in sericitic altered rocks. But it should be considered that the interpretation of the propylitic and sericitic altered rocks is based on very few samples.

The increase of LOI (loss on ignition) for advanced argillic altered rocks is due to neoformation of clay minerals, such as kaolinite, and alunite. Alunite is a diagnostic mineral for advanced argillic alteration with the bulk formula  $\text{KAl}_3(\text{SO})_4(\text{OH})_6$  and carries an unstable  $\text{SO}_4$  group (highest LOI=18.5 wt%). High LOI in propylitic altered rocks is derived from the addition of  $\text{H}_2\text{O}$  in the formation of new hydrous phases, particularly chlorite.

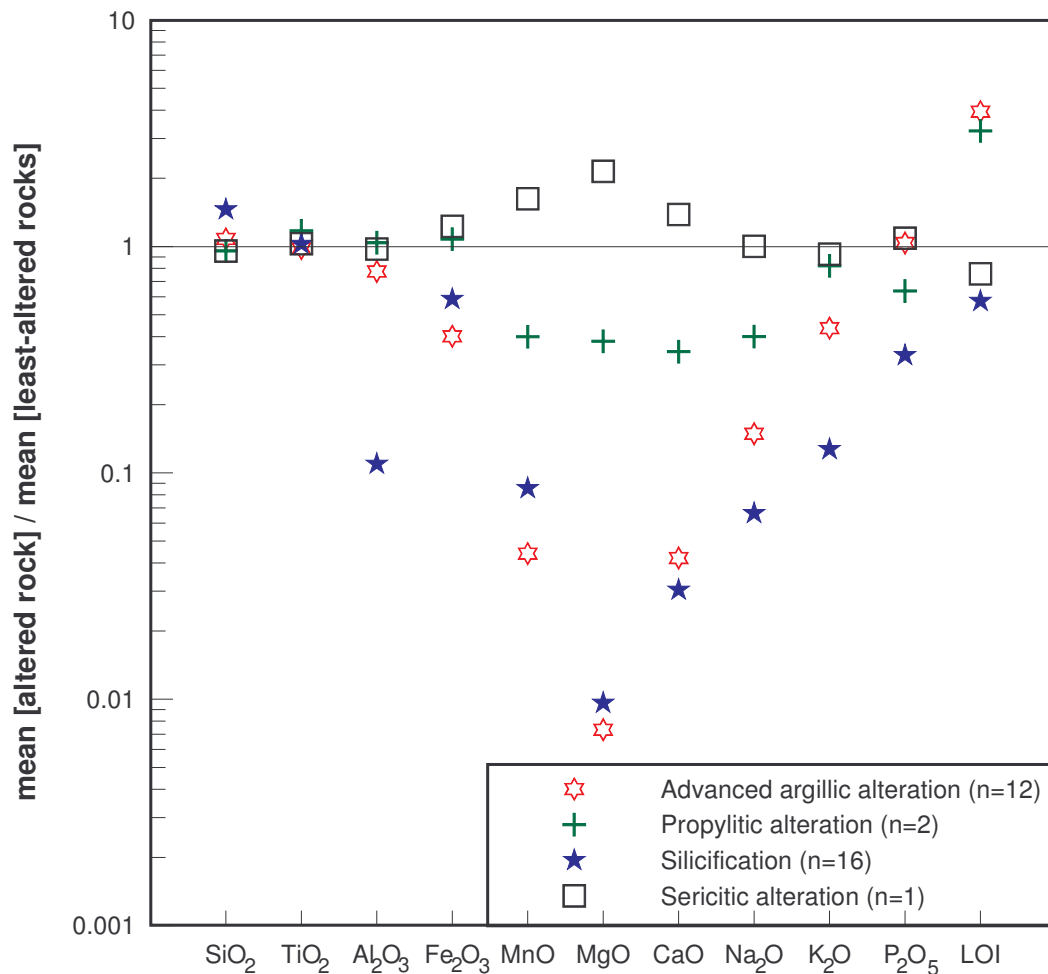


Fig. 52: Major element concentration (XRF) plus LOI (grav.) of the wall rock alteration styles at C° Millo gold prospect normalized to least-altered rocks.

Trace elements: The high field strength (HFS) elements Ti, Zr, Nb, Hf, Ta remain mainly immobile due to their low solubility. The large ion lithophile elements (LIL-elements) K, Rb and Cs are all mobile and depleted. Sr, which should behave similar due to break-down of plagioclase is enriched in advanced argillic altered rocks.

Ba (LIL-element) and U (HFS-element) are relatively soluble in aqueous liquids but remain immobile during the hydrothermal processes at C° Millo. The transition elements (Cr, Co, Ni, Cu, Zn) are mobile and depleted in the course of alteration (Fig. 53).

Hg is the most enriched element in the hydrothermal system followed by Sb, Bi and As, elements which are mobile at low temperatures. Se and Te are slightly enriched.

Of mineralogical interest is the strong depletion of Cs, Rb and K<sub>2</sub>O especially in advanced argillic altered rocks. This is due to the instability of K-bearing minerals, such as biotite and hornblende, in which Rb and Cs are substituted atomically.

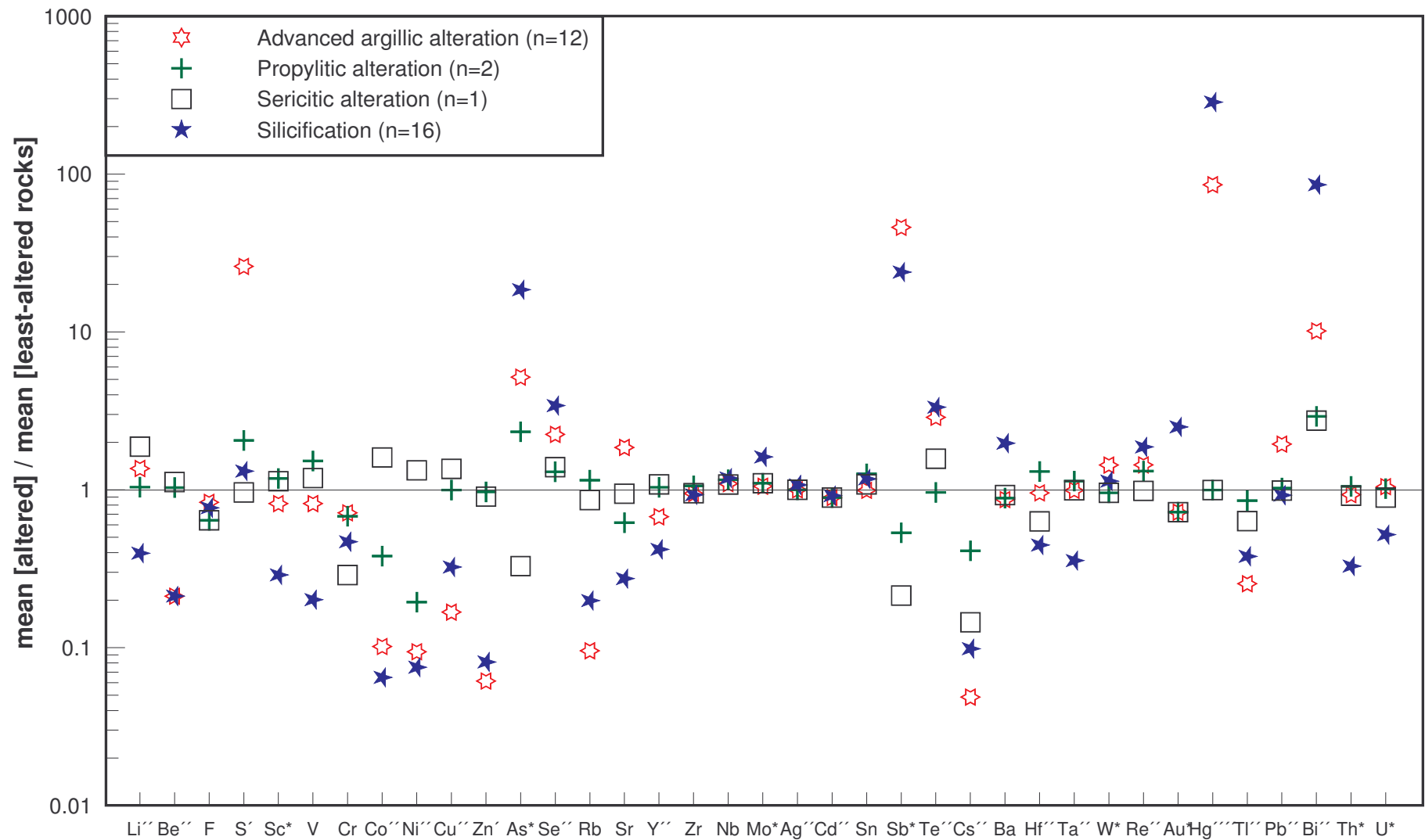


Fig. 53: Trace element concentration of the alteration types at C° Millo normalized to least-altered rock. (F, V, Cr, Sr, Zr, Nb, Sn, Ba: XRF; S, Zn: ICP; As, Mo, Sb, W, Au, Th, U: INAA; Hg: AAS-CV; others: ICP-MS).

The  $K_2O$ - $Na_2O$  variation diagram (Fig. 54) clearly distinguishes the least-altered rocks and the altered rocks.

Na is mainly related to the albite-component in feldspars and tributary to amphibole. K is related to biotite and sanidine.

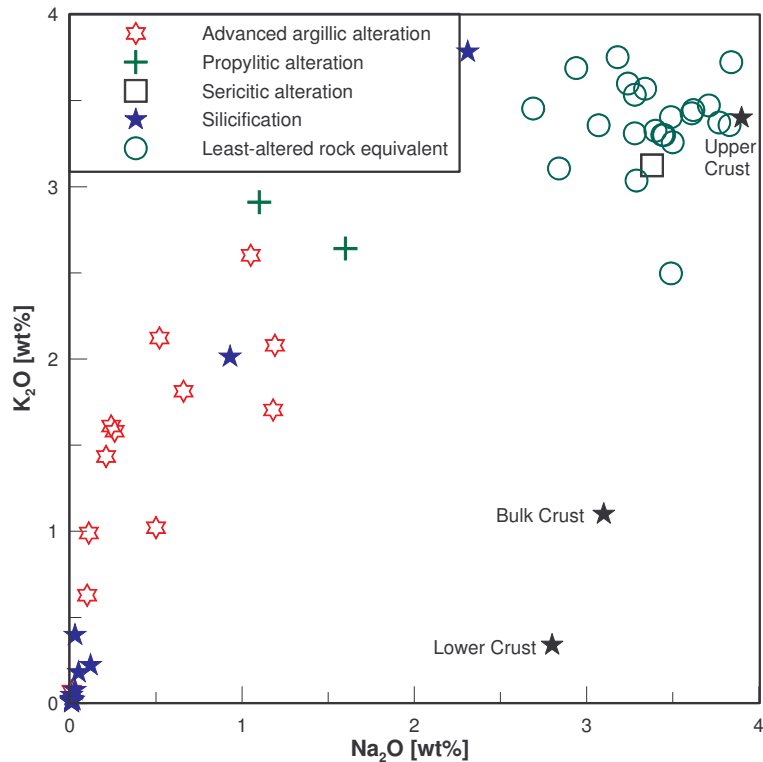


Fig. 54:  $K_2O$ - $Na_2O$  variation diagram shows the geochemical separation of the altered and least-altered rocks and the alteration-style specific depletion in the two major elements (XRF).

The sericitic altered rocks show slight depletion in  $K_2O$ , which indicates the release of K from destroyed biotite and refixation in newly formed sericite.

The propylitic alteration at C° Millo shows in contrast to MEYER & HEMLEY (1976) appreciable leaching of  $Na_2O$ .  $K_2O$  is slightly depleted. This phenomenon might be explained by opacitization of amphibole and biotite, and slight sericitization of plagioclase, which accompanies propylitic alteration and releases Na.

$Na_2O$  and  $K_2O$  are significantly leached in the course of feldspar-destructive alteration processes (advanced argillic alteration and silicification). The relatively high  $K_2O$  concentrations in comparison to  $Na_2O$  are caused by neoformation of alunite ( $KAl_3(OH)_6(SO_4)_2$ ). Extreme leaching/dilution characterizes silicification above 95 wt%  $SiO_2$ .

The K<sub>2</sub>O-CaO variation diagram (Fig. 55) shows the CaO concentrations of the least-altered rocks ranging from 1 to 5 wt%. This range is explainable by opacitization of amphibole and slight sericitization of plagioclase (especially of the anorthite-rich core). Further depletion of CaO and K<sub>2</sub>O is due to propylitic alteration and underlines destruction of the anorthite component, biotite and amphibole. Silicified and advanced argillic altered rocks are totally leached in terms of CaO.

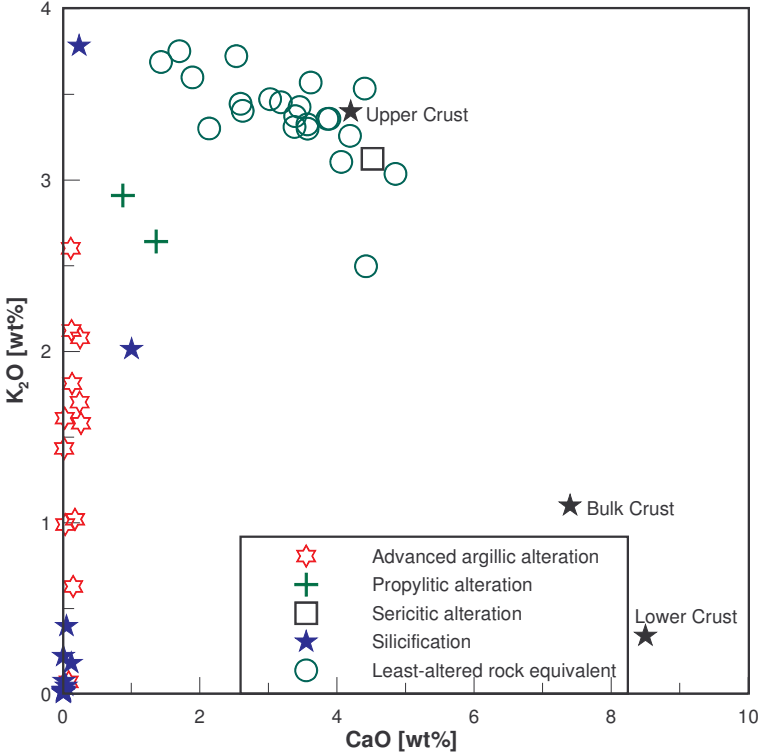


Fig. 55: CaO-K<sub>2</sub>O variation diagram showing incipient alteration of the least-altered rocks (XRF).

Fig. 56 shows the relationship of  $Al_2O_3$ ,  $(Na_2O+CaO)$  and  $K_2O$ . Destruction of plagioclase and amphibole and as a consequence thereof the decrease in  $Na_2O+CaO$  and the relative increase of  $Al_2O_3$  is appropriate to all alteration styles except for the sericitic altered rock sample. Even the least-altered rock equivalent shows a tendency towards sericite and illite (slight sericitization).

The propylitic altered rocks are not enriched in  $CaO$  and  $Na_2O$  in conflict to the microscopically observed epidote blastesis on veins and in vugs, which is possibly due to superposition of newly formed sericite and clay minerals.

The classification of the advanced argillic altered rocks into a mainly kaolinite-dominated and a more strongly alunite bearing type is indicated. In the alunite type illite and smectite minerals cannot be excluded.

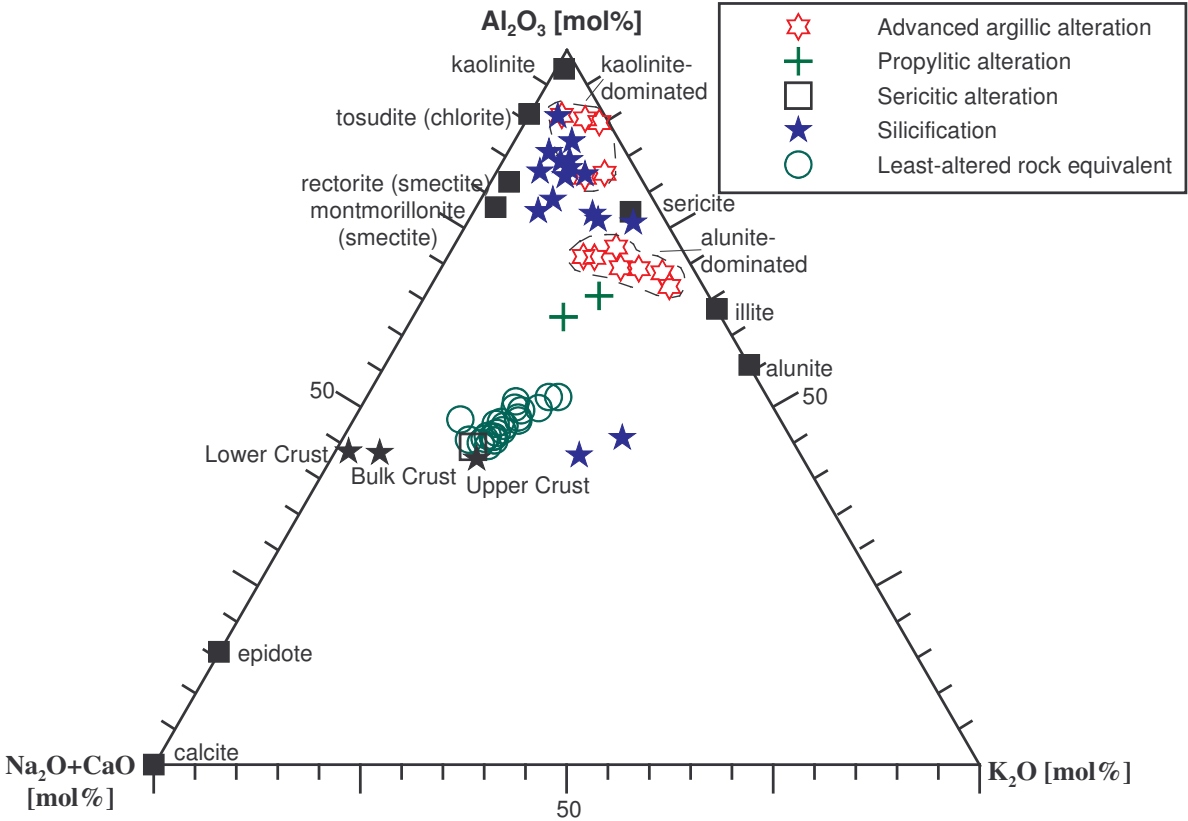


Fig. 56:  $Al_2O_3$ - $(Na_2O+CaO)$ - $K_2O$  triangular diagram showing the least-altered rocks and altered rocks of C° Millo (XRF). Reference data: kaolinite, sericite and montmorillonite (DEER et al. 1962); rectorite, tosudite, illite, alunite, epidote and calcite (www.webmineral.com).

Evidence for alunite ( $\text{KAl}_3(\text{OH})_6(\text{SO}_4)_2$ ) as a main mineral phase in advanced argillic altered rocks gives Fig. 57 (S-K<sub>2</sub>O variation diagram). It shows K<sub>2</sub>O positively correlating with S for advanced argillic altered rocks.

The solid line gives the correlation of all advanced argillic altered rocks. The solid line with lozenges represents the S to K<sub>2</sub>O wt%-ratio of pure alunite (1.36:1).

It becomes clear that S is added to the rocks, not only in the form of alunite but also as disseminated pyrite (as confirmed by ore microscopy).

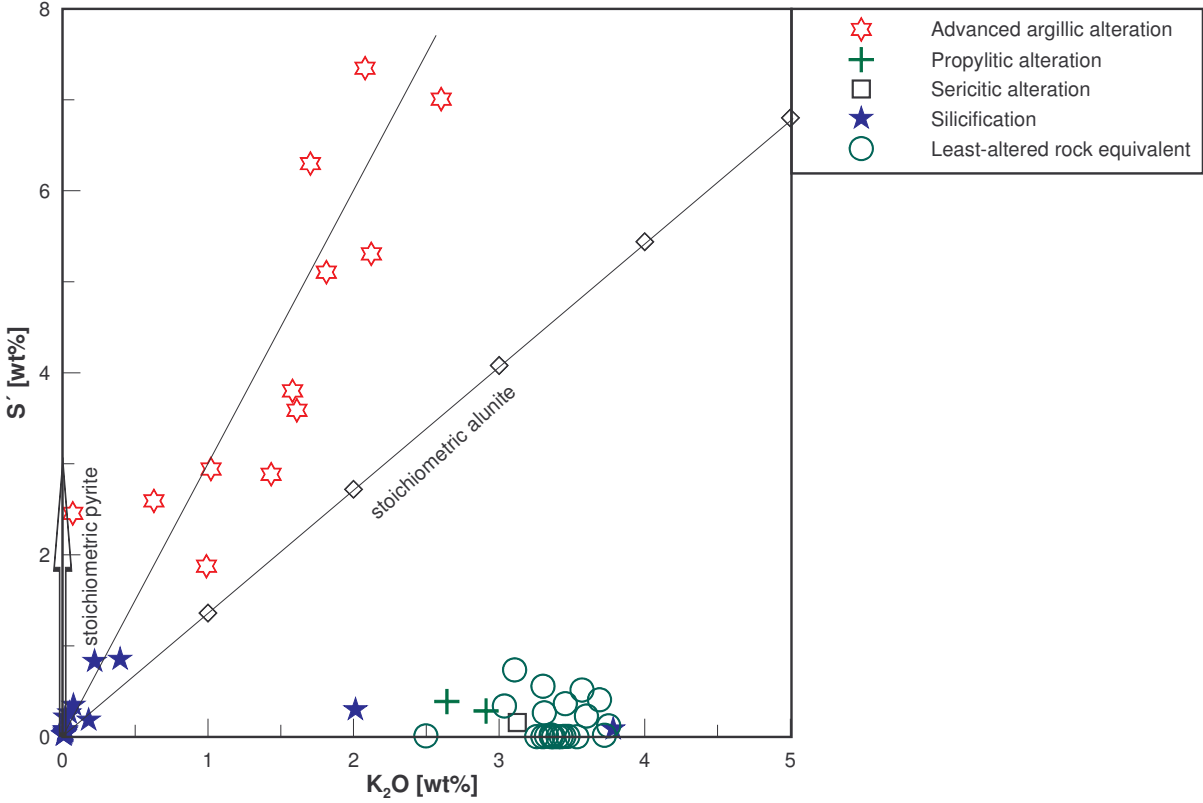


Fig. 57: S-K<sub>2</sub>O diagram (ICP-XRF): Evidence for alunite and pyrite in advanced argillic altered rocks.

The Ta-Nb variation diagram (Fig. 58) illustrates the low mobility of the HFSEs in the least-altered rocks, the propylitic altered rocks, sericitic altered rocks and in the bulk of the advanced argillic altered rocks. Crystal fractionation causes the positive correlation.

Ta depletion in silicified rocks is drastic. The strongly silicified samples are even diluted by a factor of over 10. Nb shows redistribution in strongly altered rocks and must therefore be mobile in the hydrothermal system.

This graph colours the mobility of the “immobile” HFS elements under strongly acidic conditions, because Nb must be added to compensate and to overcompensate the dilutional effect.

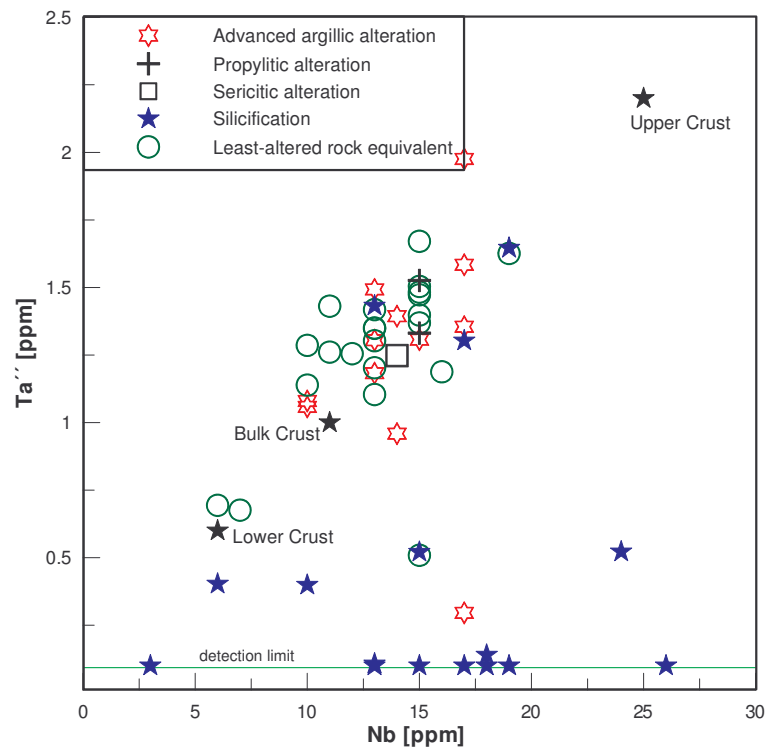


Fig. 58: Ta-Nb variation diagram showing the immobile character of the HFS elements (Ta: ICP-MS; Nb: XRF).

The Rb-K<sub>2</sub>O variation diagram (Fig. 59) shows that the least-altered rocks at C° Mollo have K/Rb ratios of 245-275 typical of intermediate volcanic rocks. The positive correlation of the two elements is explainable by atomic substitution/diadochy.

The propylitic alteration shows slight depletion of K<sub>2</sub>O, because biotite and sericite become instable. Rb is not depleted, probably because it is more firmly held in absorption positions of clay minerals than K.

The low content in Rb of the advanced argillic altered rocks indicates, in spite of elevated K, hydrothermal fractionation processes in which K becomes incorporated in alunite nearly exclusively, decoupled from Rb.

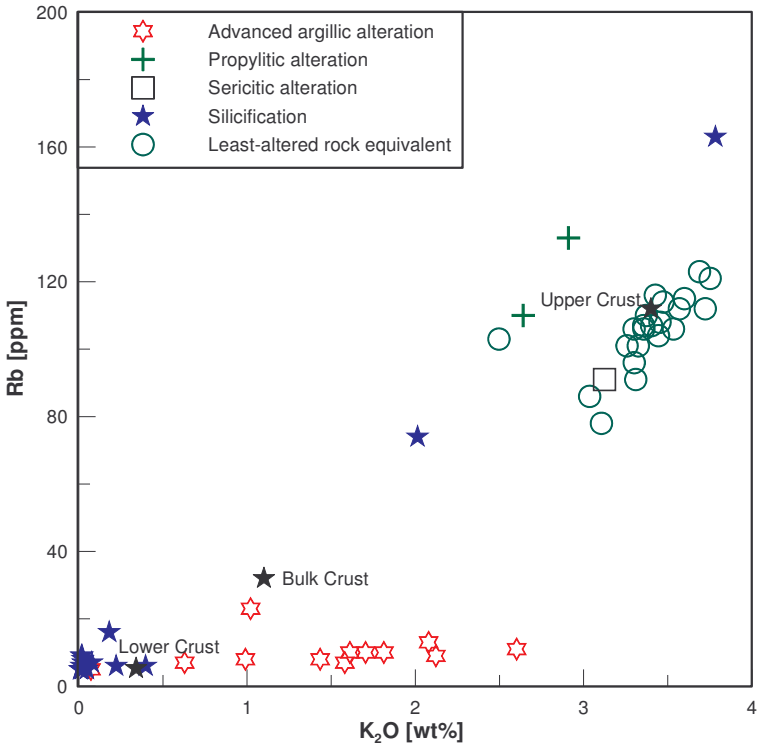


Fig. 59: Rb-K<sub>2</sub>O variation diagram (XRF).

The Zr-SiO<sub>2</sub> Harker diagram (Fig. 60) illustrates that the least-altered rock equivalent, the propylitic altered and the sericitic altered rocks have about 150-200 ppm zirconium. Advanced argillic altered rock samples have about 130-185 ppm Zr (samples >70 wt% SiO<sub>2</sub> are ignored). Advanced argillic altered rocks and silicified rocks show higher scatter in Zr. Especially the pervasively silicified rocks have both lowest and highest (20-305 ppm) Zr data.

These phenomena imply leaching of zircon due to extreme hydrothermal overprint and neoformation of zircon in some silicified rocks. Hydrothermal zircon is displayed in thin section of sample 77970 (Appendix, Photo 14) and verified by microprobe analysis.

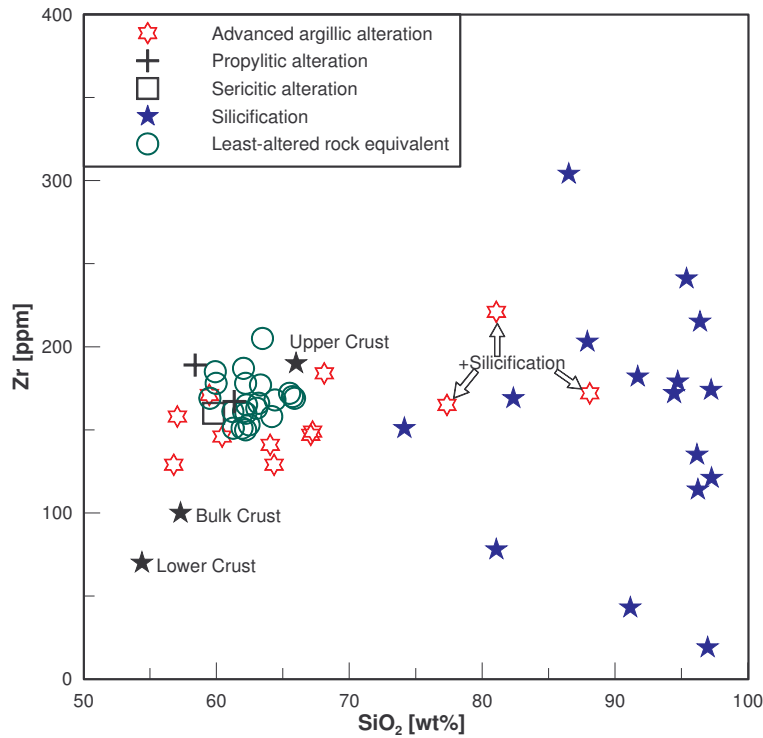


Fig. 60: Zr-SiO<sub>2</sub> Harker diagram (XRF).

Ba is even in advanced argillic altered rocks immobile while biotite and K-feldspar, the main K and therefore Ba carriers break-down (Fig. 61). The high SO<sub>4</sub><sup>2-</sup> content in the fluids responsible for alunite formation immobilizes barium because of the low solubility of BaSO<sub>4</sub>. Silicified rocks show either intensive leaching/dilution or strong enrichment of Ba (77970).

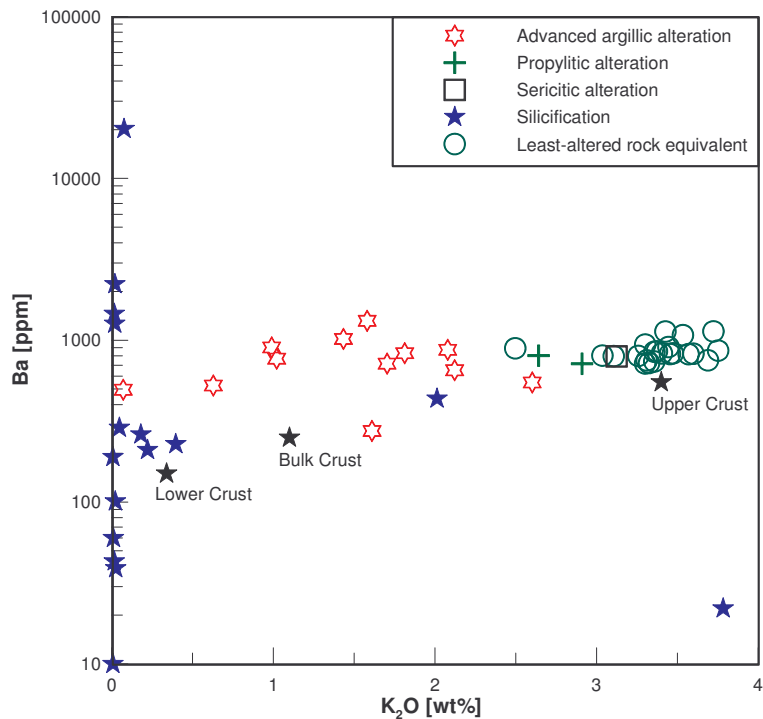


Fig. 61: Ba-K<sub>2</sub>O variation diagram illustrating the immobility of Ba (XRF).

In Fig. 62 (Zr-Ba variation diagram) the two elements do not show correlation but underline once more their drastic redistribution/solubility under extreme hydrothermal overprint, i. e. in very low pH solutions.

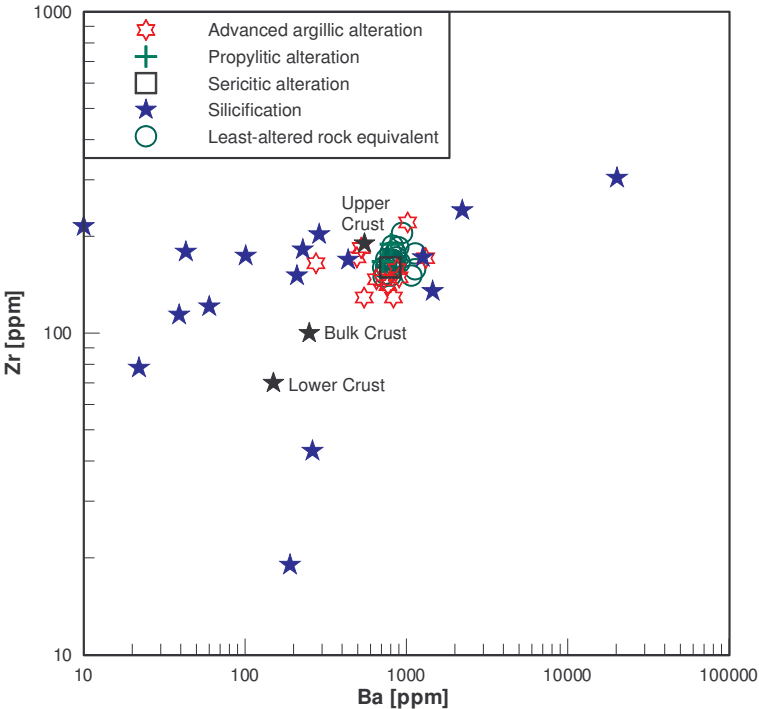


Fig. 62: Zr-Ba variation diagram illustrates the mobility of Zr and Ba in fluids (XRF).

Fig. 63: The Sr-CaO variation diagrams show the pronounced decrease in CaO during acid alteration with concomitant scatter of Sr at high level.

Sr and Ca correlate positively in the least-altered rock suite and in the advanced argillic altered rocks. This implies that Sr is related to plagioclase and kaolinite, which absorbs Sr and retains it stronger than Ca due to its more weakly hydration (KHASAWNEH et al. 1968). The absorption model explains inter alia the decrease of CaO in the hydrothermal system. The depletion of Sr in strongly silicified rocks might be explained by displacement of kaolinite by silica.

The enrichment of advanced argillic rocks in Sr in comparison to the least-altered rock suite indicates either high fluid fluxes or/and high absorption capacity of kaolinite. Atomic substitution of K by Sr in alunite is also possible, but on the other hand implausible because  $K_2O$  does not correlate with Sr in advanced argillic altered rocks.

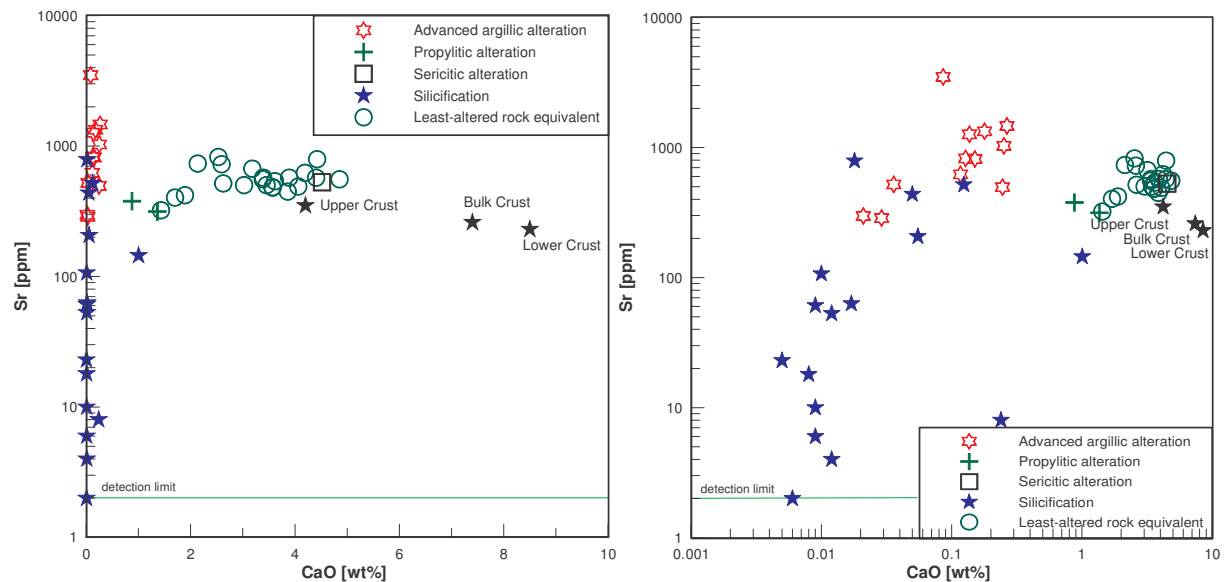


Fig. 63: Variation diagrams of Sr and CaO (XRF).

The hydrothermal system is very low in base and precious metals.

The elements of the copper group (Cu, Ag, Au) are except for rock sample 77970 (81 ppb Au) inconspicuous or near/below the detection limit.

Cu-Ni variation diagram (Fig. 64): The least-altered rocks show good correlation of Cu and Ni, which underlines their atomic affinity. The hydrothermally altered rocks are depleted in Ni and Cu, which is an expression of the high mobility of the base metals in acid fluids.

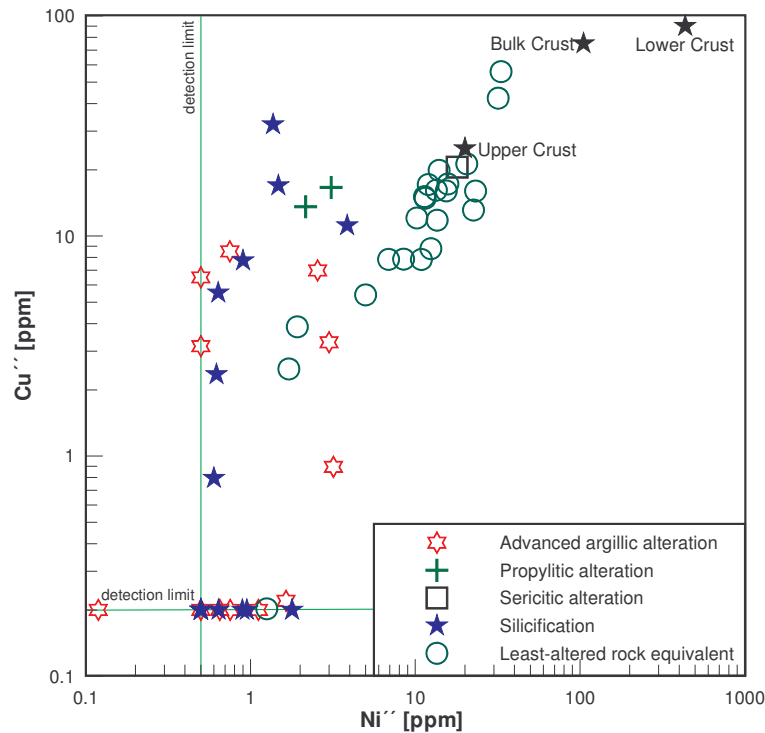


Fig. 64: Cu-Ni variation diagram shows the atomic affinity and high solubility of the two elements (ICP-MS).

Ni and Co strongly correlate and stress their similar solubility/chemical affinity (Fig. 65).

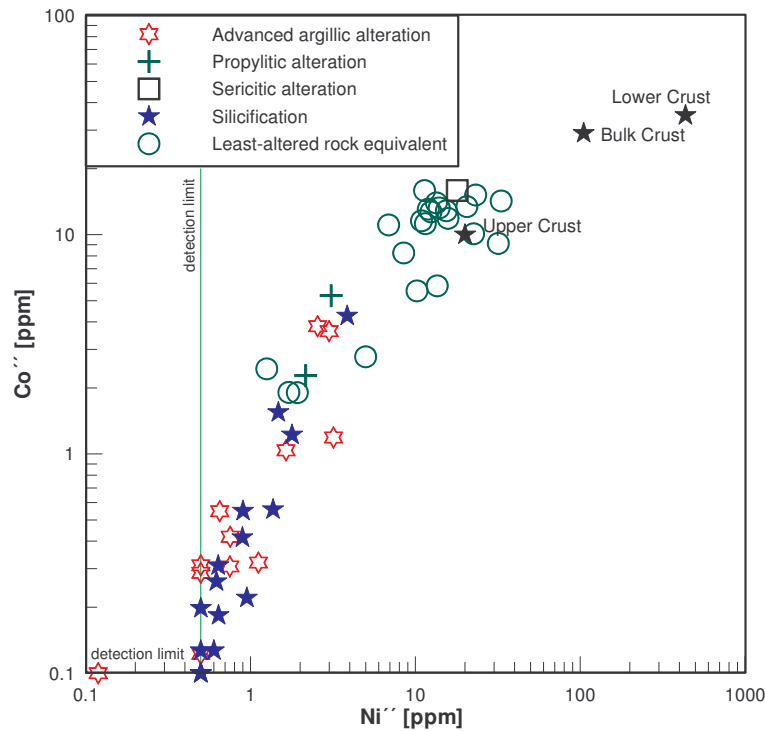


Fig. 65: Co-Ni variation diagram to illustrate the covariance of the transition elements (ICP-MS).

All handspecimens from C° Millo were measured for their magnetic susceptibility with the KT-5 susceptibility meter at the cutting surface. Rocks susceptibility is mainly an expression of the amount of magnetite.

The susceptibility-Na<sub>2</sub>O plot (Fig. 66) shows susceptibility up to  $30 \times 10^{-3}$  SI units for the least-altered rock equivalent, which responds to a normative magnetite constituent of 2.3-2.5 wt%. The magnetic susceptibility in propylitic altered rocks is lower ( $1.5-0.2 \times 10^{-3}$  SI units), which implies magnetite leaching.

In the advanced argillic, sericitic and silicified rocks susceptibility goes down to  $0.03 \times 10^{-3}$  SI units and indicates total destruction of all primary magnetite (Fig. 66), which releases V, Cr, Co, Ni as depicted in Figs. 64-65.

The relatively high magnetite content, in least-altered rocks, as reflected in magnetic susceptibility mostly  $>3 \times 10^{-3}$  SI units defines these rocks as of magnetite series (ISHIHARA 1977).

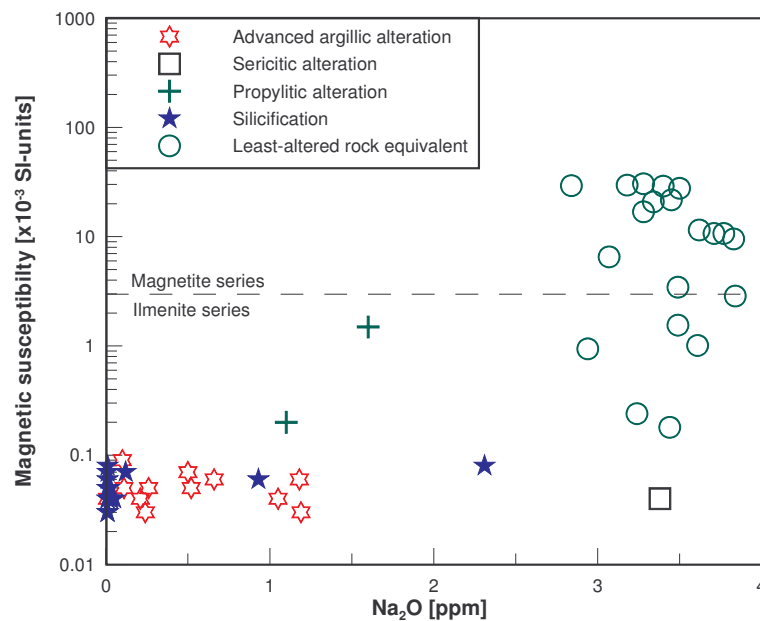


Fig. 66: Magnetic susceptibility versus Na<sub>2</sub>O plot (susceptibility meter, XRF).

Zn and Pb are plotted in Fig. 67 (Zn-Pb variation diagram). Zn shows a remarkable depletion in the hydrothermal system, which is explainable similar to Cu by its high solubility in acidic fluids. A correlation to Pb does not exist. Both elements give a scatter distribution.

Obviously is the Zn concentration relatively constant in advanced argillic altered and silicified rocks implying fixing by highly absorbing clay minerals of the kaolinite group.

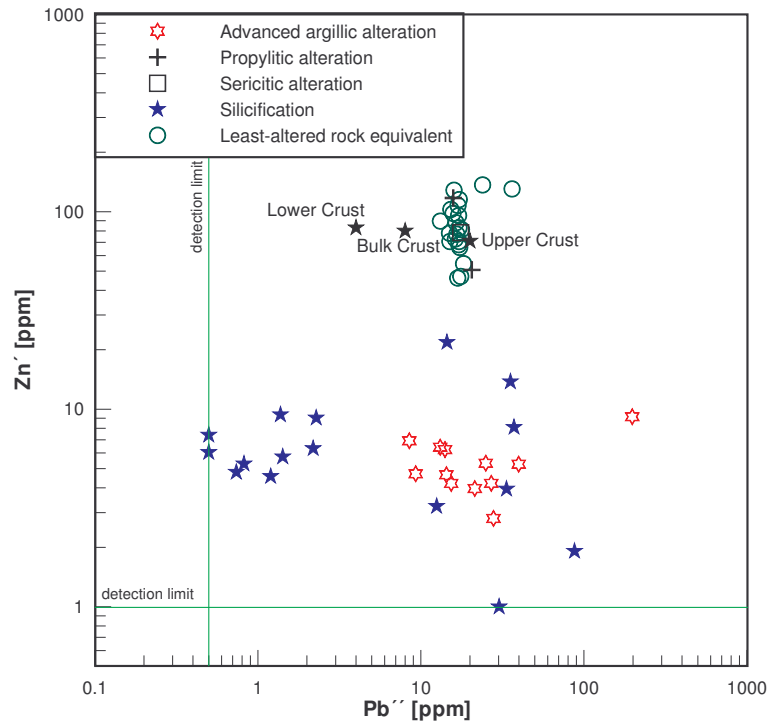


Fig. 67: Zn-Pb variation diagram (Zn: ICP; Pb: ICP-MS).

The volatile elements As, Sb, Hg, Bi and S are enriched.

In Fig. 68 (As-Sb/Bi-Sb variation diagrams) As correlates with Sb and Bi correlates vaguely with Sb.

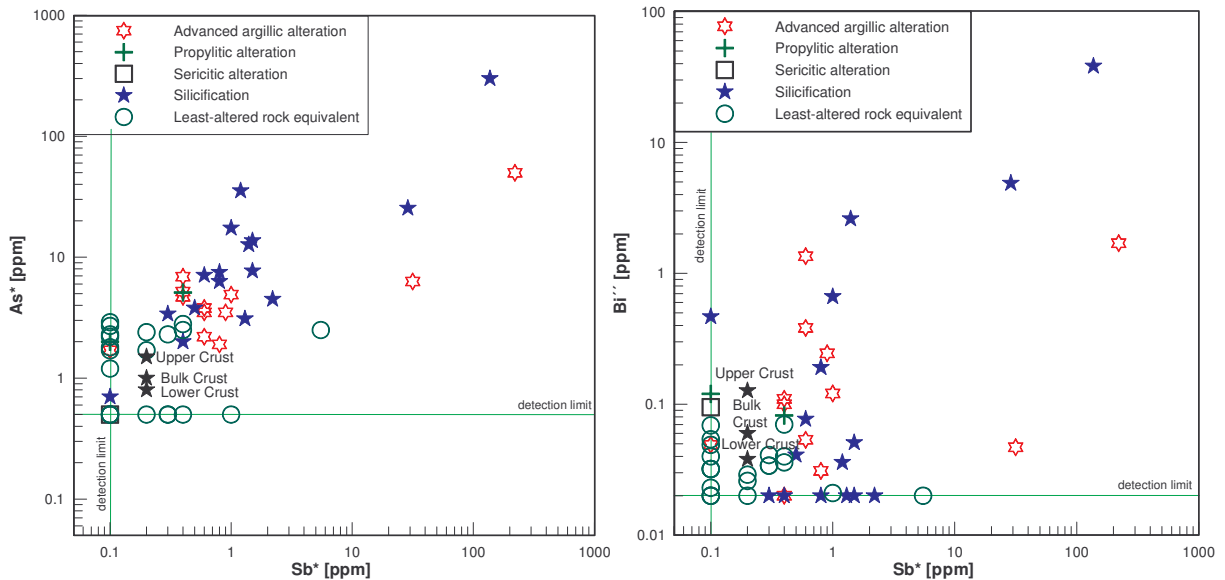


Fig. 68: As-Sb and Bi-Sb variation diagrams (As, Sb: INAA; Bi: ICP-MS).

Figs. 69 and 70 give the Hg-As and Hg-Sb distribution. These plots give scatter distributions and illustrate the strong enrichment of Hg in the hydrothermal system, of which the bulk data

range is at least, in comparison to Sb and As, one order of magnitude higher. The least-altered rocks and the propylitic and sericitic altered rocks are very low in Hg ( $\leq 5$  ppb). As shows generally higher scatter, especially in silicified rocks, whereas the Sb data are more restricted.

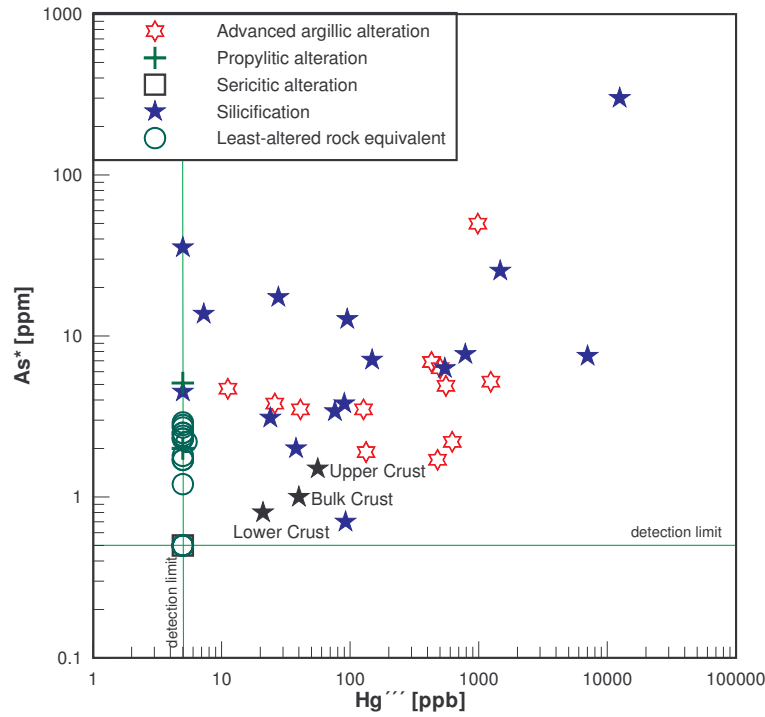


Fig. 69: As-Hg variation diagram (As: INAA; Hg: AAS-CV). UC, BC and LC data from WEDEPOHL (1995).

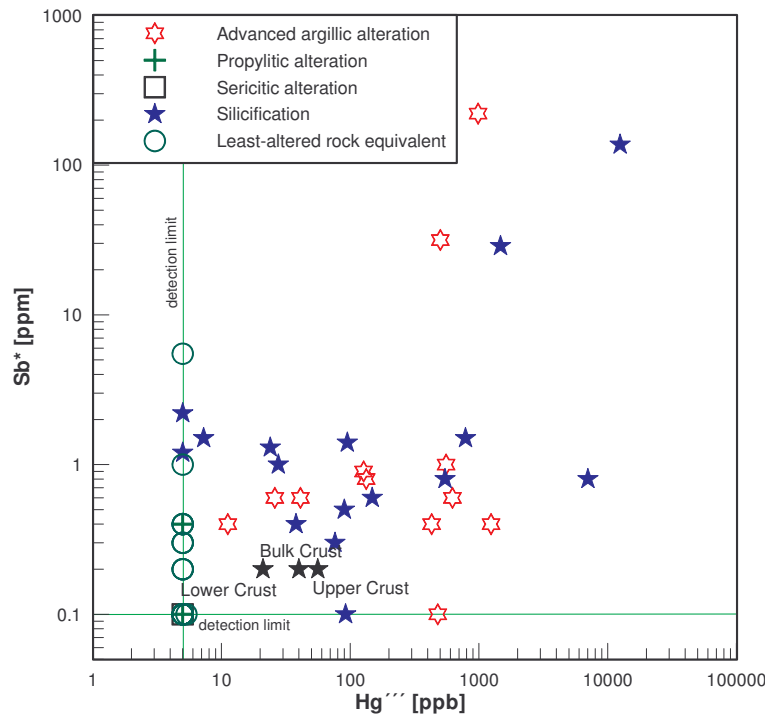


Fig. 70: Sb-Hg variation diagram (Sb: INAA; Hg: ICP-CV). UC, BC and LC data from WEDEPOHL (1995).

## 7.6 Frequency distribution of As, Sb, Ba and Hg

Trace element data tend to have a lognormal distribution (AHRENS 1954) and give a straight line in probability plots (Hazen-line). Changing slopes of the lognormal data presented in probability plots indicate several populations. These populations can be separated at inflection points (IP).

The logarithmic abscissa allows to read off the geometric mean ( $b$ ) and the standard deviation ( $s$ ) by projection of the intersection points of the Hazen-even with the median line (50 % accumulated frequency) and Hazen-even with  $b \pm 1s$  lines (16 and 84 % accumulated frequency) on the abscissa.

The INAA data set of arsenic shows a bimodal lognormal distribution with 18 % of the data below detection limit (least-altered rocks, a silicic and a sericitic altered rock sample).

Population A builds up 78.2 % of the data and has a geometric mean of 2.1 ppm with a 1s variation range of 1.1-4.0 ppm As.

This population can be described as local background, plotting near the upper crustal concentration of 1.5 ppm As. The population comprises the least-altered rocks, the advanced-argillic altered, propylitic and some silicic altered rock samples.

Population B encompasses 21.8 % of the data. The geometric mean is 20.0 ppm with a variation range of 5.8-60 ppm As. This population consists mostly of silicified samples and represents hydrothermal overprint.

The INAA data of Sb is bimodal with 31 % of data below detection limit.

Population A comprises 92.7 % of the data and has a geometric mean of 0.4 ppm Sb with 0.04-1.1 ppm.

This population consists of least-altered rocks, of advanced argillic and silicic altered rocks. Population B contains 7.3 % of all samples and has a mean of 98 ppm with one standard deviation of 21 to 420 ppm.

Population B represents the strongly altered (mainly silicic altered) rock samples.

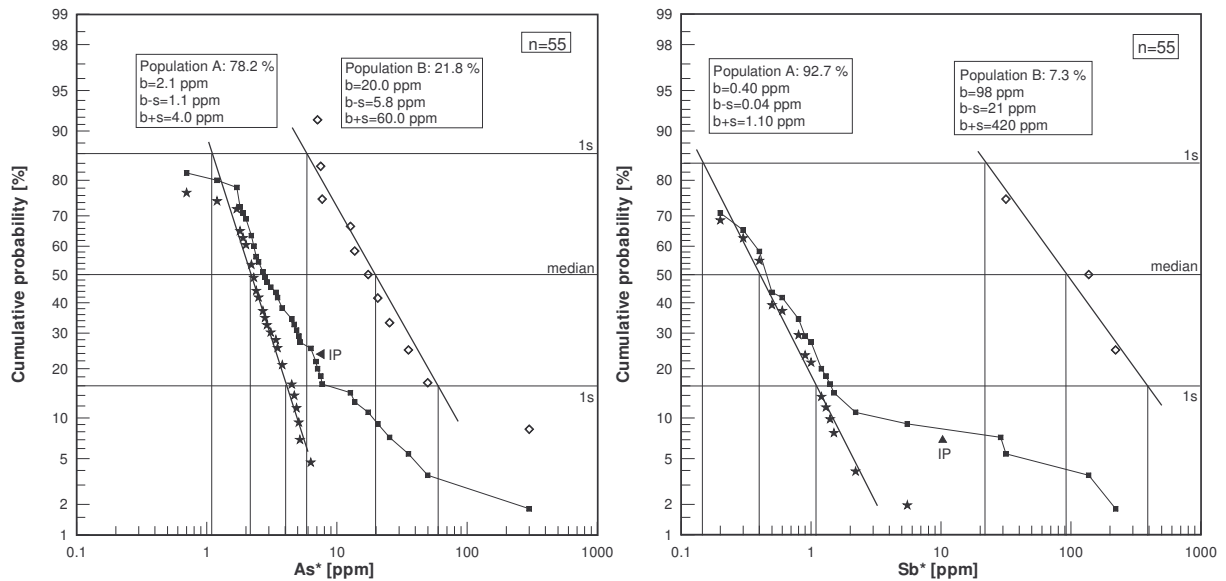


Fig. 71: Probability plots of arsenic and antimony (INAA).

All barium data (XRF) are above the detection limit and give bimodal distribution similar to Sb.

Population A (29.1 %) has a mean value of 150 ppm and one standard deviation comprises a data range from 41 to 540 ppm Ba.

Population A consists in contrast to the former ones (As, Sb) at low concentrations mainly of silicic altered (leached) rock samples. The two samples below b-1s are advanced argillic altered rocks, which indicate a further subpopulation.

The mean value of population B (70.9 %) is 910 ppm and data span for  $b \pm 1s$  from 740-1100 ppm. Population B includes the least-altered rocks with interspersed advanced argillic, propylitic, silicic and sericitic altered rocks.

Below b-1s occur two data points, which diverge distinctly from the Hazen-even because of their strong enrichment. The samples are derived from the Qda. Millo/Qda. Quelluire region and are located on faults and fissures.

The Hg data (AAS-CV) are for nearly 50 % below detection limit. The data set is interpreted to be bimodal with two slightly different gradients and an inflexion point.

Population A (83.6 % of all samples) comprises a  $b+s$  data range from 0.18 up to 94 ppb, mean value: 3.5 ppb. The data group consists of silicic and advanced-argillic altered rocks.

Population B includes 16.4 % of all data and is characterized by a mean value of 1700 ppb Hg. One standard deviation ranges from 420 to 5400 ppb. The population is built up of silicic and advanced argillic altered rock samples.

The two most enriched samples 77970 and 77971 suggest, similar to the Ba data a third population, which is due to missing samples not separated and demands further sampling in the Qda. Millo region and on the upper eastern slope of C° Millo Sur.

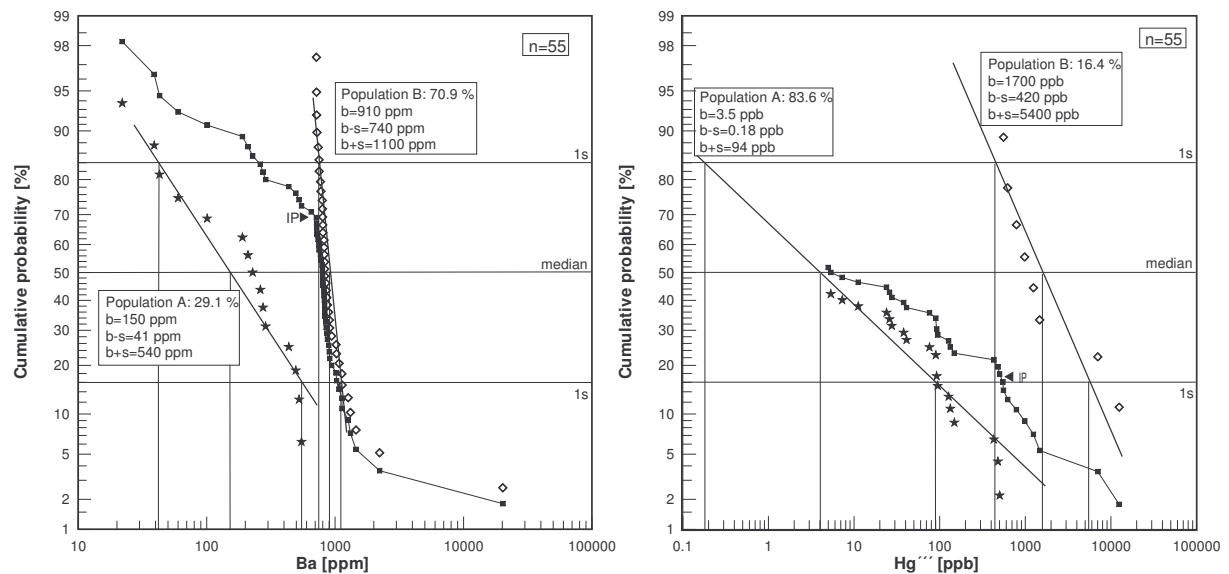


Fig. 72: Probability plots of barium and mercury (XRF, AAS-CV).

## 7.7 Spatial distribution of As, Sb, Ba, Hg and Au

The geochemical maps of the pathfinder elements As and Hg indicate two centers of the hydrothermal system, one at C° Millo Norte and the other at C° Zorrichata and Qda. Millo/Quelluire (Figs. 73 and 74).

Samples enriched in Sb are mainly located in the flat region of Qda. Millo/Quelluire (Fig. 75). The plotted Ba data are inconspicuous, except for depletion in the C° Millo region and the strongly enriched samples 77970 and 77964 at Qda. Millo/Quelluire (Fig. 76).

Au is strongly enriched in the southern Qda. Millo (77970) (Fig. 77).

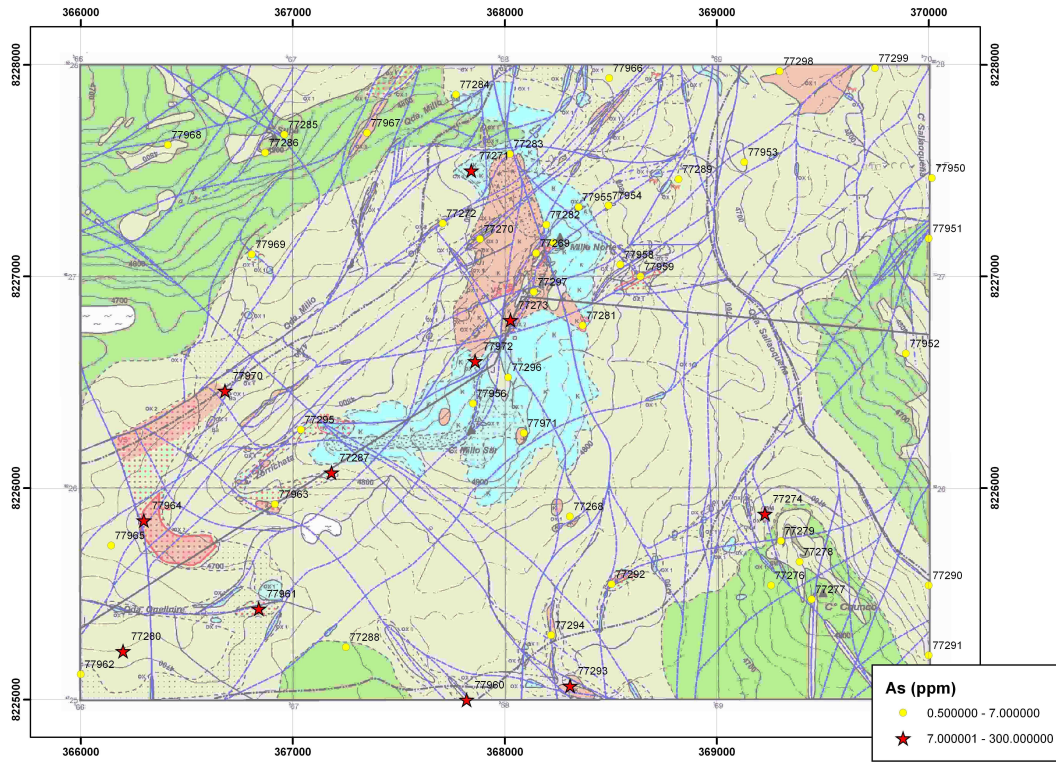


Fig. 73: As data in the study area. Yellow circles: population A, red stars population B.

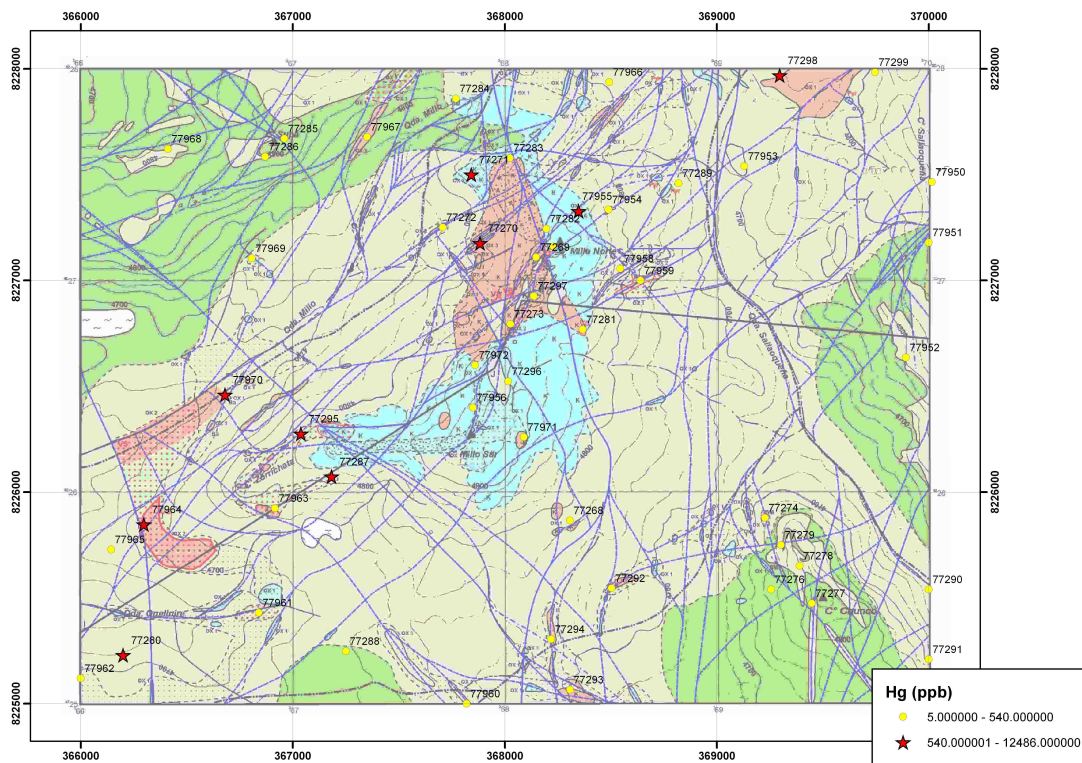


Fig. 74: Hg data in the study area. Yellow circles: population A, red stars: population B.

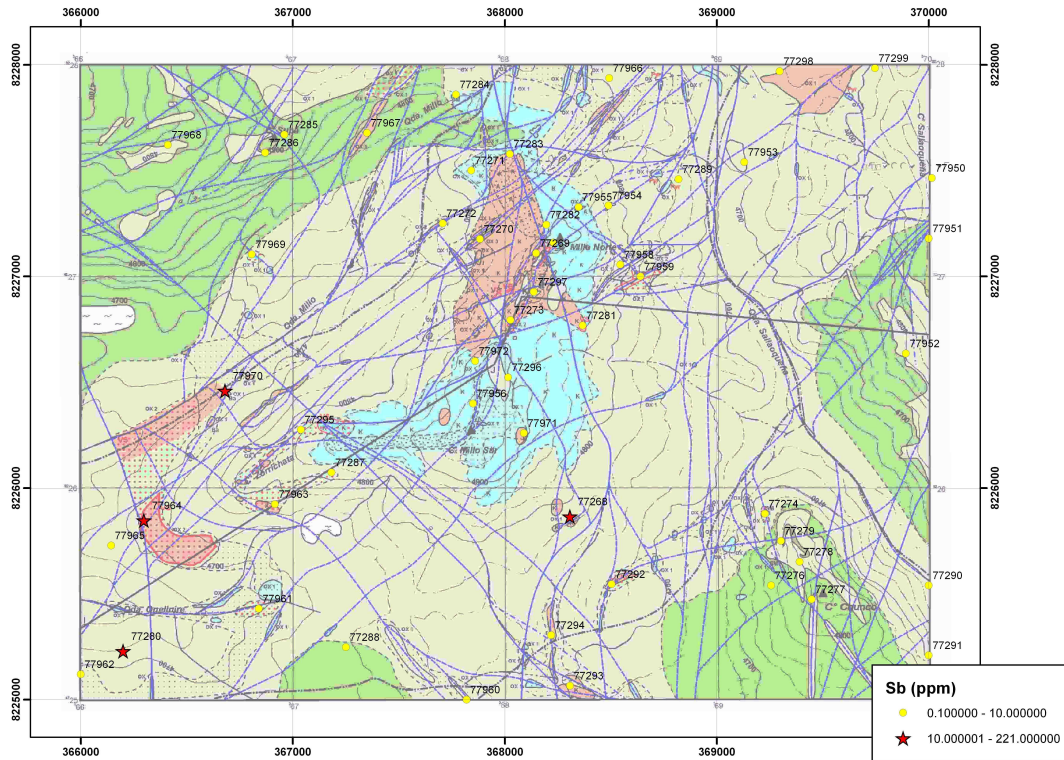


Fig. 75: Sb data in the study area. Yellow circles: population A, red stars: population B.

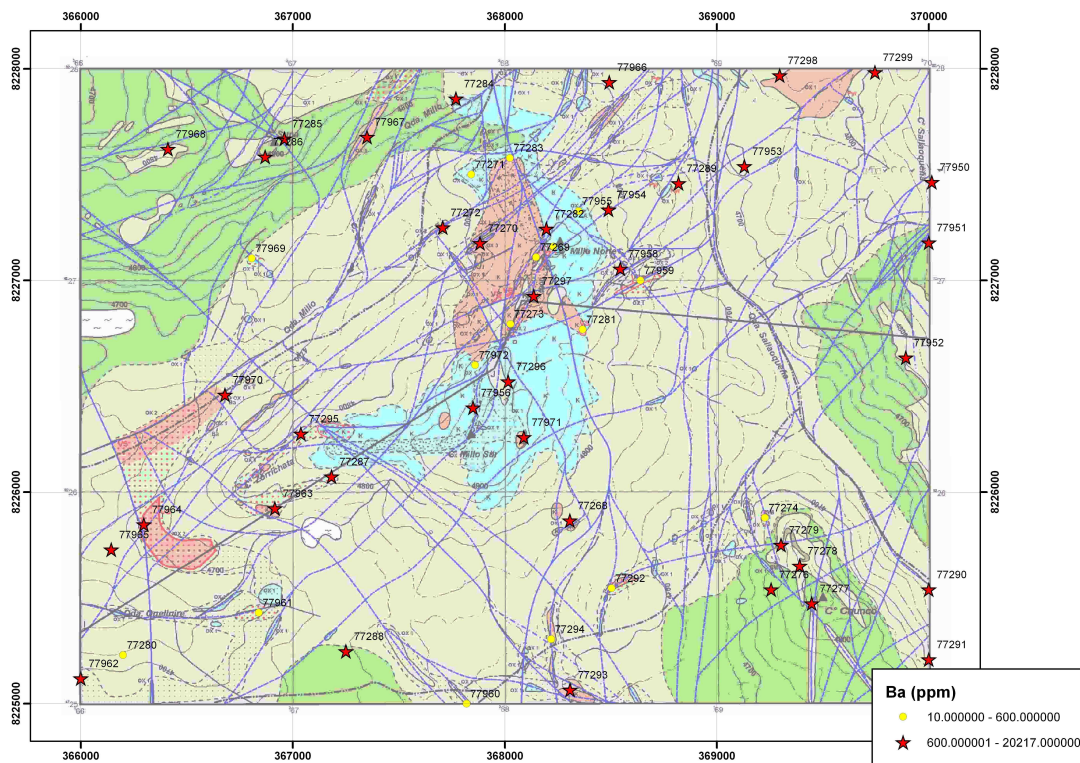


Fig. 76: Ba data in the study area. Yellow circles: population A, red stars: population B.

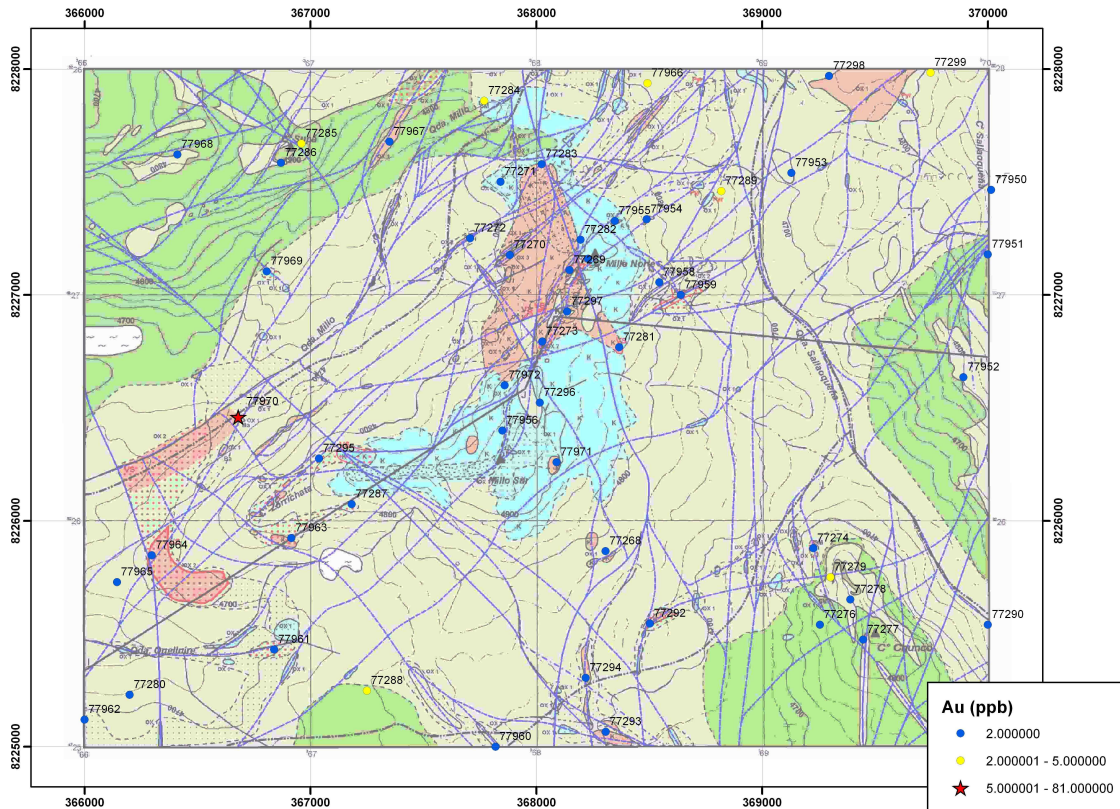


Fig. 77: Au data in the study area.

## 7.8 Physical-chemical background of the hydrothermal system

The plagioclase at C° Millo has been analysed by the RITTMAN method and RDA analysis. Most of it is andesine.

The transitions of plagioclase (andesine) and minor sanidine to mica, clay minerals and alunite can be described as follows (HEMLEY & JONES 1964, HEMLEY et al. 1969, HEMLEY et al. 1980):

### Acidic conditions:

- 1)  $3 \text{KAlSi}_3\text{O}_8 + 2 \text{H}^+ (\text{aq}) = \text{KAlSi}_3\text{O}_{10}(\text{OH})_2 + 2 \text{K}^+ (\text{aq}) + 6 \text{SiO}_2$   
 $3 \text{ sanidine} + 2 \text{H}^+ = \text{muscovite/sericite} + 2 \text{K}^+ (\text{aq}) + 6 \text{quartz}$
- 2)  $3 \text{NaAlSi}_3\text{O}_8 + \text{K}^+ + 2 \text{H}^+ = \text{KAl}_3\text{Si}_3\text{O}_{10}(\text{OH})_2 + 6 \text{SiO}_2 + 3 \text{Na}^+$   
 $3 \text{ Na-plagioclase} + \text{K}^+ + 2 \text{H}^+ = \text{muscovite/sericite} + 6 \text{quartz} + 3 \text{Na}^+$
- 3)  $0.75 \text{Na}_2\text{CaAl}_4\text{Si}_8\text{O}_{24} + 2 \text{H}^+ + \text{K}^+ = \text{KAl}_3\text{Si}_3\text{O}_{10}(\text{OH})_2 + 1.5 \text{Na}^+ + 0.75 \text{Ca}^{2+} + 3 \text{SiO}_2$   
 $0.75 \text{ andesine} + 2 \text{H}^+ + \text{K}^+ = \text{muscovite/sericite} + 1.5 \text{Na}^+ + 0.75 \text{Ca}^{2+} + 3 \text{quartz}$

- 4)  $\text{Na}_2\text{CaAl}_4\text{O}_{24} + 4 \text{H}^+ + 2 \text{H}_2\text{O} = 2 \text{Al}_2\text{Si}_2\text{O}_5(\text{OH})_4 + 4 \text{SiO}_2 + 2 \text{Na}^+ + \text{Ca}^{2+}$   
andesine + 4 H<sup>+</sup> + 2 H<sub>2</sub>O = 2 kaolinite + 4 quartz + 2 Na<sup>+</sup> + Ca<sup>2+</sup>
- 5)  $2 \text{KAl}_3\text{Si}_3\text{O}_{10}(\text{OH})_2 + 2 \text{H}^+ + 3 \text{H}_2\text{O} = 3 \text{Al}_2\text{Si}_2\text{O}_5(\text{OH})_4 + 2 \text{K}^+$   
2 muscovite/sericite + 2 H<sup>+</sup> + 3 H<sub>2</sub>O = 3 kaolinite + 2 K<sup>+</sup>
- 6)  $\text{KAl}_3\text{Si}_3\text{O}_{10}(\text{OH})_2 + 4 \text{H}^+ + 2 (\text{SO}_4)^{2-} = \text{KAl}_3(\text{SO}_4)_2(\text{OH})_6 + 3 \text{SiO}_2$   
muscovite/sericite + 4 H<sup>+</sup> + 2 (SO<sub>4</sub>)<sup>2-</sup> = alunite + 3 quartz
- 7)  $3 \text{Al}_2\text{Si}_2\text{O}_5(\text{OH})_4 + 2 \text{K}^+ + 6 \text{H}^+ + 4 (\text{SO}_4)^{2-} = \text{KAl}_3(\text{SO}_4)_2(\text{OH})_6 + 6 \text{SiO}_2 + 3 \text{H}_2\text{O}$   
3 kaolinite + 2 K<sup>+</sup> + 6 H<sup>+</sup> + 4 (SO<sub>4</sub>)<sup>2-</sup> = alunite + 6 quartz + 3 water

Neutral to alkaline conditions:

- 8)  $3 \text{CaAl}_2\text{Si}_2\text{O}_8 + \text{Ca}^{2+} + \text{H}_2\text{O} = 2 \text{Ca}_2\text{Al}_3\text{Si}_3\text{O}_{12}(\text{OH}) + 2\text{H}^+$   
3 anorthite + Ca<sup>2+</sup> + H<sub>2</sub>O = 2 epidote + 2H<sup>+</sup>

The feldspar-destructive reactions describe a chemical equilibrium depending on the cation activity (Na<sup>+</sup>, K<sup>+</sup>, Ca<sup>2+</sup>) and pH.

Fig. 78 shows the stability of some alteration and ore minerals depending on oxygen fugacity and pH at constant temperature (250°C), salinity (1 molal) and Na<sup>+</sup>/K<sup>+</sup>=10. The concentration of S varies (10<sup>-3</sup> m, 10<sup>-2</sup> m, 10<sup>-1</sup> m).

K-feldspar is stable above pH 5.2, sericite between pH 5.2 and 4.2, kaolinite below pH 4.2. Alunite (KAl<sub>3</sub>(OH)<sub>6</sub>(SO<sub>4</sub>)<sub>3</sub>) formation certainly depends on S concentration and the alunite stability field is thereof larger at higher S-concentrations (10<sup>-1</sup> mol, 3.9 pH). In lower concentrations (10<sup>-3</sup> mol) alunite is stable below pH 1.

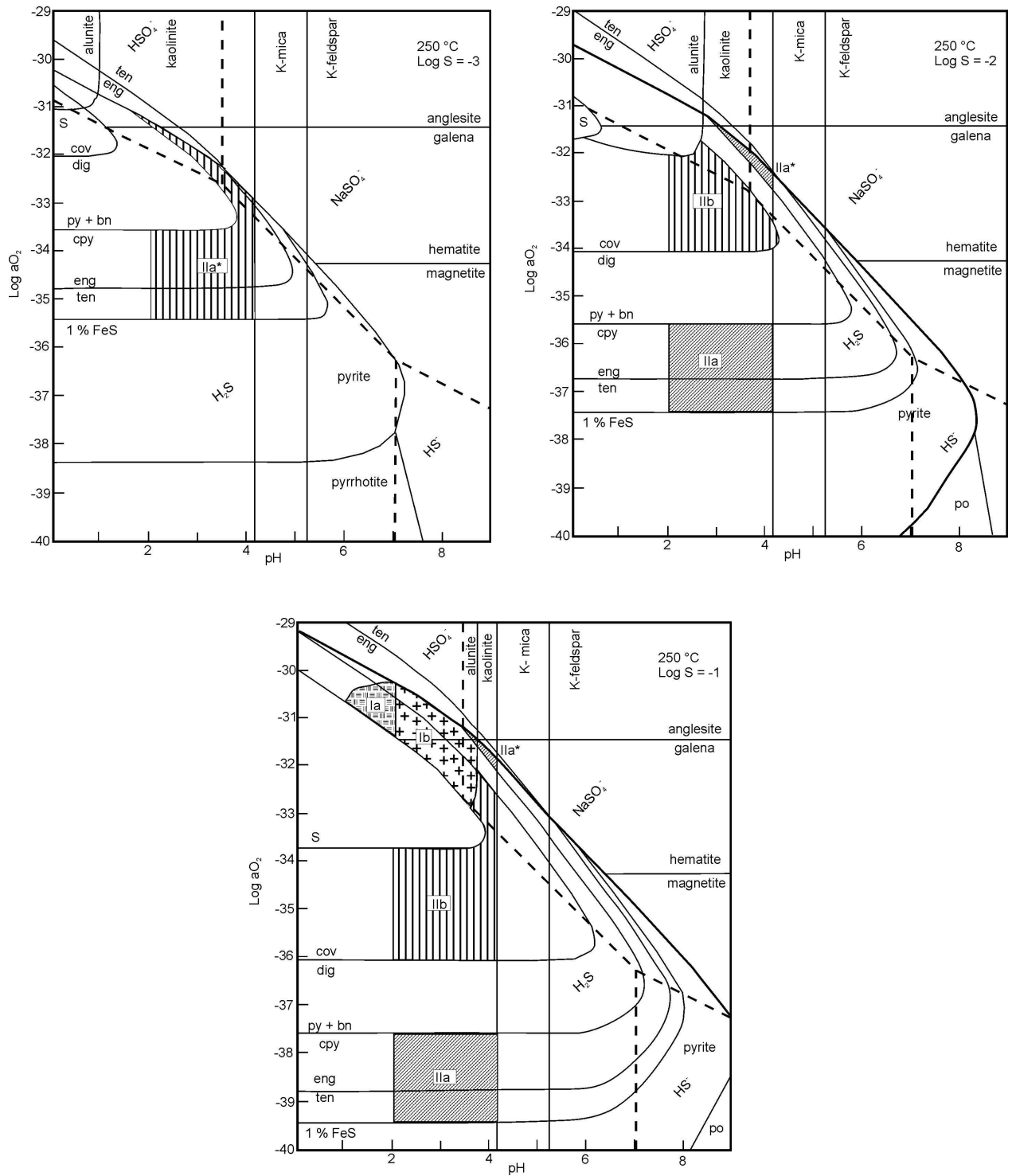


Fig. 78: Log aO<sub>2</sub>-pH diagrams for different alteration and ore minerals. Temperature: 250°C, salinity: 1 molal Na<sup>+</sup>/K<sup>+</sup>=10. Stoffregen's (1985) notation for the different mineral assemblages is used: vuggy silica (Ia), quartz-alunitite-pyrite (Ib), chalcopyrite-bearing ore assemblage (IIa) and covellite dominated ore assemblage (IIa\*), ten=tennantite, eng=enargite, cov=covellite, dig=digenite, py=pyrite, bn=bornite, cpy=chalcopyrite, po=pyrrhotite (Hayba et al. 1985).

Fig. 79 shows the stability fields for the alteration minerals at 250°C, depending on the activity of Na<sup>+</sup>, K<sup>+</sup> and H<sup>+</sup>. Possible evolution paths of the hydrothermal fluid are given.

The sericitic alteration describes albite and K-feldspar transformation to K-mica (sericite).

All hydrothermal mineral assemblages observed can be explained by a fluid which progressively becomes more and more acid.

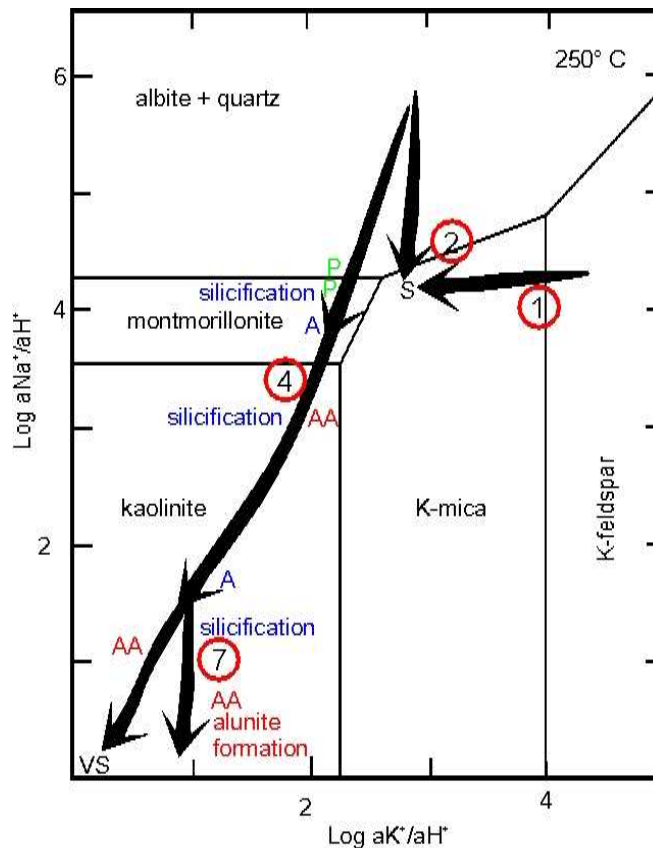


Fig. 79: Activity diagram for the phases in the system CaO-Al<sub>2</sub>O<sub>3</sub>-K<sub>2</sub>O-H<sub>2</sub>O at 250 °C (adapted from HENLEY & BROWN 1985). Numbers indicate equations. P=propylitic alteration, S=sericitic alteration, A=argillic alteration, AA=advanced argillic alteration.

Fig. 80 shows the experimentally determined stability fields of K-feldspar, muscovite, kaolinite and alunite in terms of K<sub>2</sub>SO<sub>4</sub> and H<sub>2</sub>SO<sub>4</sub> concentrations at 200 and 300°C. The system resembles the high-sulfidation type because it is oxydizing and S-rich.

The alteration path K-feldspar-muscovite-kaolinite and alunite can be seen as a result of decreasing T and pH.

Due to total protolysis of sulfuric acid the pH can be directly determined. At 200°C alunite is stable below pH 2.7 and at 300°C below pH 2.

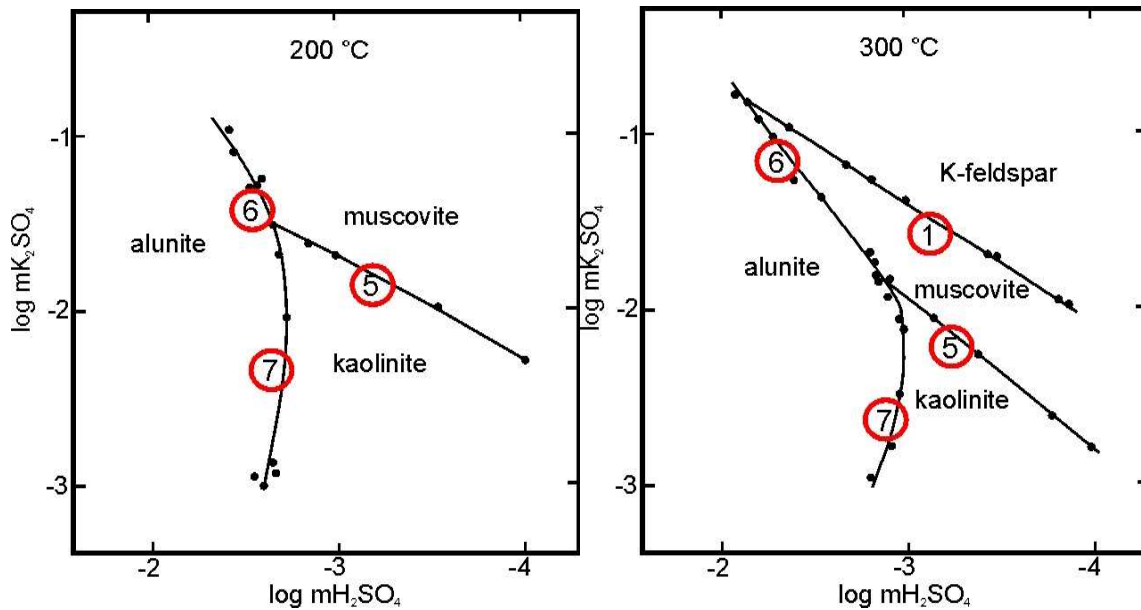


Fig. 80: Experimentally determined phase relations in the system  $K_2O-Al_2O_3-SiO_2-H_2O-SO_3$ . Total pressure is 15000 psi (adapted from HEMLEY et al. 1969).

The hydrothermal fluid: The absence of pyrophyllite and dickite in the advanced-argillic altered rocks at C° Millo indicate temperatures below 220°C (THOMPSON et al. 1996, comp. Fig. 81).

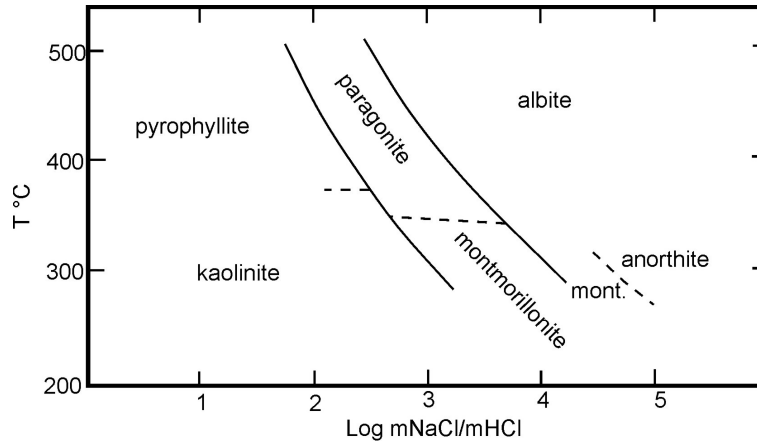


Fig. 81: Equilibrium relations in the system  $Na_2O-Al_2O_3-SiO_2-H_2O$  (adapted from MEYER & HEMLEY 1967)

The high amount of kaolinite and granular quartz in argillic altered and silicified rocks define a temperature range of about 100-200°C. The veins and flats of chalcedony imply a maximum temperature of about 160°C (Fig. 82).

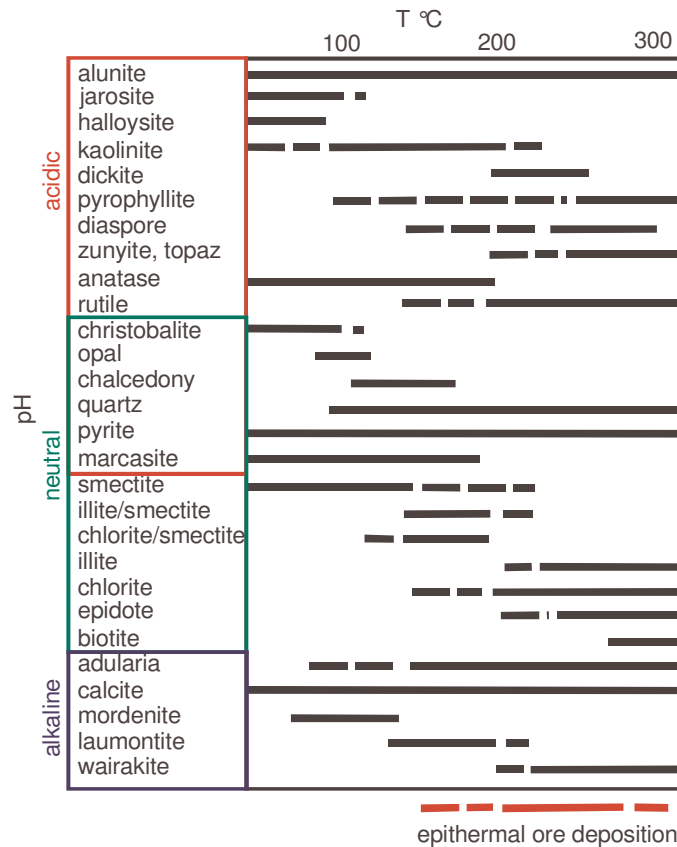


Fig. 82: Temperature stability of hydrothermal minerals of the epithermal environment, arranged by their stability with respect to pH (data from: HENLEY et al. (1983), HEDENQUIST et al. (1995)).

The indicator minerals of the propylitic-alteration imply temperatures around 200°C.

Epidote is stable above 200°C. Muscovite (sericite) is produced above 200°C, of which the well-formed, fine-grained phase at C° Millo is typical for a temperatures around 200°C (THOMPSON et al. 1996).

Pure illite is stable above 200°C. At less than about 200°C, interlayered illite/smectite or discrete smectite prevails. Chlorite can be stable above 160°C.

In summary a temperature of about 200°C for the bulk of the acid leached zone appears probable.

The veins and flats of chalcedony are thought to be generated superficially, at paleowater table and are therefore more cooled.

Residual quartz traces the most acidic parts of the hydrothermal system (mainly veins). Zoning of the argillic alteration halo from an inner kaolinite-rich part to an outer, smectite-bearing part, depends on pH.

## 8. The hydrothermal system

Most of the intensive hydrothermal alteration in the study area is related to the stratigraphically lowest rocks of the Barroso Group, which are built of pyroclastic rocks and ignimbrites.

The hydrothermal system (hypogene alteration) indicates fluid temperatures of about 200°C. A paleo-depth approximation based on the hydrostatic boiling curve implies a depth of about 120-140 m.

Both parameters define an epithermal system, which typically forms at temperatures between 50 and 350 °C in shallow crustal regions (<1.5 km/500 bar) (SILLITOE 1993).

The generation of epithermal systems is favored by thick volcanic sequences of pyroclastic rocks or lavas mainly related to volcanic domes and stratovolcanoes, which are thought to be spatially and temporally related to deeper magma chambers (5-10 km). The thermal anomaly heats meteoric water; fluids rise up and form convection cells (Fig. 83).

Thick volcanic sequences allow kilometer-wide convection cells. Itself favored to form, as at C° Millo, in unwelded/partly welded ignimbrites due to their high porosity and permeability.

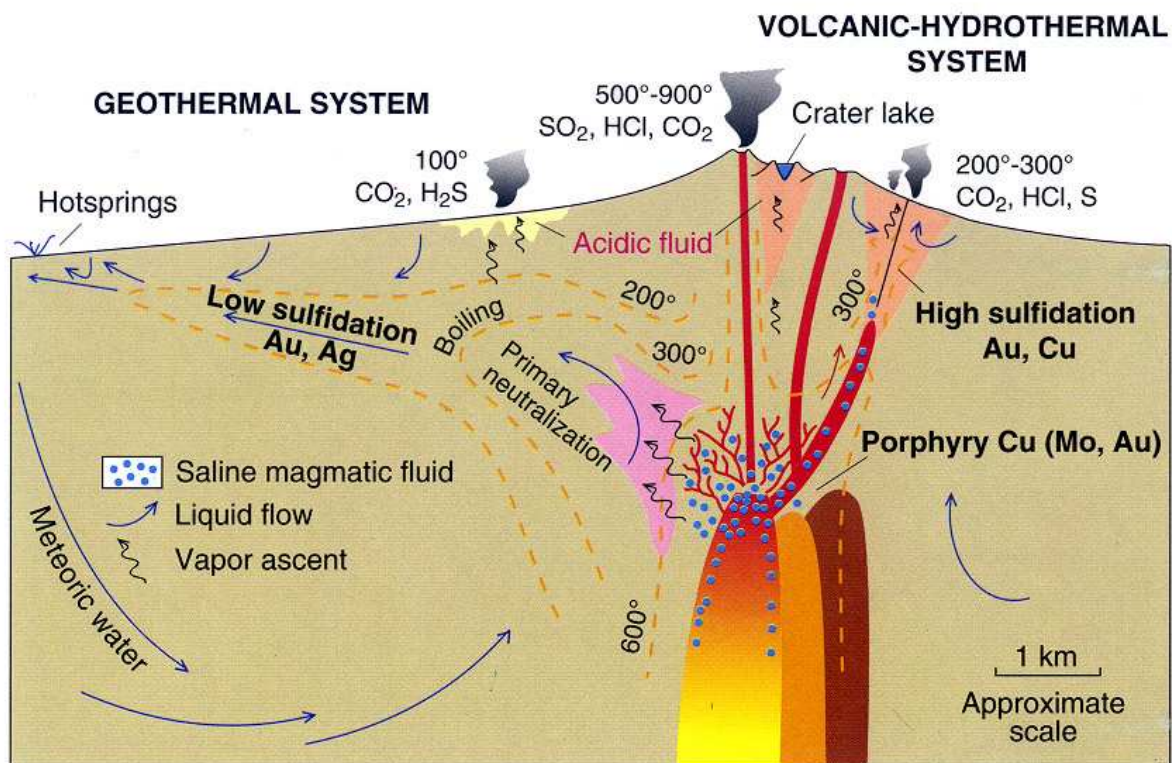


Fig. 83: Schematic cross-section showing shallow sub-volcanic intrusions and associated stratovolcano, and environments deduced for formation of porphyry Cu, and high- and low-sulfidation epithermal ore deposits (HEDENQUIST & LOWENSTERN 1994).

Epithermal systems are divided into the high-sulfidation type (HS), also called acid-sulfate type and the low-sulphidation type (LS), which is also called the adularia-sericite type. The HS type is characterized by acid, sulphur-rich, oxydized fluids (HEALD et al. 1987).

LS fluids are suggested to possess a volumetrically lesser magmatic contribution of either acid volatiles or low salinity brines (Fig. 83).

Most HS deposits are linked genetically to subalkalic rocks ranging from andesitic to rhyodacitic chemism, which also explains the tectonic setting of most HS in subduction-related, volcano-plutonic arcs. Rhyolitic melts are likely to evolve volatiles relatively poor in SO<sub>2</sub> and potentially unable to generate a low-pH fluid (HS) (HEALD et al. 1987).

Several models in different topographic “floors” and environments lead to acid-sulphate alteration (HAYBA et al. 1985), of which the following equation describes acid-sulphate alteration connected to volatile release from an underlying magma chamber. This type seems to be most important at C° Millo (Fig. 84a, Enclosure 4):



The reaction shows disproportionation of magmatically exsolved SO<sub>2</sub> gas, in the presence of water to sulfuric acid and H<sub>2</sub>S gas and results in the development of hypogene hydrochloric-sulfuric acid water with a pH of about 1, sufficiently acid to leach most components, including Al, from the rock. A siliceous residue is left and recrystallizes to quartz (vuggy quartz). The water is rich in sulphate and bears cations (Na<sup>+</sup>, K<sup>+</sup> and Ca<sup>2+</sup>).

Where the acid fluid intersects a permeable lithology or structure, flow will occur along the most permeable channel, down the hydraulic gradient. This is realized in the subvolcanic pyroclastic rock and in the ash flow tuffs at C° Millo. Moreover appear to be the subvolcanic pyroclastic rock and the faults/fissures the most important water channels, which fed the hydrothermal system (Enclosure 4).

The hypogene type of acid-sulphate alteration forms crystalline alunite (“baguette” and needle-like alunite), which is characteristic in the advanced argillic halo of C° Millo region and at some preserved patches of advanced argillic alteration incorporated in less altered rocks.

Boiling of the ascending fluid is the consequence of pressure release during upward fluid percolation. Boiling releases steam plus other volatile phases such as H<sub>2</sub>S and minor SO<sub>2</sub>, CO<sub>2</sub>, NH<sub>3</sub> which further migrate upwards.

Boiling beneath C° Millo Norte most likely took place in the channelways of subvolcanic pyroclastic rock and/or at the base of the pyroclastic rock suite, where permeability is elevated. At southern Qda. Millo boiling happened beneath the 4700 m horizon of silicification, where brecciated rocks are reported from faults (77970).

In contact with the atmosphere, i. e. just above the paleo-water table (vadose zone), sulfuric acid is generated by oxidation of H<sub>2</sub>S (Fig. 84b):



The sulfuric acid percolates back and acidifies the cool and oxidizing steam-heated ground waters which overly the deeply circulating hydrothermal cell. Flow will occur down the hydraulic gradient towards drainages (SILLITOE 1993) (Fig. 84b).

The resulting steam-heated acidic fluids with pH>2 cause advanced argillic alteration (HEDENQUIST 2000), with characteristic powdery, porous texture, as observed on central C° Millo in crystal-bearing ashtuff (“sandy silica”). The absence of residual silica (SiO<sub>2</sub>>95%) at the crater region of C° Millo Norte is due to Al insolubility above pH 2.

Typical epithermal metals, other than mercury and arsenic, are generally absent in this superficial area, because they do not undergo appreciable volatile transport at the low temperatures involved (100-120°C) (HEDENQUIST 2000).

Acid-leached zones might be very thick, where paleo-water tables fall continuously, as in arid regions and (or) beneath topographic highs (exemplified by the C° Millo stratovolcano).

Horizontally lying zones of silicification are a typical feature of shallow HS deposits (SILLITOE 1993) and are developed in Qda. Millo/Qda. Sallaoqueña and Cerro Chunco following the 4700 m contour line, and at 4800 m and 4900 m at C° Zorrichata/C° Millo.

The silicification is massive and dense. This might lead to sealing of fractures resulting in formation of hydrothermal breccias, as observed in 77273, 77964, 77970 (see above).

Such silicified horizons are believed to be generated at paleo-water tables. Sulphur, Nevada, and Wau, Papua New Guinea (SILLITOE et al. 1984) provide documented examples of

silicified horizons still overlain by acid-leached rock, similar to C° Millo. Silicified horizons stripped of their overlying acid-leached zones form ridges, commonly called “silica caps”, as observed in the upper Qda. Millo.

Silicification at water tables probably results from downward remobilization of silica by low pH condensates in overlying acid-leached zones. Furthermore, kaolinite (argillic) alteration is also caused by downward draining of acid pH condensates and difficult to separate from hypogene argillic alteration (SILLITOE 1993).

The zonation of the alteration halos at C° Millo, and the locally well-crystallized (“baguette”-like) alunite indicates the upper part of hypogene acid-sulphate alteration (SILLITOE 1993). Whereas the very fine-grained alunite (C° Millo Norte), and the horizons of silicification represent acid leaching by steam-heated overprinting near the paleo-surface (<50 m ?).

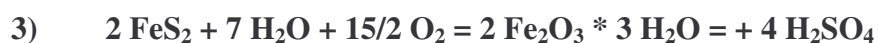
Ore-bearing silica commonly survives the acidic overprint, as at Borealis and Paradise Peak, Nevada (SILLITOE 1993), therefore it can be assumed that the upper hydrothermal system at C° Millo has been “barren” before the steam-heated overprint.

A drop of the water table during and after hydrothermal alteration is indicated/shown in the C° Millo region. The uppermost horizon of dense silica at C° Millo Sur (4900 m) and the present day discharge system at Qda. Millo at 4700 m indicate an erosional rate of at least about 200 m since the first near-surface “steam-heated overprint”.

The drop of the paleo-water table seems most likely to be due to uplift and valley incision during hydrothermal activity, and (or) to waning of the hydrothermal system.

The third possibility to generate sulfuric acid is the alteration/weathering of sulfide ore (mainly pyrite) under oxic conditions (Fig. 84c).

This alteration occurs similar to steam-heating in the vadose zone and is controlled by the position of the water table. Temperature is limited to a maximum of 30 to 40°C (HEDENQUIST 2000). Acid waters may drain downward locally along faults and open fractures. In the study area this type of advanced argillic alteration is evident from field examination by plenty of limonite staining, in thin section by secondary clays and jarosite and by pyrite oxydation in polished sections.



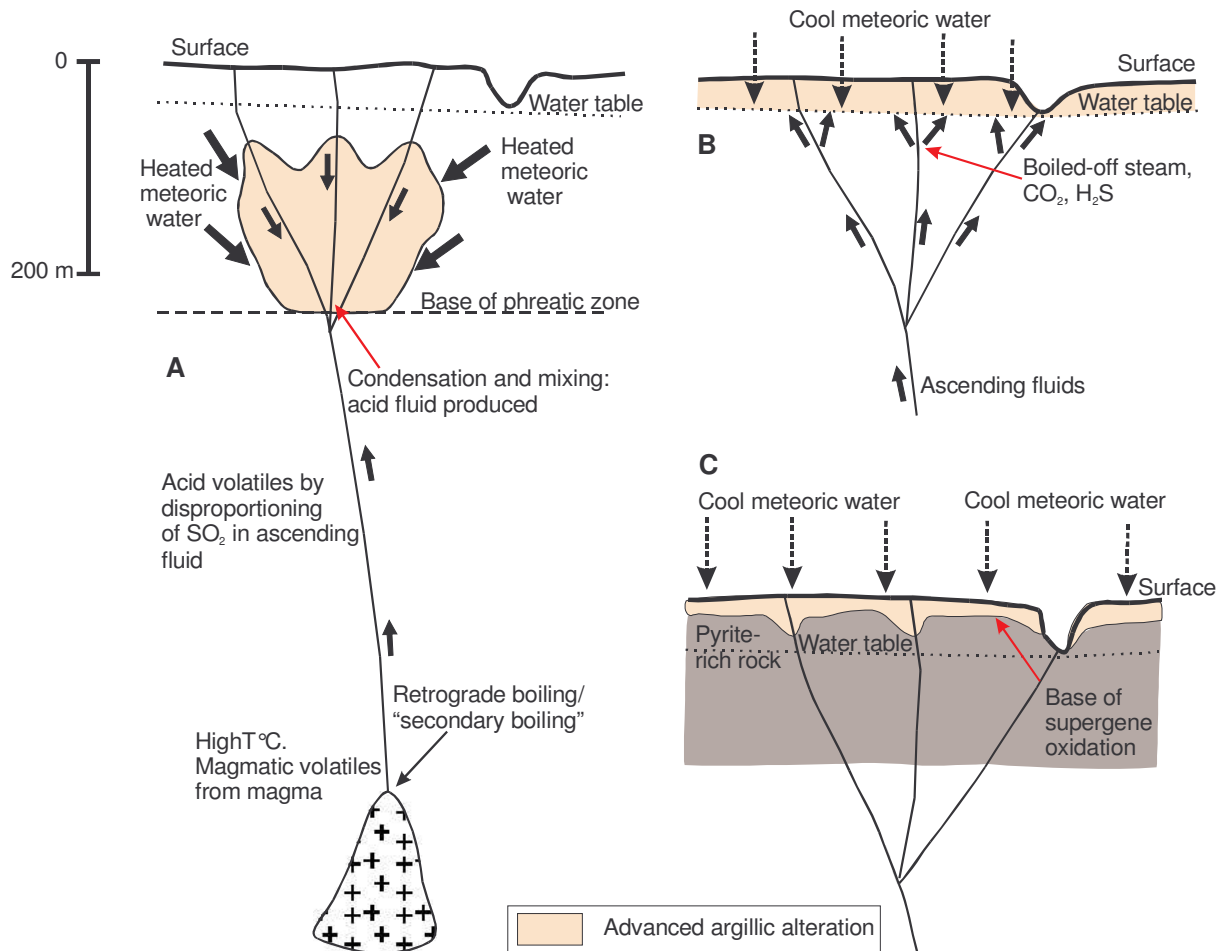
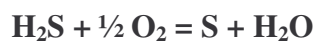


Fig. 84: Origins of three types of advanced argillic alteration: (A) deep hypogene due to condensation of acidic magmatic volatiles and dissolution of condensate in meteoric water; (B) shallow hypogene (acid leaching) due to oxidation of H<sub>2</sub>S in the vadose zone; and (C) supergene due to oxidation of sulphides above a water table (adapted from SILLITOE 1993).

The sulphur rich, argillic altered solfatara-rock south of C° Mollo can be explained similar to the steam-heated acid-sulphate alteration. Released H<sub>2</sub>S ascends on faults or fissures and sulfur and sulfuric acid are formed in contact with atmospheric oxygen.



H<sub>2</sub>S is probably delivered by subsurface boiling processes. The presence of native sulfur suggests that the hydrothermal system was active in subrecent times.

However, H<sub>2</sub>S can also form as a direct degassing product from magma.

## **9. Conclusion**

The paragenesis of the alteration minerals at C° Millo indicates fluid temperatures of about 200°C for the hypogene alteration zone, which is, according to HEDENQUIST (1995) the lowest limit for epithermal gold mineralization. This implies that the hydrothermal system at C° Millo is exposed at its uppermost level only.

As and Hg are enriched in the C° Millo region, but the highest anomalies of Au, Ag, Ba, Hg, As and Sb lie in between Qda. Millo and Qda. Quelluire i.e in the lowest topographical parts of the hydrothermal system.

Nearly all anomalies in the study area appear to be bound to faults and fissures, which might indicate leakage from a precious metal deposit below. The solfatara at southern C° Millo and the hydraulic fractured gold-bearing sample (77970) in Qda. Millo and the steam-heated area at C° Millo Norte imply boiling. Boiling is the critical process responsible for gold precipitation from bisulfide-complexes.

Minas Buenaventura focussed on the C° Millo region for channel sampling (Trinchera III and IV) and drilling (Cerro Millo Norte/Sur, Enclosure 6).

Based on this study drilling in Qda. Millo at sample point 77970 (366680/8226460) to a depth of about 300 m is recommended.

A second drilling point is indicated at C° Millo Norte at the steam-heated top in strongly faulted subvolcanic pyroclastic rock material (368080/8227350).

There is a good chance for deeper boiling horizons and gold enrichment. C° Millo can be compared in its principal geological style with Yanacocha, which is also a shallow, volcanic hosted high-sulfidation system and which shows plenty of steam-heating and supergene features (SILLITOE 1999).

## References:

- AHRENS, L. H. (1954): The log-normal distribution of the elements. – *Geochimica et Cosmochimica Acta*, **5**: 48-73.
- ANDERS, E. & GREVESSE, N. (1989): Abundances of the elements: Meteoritic and solar. – *Geochimica et Cosmochimica Acta*, **53**: 197-214.
- ANONYMUS (w.y.): [Internet://www.webmineral.com].
- ANONYMUS (2004): [Internet:// www.geologix.da/s/puno.asp].
- ARAMAKI, S., ONUMA, N. & PORTILLO, F. (1984): Petrography and major element chemistry of volcanic rocks of the Andes, southern Peru. - *Geochemical Journal*, **18**: 217-232.
- BAILEY, J. C. (1981): Geochemical criteria for a refined tectonic discrimination of orogenic andesites. – *Chemical Geology*, **32**: 139-154.
- BENAVIDES-CÁCERES, V. (1999): Orogenic evolution of the Peruvian Andes: The Andean Cycle. - In: Skinner, B. J. (ed.): *Geology of Ore Deposits of the Central Andes*. Society of Economic Geologists, Special Publication **7**: 71-107.
- CARLIER, G., LORAND, J.-P., BONHOMME, M. & CARLOTTO, V. (1996): A reappraisal of the Cenozoic inner arc magmatism in Southern Peru: consequences for the evolution of the Central Andes of the past 50 Ma. 3rd International Symposium of Andean Geodynamics. - ISAG, Paris, 551-554.
- CARR, P. F. (1985): Geochemistry of late Permian shoshonitic lavas from the southern Sydney Basin. – In: SUTHERLAND, F.L., FRANKLIN, B.J. & WALTHO, A.E. (eds.): *Volcanism in eastern Australia*. Geologic Society of Australia, Diverse Publication, **1**: 165-183.
- Carte Géologique Des Terrains Paléozoïques Et Précambriens Du Pérou Et De Bolivie. – 1:5000000 – In: DALMAYRAC, B., LAUBACHER, G., MAROCCO, R., MARTINEZ, C., MÉGARD, F., PAREDES, J. & TOMASI, (1974): *Cahiers O.R.S.T.O.M., série Géologie*, **VI**.
- CHAPPEL, B. W. & WHITE, A.J.R. (1974): Two contrasting granite types. – *Pacific Geology*, **8**: 173-174.
- DEER, W. A., HOWIE, R. A., ZUSSMAN, J. (1962): *Rock forming minerals*. – Vol. 3 Sheet Silicates: 270 pp; London (Longmans).
- DIETRICH, A. (1999): Metallogenie, Geochemie und Schmelzeinschluß-Untersuchungen von tin porphyry und copper porphyry Lagerstätten der zentralen Anden (Bolivien, Chile). – *Clausthaler Geowissenschaftliche Dissertationen*, **57**: 198 pp., 86 fig., 17 tab.
- EWART, A. (1982): The mineralogy and petrology of Tertiary-Recent orogenic volcanic rocks with special reference to the andesitic-basaltic composition range. – In: THORPE, R. S. (ed.): *Andesites*: 15-87, Chichester (Wiley).
- FAURE, G. (2001): *Origin of Igneous Rocks. The Isotopic Evidence*. – 496 pp., 420 fig., 60 tab.; (Springer).
- FLOYD, P. A. & WINCHESTER, J. A. (1975): Magma type and setting discrimination using immobile elements. – *Earth and Planetary Science Letters*, **27**: 211-218.

- GLADNEY, E. S. & ROELANDTS, I. (1988): Compilation of Elemental Concentration Data for USGS BHVO-1, MAG-1, QLO-1, RGM-1, SCo-1, SDC-1, SGR-1 and STM-1. - *Geostandards Newsletter*, **12**: 253-362.
- HAMPEL, A. (2002): The migration history of the Nazca Ridge along the Peruvian active margin: a re-evaluation. – *Earth and Planetary Science Letters*, **203**: 665-679.
- HARMON, R. S., BARREIRO, B. A, MOORBATH, S., HOEFS, J., FRANCIS, P. W., TORPE, R.S., DERUELLE, B., MCHUGH, J., VIGLINO, J.A. (1984): Regional O-, Sr-, and Pb-isotope relations in Late Cenozoic calc-alkaline lavas of the Andean Cordillera. - *Geological Society of London*, **141**: 803-822.
- HART, S. R. (1988): Heterogeneous mantle domains: signatures, genesis and mixing chronologies. – *Earth and Planetary Science Letters*, **90**: 273-196.
- HAYBA, D. O., BETHKE, P. M., HEALD, P. & FOLEY, N. K. (1985): Geologic, Mineralogic, and Geochemical characteristics of Volcanic-Hosted Epithermal Precious-Metal Deposits. – In: BERGER, B. R. & BETHKE, P. M. (eds.): *Geology and Geochemistry of Epithermal Systems*. – *Reviews in Economic Geology*, **2**: 129-167.
- HEDENQUIST, J. W. (1995): *Short Course: Epithermal Gold Deposits: Styles, Characteristics, and Exploration*. – *The Society of Resouce Geology*.
- HEDENQUIST, J. W., ARRIBAS, M. A. & GONZALEZ-URIEN, E. (2000): Exploration of epithermal gold deposits. – In: Hagemann, S. G. & Brown, P. E. (eds.): *Gold in 2000*. – *Reviws in Economic Geology*, **13**: 245-277.
- HEDENQUIST, J. W. & LOWENSTERN, J. B. (1994): The role of magmas in the formation of hydrohermal ore deposits: *Nature*, **80**: 519-527.
- HEMLEY, J. J. & JONES, W. R. (1964): *Chemical Aspects Of Hydrothermal Alteration With Emphasis On Hydrogen Metasomatism*. – *Economic Geology*, **59**: 538-569.
- HEMLEY, J. J., HOSTETLER, P. B., GUDE, A. J. & MOUNTJOY, W. T. (1969): Some Stability Relations of Alunite. – *Economic Geology*, **64**: 599-612.
- HENLEY, R. W. & BROWN, K. L. (1985): *A Practical Guide to the Thermodynamics of Geothermal Fluids and Hydrothermal Ore Deposits*. – In: BERGER, B.R. & BETHKE, P.M. (eds.): *Geology and Geochemistry of Geochemistry of Epithermal Systems*. – *Reviews in Economic Geology*, **2**: 25-44.
- INNOCENTI, F., MANETTI, P., MAZZUUOLI, R. PASQUARE, G., AND VILLARI (1982): *Anatolia and north-western Iran*. – In: THORPE, R. S. (ed.): *Andesites*: 327-349; Chichester (Wiley).
- IRVINE, T. N. AND BARAGAR, W. R. A. (1971): *A guide to the chemical classification of the common volcanic rocks*. – *Canadian Journal of Earth Sciences*, **8**: 523-548.
- JAILLARD, E., HÉRAIL, G., MONFRET, T., DÍAZ-MARTÍNEZ, E., BABY, P., LAVENU, A. & DUMONT, J. F. (2000): *Tectonic Evolution of the Andes of Ecuador, Peru, Bolivia and northernmost Chile*. – In: CORDANI, U. G., MILANI, E. J., THOMAZ FILHO, A., CAMPOS, D.A. (eds.): *Tectonic Evolution of South America*: 481-559.
- JAMES, D. E., BROOKS, C., CUYUMBA, A. (1976): *Andean Cenozoic volcanism: Magma genesis in the light of strontium isotopic composition and trace-element geochemistry*. – *Geological Society of America Bulletin*, **87**: 592-600.

- JAMES, D. E. (1982): A combined O, Sr, Nd, and Pb isotopic and trace element study of crustal contamination in central Andean lavas. Part I: Local geochemical variations. - *Earth and Planetary Science Letters*, **57**: 47-62.
- JAMES, D. E. & SACKS, I. S. (1999): Cenozoic Formation of the Central Andes: A Geophysical Perspective. – In: SKINNER, B. J: *Geology and ore deposits of the Central Andes*. Society of economic geologists, inc. Special Publication, **7**: 1-25.
- JENKS, W. F. (1946): Preliminary note on geologic studies of the Pacific slope in southern Peru. - *American Journal of Science*, **244**: 367-372.
- KONTAK, D. J., PICHAVANT, M. & CLARK, A. H. (1984): Petrology of the Pliocene peraluminous volcanics from Marsuani, SE Peru. - *American Geophysical Union Transactions*, **65**.
- KUNO, J. (1966): Lateral variation of basalt magma type across continental margins and island arcs. - *Bulletin of Volcanology*, **29**: 195-222.
- LEBAS, M. J., LEMAITRE, R. W., STRECKEISEN, A. & ZANETTIN, B. (1986): A Chemical Classification of Volcanic Rocks Based on the Total Alkali-Silica Diagram. – *Journal of Petrology*, **27**: 745-750.
- LEHMANN, B. (1978): A Precambrian Core Sample from the Altiplano/Bolivia. – *Geologische Rundschau*, Special Publication, **67**: 270-278; Stuttgart (Enke).
- MACDONALD, G. A. (1968): Composition and origin of Hawaiian lavas. – In: COARS, R. R., HAY, R. S. & ANDERSON, C. A. (eds.): *Studies in volcanology: a memoir in honour of Howel Williams*. - *Geologic Society of America Memoires*, **116**: 477-522.
- MCDONOUGH, W. F. & SUN, S.-S. (1995): Composition of the Earth. - *Chemical Geology*, **120**: 223-253.
- MCKEE, E. H., & NOBLE, D. C. (1989): Cenozoic tectonic events, magmatic pulses, and base- and precious-metal mineralization in the Central Andes. - In: ERICKSEN, G. E., CANAS PINOCHET, M. T. & REINEMUND, J. A. (eds): *Geology of the Andes and its relation hydrocarbon and mineral resources: Circum-Pacific Council for Energy and Mineral Resources Earth Sciences Series*, **11**: 189-194.
- MEYER, C. & HEMLEY, J. J. (1967): Wall rock alteration. – In: BARNES, H. L. (ed.): *Geochemistry of Hydrothermal Ore Deposits*. – 166-235; New York (Holt, Rinehart & Winston).
- MIDDLEMOST, E.A.K. (1985): *Magmas and magmatic rocks*. London. – 280 pp.; London (Longman).
- KHASAWNEH, F. E., JUO, A. S. R., BARBER, S. A. (1968): Soil properties influencing differential Ca to Sr absorption. - *Soil Science Society American Proceedings*, **32**: 209.
- PALACIOS, O., DE LA CRUZ, J., DE LA CRUZ, N., KLINCK, B. A., ALLISON, R. A., HAWKINS, M. P. (1993): *Geología de la Cordillera Occidental y Altiplano al oeste del Lago Titicaca - Sur del Peru*. - 257 pp.; Lima, Peru.
- PEARCE, J. A., HARRIS, N. B. W. & TINDLE, A. G. (1984): Trace element Discrimination Diagrams for the Tectonic Interpretation of Granitic Rocks. – *Journal of Petrology*, **25**: 956-983.
- PEARCE, J. A. (2002): *Geochemical Fingerprinting of Igneous Rocks, Short Course*. [Internet: [http://www.earth.cf.ac.uk/people/summaries/JAP\\_Fingerprinting2.ppt](http://www.earth.cf.ac.uk/people/summaries/JAP_Fingerprinting2.ppt)].

- PECCERILLO, A. & TAYLOR, S. R. (1976): Geochemistry of Eocene calcalkaline volcanic rocks from the Katsamonu area, northern Turkey. - *Contributions to Mineralogy and Petrology*, **58**: 63-81.
- RICKWOOD, P.C. (1989): Boundary lines within petrologic diagrams which use oxides of major and minor elements. – *Lithos*, **22**: 247-263.
- ROLLINSON, H. (1993): *Using geochemical data*, - 352 pp.; Essex (Longman).
- SCHMINCKE, H.-U. (2004): *Volcanism*. – 324 pp., 401 fig., Berlin (Springer).
- SIMKIN, T., UNGER, J. D., TILLING, R. I., VOGT, P. R. & SPALL, H. (1994): This dynamic planet. World map of volcanoes, earthquakes, impact craters and plate tectonics.
- SILLITOE, R. H., GRAUBERGER, G. L. & ELLIOT, J. E. (1984): Gold deposits and hydrothermal eruption breccias associated with a maar volcano at Wau, Papua New Guinea. - *Economic Geology*, **79**: 638-655.
- Sillitoe, R. H. (1993): Epithermal Models: Genetic Types, Geometrical Controls and Shallow Features. – In: KIRKHAM, R.V., SINCLAIR, W. D.; THORPE, R. I. & DUKE, J. M. (eds.) *Mineral Deposit Modeling: Geological Association of Canada, Special Paper 40*: 403-417.
- SIMMONS, S. F.: Unpublished data, - 92 pp.
- SMITH, R.L. (1960): Zones and Zonal Variation in Welded Ash Flows. – USGS Prof. Paper, **354-F**: 149-159.
- STOFFREGEN, R., (1985): Genesis of acid-sulfate alteration and Au-Cu-Ag mineralization at Summitville, Colorado. – Ph.D. thesis, University of California (Berkeley) [unpublished].
- TAYLOR, S. R. & MCLENNON, S. M. (1985): *The Continental Crust: its Composition and Evolution*. - 299 pp.; (Blackwell).
- THOMPSON, A. J. B. & THOMPSON, F. J. H. (Eds.) (1996): *Atlas of Alteration. A Field And Petrographic Guide To Hydrothermal Alteration Minerals*. – 119 pp.; (Alpine Press).
- TILTON, G. R. & BARREIRO, B. A. (1980): Origin of lead in Andean calcalkaline lavas, southern Peru. – *Science*, **210**: 1245-1247.
- TROLL, C., BLÜTHGEN, J. & WEISCHET, W. (1980): *Allgemeine Klimageographie*. – 3rd ed., 887 pp.; Berlin (de Gruyter).
- WEBERBAUER, A. (1945): *El mundo vegetal de los Andes peruanos. Estudio fisiogeográfico*. - 776 pp, Lima.
- WEDEPOHL, K. H. (1995): The composition of the continental crust. - *Geochimica et Cosmochimica Acta*, **59**: 1217-1239.
- WINCHESTER, J. A. & FLOYD, P. A. (1977): Geochemical discrimination of different magma series and their differentiation products using immobile elements. – *Chemical Geology*, **20**: 325-343.
- WINCHESTER, J. A. & FLOYD, P. A. (1977): Chemical discrimination of different magma series and their differentiation products using immobile elements. – *Earth and Planetary Science Letters*, **133**: 227-237.

- WÖRNER, G., AITCHESON, S.J., HARMON, R.S., MOORBATH, S., SCHNEIDER, A., SOLER, P., SORA-ESCALANTE, E., STEELE, G., & SWAINBANK, I. (1995): Pb isotopes define basement domains of the Altiplano, central Andes. – *Geology*, **23**: 555-558.
- WRIGHT, V.P., SLOAN, R.J., VALERO GARCES, B. & GARVIE, I.A.J. (1992): Groundwater ferricretes from the Silurian of Ireland and Permian of the Spanish Pyrenees. - *Sedimentary Geology*, **77**: 37-49
- ZANETTIN, B. (1984): Proposed new chemical classification of volcanic rocks. - *Episodes*, **7**: 19-20.

## Appendix

### Abbreviations

C°	Cerro/Mountain
HS	High-sulfidation
Lag.	Laguna/Lake
LS	Low-sulfidation
nic	nicols
PPL	parallel nicols
PS	Polished section
Qda.	Quebrada/Valley
TS	Thin section
XPL	crossed nicols

### Glossary of terms

alotriomorphic	see anhedral
anhedral	a grain lacking well-developed crystal faces
aphanitic	synonymous with microcrystalline but including cryptocrystalline
autolith	an inclusion in an igneous rock to which it is genetically related
crystallite	occurring in the groundmass of igneous rocks, they are not referable to any definite mineral species or crystal form. They present early efforts toward crystallization.
cryptocrystalline	adjective for rock or groundmass in which the crystals are too small to be separately distinguished under a polarizing microscope, grain size less than 0.001 mm
euohedral	idiomorphic, - bound by crystal faces

ghost	phantom, - a visible outline of a former crystal shape or other rock structure that has been partly or completely obliterated
glomerocryst	an aggregate of crystals of the same mineral
very coarse-grained	grain size larger than 3 cm
coarse-grained	grain size between 0.5 and 3 cm
medium-grained	grain size between 1 and 5 mm
fine-grained	grain size between 0.1 and 1 mm
very fine-grained	grain size between 0.1 and 0.01 mm
holocrystalline	adjective for a rock consisting only of crystals
hiatal	adjective for the texture of inequigranular rocks in which the sizes of the crystals vary gradually but form a broken series or where two or more sizes are notably different from one another as in porphyritic rocks.
hypocrystalline	adjective for a rock that is partly glassy, partly crystalline.
microcrystalline	micromeritic, - adjectives for a crystalline rock or matrix in which the individual crystals can only be distinguished under the microscope.
microlite	a microscopic crystal that polarizes light and has some determinable optical properties
opacitization	result of post eruption oxydation and dehydration generating swarms of opaque microscopic grains in rocks, especially as rims that develop mainly on biotite and hornblende.
penetration twin	interpenetration twins, - individuals appear to have grown through one another
phanerocrystalline	phaneritic, - adjective for holocrystalline rocks in which the crystals of the essential minerals can be distinguished by naked eye.
phantom	see ghost

pilotaxitic	adjective for the texture of holocrystalline porphyritic rocks in which the groundmass consists essentially of lath-shaped feldspar microlites, often showing a more or less noticeable flow arrangement.
poikilitic	adjective for a texture in igneous rocks in which small crystals are irregularly scattered without common orientation in a larger crystal of another mineral.
porphyritic	adjective for a texture of an igneous rock in which phenocrysts are set in a finer groundmass, which may be crystalline and/or glassy.
porphyro-aphanitic	adjective for a rock consisting of cryptocrystalline groundmass and microphenocrysts
seriate	adjective for the texture of inequigranular rocks where the sizes or the crystals vary gradually or in a continuous series.
subhedral	adjective for those minerals on a rock that are only partly bounded by their own crystal faces. The terms hypidiomorphic, hypautomorphic and subidiomorphic are also used to indicate rocks or rock textures characterized by predominance of subhedral minerals.
trachytic	adjective for a texture characteristic for trachytes, the groundmass is commonly holocrystalline or with a small amount of glassy residue. It consists essentially of lath-shaped feldspar microlites with some degree of flow alignment.

## Photographs

Photo 1      Cerro Millo from northern Cerro Sallaoqueña, direction of view: W

The photo shows the east-slope of Cerro Millo, the camp in Quebrada Sallaoqueña (foreground, white point) and in the background Cerro Supa. Light colored areas indicate intensive argillic to advanced argillic alteration.

Photo 2      Cerro Millo from northern Cerro Supa; direction of view: SE

The photo shows Quebrada Millo in the foreground and the dikes related to the outfanning Millo fault in the left part of the photo. The upper part of Cerro Millo is formed by pyroclastic rocks. In the upper right corner, the “shoulder of Cerro Millo” which is part of the eruption fissure on the mountain ridge of Cerro Millo is evident.

Photo 3      Southern Cerro Sallaoqueña (left part) and Cerro Chunco (right part) cut by Quebrada Sallaoqueña from Cerro Millo Sur; direction of view: SE

In the right foreground Trinchera IV crosses a turtle back-shaped outcrop of strongly altered ignimbrite (light line).

The top of Cerro Chunco is formed by porphyritic lava, underlain by block-lavas, which are easier to erode. The eastward dip of the strata is evident.

Note vast areas of sandy sediment cover in all pictures.



Photo 4      Cerro Sallaoqueña from the silicified top of Cerro Millo Sur; the lowest part of Cerro Chunco can be seen in the right part of the photo; direction of view: E

The mountain ridge is built up of block-lavas and porphyritic lavas. The dark patch in the south represents a font, where iron-bearing water is oxydized.

Photo 5      Cerro Millo Norte; direction of view: NW

The dashed line markes probable extent of the northern vent area, filled with subvolcanic pyroclastic rock material. The strata dip at Cerro Millo Norte from this point cupola-like to N, W and E.

Photo 6      Eastern slope of Cerro Millo from central Cerro Millo, on the left side, in the shadow lies Cerro Supa; direction of view: NNW

The oval in the foreground of the photo cut by Trinchera IV (light line in the right part of the photo) belongs to one pyroclastic flow/cooling unit and indicates besides the layering in the background that Cerro Millo strata dip on the eastern slope to E.

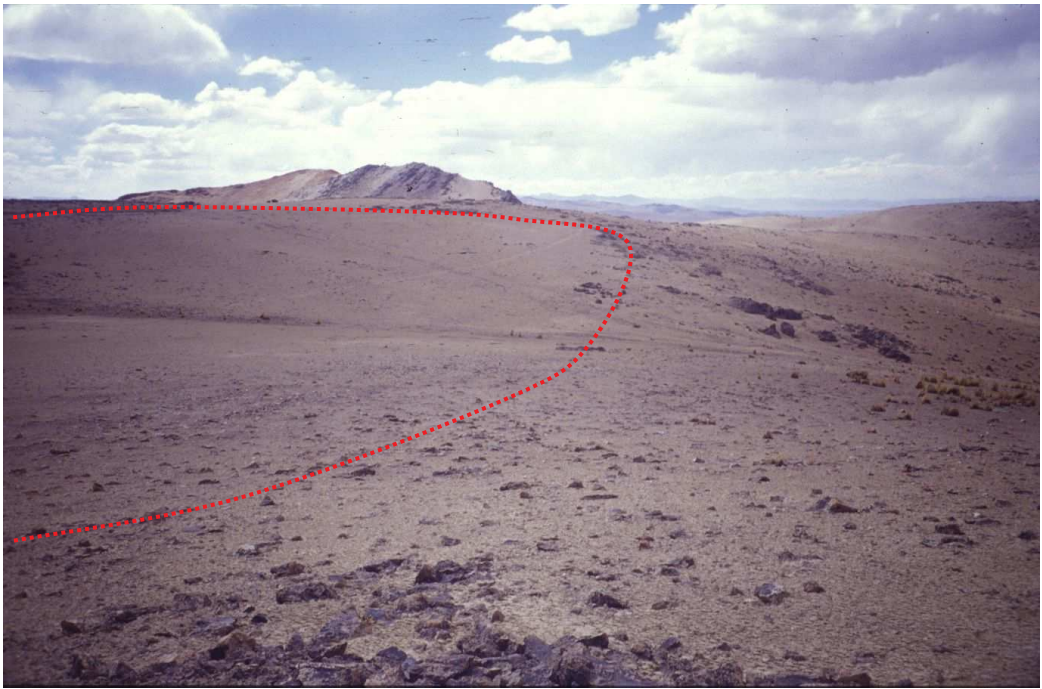


Photo 7      Front of an ignimbrite at Cerro Millo Sur (77971); direction of view: NE

The unit follows similar to the units on the western slope of Cerro Millo the slope of C° Millo. The notch at the base of the cooling unit, derived from lower degrees of welding and therefore better weatherability is distinct.

Photo 8      Top of Cerro Chunco; direction of view: N

The porphyritic lava shows vertical jointing features expressed in separation of columns up to 3 m in height.



Photo 9 Part of the large dike in Quebrada Sallaoqueña; direction of view: W

The vertical layering of the dike is expressed by vertical parting.

Photo 10 Flow folded porphyritic lava of the Millo event at the west-slope of Cerro Millo (outcrop 255); direction of view: NE

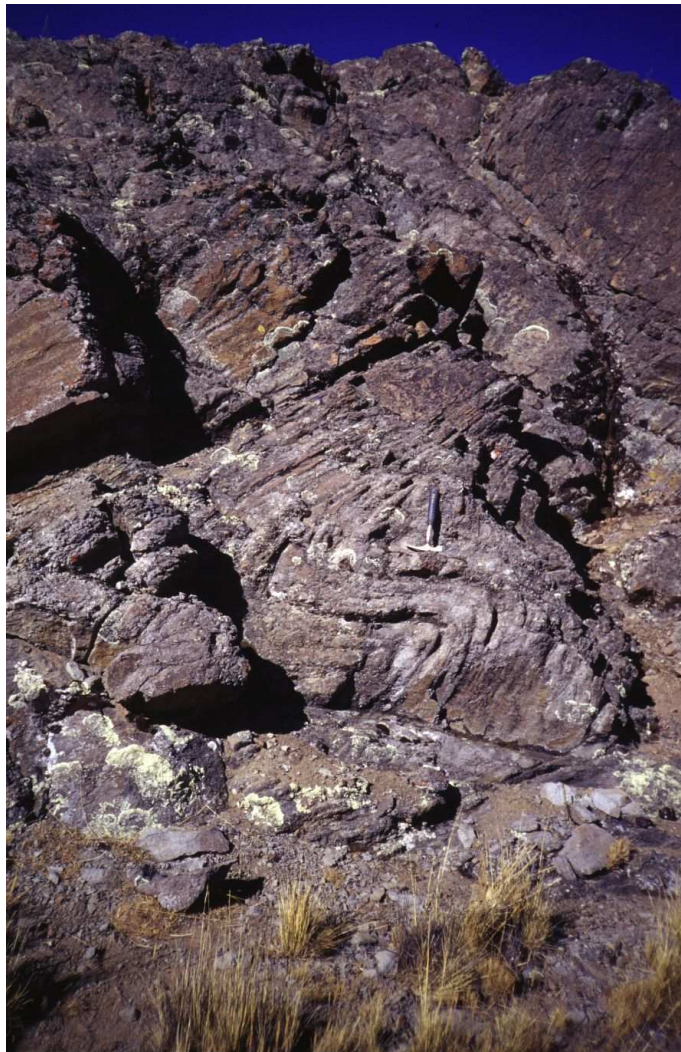
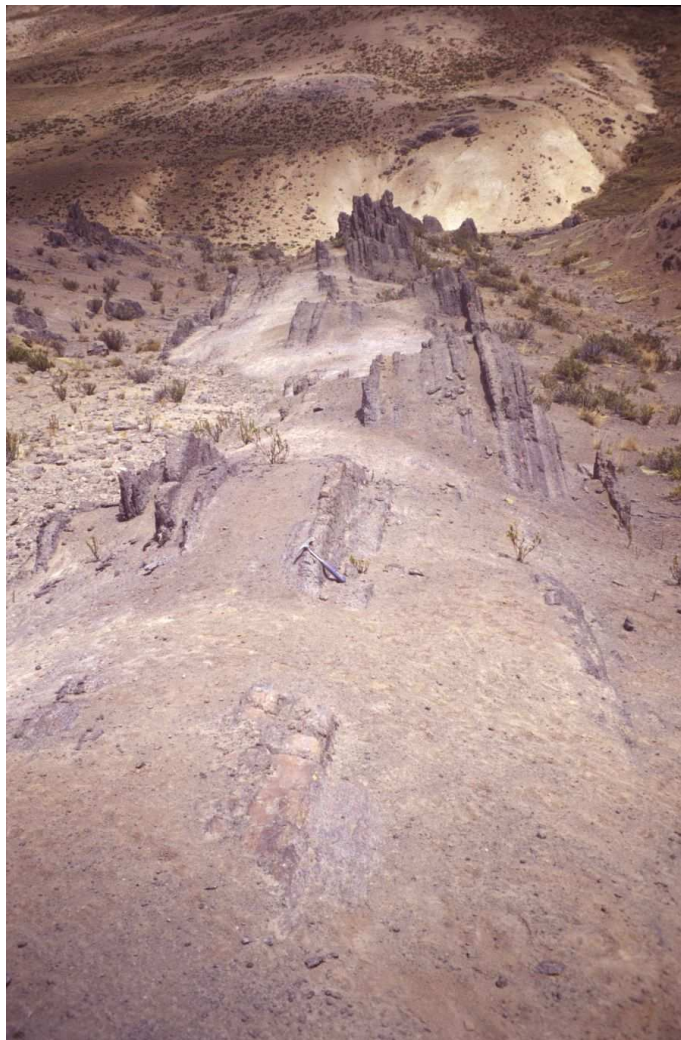


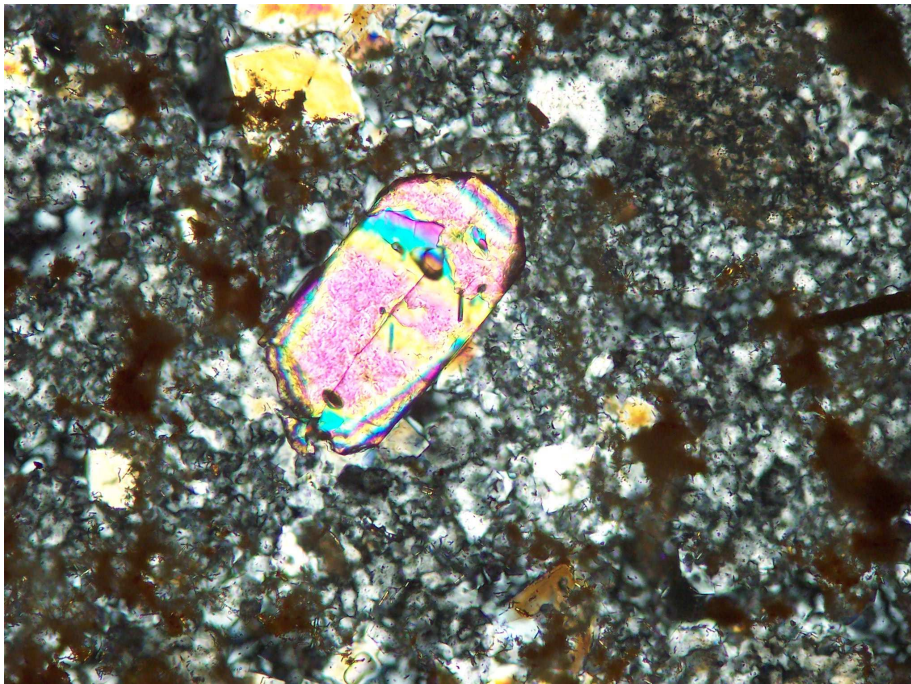
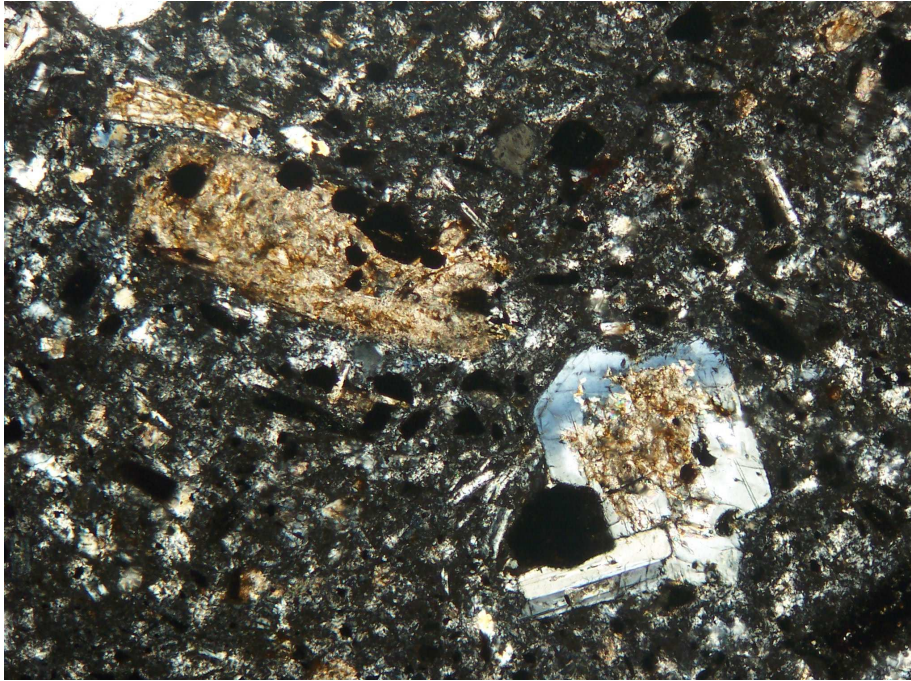
Photo 11 Silicified horizon at 4700 m at the west-slope of Cerro Zorrichata. Cerro Millo is on the right. In the background lies Cerro Supa; direction of view: N.

Photo 12 Silicified crest (creston) located at a fissure at the west-slope of Cerro Zorrichata. The rock is coated with iron oxides and iron oxyhydroxides. In the background can be seen Lag. Calacruz and Cerro Supa.



Photo 13 Propylitically altered porphyritic lava (TS 77966; XPL). Phenocrysts and microlites of plagioclase are altered to carbonate. Length of lower picture rim: 5.06 mm.

Photo 14 Hydrothermal zircon in strongly silicified rock (TS 77970; XPL). The mineral is set in a groundmass of fine-grained quartz and kaolinite. Length of lower picture rim: 1.34 mm.



## Tables

- Tab. 1: Metal content, structure and mineralogy of mines marked in Fig. 6  
(adapted from PALACIOS et al. 1993).
- Tab. 2: Normative constituents (CIPW) of the unaltered and weakly altered  
volcanic rocks at C° Millo, SE Peru.
- Tab. 3: Geochemical data of C° Millo rocks
- Tab. 4: Field data of Cerro Millo

sample	East	North	altitude [m]	sample area	rock type
77275	369804	8225074	4780	5x2	Latite (lava)
77276	369256	8225540	4823	6x2	Andesite-latite (lava)
77277	369448	8225474	4878	3x1	Trachyte-dacite (lava)
77279	369303	8225751	4819	3x2	Trachyte-dacite (lava)
77284	367770	8227860	4810	4x3	Andesite-trachyte (lava)
77285	366960	8227670	4475	4x4	Andesite-trachyte (lava)
77288	367251	8225248	4767	3x1	Andesite-trachyte (lava)
77289	368820	8227460	4734	6x2	Andesite-trachyte (lava)
77290	370000	8225540	4680	3x2	Latite-dacite (aph. lava)
77291	370000	8225210	4710	4x4	Latite-dacite (aph. lava)
77296	368016	8226523	4909	4x1	Andesite-latite (dike)
77297	368137	8226927	4917	2x1	Andesite-latite (dike)
77299	369746	8227984	4854	5x3	Dacite (lava)
77950	370014	8227465	4925	2x1	Dacite (block-lava)
77951	370000	8227180	4875	3x2	Dacite (lava)
77952	369892	8226636	4840	10x3	Andesite-latite (block-lava)
77953	369130	8227540	4711	3x1	Andesite (dome)
77954	368489	8227335	4829	10x10	Andesite (Hbl-dike)
77958	368545	8227056	4820	3x2	Andesite-trachyte (lava)
77965	366144	8225729	4704	4x2	Andesite (lava)
77966	368493	8227938	4788	3x2	Andesite-trachyte (lava)
77968	366411	8227622	4802	4x1	Andesite (block lava)
77270	367883	8227177	4845	5x3	Latite (pyroclastic rock, undiff.)
77955	368348	8227328	4880	6x2	Andesite-trachyte (lava)
77282	368196	8227245	4945	7x2	Latite (pyroclastic rock, undiff.)
77272	367707	8227251	4821	6x2	Andesite-trachyte (lava)
77268	368307	8225866	4810	10x2	Latite (pyroclastic rock, undiff.)
77967	367350	8227679	4800	5x4	Andesite-trachyte (lava)
77283	368024	8227579	4897	6x4	Latite (subvolcanic pyroclastic rock)
77298	369297	8227970	4748	6x4	Andesite-trachyte (lava)
77963	366916	8225924	4780	3x1	Latite (pyroclastic rock, undiff.)
77294	368219	8225305	4756	3x2	Latite (Amph.-olivine-bearing lava)
77280	366200	8225230	4650	2x1	Andesite (lava)
77971	368090	8226260	4902	4x1	Latite (ignimbrite, partly welded)
77961	366840	8225430	4698	8x4	Andesite-trachyte (lava)
77972	367860	8226600	4911	3x2	Latite (ashtuff)
77292	368504	8225546	4749	1x1	Andesite-trachyte (lava)
77957	368230	8227160	4921	8x3	Latite (pyroclastic rock, undiff.)
77281	368367	8226769	4859	6x3	Latite (ignimbrite unwelded)
77287	367183	8226074	4834	2x2	Latite (pyroclastic rock, undiff.)
77964	366298	8225848	4746	2x2	Andesite (lava)
77959	368640	8227000	4768	5x4	Andesite-trachyte (lava)
77295	367038	8226276	4842	5x2	Latite (pyroclastic rock, undiff.)
77269	368148	8227110	4929	6x2	Latite (subvolcanic pyroclastic rock)
77969	366807	8227105	4778	5x2	Andesite (lava)
77273	368027	8226794	4887	8x3	Latite (subvolcanic pyroclastic rock)
77970	366680	8226460	4786	4x3	Andesite (lava)
77274	369227	8225879	4744	4x3	Andesite-latite (lava)
77960	367820	8225000	4736	6x2	Andesite-trachyte (lava)
77271	367842	8227501	4832	5x4	Latite (ignimbrite unwelded)
77956	367850	8226400	4941	3x1	Latite (subvolcanic pyroclastic rock)
77278	369391	8225652	4835	7x3	Latite (block-lava)
77286	366870	8227585	4950	2x1	Andesite (block-lava)
77293	368308	8225066	4700	8x5	Latite (debris flow, lahar)
77962	366000	8225120	4725	2x2	Andesite (porphyro-afanitic lava)

sample	alteration	SiO <sub>2</sub>	TiO <sub>2</sub>	Ti	Al <sub>2</sub> O <sub>3</sub>	Al	Fe <sub>2</sub> O <sub>3</sub>	Fe	MnO	Mn	MgO	Mg
		wt%	wt%	wt%	wt%	wt%	wt%	wt%	wt%	ppm	wt%	wt%
		XRF	XRF	ICP	XRF	ICP	XRF	INAA	XRF	ICP	XRF	ICP
77275	least-altered, slight sericitization	62.20	0.831	0.60	16.92	3.57	5.72	3.94	0.067	656	0.68	0.23
77276	fresh	62.04	0.819	0.56	17.34	3.29	5.70	4.15	0.066	604	0.42	0.08
77277	least-altered, slight sericitization	63.04	0.777	0.56	16.38	4.79	5.33	3.89	0.089	825	1.22	0.78
77279	fresh	63.47	1.032	0.80	15.35	4.24	4.05	2.87	0.016	150	0.39	0.24
77284	least-altered, slight propylitic	63.32	0.829	0.60	16.50	3.54	4.57	3.27	0.026	248	0.74	0.27
77285	fresh	63.18	0.878	0.66	16.97	3.73	3.99	2.70	0.024	240	0.68	0.26
77288	fresh, opacitized	61.27	0.796	0.62	15.86	7.88	5.18	3.67	0.172	1651	2.55	2.20
77289	least-altered, slight propylitic	62.46	0.743	0.58	15.15	6.88	4.95	3.42	0.105	1005	2.01	1.76
77290	least-altered, slight propylitic	64.17	0.644	0.46	16.04	3.12	4.28	2.89	0.017	166	1.10	0.53
77291	least-altered, slight propylitic	61.93	0.733	0.55	16.01	3.51	5.27	3.68	0.127	1186	2.16	1.43
77296	least-altered, slight propylitic	61.24	0.812	0.61	16.24	6.09	5.13	3.40	0.149	1386	2.88	2.25
77297	least-altered, slight propylitic	62.27	0.835	0.66	16.38	8.54	5.07	3.06	0.082	762	1.88	1.80
77299	least-altered, slight propylitic	65.73	0.824	0.66	15.08	3.49	3.52	2.58	0.024	216	0.40	0.23
77950	least-altered, slight propylitic	65.88	0.790	0.63	15.32	3.76	3.47	2.47	0.008	79	0.21	0.14
77951	fresh	64.41	0.738	0.56	16.21	3.74	4.43	2.99	0.026	246	0.65	0.33
77952	least-altered, slight propylitic	65.51	0.827	0.54	16.13	3.98	3.03	2.14	0.008	70	0.27	0.17
77953	least-altered, slight propylitic	62.22	0.740	0.53	15.45	3.64	4.76	3.11	0.080	743	2.02	1.36
77954	least-altered, slight propylitic	62.20	0.738	0.59	15.43	10.62	4.74	3.10	0.078	796	2.04	2.06
77958	least-altered, slight propylitic	59.98	0.904	0.68	15.14	7.08	5.46	3.67	0.119	1110	2.93	2.42
77965	least-altered, slight propylitic	59.92	0.895	0.73	17.15	8.97	5.40	3.52	0.100	901	1.61	1.54
77966	least-altered, slight propylitic	59.51	0.956	0.75	16.52	8.71	6.15	4.11	0.121	1134	2.22	1.99
77968	least-altered, slight propylitic	62.04	0.801	0.55	15.64	3.38	3.78	2.58	0.039	360	0.96	0.60
77270	adv. argillic, A>K	57.06	0.739	0.62	15.24	5.81	1.20	0.99	0.004	32	0.01	0.01
77955	adv. argillic, A>K	56.79	0.677	0.55	15.35	5.56	1.52	1.13	0.002	8	0.01	0.01
77282	adv. argillic, A>K	60.43	0.764	0.62	13.56	5.04	2.61	1.93	0.001	6	0.01	0.01
77272	adv. argillic, K>A	67.10	0.755	0.58	11.32	4.62	1.48	1.18	0.004	35	0.01	0.01
77268	adv. argillic, K>A	64.34	0.649	0.51	12.26	4.68	3.30	2.55	0.008	42	0.01	0.01
77967	adv. argillic, K>A	59.47	0.735	0.50	18.24	6.04	1.29	0.99	0.002	12	0.01	0.01
77283	adv. argillic, K>A + silicification	77.35	0.952	0.77	7.54	3.06	0.86	0.71	0.004	37	0.01	0.01
77298	adv. argillic, K>A	64.05	0.658	0.51	13.90	5.02	4.30	3.28	0.002	12	0.01	0.01
77963	adv. argillic, K>A + silicification	81.07	1.158	0.95	6.12	2.63	0.46	0.37	0.004	25	0.01	0.01
77294	adv. argillic, K>A	68.12	0.905	0.69	14.78	5.41	2.31	1.66	0.002	18	0.01	0.01
77280	adv. argillic, K>A + silicification	88.10	0.859	0.69	2.98	1.34	3.07	2.42	0.002	20	0.01	0.01
77971	adv. argillic, K>A	67.24	0.731	0.59	18.08	5.16	0.35	0.26	0.002	12	0.01	0.01
77961	silicification	97.27	0.877	0.31	0.20	0.07	0.56	0.44	0.004	24	0.01	0.01
77972	silicification + argillic (kao)	97.23	1.524	0.36	0.32	0.20	0.15	0.13	0.002	15	0.01	0.01
77292	silicification	96.97	0.139	0.12	0.23	0.11	1.38	0.99	0.011	125	0.01	0.01
77957	silicification + argillic (kao)	96.40	1.076	0.22	0.25	0.14	1.26	0.90	0.004	22	0.01	0.01
77281	silicification	96.24	0.876	0.37	0.57	0.36	1.02	0.81	0.001	8	0.01	0.01
77287	silicification + propylitic	96.17	0.635	0.48	0.28	0.17	1.52	1.25	0.001	11	0.01	0.01
77964	vuggy silica	95.38	1.038	0.86	0.33	0.13	1.52	1.13	0.013	161	0.01	0.01
77959	vuggy silica	94.72	0.962	0.61	0.74	0.35	2.00	1.59	0.002	12	0.01	0.01
77295	silicification + argillic (kao)	94.45	0.976	0.34	0.34	0.12	2.46	1.88	0.007	138	0.01	0.01
77269	silicification	91.71	1.020	0.81	2.76	1.29	0.51	0.43	0.003	31	0.01	0.01
77969	silicification + argillic (kao)	91.15	0.242	0.20	3.49	1.36	0.30	0.23	0.007	42	0.01	0.01
77273	silicification + adv. argillic	87.92	0.990	0.81	1.05	0.56	6.94	5.83	0.006	59	0.01	0.01
77970	silicification + adv. argillic	86.52	1.314	0.81	0.75	0.33	5.46	3.66	0.009	76	0.01	0.01
77274	silicification + argillic (smectite)	82.35	0.788	0.24	5.39	2.31	1.77	1.33	0.014	145	0.06	0.06
77960	silicification + propylitic	81.07	0.080	0.07	9.44	3.00	0.58	0.46	0.007	49	0.01	0.01
77271	silicification + argillic (kao)	74.15	0.836	0.28	1.99	0.85	16.86	12.10	0.005	66	0.01	0.01
77956	sericitic	59.79	0.838	0.63	15.63	7.02	5.81	3.84	0.114	1063	2.93	2.40
77278	propylitic	58.40	1.056	0.86	16.70	5.38	5.84	4.39	0.029	264	0.62	0.47
77286	propylitic	61.34	0.858	0.67	16.68	4.61	4.35	2.94	0.027	245	0.42	0.31
77293	all alteration styles + ferricrete	46.46	0.683	0.48	10.03	3.35	25.37	17.60	0.009	81	0.24	0.10
77962		68.60	0.455	0.36	15.74	4.25	2.55	1.80	0.046	405	0.19	0.01

sample	CaO	Ca	Ca	Na <sub>2</sub> O	Na	K <sub>2</sub> O	K	P <sub>2</sub> O <sub>5</sub>	P	LOI	total	Li	Be	F	S
	wt%	wt%	wt%	wt%	wt%	wt%	wt%	wt%	wt%	wt%	wt%	ppm	ppm	wt%	wt%
	XRF	ICP	INAA	XRF	INAA	XRF	ICP	XRF	ICP	Grav.		ICP-MS	ICP-MS	XRF	ICP
77275	3.391	3.03	3	3.77	2.74	3.373	3.63	0.267	0.109	2.16	99.379	8.3	1.8	0.07	0.001
77276	2.625	2.22	2	3.49	2.70	3.404	3.68	0.160	0.051	3.37	99.434	3.0	1.6	0.05	0.001
77277	3.889	3.55	4	3.83	2.99	3.358	3.53	0.255	0.112	1.19	99.358	14.9	1.7	0.08	0.001
77279	2.136	1.62	1	3.44	2.63	3.301	3.98	0.332	0.164	5.82	99.337	6.0	1.8	0.05	0.556
77284	2.532	2.13	2	3.84	2.94	3.723	3.95	0.355	0.143	2.95	99.385	4.9	1.6	0.05	0.018
77285	2.594	2.29	2	3.62	2.63	3.445	3.50	0.228	0.087	3.79	99.399	5.6	1.7	0.05	0.005
77288	4.190	4.07	4	3.50	2.57	3.258	4.17	0.287	0.155	2.27	99.333	5.9	2.1	0.08	0.003
77289	3.861	3.67	4	3.07	2.32	3.357	3.60	0.250	0.132	2.89	98.846	4.7	2.1	0.14	0.021
77290	3.455	2.89	3	3.61	2.78	3.426	4.05	0.212	0.092	2.38	99.334	7.7	1.2	0.06	0.001
77291	4.405	3.87	4	3.28	2.57	3.534	3.73	0.255	0.114	1.61	99.314	3.5	1.6	0.06	0.001
77296	3.381	3.03	3	3.28	2.41	3.310	2.93	0.271	0.130	2.68	99.373	2.5	2.4	0.05	0.264
77297	3.617	3.35	3	3.34	2.51	3.569	4.68	0.281	0.151	1.97	99.294	3.8	2.9	0.05	0.515
77299	1.434	0.90	1	2.94	2.28	3.689	4.72	0.222	0.111	5.56	99.423	3.0	1.8	0.05	0.407
77950	1.892	1.19	2	3.24	2.57	3.599	4.01	0.230	0.117	4.78	99.419	5.1	1.6	0.05	0.229
77951	3.025	2.45	1	3.71	2.78	3.472	3.79	0.244	0.111	2.47	99.385	8.4	1.9	0.06	0.005
77952	1.701	1.17	3	3.18	2.48	3.752	3.34	0.393	0.158	4.59	99.391	5.2	1.3	0.05	0.121
77953	3.572	3.22	3	3.45	2.41	3.300	3.52	0.258	0.119	3.38	99.230	5.7	2.0	0.06	0.001
77954	3.569	3.76	4	3.4	2.44	3.325	3.57	0.262	0.151	3.48	99.262	6.1	2.0	0.05	0.008
77958	4.063	3.83	4	2.84	2.04	3.106	4.07	0.338	0.167	4.07	98.950	4.5	2.3	0.09	0.735
77965	4.424	4.11	4	3.49	2.51	2.497	2.95	0.445	0.244	3.45	99.381	3.4	2.8	0.05	0.011
77966	4.854	4.64	4	3.29	2.38	3.036	3.61	0.313	0.165	2.24	99.210	6.2	2.1	0.08	0.339
77968	3.182	2.66	3	2.69	1.91	3.454	3.36	0.350	0.148	6.39	99.326	3.9	2.6	0.05	0.364
77270	0.252	0.22	1	1.19	0.98	2.079	3.14	0.338	0.186	18.63	96.742	0.7	0.1	0.05	7.346
77955	0.117	0.06	1	1.05	0.79	2.602	3.71	0.130	0.067	18.19	96.438	0.5	0.3	0.05	7.007
77282	0.246	0.21	1	1.18	0.89	1.704	2.42	0.260	0.137	16.89	97.655	0.5	0.3	0.05	6.298
77272	0.128	0.11	1	0.52	0.44	2.122	2.98	0.191	0.098	13.90	97.530	0.5	0.3	0.05	5.307
77268	0.137	0.12	1	0.66	0.52	1.813	2.67	0.240	0.129	14.83	98.247	2.3	0.9	0.05	5.105
77967	0.266	0.21	1	0.26	0.22	1.581	2.32	0.745	0.370	16.56	99.159	3.7	0.3	0.05	3.801
77283	0.029	0.02	1	0.24	0.19	1.611	2.35	0.088	0.046	9.87	98.554	1.4	0.1	0.05	3.588
77298	0.179	0.16	1	0.50	0.42	1.021	1.35	0.455	0.230	13.98	99.055	28.3	1.3	0.05	2.942
77963	0.021	0.01	1	0.21	0.06	1.434	2.19	0.086	0.045	8.31	98.883	4.5	0.1	0.05	2.885
77294	0.151	0.14	1	0.10	0.09	0.629	0.83	0.439	0.218	11.93	99.376	16.7	0.4	0.07	2.593
77280	0.086	0.09	1	0.01	0.02	0.072	0.11	0.436	0.227	3.24	98.865	16.5	0.6	0.06	2.456
77971	0.036	0.03	1	0.11	0.10	0.990	1.37	0.101	0.053	11.64	99.290	15.3	0.2	0.05	1.875
77961	0.012	0.02	1	0.01	0.01	0.011	0.03	0.026	0.010	0.67	99.650	2.5	0.1	0.05	0.021
77972	0.005	0.02	1	0.01	0.01	0.023	0.05	0.010	0.002	0.38	99.664	0.5	0.2	0.05	0.063
77292	0.009	0.01	1	0.01	0.01	0.008	0.03	0.030	0.018	0.89	99.687	1.0	0.2	0.05	0.024
77957	0.006	0.01	1	0.01	0.01	0.008	0.02	0.027	0.008	0.64	99.691	0.8	0.2	0.05	0.018
77281	0.012	0.02	1	0.01	0.02	0.025	0.05	0.028	0.011	0.85	99.642	0.7	0.2	0.06	0.077
77287	0.008	0.02	1	0.01	0.02	0.016	0.03	0.007	0.006	0.80	99.457	2.5	0.1	0.05	0.076
77964	0.010	0.01	1	0.02	0.02	0.020	0.03	0.019	0.009	0.97	99.330	2.9	0.1	0.05	0.217
77959	0.017	0.02	1	0.01	0.01	0.016	0.04	0.068	0.033	1.09	99.635	2.1	0.4	0.05	0.037
77295	0.009	0.01	1	0.01	0.02	0.019	0.03	0.043	0.016	1.18	99.504	3.0	0.2	0.05	0.052
77269	0.055	0.08	1	0.03	0.03	0.397	0.62	0.110	0.058	2.97	99.575	0.5	0.2	0.05	0.853
77969	0.124	0.13	1	0.05	0.05	0.181	0.26	0.164	0.085	3.82	99.538	7.5	0.5	0.05	0.185
77273	0.050	0.06	1	0.01	0.01	0.048	0.09	0.207	0.112	2.28	99.511	1.3	0.5	0.05	0.263
77970	0.018	0.02	1	0.03	0.01	0.077	0.10	0.119	0.060	2.06	96.367	1.3	0.5	0.05	0.347
77274	1.004	1.05	1	0.93	0.73	2.013	2.82	0.592	0.162	4.62	99.531	1.6	1.2	0.05	0.299
77960	0.239	0.18	1	2.31	1.69	3.783	4.12	0.006	0.004	2.11	99.635	6.6	2.0	0.05	0.087
77271	0.009	0.01	1	0.12	0.12	0.222	0.31	0.036	0.017	5.34	99.578	0.5	0.1	0.05	0.830
77956	4.519	4.15	4	3.38	2.49	3.124	3.52	0.307	0.152	2.53	98.972	10.4	2.2	0.05	0.158
77278	1.363	1.02	1	1.60	1.28	2.641	3.17	0.173	0.088	10.99	99.412	6.8	1.9	0.05	0.388
77286	0.877	0.60	1	1.10	0.81	2.910	3.51	0.186	0.093	10.65	99.398	4.7	2.1	0.05	0.285
77293	0.331	0.25	1	0.46	0.36	1.321	1.73	0.272	0.133	14.17	99.346	4.8	0.8	0.05	1.944
77962	2.035	1.63	2	4.25	3.27	4.289	4.07	0.128	0.057	1.16	99.443	12.6	2.1	0.05	0.004

sample	SO <sub>3</sub>	Cl	Sc	Sc	V	V	V	Cr	Cr	Co	Co	Co	Ni	Ni
	wt%	wt%	ppm	ppm	ppm	ppm	ppm	ppm	ppm	ppm	ppm	ppm	ppm	ppm
	XRF	XRF	XRF	INAA	XRF	ICP	ICP-MS	XRF	INAA	XRF	ICP-MS	INAA	XRF	ICP-MS
77275	0.02	0.015	10	10.2	77	102	85	38	47	11	13.4	12	17	20.5
77276	0.01	0.041	10	10.1	48	72	51	26	34	13	11.9	13	12	15.8
77277	0.01	0.040	10	10.6	89	99	78	18	27	14	12.8	13	13	15.4
77279	0.06	0.036	11	10.6	90	127	83	53	62	4	2.8	4	3	5.0
77284	0.02	0.016	10	10.0	89	114	71	49	63	4	5.8	7	12	13.6
77285	0.01	0.041	12	11.1	126	158	108	40	50	4	5.5	6	9	10.2
77288	0.04	0.038	12	10.4	121	148	102	16	21	12	14.0	13	9	13.4
77289	0.56	0.034	9	8.2	90	112	78	11	19	11	11.2	12	3	11.5
77290	0.03	0.035	10	9.3	104	122	81	55	66	8	9.1	9	29	31.9
77291	0.01	0.056	10	9.6	113	141	94	44	62	16	14.2	14	27	33.2
77296	0.09	0.050	9	9.5	108	138	113	20	26	11	13.2	13	13	14.0
77297	0.07	0.056	12	10.3	124	141	106	18	29	14	13.1	12	9	12.0
77299	0.09	0.014	10	10.0	107	141	98	3	8	3	2.4	3	3	1.3
77950	0.06	0.041	8	8.9	65	101	61	16	25	3	1.9	2	3	1.9
77951	0.01	0.045	8	8.6	97	122	88	13	23	9	8.3	8	4	8.5
77952	0.08	0.036	8	9.1	59	79	50	6	22	3	1.9	3	3	1.7
77953	0.19	0.042	8	7.6	129	148	102	6	18	13	11.6	12	8	10.9
77954	0.19	0.042	9	7.5	137	151	114	11	18	18	12.7	12	7	12.4
77958	0.37	0.037	11	9.3	118	140	111	43	55	14	15.2	15	19	23.2
77965	0.01	0.019	8	6.7	122	151	115	3	6	13	11.1	11	4	6.9
77966	0.17	0.040	12	9.8	128	155	119	3	11	14	15.9	16	7	11.4
77968	0.05	0.066	8	8.6	105	135	96	42	49	11	10.1	10	17	22.6
77270	2.64	0.034	10	10.7	114	150	122	25	41	3	1.2	1	3	3.2
77955	3.07	0.037	5	5.1	78	103	73	23	40	3	0.1	1	3	0.5
77282	1.89	0.029	9	8.7	101	132	92	3	14	3	0.3	1	3	0.5
77272	1.96	0.030	5	6.2	65	84	64	26	36	4	0.3	1	3	1.1
77268	1.15	0.030	10	10.8	92	111	93	12	37	3	0.3	1	3	0.7
77967	0.15	0.051	12	11.1	114	138	96	37	57	3	1.0	1	3	1.6
77283	1.06	0.014	3	3.9	36	58	39	17	30	3	0.4	1	3	0.8
77298	0.33	0.046	8	7.5	95	118	89	3	9	4	0.3	1	3	0.5
77963	0.64	0.042	4	3.7	37	53	31	3	5	3	0.1	1	3	0.1
77294	0.06	0.043	14	13.1	97	125	77	8	16	3	3.6	5	3	3.0
77280	0.24	0.033	6	6.3	99	141	87	21	40	3	3.8	5	3	2.6
77971	0.19	0.043	5	4.8	74	111	78	30	38	3	0.5	1	3	0.7
77961	0.02	0.037	2	0.4	5	4	1	3	16	4	0.1	1	3	0.5
77972	0.02	0.017	2	0.4	5	5	1	3	5	3	0.4	1	3	0.9
77292	0.01	0.044	2	0.4	5	3	1	5	6	3	0.3	1	3	0.6
77957	0.01	0.020	3	2.0	18	3	1	3	11	3	0.1	1	3	0.5
77281	0.03	0.040	4	4.6	24	11	1	14	27	3	0.1	1	3	0.5
77287	0.07	0.030	3	3.7	17	26	12	16	36	3	0.1	1	3	0.5
77964	0.09	0.029	2	2.6	5	14	4	3	9	3	1.2	1	3	1.8
77959	0.01	0.036	6	6.5	13	18	7	40	58	3	0.1	1	3	0.6
77295	0.02	0.050	2	0.7	14	5	1	6	15	4	0.3	1	3	0.6
77269	0.04	0.038	3	3.5	35	42	23	3	13	3	0.2	1	3	0.6
77969	0.04	0.058	2	2.2	43	62	39	12	16	3	0.2	1	3	1.0
77273	0.05	0.034	7	7.7	38	53	34	12	17	4	0.5	1	3	0.9
77970	0.88	0.047	2	2.1	39	33	20	3	18	3	1.5	2	3	1.5
77274	0.07	0.036	3	2.8	27	43	25	5	10	7	4.3	5	3	3.9
77960	0.01	0.038	2	1.3	5	2	1	3	5	3	0.2	1	3	0.5
77271	0.05	0.037	2	2.4	36	35	27	51	77	3	0.6	1	3	1.4
77956	0.45	0.047	12	10.6	121	143	119	7	16	12	15.9	16	12	17.9
77278	0.08	0.035	12	12.5	176	223	146	3	13	4	5.3	5	3	3.1
77286	0.05	0.038	10	9.6	135	173	130	30	45	5	2.3	3	3	2.2
77293	0.14	0.039	7	7.1	99	129	102	14	30	5	1.1	1	3	1.2
77962	0.01	0.031	3	2.8	18	29	17	3	5	3	2.5	3	3	1.8

sample	Ni	Cu	Cu	Zn	Zn	Zn	Ga	Ga	Ge	As	As	Se	Se	Br
	ppm	ppm	ppm	ppm	ppm	ppm	ppm	ppm	ppm	ppm	ppm	ppm	ppm	ppm
	INAA	XRF	ICP-MS	XRF	ICP	INAA	XRF	ICP-MS	ICP-MS	XRF	INAA	ICP-MS	INAA	INAA
77275	37	25	21.3	87	96	131	22	23.1	0.4	2	2.5	0.3	3	0.5
77276	28	20	17.2	123	130	50	21	19.9	0.7	2	0.5	0.1	3	0.5
77277	38	19	16.0	91	98	115	22	19.8	0.3	3	0.5	0.1	3	0.5
77279	32	12	5.4	41	46	50	24	24.8	0.6	2	2.3	0.3	3	0.5
77284	33	14	11.8	85	90	112	24	20.4	0.2	2	2.2	0.2	3	0.5
77285	34	17	12.1	78	81	50	25	22.7	0.3	2	0.5	0.3	3	0.5
77288	31	22	16.2	99	103	127	24	20.6	0.2	2	2.4	0.3	3	0.5
77289	31	14	14.9	67	71	109	20	19.5	0.2	2	0.5	0.2	3	0.5
77290	31	42	42.3	72	78	50	22	20.3	0.1	2	0.5	0.1	3	0.5
77291	28	53	55.9	109	115	50	22	22.2	0.1	2	0.5	0.2	3	0.5
77296	27	19	19.9	81	88	82	22	22.6	0.2	2	2.9	0.4	3	0.5
77297	29	18	17.1	131	137	149	21	21.3	0.3	2	2.8	0.3	3	0.5
77299	28	10	0.2	41	47	89	20	20.7	0.4	2	1.7	0.3	3	0.5
77950	26	10	3.9	46	55	50	22	21.1	0.1	2	1.7	0.1	3	0.5
77951	29	10	7.9	65	73	50	22	22.0	0.1	2	0.5	0.3	3	0.5
77952	29	10	2.5	64	71	50	23	21.0	0.6	2	2.7	0.2	3	0.5
77953	25	10	7.8	63	68	67	21	21.2	0.2	2	1.2	0.2	3	0.5
77954	108	10	8.8	65	66	71	22	22.2	0.8	2	0.5	0.3	3	0.5
77958	26	21	16.0	77	77	50	22	22.7	0.3	2	0.5	0.3	3	0.5
77965	29	13	7.8	128	128	147	23	20.7	0.1	2	2.5	0.2	3	0.5
77966	26	22	15.1	80	83	117	22	17.7	0.2	2	2.3	0.5	3	0.5
77968	27	20	13.1	102	108	50	22	21.1	0.4	2	1.8	0.4	3	0.5
77270	34	10	0.9	6	4	50	21	21.6	0.7	2	4.9	0.5	3	0.5
77955	20	10	0.2	8	5	50	15	13.0	0.5	2	2.2	0.4	3	1.5
77282	27	10	3.2	4	3	50	16	16.0	0.4	5	3.5	1.2	3	0.5
77272	27	10	0.2	5	4	50	19	20.4	0.6	4	6.9	0.4	3	0.5
77268	27	19	8.5	7	5	50	16	18.5	0.2	4	6.3	1.3	3	0.5
77967	26	10	0.2	3	5	50	22	18.8	0.4	2	1.7	0.4	3	0.5
77283	20	10	0.2	5	7	50	11	10.9	0.2	2	1.9	0.9	3	2.1
77298	25	10	6.5	32	4	50	20	20.1	0.2	45	5.2	0.5	3	1.5
77963	20	10	0.2	4	5	50	7	7.4	0.1	3	3.5	0.1	3	0.5
77294	24	10	3.3	6	6	50	23	23.0	0.4	2	4.7	0.2	3	0.5
77280	23	21	7.0	8	9	50	19	19.6	0.7	33	49.8	0.7	3	0.5
77971	20	10	0.2	5	6	50	19	15.8	0.4	2	3.8	0.1	3	2.1
77961	20	10	0.2	3	7	50	3	0.3	0.1	8	13.7	0.2	3	5.8
77972	20	10	0.2	6	6	50	3	0.7	0.2	14	17.4	0.1	3	7.5
77292	20	10	2.4	9	9	50	3	0.5	0.1	2	4.5	0.1	3	0.5
77957	20	10	0.2	3	6	50	3	0.5	0.1	2	2.0	0.2	3	13.3
77281	20	10	0.2	3	5	50	3	0.9	0.1	2	3.1	0.2	3	2.2
77287	20	10	0.2	3	5	50	3	5.5	0.2	5	7.7	0.2	3	0.5
77964	20	10	0.2	6	4	50	4	5.9	0.2	5	25.4	0.6	3	0.5
77959	20	10	0.8	3	6	50	3	0.9	0.2	2	3.8	0.4	3	0.5
77295	20	10	5.5	6	5	50	3	0.8	0.1	2	6.3	0.2	3	1.6
77269	20	10	0.2	5	9	50	3	0.5	0.2	2	3.4	0.4	3	8.6
77969	20	10	0.2	6	8	50	7	6.7	0.1	2	0.7	0.1	3	0.5
77273	22	17	7.7	9	3	50	3	2.1	0.2	4	12.7	1.5	3	1.1
77970	20	25	17.0	3	2	50	3	10.8	0.2	260	300.0	2.1	3	0.5
77274	21	10	11.2	16	22	50	8	7.1	0.1	2	7.1	0.2	3	0.5
77960	21	10	0.2	11	14	50	14	12.6	0.1	32	35.4	0.3	3	0.5
77271	21	28	32.1	9	1	50	8	6.9	0.3	5	7.5	7.1	8	0.5
77956	28	23	20.6	80	78	50	16	21.9	0.2	2	0.5	0.4	3	0.5
77278	34	33	16.6	110	117	169	21	22.4	0.3	2	5.1	0.3	3	0.9
77286	28	16	13.6	48	51	50	24	23.1	0.3	2	2.0	0.3	3	1.8
77293	27	29	26.6	32	13	50	19	18.1	0.2	20	20.6	0.5	3	0.5
77962	28	10	0.2	56	63	50	19	20.5	0.2	2	2.0	0.3	3	0.5

sample	Rb	Rb	Rb	Sr	Sr	Sr	Y	Y	Zr	Zr	Nb	Nb	Mo
	ppm	ppm	ppm	ppm	ppm	wt%	ppm	ppm	ppm	ppm	ppm	ppm	ppm
	XRF	ICP-MS	INAA	XRF	ICP-MS	INAA	XRF	ICP-MS	XRF	ICP-MS	XRF	ICP-MS	XRF
77275	110	45.1	49	573	525	0.06	15	10.8	178	99	11	14.3	2
77276	107	41.8	61	518	358	0.05	6	5.0	161	53	13	13.0	2
77277	106	41.0	42	573	512	0.07	9	9.3	163	83	13	13.2	2
77279	96	61.4	70	734	590	0.05	5	9.2	205	163	19	19.8	2
77284	112	36.2	44	826	581	0.07	6	5.1	177	119	16	13.5	2
77285	104	34.3	42	725	532	0.06	9	8.7	166	116	15	15.7	2
77288	101	29.0	45	623	530	0.07	9	9.5	151	94	10	12.1	2
77289	107	33.1	48	448	427	0.06	10	8.3	153	94	13	14.2	2
77290	116	47.6	64	502	456	0.06	3	4.1	158	154	7	7.2	2
77291	106	41.2	51	572	537	0.07	3	5.4	151	165	6	7.4	2
77296	91	31.4	45	556	593	0.07	11	13.4	161	104	13	14.1	2
77297	112	48.0	55	538	502	0.07	12	11.1	165	95	12	13.2	2
77299	123	71.7	74	322	213	0.05	6	5.1	170	136	15	17.4	2
77950	115	73.7	82	420	328	0.05	3	4.4	169	95	15	15.5	2
77951	114	60.4	74	502	489	0.05	5	8.2	168	100	13	15.7	2
77952	121	66.9	79	403	290	0.05	4	6.8	172	96	15	7.0	2
77953	106	54.8	65	481	437	0.05	9	9.3	160	75	15	14.2	2
77954	101	49.0	58	484	485	0.08	10	10.4	150	84	11	15.9	2
77958	78	33.0	42	490	511	0.06	6	8.7	178	129	15	16.1	2
77965	103	32.9	43	793	737	0.10	12	8.5	185	172	15	17.0	2
77966	86	30.7	42	556	527	0.07	11	9.0	169	108	10	14.2	2
77968	108	55.1	70	671	552	0.07	23	15.6	187	115	13	12.9	2
77270	13	8.1	15	1029	1050	0.14	3	6.5	158	135	14	16.3	2
77955	11	3.8	15	622	546	0.08	3	2.9	129	60	10	11.5	3
77282	10	7.5	15	496	469	0.05	3	5.4	146	100	13	14.7	2
77272	9	4.9	15	825	851	0.09	3	6.3	147	79	17	17.3	2
77268	10	4.7	15	1264	1240	0.12	3	8.5	129	93	10	11.5	2
77967	7	4.7	15	1466	1120	0.12	10	10.1	171	111	14	11.2	2
77283	10	3.9	15	287	315	0.05	3	1.1	165	89	17	22.6	2
77298	23	21.7	31	1334	1290	0.12	3	9.4	141	115	13	16.0	2
77963	8	1.5	15	298	256	0.05	3	1.9	221	157	17	19.3	2
77294	7	2.0	15	816	690	0.11	3	6.4	184	126	15	14.6	2
77280	5	3.0	15	3494	3470	0.37	3	9.4	172	117	17	13.4	2
77971	8	3.7	15	521	402	0.05	3	0.4	149	50	13	12.7	2
77961	5	0.6	15	4	5	0.05	3	0.7	121	10	13	0.8	2
77972	8	2.0	15	23	30	0.05	3	0.1	174	10	26	0.2	2
77292	5	1.3	15	10	15	0.05	3	0.4	19	5	3	2.2	2
77957	5	0.4	15	2	1	0.05	3	0.6	215	10	18	0.2	2
77281	7	2.1	15	53	60	0.05	3	2.2	114	20	13	0.6	2
77287	6	1.9	15	18	22	0.05	3	2.2	135	68	10	3.7	2
77964	5	0.3	15	107	118	0.05	3	1.3	241	110	19	18.1	2
77959	9	0.8	15	63	66	0.05	7	10.9	179	53	15	5.6	3
77295	9	0.9	15	6	7	0.05	3	0.9	172	50	17	0.3	2
77269	6	4.6	15	207	195	0.05	3	1.6	182	29	19	8.3	2
77969	16	10.5	15	518	512	0.07	3	1.9	43	29	6	5.2	2
77273	5	3.2	15	438	479	0.06	3	8.5	203	102	17	14.7	2
77970	7	3.2	15	789	766	0.10	3	0.8	304	43	24	9.4	2
77274	74	78.0	63	145	151	0.05	4	11.0	169	51	15	1.6	2
77960	163	155.8	155	8	12	0.05	13	12.9	78	82	13	15.0	3
77271	6	0.7	15	61	73	0.05	3	0.7	151	19	18	7.0	2
77956	91	30.4	42	528	497	0.06	4	9.1	160	69	14	13.5	2
77278	110	92.6	119	315	277	0.05	5	6.9	189	152	15	15.7	2
77286	133	131.0	129	378	329	0.05	9	10.6	167	131	15	17.4	3
77293	30	21.7	29	511	506	0.06	3	4.0	150	88	13	11.8	2
77962	136	84.0	100	377	295	0.05	6	8.1	251	262	17	17.5	2

sample	Mo	Mo	Ag	Ag	Cd	In	Sn	Sn	Sn	Sb	Sb	Te	Cs
	ppm	ppm	ppm	ppm	ppm	ppm	ppm	ppm	wt, %	ppm	ppm	ppm	ppm
	ICP	INAA	ICP-MS	INAA	ICP-MS	ICP-MS	XRF	ICP-MS	INAA	XRF	INAA	ICP-MS	XRF
77275	2	4	0.05	5	0.2	0.1	2	1.0	0.01	5	0.4	0.1	8
77276	3	1	0.05	5	0.1	0.1	5	1.0	0.01	5	1.0	0.1	9
77277	3	1	0.05	5	0.1	0.1	2	1.0	0.01	5	0.3	0.1	5
77279	3	1	0.05	5	0.1	0.1	4	1.0	0.01	5	0.1	0.1	7
77284	3	1	0.05	5	0.1	0.1	2	1.0	0.01	5	0.1	0.1	7
77285	3	1	0.05	5	0.1	0.1	2	1.0	0.01	5	0.3	0.1	5
77288	2	1	0.05	5	0.1	0.1	2	1.0	0.01	5	0.2	0.1	10
77289	3	1	0.05	5	0.1	0.1	3	1.0	0.01	5	0.1	0.1	8
77290	3	1	0.05	5	0.1	0.1	2	1.0	0.01	5	0.4	0.1	8
77291	4	4	0.05	5	0.1	0.1	3	1.0	0.01	5	0.2	0.1	8
77296	4	4	0.05	5	0.1	0.1	3	1.0	0.01	5	0.1	0.1	6
77297	5	2	0.05	5	0.1	0.1	2	1.0	0.01	5	0.4	0.1	6
77299	3	1	0.05	5	0.1	0.1	2	1.0	0.01	5	0.2	0.1	7
77950	2	4	0.05	5	0.1	0.1	5	1.0	0.01	5	0.1	0.1	8
77951	3	1	0.05	5	0.1	0.1	2	1.0	0.01	5	0.1	0.1	5
77952	2	1	0.05	5	0.1	0.1	6	1.0	0.01	5	0.1	0.1	8
77953	3	1	0.05	5	0.1	0.1	2	1.0	0.01	5	0.1	0.1	6
77954	2	5	0.05	5	0.1	0.1	3	1.0	0.01	5	0.1	0.1	6
77958	4	2	0.05	5	0.1	0.1	2	1.0	0.01	5	0.1	0.1	5
77965	5	1	0.05	5	0.3	0.1	2	1.0	0.01	5	5.5	0.1	195
77966	5	1	0.05	5	0.1	0.1	3	1.0	0.01	11	0.3	0.1	6
77968	3	1	0.05	5	0.1	0.1	2	1.0	0.01	5	0.1	0.1	8
77270	3	1	0.05	5	0.1	0.1	3	1.0	0.01	5	1.0	0.3	5
77955	2	1	0.05	5	0.1	0.1	2	1.0	0.01	5	0.6	0.2	5
77282	2	5	0.05	5	0.1	0.1	2	1.0	0.01	5	0.9	0.2	6
77272	1	1	0.05	5	0.1	0.1	2	1.0	0.01	5	0.4	0.3	5
77268	2	3	0.05	5	0.1	0.1	4	1.0	0.01	26	31.6	0.3	6
77967	2	1	0.05	5	0.1	0.1	2	1.0	0.01	5	0.1	0.2	6
77283	1	1	0.05	5	0.1	0.1	2	1.0	0.01	5	0.8	0.6	5
77298	2	2	0.05	5	0.1	0.1	4	1.0	0.01	5	0.4	0.8	7
77963	5	1	0.05	5	0.1	0.1	3	1.0	0.01	5	0.6	0.1	8
77294	1	4	0.05	5	0.1	0.1	5	1.0	0.01	5	0.4	0.1	7
77280	5	1	0.05	5	0.1	0.2	2	1.0	0.02	217	221.0	0.4	8
77971	4	2	0.05	5	0.1	0.1	2	1.0	0.01	5	0.6	0.1	5
77961	1	3	0.05	5	0.1	0.1	5	1.0	0.01	5	1.5	0.1	5
77972	1	5	0.05	5	0.1	0.1	3	1.0	0.01	5	1	0.1	5
77292	1	3	0.05	5	0.1	0.1	2	1.0	0.01	5	2.2	0.1	5
77957	1	4	0.05	5	0.1	0.1	4	1.0	0.01	5	0.4	0.1	7
77281	1	2	0.05	5	0.1	0.1	2	1.0	0.01	5	1.3	0.1	5
77287	1	4	0.05	5	0.1	0.1	5	1.0	0.01	5	1.5	0.1	6
77964	5	5	0.05	5	0.1	0.1	6	1.5	0.01	34	28.8	0.5	7
77959	4	5	0.05	5	0.1	0.1	2	1.0	0.01	5	0.5	0.1	5
77295	1	1	0.05	5	0.1	0.1	2	1.0	0.01	5	0.8	0.1	5
77269	4	2	0.05	5	0.1	0.1	2	1.0	0.01	5	0.3	0.2	5
77969	1	1	0.05	5	0.1	0.1	2	1.0	0.01	5	0.1	0.1	7
77273	3	3	0.05	5	0.1	0.1	2	1.0	0.01	5	1.4	0.6	5
77970	2	2	0.11	5	0.1	0.1	9	2.6	0.01	152	137.0	0.6	9
77274	3	3	0.05	5	0.1	0.1	2	1.0	0.01	5	0.6	0.1	9
77960	4	1	0.05	5	0.1	0.1	2	1.0	0.01	5	1.2	0.1	8
77271	2	3	0.05	5	0.1	0.1	2	1.0	0.01	5	0.8	2.5	8
77956	6	2	0.05	5	0.1	0.1	3	1.0	0.01	5	0.1	0.2	8
77278	4	1	0.05	5	0.1	0.1	5	1.0	0.01	5	0.4	0.1	8
77286	3	3	0.05	5	0.1	0.1	2	1.0	0.01	5	0.1	0.1	8
77293	3	2	0.05	5	0.1	0.1	2	1.0	0.01	5	1.0	0.2	6
77962	2	1	0.05	5	0.1	0.1	2	1.0	0.01	5	0.1	0.1	7

sample	Cs	Cs	Ba	Ba	Ba	La	La	La (co)	La	Ce	Ce	Ce (co)	Ce
	ppm	ppm	ppm	ppm	ppm	ppm	ppm	ppm	ppm	ppm	ppm	ppm	ppm
	ICP-MS	INAA	XRF	INAA	ICP	XRF	ICP-MS	ICP-MS	INAA	XRF	ICP-MS	ICP-MS	INAA
77275	2.98	2	854	1300	1274	51	17.5	43.4	49.4	89	48.3	119.8	115
77276	3.11	3	830	1200	1176	39	10.8	37.9	47.6	65	32.6	114.8	100
77277	2.74	2	848	1300	1282	62	19.5	45.2	49.8	87	46.6	107.9	110
77279	2.57	2	940	1300	1467	46	16.1	42.8	48.8	93	42.4	112.5	110
77284	1.90	2	1135	1500	792	39	10.4	42.4	48.2	81	29.5	120.3	111
77285	2.60	3	908	1300	1314	49	13.4	45.9	56.5	103	41.4	141.9	128
77288	2.09	3	801	1200	1290	54	20.3	44.4	50.0	77	50.3	109.7	100
77289	1.67	3	739	1200	1181	38	20.3	38.4	42.5	77	43.8	82.7	76
77290	3.65	4	1133	1600	795	55	16.0	38.2	43.8	59	36.2	86.5	88
77291	3.68	4	1075	1600	760	48	22.5	38.7	39.6	74	46.6	80.4	83
77296	1.18	1	751	980	1151	65	22.7	39.2	43.1	72	53.9	92.9	93
77297	1.66	2	820	1200	1303	43	15.9	37.0	42.2	64	39.4	91.7	93
77299	2.42	3	752	1200	1147	20	8.0	36.2	41.1	58	24.9	112.1	87
77950	2.57	3	825	1000	1293	20	8.5	29.5	31.9	56	20.5	71.6	64
77951	2.45	2	829	1400	1271	57	18.0	42.0	46.5	76	45.3	105.9	92
77952	2.56	3	863	1400	1336	31	9.0	32.9	36.8	42	22.5	82.1	78
77953	2.31	3	719	840	1080	40	18.9	35.5	37.5	71	39.7	74.6	75
77954	2.63	3	723	840	1252	34	20.8	36.9	37.9	66	45.1	80.1	79
77958	0.75	1	798	1200	1214	64	20.9	39.0	41.8	61	45.5	85.2	91
77965	230.85	251	891	1100	1382	41	18.9	41.5	45.3	113	41.1	90.3	103
77966	1.26	2	804	1100	1265	26	16.0	32.9	36.5	46	37.2	76.6	80
77968	3.92	4	822	1200	1214	49	20.4	44.1	49.5	73	45.9	99.3	97
77270	0.09	1	872	1500	128	79	74.1	87.4	83.2	120	152.9	180.3	195
77955	0.10	1	548	820	108	32	12.3	17.2	17.5	44	24.7	34.4	37
77282	0.13	1	717	1100	138	74	53.0	72.5	63.5	95	96.2	131.5	121
77272	0.05	1	653	1200	161	47	56.8	60.1	57.7	84	116.9	123.7	138
77268	0.11	1	832	1400	150	43	23.9	30.9	28.7	47	49.2	63.6	76
77967	0.43	1	1318	2100	259	71	48.1	68.8	73.0	134	107.3	153.5	160
77283	0.05	1	275	430	192	20	9.0	11.6	11.2	20	15.2	19.4	20
77298	1.49	1	769	1300	227	61	43.1	56.7	54.4	77	85.5	112.6	117
77963	0.08	1	1018	1500	143	20	8.0	12.0	11.3	20	10.7	16.1	17
77294	0.44	1	525	790	406	44	33.1	44.1	46.4	84	78.5	104.5	116
77280	4.37	4	494	770	383	48	52.0	57.0	56.4	90	96.4	105.6	117
77971	0.13	1	902	1300	349	23	6.0	11.3	11.0	20	12.3	23.3	23
77961	0.06	1	60	77	109	344	0.5	0.6	0.6	20	1.0	1.2	3
77972	0.20	1	101	110	192	20	1.2	1.0	0.7	20	3.0	2.3	3
77292	0.08	1	190	260	341	20	0.5	1.0	0.5	25	1.1	2.0	3
77957	0.05	1	10	50	16	20	0.3	0.5	0.5	20	0.5	1.0	3
77281	0.11	1	39	110	81	20	4.3	4.6	3.9	20	8.1	8.7	10
77287	0.13	1	1457	2500	1249	20	1.8	1.7	1.6	20	3.0	2.9	3
77964	0.18	1	2222	3400	1845	20	1.6	2.2	2.2	20	2.4	3.3	3
77959	0.14	1	43	75	75	337	12.9	14.9	13.3	24	24.3	28.1	30
77295	0.11	1	1265	1900	1037	20	0.3	0.5	0.5	20	0.5	0.8	3
77269	0.17	1	228	380	401	20	4.5	4.0	3.6	20	9.4	8.2	9
77969	1.84	2	262	330	467	20	21.8	19.9	19.1	24	39.9	36.5	40
77273	0.19	1	288	580	506	20	23.3	25.1	22.5	33	44.2	47.7	55
77970	0.79	1	20217	26000	1689	20	7.1	8.9	9.0	24	16.6	20.9	22
77274	5.64	5	436	650	706	24	12.5	13.3	12.5	20	22.9	24.5	26
77960	10.40	8	22	50	49	23	18.1	24.9	22.3	65	36.3	50.0	51
77271	0.08	1	210	320	344	20	1.7	1.8	1.9	20	3.1	3.2	3
77956	1.85	2	794	1100	1200	32	20.3	34.1	36.3	53	42.1	70.6	78
77278	5.05	4	803	1200	1301	28	16.1	31.1	34.5	54	43.3	83.8	83
77286	5.46	4	716	1000	1104	65	28.7	61.5	66.8	126	88.0	188.4	138
77293	1.14	1	776	1400	350	20	20.4	29.4	29.9	28	40.0	57.7	60
77962	2.44	2	1026	1400	754	54	12.2	34.5	42.6	59	36.8	104.5	85

sample	Eu (co)	Eu	Gd	Gd (co)	Tb	Tb (co)	Tb	Dy	Dy (co)	Ho	Ho (co)
	ppm	ppm	ppm	ppm	ppm	ppm	ppm	ppm	ppm	ppm	ppm
	ICP-MS	INAA	ICP-MS	ICP-MS	ICP-MS	ICP-MS	INAA	ICP-MS	ICP-MS	ICP-MS	ICP-MS
77275	2.25	1.8	3.7	9.2	0.5	1.2	0.5	2.7	6.8	0.6	1.38
77276	2.17	1.6	2.0	6.9	0.3	1.0	0.5	1.5	5.4	0.3	1.04
77277	2.04	1.7	3.3	7.7	0.5	1.1	0.5	2.5	5.7	0.5	1.14
77279	2.38	2.0	3.5	9.4	0.4	1.1	0.5	2.4	6.3	0.5	1.24
77284	2.42	1.7	1.9	7.8	0.3	1.1	0.5	1.4	5.8	0.3	1.10
77285	3.59	2.4	4.0	13.6	0.5	1.8	0.5	2.9	9.9	0.5	1.84
77288	2.12	1.4	3.9	8.6	0.5	1.0	0.5	2.5	5.4	0.5	1.07
77289	1.66	1.5	3.3	6.3	0.4	0.8	0.5	2.1	4.0	0.4	0.79
77290	1.42	1.4	2.1	5.1	0.3	0.6	0.5	1.2	2.9	0.2	0.56
77291	1.47	1.5	3.0	5.1	0.3	0.6	0.5	1.6	2.8	0.3	0.50
77296	2.07	1.8	4.7	8.0	0.6	1.0	0.5	3.1	5.4	0.6	1.02
77297	2.34	2.0	3.6	8.4	0.5	1.2	0.5	2.8	6.6	0.6	1.31
77299	1.95	1.8	1.6	7.4	0.2	1.0	0.5	1.3	6.0	0.3	1.22
77950	1.79	1.4	1.6	5.5	0.2	0.7	0.5	1.1	4.0	0.2	0.75
77951	1.83	1.5	3.0	7.0	0.4	0.9	0.5	2.0	4.7	0.4	0.89
77952	2.37	1.7	2.3	8.5	0.3	1.2	0.5	1.8	6.6	0.3	1.26
77953	1.56	1.2	3.1	5.9	0.4	0.8	0.5	2.3	4.3	0.4	0.79
77954	1.59	1.6	3.2	5.7	0.4	0.7	0.5	2.3	4.2	0.4	0.78
77958	2.12	1.5	3.6	6.8	0.4	0.8	0.5	2.5	4.8	0.5	0.86
77965	2.07	1.8	3.8	8.4	0.5	1.1	0.5	2.5	5.5	0.4	0.96
77966	1.93	1.4	3.3	6.8	0.4	0.9	0.5	2.4	4.9	0.4	0.92
77968	2.04	1.6	3.8	8.2	0.5	1.1	0.5	3.0	6.4	0.6	1.36
77270	1.81	1.6	4.5	5.4	0.4	0.5	0.5	1.8	2.1	0.4	0.42
77955	0.49	0.6	1.1	1.6	0.1	0.2	0.5	0.7	1.0	0.1	0.20
77282	1.36	1.1	3.5	4.7	0.3	0.4	0.5	1.5	2.0	0.3	0.38
77272	1.72	1.7	4.6	4.8	0.3	0.4	0.5	1.4	1.5	0.3	0.29
77268	1.47	1.2	3.9	5.0	0.4	0.5	0.5	1.9	2.4	0.4	0.48
77967	2.75	2.5	6.6	9.4	0.7	1.0	0.9	3.3	4.8	0.5	0.73
77283	0.06	0.2	0.3	0.3	0.1	0.1	0.5	0.3	0.3	0.1	0.13
77298	2.14	2.0	5.8	7.7	0.6	0.8	0.5	2.9	3.8	0.5	0.62
77963	0.13	0.4	0.5	0.8	0.1	0.2	0.5	0.5	0.7	0.1	0.15
77294	1.90	2.0	4.7	6.2	0.5	0.6	0.5	2.2	3.0	0.4	0.48
77280	2.03	2.0	6.1	6.7	0.6	0.6	0.5	2.6	2.9	0.5	0.52
77971	0.36	0.4	0.4	0.7	0.1	0.2	0.5	0.2	0.4	0.1	0.19
77961	0.06	0.2	0.1	0.1	0.1	0.1	0.5	0.1	0.1	0.1	0.12
77972	0.04	0.2	0.1	0.1	0.1	0.1	0.5	0.1	0.1	0.1	0.08
77292	0.09	0.2	0.1	0.2	0.1	0.2	0.5	0.1	0.2	0.1	0.18
77957	0.10	0.2	0.1	0.2	0.1	0.2	0.5	0.1	0.3	0.1	0.20
77281	0.15	0.2	0.5	0.6	0.1	0.1	0.5	0.4	0.5	0.1	0.12
77287	0.07	0.2	0.3	0.3	0.1	0.1	0.5	0.5	0.4	0.1	0.10
77964	0.07	0.2	0.2	0.3	0.1	0.1	0.5	0.3	0.5	0.1	0.14
77959	0.48	0.7	1.7	1.9	0.2	0.3	0.5	1.8	2.0	0.4	0.46
77295	0.08	0.2	0.1	0.2	0.1	0.2	0.5	0.2	0.3	0.1	0.15
77269	0.13	0.4	0.7	0.6	0.1	0.1	0.5	0.5	0.5	0.1	0.09
77969	0.56	0.6	2.1	1.9	0.2	0.2	0.5	0.9	0.8	0.1	0.10
77273	0.88	0.9	2.6	2.8	0.4	0.4	0.5	1.8	2.0	0.4	0.47
77970	0.86	1.0	1.8	2.2	0.1	0.2	0.5	0.4	0.5	0.1	0.13
77274	0.51	0.7	1.8	1.9	0.3	0.3	0.5	1.7	1.9	0.4	0.42
77960	0.29	0.2	2.6	3.6	0.4	0.6	0.5	2.5	3.5	0.5	0.69
77271	0.05	0.3	0.1	0.2	0.1	0.1	0.5	0.2	0.2	0.1	0.10
77956	1.71	1.7	3.8	6.3	0.4	0.7	0.5	2.4	4.1	0.4	0.73
77278	1.32	1.4	2.4	4.7	0.3	0.6	0.5	1.9	3.7	0.3	0.67
77286	1.78	1.4	4.0	8.5	0.4	1.0	0.5	2.4	5.1	0.4	0.96
77293	0.95	1.0	2.2	3.2	0.2	0.3	0.5	1.1	1.6	0.2	0.32
77962	1.51	1.3	2.0	5.6	0.3	0.8	0.5	1.6	4.4	0.4	0.99

sample	Er	Er (co)	Tm	Tm (co)	Yb*	Yb (co)	Yb	Lu*	Lu (co)	Lu	Hf
	ppm	ppm	ppm	ppm	ppm	ppm	ppm	ppm	ppm	ppm	ppm
	ICP-MS	ICP-MS	ICP-MS	ICP-MS	ICP-MS	ICP-MS	INAA	ICP-MS	ICP-MS	INAA	XRF
77275	1.6	3.9	0.2	0.6	1.4	3.5	2.4	0.2	0.5	0.36	7
77276	0.8	2.9	0.1	0.4	0.7	2.3	1.5	0.1	0.4	0.23	5
77277	1.4	3.1	0.2	0.5	1.3	3.0	2.6	0.2	0.4	0.39	5
77279	1.4	3.6	0.2	0.5	1.2	3.1	2.4	0.2	0.4	0.36	7
77284	0.8	3.1	0.1	0.5	0.7	2.9	1.8	0.1	0.4	0.27	5
77285	1.4	4.9	0.2	0.7	1.4	4.7	2.3	0.2	0.6	0.34	5
77288	1.4	3.0	0.2	0.4	1.1	2.4	2.4	0.2	0.4	0.36	5
77289	1.1	2.1	0.2	0.3	1.0	1.8	2.2	0.1	0.2	0.33	5
77290	0.6	1.4	0.1	0.2	0.4	1.0	1.0	0.1	0.2	0.15	8
77291	0.8	1.5	0.1	0.2	0.5	0.9	0.9	0.1	0.2	0.14	5
77296	1.7	2.9	0.2	0.4	1.5	2.5	1.9	0.2	0.4	0.28	5
77297	1.6	3.7	0.2	0.5	1.4	3.2	2.3	0.2	0.4	0.35	7
77299	0.8	3.5	0.1	0.6	0.9	3.9	2.0	0.1	0.5	0.31	5
77950	0.7	2.3	0.1	0.3	0.6	2.3	1.5	0.1	0.3	0.23	5
77951	1.1	2.5	0.1	0.3	0.9	2.1	1.8	0.1	0.3	0.26	6
77952	1.0	3.6	0.2	0.6	1.0	3.7	2.1	0.1	0.5	0.31	6
77953	1.1	2.1	0.2	0.3	1.1	2.0	1.6	0.2	0.3	0.26	5
77954	1.3	2.3	0.2	0.3	1.3	2.2	1.7	0.2	0.3	0.25	5
77958	1.2	2.3	0.2	0.3	1.1	2.1	1.6	0.2	0.3	0.24	9
77965	1.2	2.7	0.2	0.3	1.0	2.1	2.2	0.1	0.3	0.33	5
77966	1.2	2.5	0.2	0.4	1.1	2.4	2.3	0.1	0.3	0.35	6
77968	1.7	3.6	0.2	0.5	1.5	3.3	2.9	0.2	0.5	0.44	5
77270	1.0	1.2	0.2	0.2	1.2	1.5	1.5	0.2	0.2	0.22	7
77955	0.4	0.6	0.1	0.1	0.5	0.6	0.9	0.1	0.1	0.14	5
77282	0.9	1.2	0.1	0.2	1.1	1.5	1.6	0.2	0.2	0.24	5
77272	0.8	0.9	0.2	0.2	1.1	1.2	1.9	0.2	0.2	0.28	5
77268	1.1	1.4	0.2	0.2	1.2	1.6	1.7	0.2	0.2	0.25	5
77967	1.2	1.7	0.2	0.2	0.9	1.3	1.4	0.1	0.2	0.21	7
77283	0.3	0.3	0.1	0.1	0.3	0.4	0.6	0.1	0.1	0.10	5
77298	1.2	1.6	0.2	0.2	1.1	1.5	1.5	0.2	0.2	0.23	5
77963	0.3	0.5	0.1	0.2	0.4	0.6	0.6	0.1	0.2	0.09	5
77294	1.0	1.3	0.1	0.2	0.9	1.2	1.2	0.1	0.2	0.20	5
77280	1.3	1.4	0.2	0.2	1.3	1.4	2.2	0.2	0.2	0.33	5
77971	0.1	0.2	0.1	0.2	0.2	0.3	0.4	0.1	0.2	0.06	6
77961	0.1	0.1	0.1	0.1	0.1	0.2	0.3	0.1	0.1	0.05	5
77972	0.1	0.1	0.1	0.1	0.1	0.1	0.2	0.1	0.1	0.05	5
77292	0.1	0.2	0.1	0.2	0.1	0.2	0.2	0.1	0.2	0.05	5
77957	0.1	0.2	0.1	0.2	0.1	0.2	0.4	0.1	0.2	0.06	5
77281	0.4	0.4	0.1	0.1	0.5	0.5	0.8	0.1	0.1	0.13	5
77287	0.4	0.3	0.1	0.1	0.4	0.4	0.7	0.1	0.1	0.11	5
77964	0.2	0.3	0.1	0.1	0.1	0.2	0.5	0.1	0.1	0.08	5
77959	1.2	1.4	0.2	0.2	1.0	1.2	1.8	0.2	0.2	0.25	5
77295	0.1	0.2	0.1	0.2	0.1	0.2	0.2	0.1	0.2	0.05	5
77269	0.2	0.2	0.1	0.1	0.3	0.2	0.8	0.1	0.1	0.15	7
77969	0.2	0.2	0.1	0.1	0.1	0.1	0.2	0.1	0.1	0.05	5
77273	1.2	1.3	0.2	0.2	1.2	1.3	2.1	0.2	0.2	0.31	6
77970	0.1	0.2	0.1	0.1	0.1	0.1	0.6	0.1	0.1	0.09	5
77274	1.1	1.2	0.2	0.2	1.2	1.2	1.5	0.2	0.2	0.23	5
77960	1.5	2.1	0.2	0.3	1.7	2.3	2.3	0.2	0.3	0.35	5
77271	0.1	0.1	0.1	0.1	0.2	0.2	0.5	0.1	0.1	0.08	8
77956	1.2	2.1	0.2	0.3	1.1	1.9	1.8	0.1	0.2	0.26	5
77278	1.0	1.9	0.2	0.3	1.0	1.9	1.9	0.1	0.3	0.3	9
77286	1.3	2.8	0.2	0.4	1.2	2.6	2.2	0.2	0.4	0.33	5
77293	0.6	0.8	0.1	0.1	0.6	0.8	1.0	0.1	0.1	0.15	8
77962	1.1	3.0	0.2	0.5	1.2	3.4	2.3	0.2	0.4	0.36	5

sample	Hf*	Hf	Ta	Ta*	Ta	W	W	Re	Ir	Au	Hg	Hg	TI
	ppm	ppm	ppm	ppm	ppm	ppm	ppm	ppm	ppb	ppb	ppb	ppm	ppm
	ICP-MS	INAA	XRF	ICP-MS	INAA	XRF	INAA	ICP-MS	INAA	INAA	AAS-CV	INAA	ICP-MS
77275	3.1	5	5	1.3	0.5	5	1	0.005	5	4	5	1	0.28
77276	2.0	6	7	1.3	0.5	5	1	0.006	5	2	5	1	0.25
77277	2.6	5	5	1.2	3.8	5	1	0.010	5	2	5	1	0.21
77279	4.1	6	5	1.6	2.0	5	1	0.003	5	4	5	1	0.28
77284	3.1	6	5	1.2	3.2	5	1	0.001	5	3	5	1	0.25
77285	3.3	5	5	1.5	0.5	5	1	0.001	5	3	5	1	0.51
77288	2.6	5	5	1.1	0.5	5	1	0.003	5	4	5	1	0.39
77289	2.7	5	5	1.3	0.5	5	1	0.002	5	4	5	1	0.48
77290	4.0	5	5	0.7	0.5	5	1	0.004	5	2	5	1	0.28
77291	4.3	5	5	0.7	0.5	5	1	0.001	5	5	5	1	0.26
77296	3.0	5	6	1.4	2.5	5	1	0.002	5	2	5	1	0.43
77297	2.9	5	5	1.3	0.5	5	1	0.004	5	2	5	1	0.53
77299	3.8	6	5	1.7	0.5	5	1	0.003	5	5	5	1	0.44
77950	2.9	6	5	1.5	0.5	5	2	0.002	5	2	5	1	0.32
77951	2.8	5	7	1.4	2.2	5	1	0.005	5	2	5	1	0.55
77952	2.5	5	5	0.5	0.5	5	1	0.002	5	2	5	1	0.19
77953	2.4	5	5	1.4	2.0	5	1	0.001	5	2	5	1	0.28
77954	2.4	5	9	1.4	2.6	5	1	0.001	5	2	5	1	0.28
77958	3.4	5	5	1.4	0.5	5	1	0.004	5	2	5	1	0.38
77965	4.8	5	5	1.5	1.7	5	1	0.002	5	2	5	1	9.49
77966	3.0	5	6	1.3	0.5	5	1	0.001	5	3	5	1	0.61
77968	3.1	5	5	1.1	0.5	5	1	0.004	5	2	5	1	0.60
77270	3.9	5	5	1.4	0.5	5	1	0.017	5	2	556	1	0.12
77955	2.0	4	5	1.1	0.5	5	1	0.002	5	2	622	1	0.05
77282	3.0	5	5	1.3	0.5	5	1	0.003	5	2	127	1	0.07
77272	2.5	6	5	1.4	0.5	5	1	0.007	5	2	429	1	0.09
77268	2.7	5	5	1.1	0.5	5	2	0.008	5	2	501	1	0.05
77967	3.0	5	5	1.0	1.6	5	1	0.001	5	2	479	1	0.21
77283	2.6	6	5	2.0	2.3	5	1	0.003	5	2	133	1	0.05
77298	3.3	5	5	1.5	0.5	5	1	0.002	5	2	1243	1	0.19
77963	4.6	8	5	1.6	1.7	5	2	0.003	5	2	41	1	0.05
77294	3.5	7	5	1.3	2.1	5	1	0.003	5	2	11	1	0.05
77280	3.1	6	5	0.3	1.5	5	5	0.001	5	2	985	1	1.27
77971	1.5	4	5	1.2	1.6	5	1	0.003	5	2	26	1	0.18
77961	0.4	3	5	0.1	1.2	5	1	0.003	5	2	7	1	0.07
77972	0.4	7	5	0.1	2.2	5	2	0.005	5	2	28	1	0.05
77292	0.2	1	5	0.1	0.5	5	2	0.003	5	2	5	1	0.05
77957	0.4	7	5	0.1	1.8	5	1	0.005	5	2	38	1	0.06
77281	0.6	4	7	0.1	1.0	5	1	0.002	5	2	24	1	0.06
77287	2.1	5	7	0.4	1.0	5	1	0.001	5	2	786	1	0.05
77964	3.6	8	5	1.6	1.5	5	1	0.005	5	2	1472	1	0.30
77959	1.6	6	5	0.5	1.6	5	1	0.001	5	2	90	1	0.05
77295	1.9	6	7	0.1	1.2	5	1	0.003	5	2	545	1	0.05
77269	0.8	7	5	0.1	1.3	5	1	0.005	5	2	76	1	0.06
77969	0.8	2	5	0.4	0.5	5	1	0.001	5	2	92	1	0.76
77273	3.6	9	5	1.3	1.2	5	1	0.042	5	2	95	1	0.10
77970	1.2	11	5	0.5	2.2	5	2	0.001	5	81	12486	10	1.48
77274	0.8	6	5	0.1	0.5	5	1	0.011	5	2	148	1	0.17
77960	3.4	4	5	1.4	0.5	5	1	0.002	5	2	5	1	1.39
77271	0.5	5	5	0.1	1.3	5	1	0.001	5	2	7024	6	0.05
77956	2.0	5	6	1.2	1.5	5	1	0.003	5	2	5	1	0.50
77278	4.4	6	5	1.3	0.5	5	1	0.006	5	2	5	1	0.58
77286	3.7	6	5	1.5	0.5	5	1	0.002	5	2	5	1	0.77
77293	2.4	4	5	1.1	0.5	5	1	0.004	5	2	90	1	0.23
77962	6.8	7	5	1.5	0.5	5	1	0.001	5	2	5	1	0.70

sample	Pb	Pb	Bi	Bi	Th	Th*	Th	U	U	U
	ppm	ppm	ppm	ppm	ppm	ppm	ppm	ppm	ppm	ppm
	XRF	ICP-MS	XRF	ICP-MS	XRF	ICP-MS	INAA	XRF	ICP-MS	INAA
77275	17	17.0	3	0.04	16	6.6	18.7	8	2.0	4.4
77276	13	36.3	3	0.02	16	5.2	19.9	9	1.3	4.4
77277	8	15.7	3	0.03	18	6.7	19.3	8	2.2	3.7
77279	13	16.8	3	0.03	16	7.1	16.4	6	1.6	2.8
77284	15	13.2	3	0.03	15	4.4	17.1	4	1.1	4.8
77285	18	17.7	3	0.03	16	5.5	15.3	6	1.5	4.0
77288	19	15.3	3	0.03	20	6.0	17.5	3	2.0	4.6
77289	15	15.1	5	0.05	14	5.3	16.1	3	2.6	5.6
77290	14	15.0	3	0.04	15	5.2	17.7	3	1.2	3.3
77291	15	17.2	3	0.03	10	5.3	14.1	4	2.2	2.5
77296	8	16.4	4	0.05	17	8.4	17.8	4	2.8	4.1
77297	16	23.9	3	0.07	16	5.9	17.7	8	2.3	4.9
77299	20	17.6	3	0.02	14	5.0	19.1	3	1.3	5.6
77950	18	18.3	3	0.02	18	7.3	17.9	3	1.8	4.2
77951	18	16.3	3	0.02	20	7.1	17.5	5	2.1	5.3
77952	17	17.1	3	0.03	19	6.9	20.3	5	1.6	4.3
77953	17	17.1	3	0.02	17	6.9	15.5	4	2.4	4.1
77954	8	17.3	3	0.02	22	8.1	16.5	9	2.4	4.6
77958	16	16.6	3	0.04	11	5.2	14.3	4	2.7	2.8
77965	17	16.0	3	0.02	14	3.9	15.3	5	1.9	2.6
77966	14	17.1	3	0.04	12	5.2	14.7	3	1.8	3.1
77968	14	16.9	3	0.07	15	6.1	15.2	6	1.9	3.0
77270	25	27.0	3	0.12	25	21.7	24.0	5	5.4	5.6
77955	6	9.3	3	1.35	13	6.2	9.7	3	1.7	2.0
77282	23	27.9	3	0.25	24	18.0	22.5	4	3.3	3.6
77272	15	15.3	3	0.11	16	10.8	14.0	7	2.0	3.0
77268	37	39.8	3	0.05	18	13.8	17.4	3	3.8	4.2
77967	24	25.0	3	0.05	18	13.8	21.0	4	3.4	5.5
77283	8	8.5	3	0.03	8	3.4	4.8	3	1.2	2.0
77298	25	21.4	3	0.10	21	15.7	20.0	3	3.2	4.4
77963	14	14.3	3	0.05	11	3.5	6.2	3	2.4	2.6
77294	14	14.1	3	0.02	27	21.0	29.3	9	7.4	9.8
77280	176	198.0	3	1.70	20	14.5	16.5	5	3.5	4.9
77971	14	13.1	3	0.38	11	2.7	4.7	3	1.7	3.1
77961	4	0.5	3	0.02	5	1.8	2.7	3	0.6	1.4
77972	4	2.2	3	0.67	5	0.6	0.6	3	0.1	0.5
77292	4	1.4	3	0.02	5	0.3	0.4	3	0.2	0.5
77957	4	0.5	3	0.02	6	1.0	2.4	3	0.5	1.7
77281	4	1.2	3	0.02	5	2.1	2.9	3	1.2	1.6
77287	4	0.8	3	0.05	5	1.6	1.9	4	2.2	2.0
77964	29	33.5	4	4.89	6	3.0	5.8	3	1.8	2.7
77959	4	1.4	3	0.04	13	5.9	7.9	3	1.6	2.7
77295	4	0.7	3	0.02	5	0.3	0.4	3	0.1	0.5
77269	4	2.3	3	0.02	11	3.3	4.1	5	1.3	2.2
77969	35	37.3	3	0.47	9	3.6	3.6	4	1.1	1.0
77273	6	12.5	3	2.61	11	10.2	11.8	6	3.9	4.5
77970	75	87.7	42	38.29	6	1.9	6.7	6	0.8	0.5
77274	11	14.5	3	0.08	12	12.5	13	3	3.4	4.1
77960	29	35.4	3	0.04	32	19.2	23.7	8	6.2	6.6
77271	4	30.2	3	0.19	5	1.1	1.5	3	0.7	1.0
77956	16	17.5	3	0.10	15	5.5	15.6	3	2.6	3.6
77278	13	15.8	3	0.08	11	8.9	17.2	8	2.3	3.8
77286	22	20.5	3	0.12	17	9.5	18.5	8	2.7	4.4
77293	4	17.3	3	0.31	9	9.9	17.0	3	2.7	3.0
77962	15	17.9	3	0.06	22	9.4	22.4	13	2.6	5.0

outcrop	East	North	altitude	layering	faults	fault striation	feldspar orientation	glacial striation
1	366279	8227554	4790	335/05				
2	366414	8227223	4825	350/60				
3	366529	8227304	4825	330/50				
4	368024	8227224	4852	250/30				
5	368344	8227224	4898	085/20				
6	368364	8227323	4878	070/17				
7	369289	8227954	4742	080/20				
8	369739	8227783	4828	090/60			180/10	
9	369794	8227613	4843	060/45			150/10	
10	369619	8227354	4785	350/20				
11	369954	8227104	4872	126/40				
12	369929	8226913	4862	270/30				
13	367617	8226292	4917					
14	367463	8226218	4776					
15	368866	8227476	4725					
16	368975	8227591	4730					
17	369018	8227588	4734	110/30				
18	368109	8226264	4776	120/20				
19	368084	8226386	4810					090/25
20	368088	8226446	4812					
21	368173	8226168	4871					130/25
22	368206	8226078	4830					
23	368192	8225990	4822					
24	368260	8225958	4820					
25	368223	8225996	4836					
26	368226	8225938	4832					
27	368218	8225891	4813					
28	368219	8225813	4810					
29	368271	8225933	4831					
30	368259	8225953	4833					
31	368125	8226254	4802					
32	368069	8226089	4878					
33	368029	8226022	4762					
34	368025	8225983	4874					
35	368031	8225964	4860					
36	367978	8225957	4885	170/20				
37	367960	8225956	4866					
38	367962	8225981	4887					
39	367925	8225967	4888					
40	367889	8225948	4905					
41	367840	8225932	4906					
42	367844	8226039	4932					
43	367804	8226139	4951					
44	367766	8226056	4930					
45	367742	8226002	4908					
46	367717	8226013	4895					
47	367722	8226031	4905					
48	367698	8226085	4937					
49	367680	8226105	4950					
50	367609	8226117	4947					
51	368015	8226530	4896					
52	368013	8226467	4906					
53	368004	8226434	4915					
54	369884	8226604	4802	260/45				
55	370000	8226413	4770	250/30				
56	367923	8226462	4977					
57	367900	8226494	4939					
58	367851	8226493	4941					
59	367866	8226576	4939					

outcrop	East	North	altitude	layering	faults	fault striation	feldspar orientation	glacial striation
60	367890	8226580	4928					
61	367923	8226605	4922					
62	367979	8226476	4909					
63	367984	8226703	4801					
64	368018	8226781	4911					
65	368047	8226836	4906					
66	368060	8226862	4909					
67	368090	8226975	4915					
68	368131	8227051	4919					
69	368145	8227075	4901					
70	368168	8227144	4929					
71	368208	8227089	4910					
72	368210	8226961	4891					
73	368140	8226925	4913					
74	368180	8226813	4885	090/15				
75	368175	8226794	4881					
76	368123	8227079	4919					
77	368229	8227164	4928					
78	367937	8227206	4935					
79	367741	8227339	4782					
80	367735	8227386	4866	330/60				
81	367765	8227419	4800					
82	367744	8227496	4812					
83	367739	8227439	4798					
84	367899	8227562	4889					
85	367941	8227558	4858					
86	367851	8227691	4869	190/30				
87	367743	8227805	4826	340/30				
88	367606	8227962	4845					
89	367562	8227953	4869					
90	367508	8227881	4845					
91	367433	8227871	4840					
92	367270	8227917	4892					
93	367230	8227896	4894					
94	367015	8227781	4898					
95	368290	8226942	4870					
96	367696	8227241	4776					
97	367580	8227199	4805	330/45				
98	367790	8227185	4798					
99	367826	8227174	4843					
100	367874	8227146	4843					
101	367868	8227112	4847					
102	367845	8227001	4850					
103	367858	8226975	4860					
104	367809	8226904	4855					
105	367786	8226850	4850					
106	367809	8226777	4858					
107	367960	8226803	4897					
108	367960	8226911	4890					
109	368069	8226936	4912					
110	367848	8226718	4848					
111	367596	8226730	4794					
112	367522	8226738	4810					
113	367370	8226740	4793					
114	367260	8226692	4783					
115	367254	8226597	4787					
116	367102	8226483	4796					
117	367062	8226433	4807					
118	367006	8226394	4814					
119	366955	8226371	4812					

outcrop	East	North	altitude	layering	faults	fault striation	feldspar orientation	glacial striation
120	366898	8226215	4833					
121	366873	8226169	4847					
122	366767	8226121	4801					
123	366837	8226027	4830					
124	367146	8225840	4765					
125	367201	8226072	4848					
126	367273	8226185	4870					
127	367237	8226247	4895					
128	367774	8226506	4933		340/75			
129	368378	8227572	4825					
130	368356	8227561	4832					
131	367905	8227592	4872					
132	367998	8227597	4891					
133	367922	8227903	4852					
134	368032	8227910	4834	000/30				
135	368157	8227963	4804					
136	368382	8227940	4807					
137	368551	8227794	4816					
138	368471	8227591	4812					
139	368381	8227572	4837					
140	368377	8227491	4849					
141	368337	8227414	4868					
142	368452	8227314	4847					
143	368479	8227165	4844					
144	368330	8227309	4890					
145	368511	8226844	4822					
146	368435	8226804	4847					
147	368418	8226514	4834					
148	368398	8226310	4835	120/75				
149	368336	8226198	4844					
150	368378	8225838	4789					
151	368295	8225785	4787	130/60	150/70	060/10	070/10	
152	368169	8225643	4780		120/70	060/75	070/75	
153	368454	8225609	4758					
154	368315	8225345	4748					
155	368855	8227517	4726					
156	369983	8225611	4639					
157	369980	8225364	4643	230/15				
158	369968	8225278	4706					
159	369872	8225425	4694	225/60				
160	369785	8225558	4687	265/28				
161	369644	8225772	4678	270/50				
162	369664	8225865	4668	180/35				
163	369839	8225837	4657					
164	369919	8225678	4648	350/15				
165	369816	8225267	4773	260/15				
166	369764	8225329	4776					
167	369735	8225370	4787		290/90			
168	369702	8225429	4776				060/10	
169	369703	8225453	4777					
170	369474	8225440	4849		220/35	195/30		
171	369178	8227571	4743		130/80			
172	369257	8227423	4762		230/35	230/30		
173	369415	8227365	4782				060/10	
174	369680	8227329	4838					
175	369669	8227262	4827					
176	369715	8227187	4818		130/80			
177	369574	8227128	4788					
178	368867	8227677	4741	000/00				
179	368878	8227832	4747		095/80			

outcrop	East	North	altitude	layering	faults	fault striation	feldspar orientation	glacial striation
180	368879	8227895	4753	000/00				
181	368998	8227998	4745		110/80			
182	369216	8227939	4757					
183	369603	8227954	4797	100/10				
184	369751	8227992	4843	110/60			110/10	
185	369836	8227756	4887					
186	369915	8227552	4899	110/30			010/00	
187	369847	8227099	4856		300/50			
188	369954	8226244	4745	270/40				
189	369454	8226754	4712	045/90				
190	370009	8226121	4783	250/30				
191	369995	8226029	4746		290/80			
192	369785	8226943	4780					
193	369633	8226758	4719					
194	369637	8226754	4740	335/85			vertical	
195	369648	8226823	4759	270/90			vertical	
196	369567	8226876	4748	250/80			vertical	
197	369642	8226740	4740					
198	369167	8225972	4716	290/20				
199	369464	8225209	4774		090/70		010/20, 190/15	
200	369710	8225150	4780	305/30				
201	369534	8225200	4775					
202	369739	8226703	4735	225/20				
203	369534	8225241	4805					
204	369634	8225505	4798					
205	369322	8225759	4823					
206	369411	8225685	4824					
207	369805	8225072	4780	320/50			120/00 o.310/00	
208	370000	8225167	4752	000/00				
209	369407	8225614	4848	180/15			090/00	
210	369769	8225335	4772	000/00				
211	367394	8227756	4810		145/85			
212	367340	8227952	4880					
213	366704	8227984	4864		N45E			
214	366135	8227953	4725	330/30				
215	366110	8227755	4728	135/30				
216	366777	8227759	4881					
217	367263	8227905	4861					
218	366866	8227647	4944					
219	366831	8227547	4881					
220	366753	8227538	4898					
221	366755	8227534	4883					
222	369739	8225623	4673	270/35				
223	366304	8227297	4911	330/20				
224	366140	8226710	4774	80/10			150/00	
225	366118	8226967	4755					
226	366060	8226664	4737	350/30				
227	366218	8226418	4689	330/80				
228	366650	8226040	4813					
229	366700	8226041	4813					
230	368766	8226621	4741					
231	366573	8225899	4782					
232	366464	8225848	4767	195/15				
233	366300	8225883	4745	45/15				
234	366060	8225303	4701					
235	366223	8225029	4742					
236	366785	8225277	4748	80/25				
237	366848	8225437	4751					
238	368106	8226254	4901					
239	368153	8226205	4873					

outcrop	East	North	altitude	layering	faults	fault striation	feldspar orientation	glacial striation
240	368204	8226223	4856					
241	368239	8226183	4852					
242	367945	8226150	4919					
243	368039	8226269	4916					
244	367685	8226112	4952					
245	367505	8226181	4904					
246	367359	8226208	4907					
247	367184	8226235	4877					
248	366926	8226243	4834		225/90	225/89		
249	367006	8226279	4834		305/85			
250	367164	8226309	4851		220/90	220/89	vertical	
251	367486	8226261	4885					
252	366792	8226807	4727					
253	366870	8227048	4770					
254	366852	8227089	4779					
255	366985	8226494	4773					
256	367966	8226604	4918					
257	368375	8227122	4889					
258	368083	8226402	4910					
259	367992	8226080	4910					
260	368237	8226298	4869					
261	368383	8226394	4845	000/90				
262	368496	8226993	4770					
263	368696	8227149	4800		000/90			
264	368502	8227130	4828					
265	368281	8227410	4880					
266	368329	8227700	4858					
267	368205	8227665	4883					
268	368238	8227533	4847					
269	368085	8227047	4906					
270	367672	8226855	4827					
271	368006	8226894	4896					
272	367807	8226778	4858					
273	367824	8227683	4839	195/30				
274	367733	8227612	4827	195/40			280/00	
275	367774	8227584	4818	140/60			220/35	
276	367879	8227550	4875	165/35			230/66	
277	367619	8226735	4821					
278	367135	8225365	4750					
279	367497	8225276	4752					
280	368832	8226877	4728	090/25			180/10	
281	368967	8225902	4710					
282	368720	8225090	4723	220/25			130/00	
283	368306	8225068	4700					
284	369127	8227239	4742	315/90			225/90	
285	268356	8227220	4893	80/25				
286	368368	8226781	4864	100/25				
287	368271	8226750	4863					
288	368206	8226362	4872					
289	367863	8225776	4804					
290	367807	8225779	4845	160/20				
291	367755	8225874	4855	180/20				
292	367636	8225898	4854	229/25				
293	366771	8225336	4736	165/42				
294	365985	8225025	4720	310/45				
295	366214	8225007	4737	030/60				
296	367042	8225970	4793	200/20				
297	367128	8226044	4822	200/20				
298	367139	8226142	4825	210/25				
299	367275	8226143	4866					

outcrop	East	North	altitude	layering	faults	fault striation	feldspar orientation	glacial striation
300	368619	8227729	4788	080/50				
301	368550	8227842	4798					
302	368322	8227741	4855	150/30			060/10	
303	368098	8227521	4884	095/15				
304	367849	8227656	4858	120/80				
305	366582	8227597	4840					
306	366676	8227532	4873	335/25				
307	366725	8227501	4877	250/45				
308	366972	8227170	4777	330/60				
309	367201	8227250	4765	280/70				
310	367479	8227434	4794	150/50			230/00	
311	367609	8227521	4816	155/55				
312	367873	8227590	4871	180/56				
313	368023	8227612	4891	240/30			150/00	
314	367921	8227459	4898	260/30				
315	368052	8227562	4875					
316	368084	8227668	4885	002/30				
317	368143	8227767	4896	330/10				
318	367928	8227642	4852					
319	367953	8227376	4892	260/30				
320	367984	8227277	4888	265/25				
321	368190	8227298	4917	035/20				
322	368188	8227180	4935	140/20				
323	368140	8227128	4921	245/20				
324	368092	8227018	4915	290/20				
325	368081	8226956	4910	305/20				
326	368045	8226978	4812	110/15				
327	368033	8226857	4901	110/45				
328	367890	8226873	4873	270/35				
329	368046	8226746	4904	105/17				
330	368007	8226667	4912	075/20				
331	367862	8226575	4914	325/30				
332	367859	8226500	4946	090/10				
333	367872	8226395	4955	135/40				
334	367854	8226380	4959	280/30				
335	367863	8226289	4967	135/30				
336	367810	8226279	4972	280/30				
337	369279	8225703	4750	045/05				
338	369379	8225863	4777	270/05				
339	368499	8225543	4722	135/30				
340	368199	8225233	4723	330/20				
341	368235	8226172	4775	130/42				
342	366039	8225102	4710	080/20				
343	366079	8225643	4668	205/60				
344	366599	8226323	4690	70/22				
345	366860	8226570	4625	040/15				
346	367529	8225763	4785	240/20				
347	367999	8226173	4814	100/15				
348	367639	8226373	4772	040/35				
Camp	368851	8227452						